Copy 1001

NORAD GENERAL PERTURBATION THEORIES:

AN INDEPENDENT ANALYSIS

by

Darrell Lee Herriges

B.S., United States Air Force Academy (1978)
M.S., Troy State University (1984)

Submitted in partial fulfillment of the
requirements for the degree of

MASTER OF SCIENCE IN AERONAUTICS AND ASTRONAUTICS

at the

MASSACHUSETTS INSTITUTE OF TECHNOLOGY

January 1988

© The Charles Stark Draper Laboratory, Inc., 1988

Signature of Author: Darrell Lee Herriges
Department of Aeronautics and Astronautics
15 January 1988

Certified by: Paul Cefola
Paul J. Cefola, Thesis Advisor
Lecturer, Department of Aeronautics and Astronautics

Accepted by: Harold Y. Wachman
Professor Harold Y. Wachman
Chairman, Aeronautics and Astronautics Graduate Committee

NORAD GENERAL PERTURBATION THEORIES:

AN INDEPENDENT ANALYSIS

by

Darrell Lee Herriges

Submitted to the Department of Aeronautics and Astronautics in January 1988 in partial fulfillment of the requirements for the degree of Master of Science in Aeronautics and Astronautics.

ABSTRACT

This thesis accurately incorporates the NORAD general perturbation theories SGP, GP4/DP4 and HANDE into the Draper Laboratory modified Goddard Trajectory Determination System orbit computation program. Actual SPADOC 4B Fortran source code for the NORAD theories, that was obtained from the Ford Aerospace Corporation, formed the basis for this incorporation. This incorporation supports comparisons of the NORAD general perturbation theories with conventional special perturbations and with other more recent analytical and semianalytical satellite theories. It is not presently possible to perform such comparisons within a single orbit computation program with consistent treatment of force models, coordinate systems and time references. This system will be uniquely able to support analyses of the accuracy with which orbits can be determined and predicted with NORAD tracking data.

Both orbit generator and differential correction test cases are analyzed. The orbit generator results provide strong confidence in the accuracy of the incorporation. Differential correction analyses include both geosynchronous and low altitude cases. For simulated data analysis, a Precise Conversion of Elements procedure was utilized whereby a given NORAD theory was used to obtain a differential correction fit to simulated observations. These observations were in the form of a position and velocity truth file that was created by the numerical evaluation of the equations of motion for each NORAD theory. A subsequent ephemeris, based upon this differential correction fit, is generated and compared with the corresponding reference orbit. The real data analysis employs a Differential Correction/Ephemeris Comparison procedure in which a designated NORAD theory processes real observations. The resulting orbit is compared to a differential correction fit of the same data with a high precision theory. Numerical results are available.

Thesis Supervisor: Paul J. Cefola, Ph.D
Section Chief
Air Force and Defensive Systems Department
The Charles Stark Draper Laboratory

Lecturer
Department of Aeronautics and Astronautics
Massachusetts Institute of Technology

ACKNOWLEDGEMENTS

First of all, I thank Elba Santos and Christine Aufiero for preparing this thesis. Without both of your efforts we would read no further.

I thank my wife, Bev-Ann, and my children, Audra and Travis, for their understanding and encouragement. Their continued patience and sacrifice have allowed me to complete this document in a complete and timely manner. I am also grateful to Bev-Ann's parents, Bob and Beverly, for all of their support throughout our entire stay in Boston.

My opportunity for this graduate education was made possible by AFIT's Senior Commander Sponsored Education Program. I hope that my efforts reflect the value of this program and provide motivation for its continued support.

I must mention three Air Force officers who played a key role in getting me into MIT. These former instructors are: Colonel Ferguson, Lieutenant Colonel Schade, and Lieutenant Colonel Torrey. I thank all of you for taking the time to recommend a former student and making this experience possible.

This thesis would not have been possible without the cooperation and assistance of the following individuals and the organizations that they represent: Colonel Paul Nielsen (ESD), Colonel Eric Sundberg (AFSPACECOM/DOA), and Mr. Roger Mansfield and Mr. Jon Kolb, both of the Ford Aerospace Communications Corporation. I am especially grateful for the efforts of Mr. Roger

Mansfield and his staff for providing the SPADOC Fortan computer code and the orbit generator test cases that were used in this analysis. I thank Mr. Frans C. Kes of Telesat Canada for providing the ANIK D2 tracking data that provided the excellent test case for the geosynchronous study. I also appreciate the efforts of MSgt Michael D. Ruff and the NORAD Historical Data System (LKWSA) staff for providing outstanding support throughout this thesis.

I owe a special thanks to Draper Laboratory President, Ralph Jacobson; ROTC detachment Commander, Colonel Gary Nelson; and Dr. David Burke, Draper Laboratory Education Director. I thank all of you for taking a personal interest in my career and I sincerely appreciate all of your efforts.

As for the Draper Laboratory Education Department, I thank you; Dr. David Burke, Vilma Dunham and Shirley Grady for creating my 'home' away from home in the carpeted halls of the seventh floor. I appreciate your personal support and our continuing companionship.

I am grateful for the professional advice received from members of the Space Systems Analysis Section to include: Mr. Leo Early, Dr. Ronald Proulx, Dr. Mark Slutsky and Mr. Wayne McClain. I also thank Mark and Wayne for their insights and a willingness to listen to a sometimes confused researcher. To Gary Holden and Nan Cook, your Macintosh advice, knowledge and support have been invaluable. I thank my peers: Robert Polutchko, Shuur Ahmed, Dr. Elaine Wagner, Avram Tetewsky, Dr. Bob Herklotz, Rob Saner, Dr. Mark Lane, Neil McCasland, Mark Stephenson, and Craig Seymour. Your help and friendship have been the key to my success and my

well being. I only hope that I can return as much to you. I especially thank Major (selectee) Neil McCasland and his wife, Dr. Susan Wilkerson for "adopting" me during the last month of writing this thesis. Even though I seldom saw either of you, I am truly appreciative of your generosity and understanding.

It has been both motivational and a priviledge to be a student of the following distinguished instructors: Dr. Richard Battin, Dr. John Vinti, Dr. Walter Hollister and Dr. Paul Cefola. As my thesis advisor, I thank Dr. Cefola for his leadership, technical guidance, extraordinary availability, and for having a seemingly unlimited patience. I am also indebted to him for providing a comprehensive introduction to the "business" of applied astrodynamics.

To my mother, Joyce Roemer, and my grandmother, Ramona Boyd, I thank you both for developing my desire to attain an excellent education. This thesis and my graduation from MIT represents a measure of your success.

Permission is hereby granted by the Charles Stark Draper Laboratory, Inc., to the Massachusetts Institute of Technology and to the Air Force Institute of Technology to reproduce any or all of this thesis.

TABLE OF CONTENTS

Chapter		Page
1	INTRODUCTION	15
1.1	Motivation	15
1.2	Need for an Independent Analysis	18
1.3	Overview of Thesis	37
2	BACKGROUND	42
2.1	NORAD General Perturbation Theories	42
2.1.1	SGP Satellite Theory	43
2.1.2	GP4 Satellite Theory	46
2.1.3	DP4 Satellite Theory	52
2.1.4	HANDE Satellite Theory	55
2.2	The Goddard Trajectory Determination System	61
2.2.1	Overall GTDS Capabilities	61
2.2.2	GTDS Cowell Special Perturbations Orbit Generator	67
2.2.3	Draper Semianalytical Satellite Theory (DSST)	70
2.3	Pertinent Coordinate Systems	75
3	INCORPORATION OF THE NORAD THEORIES INTO GTDS	84
3.1	Overview	84
3.2	Input Data	90
3.2.1	Orbit Generator Input Data	90
3.2.2	Differential Correction Input Data	93
3.3	Processing	94
3.3.1	Key Common Blocks	94
3.3.2	Input Data Processing (SETRUN, SETORB)	96
3.3.2.1	SETRUN	96
3.3.2.2	SETORB	100
3.3.3	Initialization	101
3.3.3.1	Initialization of Time and Coordinate Systems	101
3.3.3.2	Initialization of Semimajor Axis	104
3.3.3.3	Initialization of Element Set Arrays	105
3.3.3.4	Initialization of HANDE	106
3.3.3.5	Initialization of Drag Solve-for Parameters and Flags	106

3.3.4 Solve Table Set-Up (SOLTAB) 109
3.3.5 Restart (ORBIT, RESINS) 109
3.3.5.1 Restart for SGP (RESSGP, SGPAST) 110
3.3.5.2 Restart for GP4/DP4 (RESGP4, GP4IC2, GP4AST) 111
3.3.5.3 Restart for HANDE (RESHAN, DCIN2B, HANAST) 113
3.3.6 Solve Parameter Titles (GVCVL) 118
3.3.7 Output at Request Time (ORBIT, ORBITS, ORBSGP, ORBGP4, ORBHAN) 118
3.3.7.1 Position and Velocity 118
3.3.7.2 Partial Derivatives 119
3.3.8 Observation Modelling 126
3.3.8.1 Position and Velocity Data (OBSPCE, ROTKEY, ROTRAN) 126
3.3.8.2 Tracking Data (OBSTRK) 127
3.3.9 Parameter Reset (PSET) 127
3.3.10 Output Report Modifications 127
3.4 Output Data 128
3.5 SPADOC Subroutines 128

4 ORBIT GENERATOR TEST CASES 133
4.1 SGP Orbit Generator 136
4.2 GP4/DP4 Orbit Generator 138
4.3 HANDE Orbit Generator 144
4.4 State Transition Matrix Analysis 146
4.4.1 Finite Differencing 148
4.4.2 SGP State Transition Matrix 153
4.4.3 GP4/DP4 State Transition Matrix 157
4.4.4 HANDE State Transition Matrix 162

5 DIFFERENTIAL CORRECTION TEST CASES 166
5.1 Test Methodology 166
5.2 Low Altitude Case 172
5.2.1 PCE Fits to a Specified NORAD Reference Ephemeris 175
5.2.1.1 SGP Low Altitude DC Comparison 176
5.2.1.2 GP4 Low Altitude DC Comparison 177
5.2.1.3 HANDE Low Altitude D.C. Comparison 179

5.2.2 Fits to Real Data (NSSC 10299) 180
5.2.2.1 Fit Span Comparisons 185
5.2.2.1.1 DSST Analysis 185
5.2.2.1.2 GP4 Analysis 188
5.2.2.1.3 HANDE Analysis 197
5.3 Geosynchronous Case 206
5.3.1 PCE Fit to the DP4 Propagation Trajectory 207
5.3.1.1 DP4 Geosynchronous DC Comparison 209
5.3.2 Fits to TELESAT ANIK D2 Tracking Data 211
5.3.2.1 DSST Analysis 214
5.3.2.2 DP4 Analysis 217

6 CONCLUSIONS/FUTURE WORK 234
6.1 Summary 234
6.2 Conclusions 238
6.3 Future Work 240

LIST OF REFERENCES 310
BIOGRAPHY 321

LIST OF APPENDICES

Appendix		Page
A	Overview of General and Special Perturbation Methods	247
B	Subroutine G2MEOE Mathematics	263
C	A Comparison GTDS and SPADOC Partial Derivative Equations	275
D	Finite Differencing Theory	279
E	A Review of the Generalized Method of Averaging	282
F	User Guide Data	293

LIST OF FIGURES

Figure		Page
2-1	The Celestial Sphere	77
2-2	Nutation	79
3-1	Basic GTDS Orbit Generator Architecture	85
3-2	Overview of GTDS Implementation of NORAD/SPADOC GP Satellite Theories	87
3-3	Overview of SGP Software	112
3-4	Overview of GP4/DP4 Software	114
3-5	Overview of HANDE Software	117
3-6	Members of the AG2STM Array from Subroutine G2MEOE	120
3-7	Reordered AG2STM Matrix, AGRSTM	121
3-8	GTDS B_2 Matrix	124
5-1	DSST Low Altitude Observation Processing Summary	184
5-2	GP4 Low Altitude Observation Processing Summary	189
5-3	GP4-DSST Radial Differences Day 5	191
5-4	GP4-DSST Cross-Track Differences Day 5	192
5-5	GP4-DSST Along-Track Differences Day 4	193
5-6	GP4-DSST Along-Track Differences Day 5	194
5-7	GP4-DSST Mean Longitude Differences Day 4	195
5-8	GP4-DSST Mean Longitude Differences Day 5	196
5-9.	HANDE Low Altitude Observation Processing Summary	198
5-10	HANDE-DSST Radial Differences Day 5	200
5-11	HANDE-DSST Cross-Track Differences Day 5	201
5-12	HANDE-DSST Along-Track Differences Day 4	202
5-13	HANDE-DSST Along-Track Differences Day 5	203
5-14	HANDE-DSST Mean Longitude Differences Day 4	204
5-15	HANDE-DSST Mean Longitude Differences Day 5	205
5-16	DSST Geosynchronous Observation Processing Summary	215

5-17 DP4 Geosynchronous Observation Processing Summary 218
5-18 DP4-DSST Fit Span Radial Differences 220
5-19 DP4-DSST Fit Span Cross-Track Differences 221
5-20. DP4-DSST Fit Span Along-Track Differences 222
5-21 DP4 and DSST Fit Span Longitude of Ascending Node Histories 223
5-22. DP4-DSST Fit Span Mean Longitude Differences 224
5-23 "Modified" DP4 Geosynchronous Observation Processing Summary 226
5-24 "Modified DP4" -DSST Fit Span Radial Differences 229
5-25 "Modified DP4" -DSST Fit Span Cross-Track Differences 230
5-26 "Modified DP4" -DSST Fit Span Along-Track Differences 231
5-27 "Modified DP4" and DSST Fit Span Longitude of Ascending Node Histories 232
5-28 "Modified DP4" -DSST Fit Span Mean Longitude Differences 233

LIST OF TABLES

Table		Page
1-1	Maximum m-daily Errors (meters)	24
1-2	WGS 72 and WGS 84 Ellipsoid Parameters	29
3-1	Element Set Definitions	89
3-2	Key Common Blocks	95
4-1	Characteristics of the Satellites Used in the Orbit Generator Test Cases	134
4-2	Benchmark of Spacetrack Report #3 SGP Test Case	137
4-3	Benchmark of FACC GP4/DP4 Test Case for Satellite #4282 (Low Earth Orbit)	140
4-4	Benchmark of FACC GP4/DP4 Test Case for Satellite #7250 (Geosychronous)	141
4-5	Benchmark of FACC GP4/DP4 Test Case for Satellite #9494 (Near Decay)	142
4-6	Benchmark of FACC GP4/DP4 Test Case for Satellite #10455 (Molniya)	143
4-7	Benchmark of FACC HANDE Test Case for Satellite #4282 (Low Earth Orbit)	145
4-8	Finite Differencing Analysis for $\delta\lambda/\delta ko$	151
4-9	Finite Differencing Analysis for $\delta\lambda/\delta ho$	152
4-10	DSST B2 Matrix vs SGP "Modified" AGRSTM Array at Epoch + 1 Day	155
4-11	DSST B2 Matrix vs SGP "Modified" AGRSTM Array at Epoch + 1 Day	156
4-12	DSST B2 Matrix vs GP4/DP4 "Modified" AGRSTM Array at Epoch + 1 Day	158
4-13	DSST B2 Matrix vs GP4/DP4 "Modified"AGRSTM Array at Epoch + 1 Day	159
4-14	DSST B2 Matrix vs HANDE "Modified" AGRSTM Array at Epoch + 1 Day	163
4-15	DSST B2 Matrix vs HANDE "Modified" AGRSTM Array at Epoch + 1 Day	164

5-1 Initial Parameters of the low altitude orbit for PCE....173
5-2 Differential Correction Parameters Used in Low Altitude PCE....175
5-3 SGP Low Altitude PCE Results....177
5-4 GP4 Low Altitude PCE Results....178
5-5 HANDE Low Altitude PCE Results....180
5-6 Initial Parameters of NSSC 10299....182
5-7 Force Model Used in the DSST "truth" Model for the Low Altitude Case (NSSC 10299)....183
5-8 Results of DSST for NSSC 10299, Days 1-3....187
5-9 Results of DSST DC for NSSC 10299, Days 4-6....187
5-10 Results of the GP4 DC for NSSC 10299, Days 4-6....190
5-11 Results of HANDE DC for NSSC 10299, Days 4-6....199
5-12 Initial Parameter of Geosynchronous Orbit for PCE....208
5-13 DP4 Geosynchronous PCE Results....210
5-14 Force Model Used in the DSST "truth" Model for the Geosynchronous (ANIK D2) Case....213
5-15 Initial Parameters of ANIK D2 Reference Orbit....213
5-16 Results of DSST DC for Merged Telesat Data....216
5-17 Results of DP4 DC for Merged Telesat Data....219
5-18 Comparison of DP4 Theory with Converged DSST (D2)....219
5-19 Results of "Modified" DP4 DC for Merged Telesat Data....227
5-20 Comparison of "Modified" DP4 Theory with Converged DSST (D2)....228
6-1 Summary of Real Data Low Altitude Results....237
6-2 Summary of Real Data Geosynchronous Results....237

Chapter 1

INTRODUCTION

1.1 Motivation

Today there is a need to cooperate among all astrodynamic, mathematical, and computer software professionals. As a nation, the United States lagged behind the Soviet space program from the launch of Sputnik until we put men on the moon. On July 20th, 1969, The United States of America became the leader in space. What has happened to this position of leadership?

According to the following quotes from an article in TIME magazine, 5 October, 1987, the Soviets have overtaken our leadership role. Says Genevie've Debouzy, of the French space agency: "The seminars that ten years ago would have been given at the Goddard Space Flight Center are now given in Moscow." Says Heinz Hermann Koelle, a West German space-technology professor and former director of future projects at NASA's Marshall Space Flight Center: "American pre-eminence in space simply no longer exists." These comments are well supported by the Soviets' present and upcoming space developments.

The USSR's most notable development is their successful launch of Energia, a booster with a 100 ton payload capability. This exceeds our shuttle capability which has a maximum thirty-four ton capability [1]. The United States will not have a counterpart to

Energia until 1993 at the earliest, since we have abandoned the Saturn V program [2].

Although the Soviets do not have, as of now, an operational space shuttle, there are space experts who think that the USSR could launch a shuttle within the next twelve months. In 1983, after the splashdown of Cosmos 1445, the U.S. Department of Defense announced that the Soviets were pursuing a two-pronged program that included a Columbia-sized shuttle and a smaller space plane. This statement was partially substantiated when, in 1987, the USSR officially announced that they were pursuing a space shuttle program. It is of further interest to note that the Soviets have improved upon our shuttle design. They have installed a set of air-breathing jet engines which will allow cosmonauts to maneuver their vehicle during the landing phase and, if necessary, to fly to an alternate landing strip. Even though it is unclear that the USSR is actually developing a smaller space plane, Jurgen Esders, a West German member of the European Parliament, thinks that the Soviets will launch a space plane in the near future.

Additional Soviet plans include: probes to asteroids, Venus, the Martian moons, and to the surface of Mars itself; permanently manned space stations; and colonization of both the moon and Mars. We could overlook the Soviets' present initiatives, impending developments, and plans for the future. We may speculate that the Soviet economy cannot support such an aggressive program, and that the U.S. will eventually regain its leadership role in space. But

Mikhail Gorbachev provides motivation for us to think otherwise. He gives the Soviet space program a high priority when he states, "We do not intend to slacken our efforts and lose leading positions in space exploration [2]."

Why have we fallen behind? What is different now, than during the Apollo era? It is possible that the leadership provided by scientist Roald Z. Sagdeyev, head of the Soviet Institute of Space Research (known as IKI), is responsible for their lead in almost all areas of space exploration with the notable exception in electronic technology [1]. However, another possible answer lies in the change of attitude within the U.S. aerospace community since the time of the Apollo program. This change of attitude is reflected in a quotation appearing in the Boston Globe on August 4th, 1987, from the outgoing president of Draper Laboratory, Robert Duffy, as he described earlier times at the lab, "...days where technical competence, team spirit, and partnership between sponsor and performer were viewed as the way to get tough, new, demanding jobs done [3]." Also, in our quest to fulfill President John F. Kennedy's goal, "...to put a man on the moon by the end of this decade," the aerospace community was a team. We were dedicated to a common purpose and were therefore, pursuing a higher common ground. Today, we need to regain this attitude of team cooperation. The objective of this attitude is to foster and promote an atmosphere of open-mindedness which allows all appropriate professionals to contribute. It is not an attitude which implies

incompetence nor outmoded methods, but rather an attitude which seeks to go forward and contribute to a higher common goal. It is my intention to foster this attitude among the appropriate agencies that develop and implement general perturbation theories for NORAD. We need to listen to new ideas, new information, and better ways of doing business; and then we must exploit these new technologies with vigor. It is with this attitude that I pursue this thesis.

The specific objective of this thesis is to describe the analysis, software development, and testing necessary to incorporate the NORAD SGP, GP4/DP4 and HANDE general perturbation theories into the Draper Laboratory modified Goddard Trajectory Determination System (GTDS) orbit computation program. The resulting software capability will provide a unique environment for comparing the NORAD GP theories with conventional Special Perturbations and with the comprehensive Semianalytical Satellite Theory previously developed at Draper Laboratory.

1.2 Need for an Independent Analysis

There are at least five major factors which influence the performance of an orbit determination system. According to a 1976 memo for record, written by Dr. H. B. Wackernagel, then, of the Space

Computation Center (SCC[1]) Development Division, four of these factors include [34]:

1. The completeness and mathematical rigor of the perturbation theory.

2. The models used to approximate the physical world including geopotential and atmospheric density. This factor also includes the mathematical models of the tracking data and the tracking data error statistics assumed in the orbit determination data processing.

3. The observational data, in terms of the intrinsic quality, as well as their distribution in time and space, and their quantity.

4. The available computing hardware, in terms of precision, quality, and storage capability.

The fifth significant factor is the total number of objects which must be supported by the available tracking sensors and computing hardware. The following paragraphs take a critical look at each of these factors as they apply to NORAD's orbit determination system.

NORAD uses both general perturbation (GP) and special perturbation (SP) theories. (See Appendix A for an overview of general and special perturbation methods.) The vast majority of

---

1 The SCC is now the Space Surveillance Center [SSC] [4].

NORAD's tasking utilizes GP theories, and therefore, this discussion will focus on those GP theories. (See Section 2.1 for a detailed review of NORAD's GP theories.) The most current low altitude model is the Cranford (1970) GP4 theory. NORAD defines low altitude, or near-earth objects as those having a period less than 225 minutes and high altitude or deep space, as those objects having periods greater than or equal to 225 minutes [5]. This theory incorporates the J_2, J_3 and J_4 [5] zonal harmonics coupled with certain second order secular terms of the geopotential [6]. The atmospheric density is represented by a power density function [7]. The most current deep space GP theory is the Hujsak and Hoots (1977) DP4 theory. This theory is an extension of the GP4 theory with a more sophisticated gravitational model which includes additional first order lunar and solar terms. The DP4 theory also includes twelve hour high eccentricity and twenty-four hour tesseral and sectoral resonance terms. Although sections 2.1.2 and 2.1.3 present a detailed synopsis of GP4 and DP4 capabilities, a critical look at the limitations of these theories can provide insight for potential improvements.

A major drawback of both of these theories is the lack of flexibility within their computer code [8]. In other words, if you want to incorporate additional geopotential effects, or perhaps new atmospheric effects, both GP4 and DP4 would require extensive modifications. This point is clearly supported by the fact that it has taken approximately fifteen to twenty years since GP4 and DP4

became operational, to introduce NORAD's new HANDE model which is planned to be operational in the early 1990's [9].

Another limitation of both of these theories is that they are tailored to specific classes of orbits [8]. Although these classes may encompass many objects of concern, there is a significant loss in accuracy when looking at other classes of orbits. (See section 2.1.2 for a detailed example.) This limitation is primarily due to the gravitational effects which the NORAD GP theories neglect. These include [8]:

1. The m-daily effects due to non-resonant tesseral harmonics.

2. The short-periodic effects due to: low degree and order tesseral harmonics; and lunar-solar point mass perturbations.

3. The long-periodic and secular effects due to higher order zonals, resonant tesseral harmonics, and higher order lunar-solar terms.

It is important to both understand what these effects are, and the significance of neglecting these effects. To gain an understanding of these concepts, I will present a brief synopsis of a 1978 memorandum written by Dr. Paul Cefola, to W. G. Denhard, then,

Department Head of Air Force Programs at Draper Laboratory. The synopsis begins with Kaula's potential [10]:

$$U = \frac{\mu}{a} \sum_{l=2}^{N} \left(\frac{R_e}{a}\right)^l \sum_{m=0}^{l} \sum_{p=0}^{l} F_{lpq}(i) \sum_{q=-\infty}^{\infty} G_{lpq}(e)\, S_{lmpq}\,(\omega, M, \Omega, \theta) \qquad (1.1)$$

where: $a, e, i, \omega, \Omega, M$ = classical orbital elements

and

$G_{lpq}(e)$ = polynomials in the eccentricity

$F_{lmp}(i)$ = polynomials in the cosine of the orbital inclination

θ = Greenwich hour angle

and

$$S_{lmpq} = \begin{bmatrix} C_{lm} & \text{for} & (l-m) \text{ even} \\ -S_{lm} & \text{for} & (l-m) \text{ odd} \end{bmatrix} \cos\left[(l-2p)\omega + (l-2p+q)M + (\Omega-\theta)m\right]$$

$$+ \begin{bmatrix} S_{lm} & \text{for} & (l-m) \text{ even} \\ C_{lm} & \text{for} & (l-m) \text{ odd} \end{bmatrix} \sin\left[(l-2p)\omega + (l-2p+q)M + (\Omega-\theta)m\right] \qquad (1.2)$$

The zonal harmonics, $J_2, J_3, \ldots$ commonly appearing in the NORAD GP theories correspond to the $(C, S)_{lm}$ in equation (1.2) as follows:

$$J_2 = -C_{2,0}, \quad J_3 = -C_{3,0}, \text{ etc.}$$

The m-daily effects due to non-resonant tesseral harmonics occur when the following conditions are met in equation (1.1):

$$m \neq 0, \qquad (l - 2p + q) = 0 \qquad \text{and,}$$

$$(l - 2p)\,\dot{\omega} + (l - 2p + q)\,\dot{M} + (\dot{\Omega} - \dot{\theta})\,m \neq 0 \qquad (1.3)$$

When equation (1.3) is substituted into equation (1.2), the resulting argument of the trigonometric terms is: $(l - 2p)\,\omega + m\,(\Omega - \theta)$. Thus, the Greenwich hour angle, θ, is the fastest variable for this subset of the S_{lmpq} terms. The name, 'm daily,' comes from the fact that these terms repeat m times per day. Cefola references the following table[2] of periodic errors, (See Table 1-1) or m-daily effects for low altitude orbits, which he confirmed as part of a research project at MIT in 1979. The significance of neglecting these m-daily terms in a batch least squares orbit determination process is that the observation span must be at least several times the neglected period in order to obtain an accurate solution. Thus, the truncation of the satellite theory can limit the ability of the orbit determination process to generate an accurate orbit prediction from a short arc of observation data.

---

2 This table was originally generated by Dr. Hunt Small at Lockheed Missiles and Space Company.

Table 1-1. Maximum m-daily Errors (meters)

Harmonic	Radial	Cross-Track	In-Track
J_{22}	---	260	790
J_{31}	300	---	600
J_{32}	65	---	130
J_{33}	75	---	150
J_{41}	---	225	590
J_{42}	---	90	270
J_{43}	---	75	210
J_{44}	---	40	100

Geopotential tesseral short-periodics occur when the following conditions are met in equation (1.1):

$$m \neq 0, \qquad (l - 2p + q) \neq 0 \qquad \text{and,}$$

$$(l - 2p)\,\dot{\omega} + (l - 2p + q)\dot{M} + (\dot{\Omega} - \dot{\theta})\,m \neq 0 \qquad (1.4)$$

With this combination of indices, the argument of the trigonometric terms in equation (1.2) becomes a linear combination of the satellite

mean anomaly and the Greenwich Hour Angle. The Harmonic Analysis Program [11] results suggest errors from neglecting these terms in the 100-200 meter range for tesseral harmonics of degree and order up to three for low altitude orbits [12]. This analysis is further supported by the work of Kaniecki (1979) [13] and Proulx, et al [14]. The impact of neglecting the tesseral short-periodics is less severe than neglecting the tesseral m-dailies. This is due to generally higher frequencies and smaller magnitudes associated with the tesseral short-periodics.

The lunar-solar short-periodics are important for high altitude orbits. For example, the lunar-solar short-periodics include the dominant short periodic motion in the semimajor axis for the geosynchronous equatorial orbits.

Long-periodic and secular (zonal) terms result when m = 0, and (l-2p+q) = 0 in equation (1.1). Therefore, these terms have no dependence on either the satellite mean anomaly or the Greenwich Hour Angle. Zeis investigates the effects of neglecting odd zonal harmonics $J_5 - J_9$, for medium altitude orbits near the critical inclination (which is $\cong 63.43$ degrees) and shows that the eccentricity errors are quite significant without these harmonics [15]. Also, Mueller [16] shows that neglecting the long-periodic and secular zonal terms with degree greater than five (Mueller's case was J_6 through J_{18}) may cause positional errors on the order of 500 to 1000 meters after just ten revolutions of a sixteen revolutions/day satellite.

Tesseral resonance terms result when the following conditions are met in equation (1.1):

$$m \neq 0 \qquad \text{and} \qquad (l - 2p)\,\dot{\omega} + (l - 2p + q)\dot{M} + (\dot{\Omega} - \dot{\theta})\,m \cong 0 \qquad (1.5)$$

This condition occurs when the satellite mean motion is some multiple of the Earth's rotation rate. This is exactly the case for such important orbits as the twelve hour, high eccentricity Molniya orbit and the synchronous equatorial orbit.

Higher order long period lunar-solar terms are likely to have a noticeable impact at geosynchronous and higher altitudes.

In summary, the current NORAD GP theories obviously can be improved. In all fairness it should be noted that the driving force behind the SGP (1966), GP4 (1970) and DP4 (1977) theory developments was processing efficiency. Run time was minimized to allow processing of more element sets at more frequent time intervals. Additionally, an assumption was made that by minimizing run time, there would be more CPU time available for more frequent element set update. Perhaps this assumption is not necessarily correct. By improving the current prediction capabilities of the NORAD GP theories, the required tasking frequency may actually decrease. The question remains as to what price would have to be paid to make such improvements. For example, there would be value in determining how much more computational run time one would

incur for a corresponding change to improve a theory's accuracy. It would also be worthwhile to investigate an alternative theory which would incorporate desired improvements and be capable of adopting upcoming changes.

The second factor to examine in the overall orbit determination system is the physical models used to approximate the real world. The following development will look at both the geopotential models and atmospheric density models which NORAD uses, and other models which are available in the aerospace community.

According to NORAD's 1982 SCC Mathematical Foundation Text [17], the SCC has four available geopotential models. Briefly, these models include: a World Geodetic System (WGS) 72 geopotential model truncated to the eighth order and degree, the Naval Weapons Laboratory (NWL)-8C twelfth order zonal and nonzonals as derived by Kozai, a sixteenth order model (unspecified), and the Goddard Earth Model GEM 2 coefficients (1972) [17].

Since the preparation of the SCC specifications, the development of geopotential models has continued. As of September 1982, accuracy tests on the most recent GEM gravity models for the representation of the Earth's gravity field, showed that there was steady improvement in these models with time [18]. The accuracy of determining the spherical harmonic coefficients of the Earth's gravitational field was as follows: 100% accuracy for n = (2-6), 90-

99% for n = (7-10,) 55-80% for n = (11-14), and less than 50% for n greater than 15 [18]. Some of these GEM models are based solely on satellite observational data. For example, the GEM9 (1978) gravity model is based on optical, laser and electronic observations taken on thirty-one satellites [19]. Other gravity models combine satellite observation data with surface gravimetry. The GEM10B (1978) is a gravitational model complete to degree and order thirty-six, and is based on camera, laser and radio-frequency tracking data from thirty satellites; and surface gravity measurements, in the form of 1654 five degree by five degree mean gravity anomalies and 1000 GEOS-3 altimetry passes [20]. Furthermore, a new gravity model GEM-L2 (1985), uses a combination of GEM9 data and extremely accurate, two to five centimeter precision, laser ranging from NASA's laser Geodynamics Satellite LAGEOS. The use of the GEM-L2 model yields smaller LAGEOS positioning errors. Specifically, using the GEM9 model would yield one meter errors, but the use of GEM-L2 decreases the errors to approximately twenty-five centimeters [21]. There also exists other experimental GEM models, such as the GEM10C, which is complete to degree and order 180 [20]. Of these models, GEM 10B is considered desirable for low altitude cases and GEM-L2 is desirable for the high altitude orbits [22].

The WGS 72 model was the result of a major DOD effort that included five years of data collection within the DOD and scientific community [23]. The model includes twenty-fourth degree and order geopotential harmonics, Doppler and optical satellite observations,

surface gravity data, and astrogeodetic data available through 1972 [23]. Since the 1972 effort, a new WGS model has been under development. This model is an improved DOD model and is designated as the WGS 84 model. Table 1-2 presents a summary of differences between WGS 72 and WGS 84 ellipsoid parameters.

Table 1-2. WGS 72 and WGS 84 Ellipsoid Parameters

ELLIPSOID PARAMETERS	NOTATION	WGS 72	WGS 84	DIFFERENCE*
SEMIMAJOR AXIS	a	6378135 m	6378137 m	2 m
FLATTENING	f	1/298.26	1/298.257223563	0.3121057×10^{-7}
ANGULAR VELOCITY	ω	$7292115.147 \times 10^{-11}$ rad s^{-1}	7292115×10^{-11} rad s^{-1}	-0.147×10^{-11} rad s^{-1}
SECOND DEGREE ZONAL	$\bar{C}_{2,0}$	-484.1605×10^{-6}	$-484.16685 \times 10^{-6}$	-0.00635×10^{-6}
GRAVITATIONAL CONSTANT (MASS OF EARTH'S ATMOSPHERE INCLUDED)	GM	3986008×10^{8} m^3 s^{-2}	3986005×10^{8} m^3 s^{-2}	-3×10^{8} m^3 s^{-2}
GRAVITATIONAL CONSTANT (WITHOUT MASS OF EARTH'S ATMOSPHERE)	GM '	3986005×10^{8} m^3 s^{-2}	3986001.5×10^{8} m^3 s^{-2}	-3.5×10^{8} m^3 s^{-2}

*WGS 84 MINUS WGS 72

Future developments could significantly enhance all of the geopotential models. In the 1990's the U.S. Geopotential Research Mission (GRM), which includes two satellites in a 160 kilometer

circular polar orbit, may provide a dramatic breakthrough in gravity field modeling [20].

Although all of these advances in geopotential study may not be applicable nor useable in NORAD's operations, it may be prudent to investigate what information can be of use. Of course it would be necessary to evaluate cost tradeoffs in terms such as computational complexity versus increased accuracy as well as the overall impact on operations.

The current atmospheric density model of GP4 and DP4 is based on the work of Lane (1965) and assumes a static, nonrotating, spherically symmetrical atmosphere that is modeled with a power density function. (See section 2.1.2 for details.) NORAD's proposed HANDE model makes a significant improvement to the density model, by incorporating a dynamic atmosphere, as defined by Hoots and France (1987). (See section 2.1.4 for details.) It appears that HANDE will be able to incorporate future atmospheric developments. This is significant because the 1986 Presidential Commission on Space anticipates, as a result of our upcoming space station, projected for 1994, that solar studies will reveal more complete information on the solar cycle and solar flares [24] which will significantly impact the potential accuracy of perturbation theories.

The third factor which plays a crucial role in the orbit determination system is the observational data. Observational data availability and accuracy has been enhanced by the recent NORAD

Space Sensor Network updates: Cobra Dane and Pave Paws Phased Array Radars, and the Ground-based Electro-Optical Deep-Space Surveillance (GEODSS) system [25]. Also, since 1976, the deep space radars, specifically, Millstone Hill Radar and Altair have been upgraded [26]. Today, the sensors of the NORAD Space Sensor Network[3] include the following [17]:

1. The Navy Space Surveillance System (SPASUR)

   This system includes nine field stations within the continental United States, specifically: three transmitter sites, two high-altitude receivers, and four low-altitude receivers.

2. The Air Force SPACETRACK

   This system consists of numerous radars, Baker-Nunn cameras, and a Ground-based Electro-Optical Deep Space Surveillance (GEODSS) system. Specific radar types include: Cobra Dane and Pave Paws phased array radars, detection radar fans, tracking radars, and a Perimeter Acquisition Radar (PAR) from the cancelled Safeguard ABM system.

3. Co-Operating Sensors

   These sensors include: the Eastern Test Range tracking radars, Smithsonian Astrophysics Observatory Baker-Nunn cameras,

---

3 The NORAD Space Sensor Network was formerly the Space Detection and Tracking System (SPADATS) [4].

Space and Missile Test Center tracking radars, and the Pacific Missile Range tracking radars.

4. Other Sensors

This group is comprised of: Over the Horizon (OTH) tracking radars; the USAF Satellite Control Facility; NASA tracking networks and the Worldwide Satellite Observation Network; other tracking radars; and electro-optical sensor sites [27].

The location of each Network component is listed in references [4] and [27].

The fourth factor to evaluate in the NORAD system is computer hardware. Presently, the SSC operates on the Honeywell 6080 computer. According to Lt Col Sundberg, Headquarters (HQ) Air Force Space Command (AFSPACECOM), the SSC may upgrade to the IBM 3083 in the 1990's [28]. Ford Aerospace Corporation personnel, who are presently writing the new SPADOC 4B computer code use the IBM 3083 computer. Their software is compatible with the CSDL IBM 3090 computer. This potential upgrade of computer hardware is significant because of the increased processing capability of the IBM 3083 versus the Honeywell 6080. This hardware will provide more available CPU time with improvements to the existing GP theories.

The final factor, and perhaps most difficult to control, is the total number of objects which NORAD must track. NORAD is responsible for both maintaining general perturbation element sets

on all man-made space objects, and special perturbation element sets on specified support missions. For the purposes of tasking support, all missions are assigned to one of the following areas: catalog maintenance, deep space or special missions. Catalog maintenance is the routine task of maintaining general perturbation element sets on all satellites in earth orbit [17]. This is not a trivial matter, because as of 13 August, 1987, NORAD was maintaining a catalog of over 7000 objects [29]. Furthermore, NORAD has stated in their Space Computation Center, SCC, mathematical foundation reference text, "The catalog of satellites has grown too large to continue using the early operational concept of allowing all sensors to observe all satellites. The finite capabilities of the SPADATS (now, the NORAD Space Sensor Network) sensor system must now be used in a systematic and coordinated manner to insure that the large number of satellites are all observed at a frequency adequate to support orbit element maintenance. Satellites will become lost if not enough observations are obtained or, if too many observations are collected, the computer center becomes saturated [17]." Deep space missions are simply those missions associated with satellites having apogees greater than 3000 nautical miles but still requiring GP element sets. Special missions include: new launches, maneuvers, breakups, and other special activities. Typically, these missions require a much greater number of observations due to the requirement to generate special perturbation element sets [17].

Due to the extremely large number of catalogued satellites, relative to the special missions, the key issues are catalog maintenance and deep space missions. Specifically, according to Lt Col Eric Sundberg, "With 7000 objects our system is close to being fully loaded in terms of available sensor resources and data processing capacity in Cheyenne Moutain. This problem will become critical in the near future because there is a reasonable probability the catalog will have to double or triple in size within the next few years [29]." This concern is further developed in a paper entitled, "The SMART Catalog," which was presented at the AAIA/AAS Astrodynamics Specialist Conference, Kalispell, Montana, 10-13 August, 1987, by Major David Cooke, also of HQ AFSPACECOM. In this paper he states that the USAF Space Command is exploring a new concept called the SMART Catalog, which is designed to improve satellite tracking efficiency and expand the current catalog to include very small debris, on the order of a few centimeters, or less. The concern over very small debris was highlighted on space shuttle flight STS-7, where a 0.2 mm fleck of aluminum oxide paint made a small crater in the orbiter's window. The magnitude of the space debris problem has increased tremendously due to four major satellite breakups which have occurred since September 1985. There were two planned low altitude breakups and two unintentional breakups at high altitude. The two planned breakups were the Solwind ASAT experiment and the Delta 180 Strategic Defense Initiative (SDI) experiment [30]. The Solwind ASAT experiment was actually the elimination of Air Force satellite P78-1. An F-15

fighter plane launched a miniature homing vehicle [25] to destroy the satellite which was in a low, (514 - 541 kilometer), polar orbit [31]. The SDI Delta 180 experiment was a space intercept and collision test between the second and third Delta stages that made head-on contact at a closing speed of 1.8 miles per second. The experiment created two satellite debris clouds that passed through each other and entered into orbits which centered on the original orbits of the two stages [32]. Both of these breakups have almost entirely reentered due to their relatively low altitude. However, the main pressure vessel breakup of the French Ariane rocket body, and the spontaneous booster failure of the Soviet Cosmos 1813 satellite, have created orbiting debris clouds that will remain in orbit for years to come since both of these bodies are at much higher altitudes. The impact of this additional debris has been to increase NORAD's Average Daily Observations (OBS) from thirty to forty thousand, to over 60,000 [30].

The upcoming Stategic Defense Initiative (SDI) program may further challenge NORAD's present capabilities. SDI is a multilayered, multitechnology approach to ballistic missile defense (BMD) which shows the promise of achieving the capability to intercept a high percentage of offensive nuclear weapons after they have been launched at the U. S. This approach includes attacks

against ballistic missiles in each phase of their flight with weapons that destroy these missiles using various technologies [33]. As a component of this BMD, SDI could require hundreds of orbiting surveillance and weapons platforms. NORAD is the only organization with any experience in maintaining the orbital elements of large numbers of space objects and it is natural to expect that deployment of SDI will result in more strain on NORAD's capabilities.

The overall impact of the increased number of objects tracked by NORAD will test NORAD's present and near future capabilities in terms of: sensor tracking requirements, orbit determination accuracy, computational run time, and computer storage requirements. Since this increase in objects is essentially a given parameter, attention must therefore focus on the other factors for possible improvements to NORAD's orbit determination system. Dr. Wackernagel summarizes the criterion for selecting the proper focus. He states that normally one of the factors which influence the performance of an orbit representation module is dominant (least accurate), and therefore determines the overall performance of the module [34]. With this perspective in mind, and after taking a critical look at these factors, it appears that NORAD has made or planned for significant improvements in the quality and quantity of observational data, computer hardware capabilities, and the proposed dynamic atmosphere within the HANDE model. However, it seems that improvements can be made in the area of understanding the limitations associated with the GP theories themselves. In light

of these considerations and impending future developments, it would seem prudent to accomplish an independent analysis of NORAD's GP theories to both verify present capabilities and examine possible improvements to these theories. This analysis should provide the tools, resources, and data needed to evaluate applicable tradeoffs.

1.3 Overview of Thesis

The overall objective of this thesis is to accurately incorporate the SGP, GP4/DP4, and HANDE general perturbation theories into the Draper Laboratory modified Goddard Trajectory Determination System (GTDS) orbit computation program. Additionally, this thesis will analyze both low altitude and geosynchronous test cases in order to provide examples of each theory's orbit determination accuracy. Furthermore, this incorporation of GP theories into the GTDS program will allow for rigorous comparison with both the GTDS Cowell-based special perturbation theory (SP) and the Draper Semianalytical Satellite Theory (DSST). Such a comparison is not presently possible within a single existing computer program with consistent force models and coordinate systems. A comparison with DSST is of special interest because the DSST is [8]:

1. Highly flexible, and easy to modify at the time of application.

2. Computationally more efficient than SP theories.

3. Almost as accurate as SP theories.

4. A possible alternative to GP theories.

5. A possible supplement to the present NORAD GP theories.

Chapter Two provides a review of both NORAD GP theories and GTDS capabilities including the DSST. Additionally, this chapter explains the technical differences between the NORAD and GTDS coordinate frames.

Chapter Three is a detailed description of the actual incorporation effort. The overall design approach is to incorporate the NORAD GP computer code into the existing GTDS ephemeris generation architecture. This architecture includes: a one time initialization, an initialization which is dependent upon the epoch orbital element values, and output at a request time. Eleven interface subroutines were created, thirty-two GTDS subroutines were modified and four SPADOC subroutines, aside from the SPADOC error and minor utility routines, were modified to complete this incorporation. In addition, forty-seven SPADOC subroutines and block datas were compiled without modifications and linked with GTDS. In order to establish accurate benchmark test runs and create a credible analysis capability, an intentional effort was made to minimize modifications to the NORAD-based software. Chapter Three follows the standard software documentation outline: inputs,

processing, and outputs. Within the discussion of processing, the functions are presented in the order that they would occur in a GP differential correction run.

Chapter Four presents orbit generator cases for each GP theory. The first three sections of this chapter compare orbit generator test cases, supplied from both NORAD and Ford Aerospace Corporation, to the results generated by the incorporated orbit generators. The results of these comparisons provide strong confidence in the accuracy of this incorporation. Additionally, Chapter Four analyzes the partial derivatives in the state transition matrix. A single-sided finite differencing technique is used to establish confidence in the accuracy of the partial derivative incorporation.

Chapter Five presents differential correction test cases for both geosynchronous and low altitude cases. The analyses incorporate both simulated and real data. Actual NORAD tracking data is used for the low altitude NSSC 10299 satellite; both owner/operator supplied precision ranging data and NORAD tracking data are used for the geosynchronous TELESAT ANIK D2 satellite.

Chapter Six summarizes the newly developed analysis capability and test case results. This chapter also presents conclusions and ideas for future research and analysis.

Appendix A provides an overview of general and special perturbation methods as well as the advantages and disadvantages of each of those methods.

Appendix B presents the mathematical equations of the SPADOC subroutine G2MEOE by theory type. The G2MEOE subroutine calculates partial derivative terms, including the state transition matrix. Within this subroutine, each NORAD theory type yields slightly different expressions for some of the elements of the state transition matrix.

Appendix C is a discussion of a mathematical comparison of the GTDS B_2 matrix equations and the corresponding SGP theory partial derivative equations as derived in Appendix B. This comparison highlights the fact that the SGP theory equations, with the exception of those terms which are dependent on the derivative of the mean longitude at epoch, match precisely the GTDS B_2 matrix equations.

Appendix D provides some background on finite differencing theory. This appendix supports Chapter Four.

Appendix E is a review of the generalized method of averaging. This method is an integral part of the DSST, as well as NORAD's DP4 and HANDE theories.

Appendix F presents user guide data: revisions and additions to the GTDS Keyword Cards and a sample input deck for HANDE and DP4 differential correction runs.

Chapter 2

BACKGROUND

The NORAD GP theories consist of a conglomeration of efforts and modifications which have occurred over the last twenty to twenty-five years. As a result of this development it is of the utmost importance to identify element sets or states by their respective theory type. This critical point is alluded to by Felix R. Hoots and Ronald L. Roehrich in their opening paragraph to Spacetrack Report Number Three, "...one must be careful to use a prediction method which is compatible with the way in which the elements were generated [5]." A further distinction to be aware of is NORAD's use of a unique coordinate frame. Additionally, the definition of the term "mean", will vary with each NORAD theory type and with the GTDS program. One can draw conclusions and do analyses only with these points in mind. This chapter will explain these inherent differences with a thorough review of NORAD's GP theories, the GTDS program at Draper Laboratory (CSDL), and the appropriate coordinate frames.

2.1 NORAD General Perturbation Theories

NORAD presently uses three GP theories to update the space catalog: SGP, GP4, and DP4. In the early 1990's, Space Command

plans to convert to a new, improved and more accurate ephemeris prediction model called HANDE [9]. Presently, Ford Aerospace Corporation (FACC), Colorado Springs, Colorado, is developing Space Defense Operations Center (SPADOC) 4B Fortran source code for all of these general perturbation theories for the USAF Electronic Systems Division (ESD), Hanscom AFB, Massachusetts. Although code is also being written for NORAD's Semianalytical Satellite Theory (SALT), no benchmarks are as of yet available and, accordingly, NORAD's SALT theory will not be discussed.

2.1.1 SGP Satellite Theory

The Simplified General Perturbation (SGP) theory was developed by C.G. Hilton and J. R. Kuhlman (1966) and is used for near-earth satellites [5]. As a historical note, SGP is actually a truncated form of AGP, which was a more comprehensive GP theory developed in 1961 by Aeronutronic, a division of Philco-Ford Corporation, Newport Beach, California. This Aeronutronic Complete First-Order General Perturbations (AGP) theory included: first and second order secular terms, and long and short periodic expressions of first order with coefficients of second, third, and fourth zonal harmonics (J_2, J_3 and J_4). AGP was modified for use where maximum computational efficiency along with moderate prediction accuracy was needed [35]. As an example, when SGP is used to process observations, there is a computational speed advantage of

fifty to one over that of special perturbations (SP) [34]. This is due to the small number of observations included in a typical GP differential correction [36], as contrasted with the very large number of integration steps required for SP over a typical observation span. As a rule-of-thumb, SP processing requires fifty to one hundred steps per revolution. So, SP might require several thousand integration steps over a typical GP observation span [8]. This modification of AGP was called Simplified General Perturbations (SGP) and was optimized for low eccentricity and non-equatorial orbits. Specifically, the SGP perturbative terms are: the zonal harmonics J_2 and J_3, secular and long periodic terms truncated to the square of the eccentricity $O(e^2)$, and a few selected short period terms from the AGP theory [37]. The SGP theory uses a simplification of the work of Kozai (1959) for its gravitational model [6,9]. This implies, and indeed the actual Fortran code verifies that SGP uses the Kozai mean motion which is defined as [38] :

$$n = n_0 + \frac{A_2}{p^2} (n_0) (1 - \frac{3}{2} \sin^2 i) \sqrt{1 - e^2} \qquad (2.1)$$

where:
- n = Kozai mean motion
- n_0 = unperturbed mean motion
- p = semi-parameter
- i = inclination
- e = eccentricity

A_2 is taken to be of the first order of small quantities, and is equivalent to[1] $(\frac{3}{2}J_2)$.

Alternately [39];

Since

$$\dot{M}_0 = \frac{3}{2} J_2 \left(\frac{a_e}{p}\right)^2 n_0 \left(1 - \frac{3}{2} \sin^2 i\right) \sqrt{1 - e^2} \qquad (2.2)$$

Kozai mean motion = Brouwer mean motion + $\dot{M}_0$

This alternate form of equation (2.1) must be considered in the initialization of elements which come from the NORAD Historical Data System and are input into the GP4 model. This relation is particularly important to make an accurate "a" to "n" transformation in the subroutine RESSGP[2].

SGP also assumes the drag effect on mean motion to be a quadratic in time. Specifically, this drag assumption results in a cubic variation in the secular longitude with time. Furthermore, the drag effect on eccentricity is modeled in such a way that perigee height remains constant [5]. Lastly, the SGP model defines a "mean" element set as one having the gravitational perturbations removed

---

1 Note: From Brouwer (1959) [3] $-(\frac{2}{3}A_2) = -(J_2R^2)$ Where $R = 1$,

$\therefore \; A_2 = \frac{3}{2} J_2$.

2 See Chapter Three for a complete description of the subroutine RESSGP.

[40]. The actual equations used in this theory are listed in reference [5].

2.1.2 GP4 Satellite Theory

GP4 or SGP4 is a theory developed by Ken Cranford in 1970 and is used for near-earth satellites. This model is based on a simplified version of Lane's (1965) and Lane and Cranford's (1969) drag theory [6]. Lane (1965) developed the atmospheric model which assumes a static, nonrotating, spherically symmetrical atmosphere that is modeled with a power density function. Specifically, this function is:

$$\rho = \rho_0 \left(\frac{q_0 - s}{r - s} \right)^{\tau} \tag{2.4}$$

where:

ρ = density at the radial distance, r

ρ_0 = atmospheric density at the radial reference height

q_0 = a geocentric reference distance

r = radial distance to the satellite

The two parameters, τ and s are disposable parameters which appear as constants in the final integrated drag equations of motion. They are to be chosen to fit the power density function to the best available atmospheric data [7]. Lane and Cranford (1969) eliminated the small eccentricity and inclination divisor problem by developing drag equations that do not use the terms $\frac{1}{\sin I}$ or $\frac{1}{e}$ as coefficients [41]. The GP4 geopotential theory is based on a simplification of Brouwer's theory [42]. This potential includes the zonal harmonics J_2, J_3 and J_4, coupled with certain second order secular terms [6]. These higher order terms are based on the following criterion of Lane and Cranford (1969): terms contributing more than 600 meters in position error over a prediction span of at least ten days, will be retained[3] [41].

Additionally, NORAD's adaptation of Brouwer's theory shows a strong dependency on low eccentricity. The following development [12] of the NORAD modifications to Brouwer's secular variations in the mean elements within the GP4 theory, provides an insight to this low eccentricity dependency. Brouwer's formulas for the secular variations are:

l'' = "mean" mean anomaly

---

3 Of historical interest, is the fact that the GP4 theory is actually a subset of an earlier theory, AFGP4, which included the zonal harmonics J_2, J_3, J_4 and J_5 [17].

$$= \quad n_0 t \left\{ 1 + \frac{3}{2}\gamma_2 \eta(-1 + 3\theta^2) + \frac{3}{3^2}\gamma_2 \eta[-15 + 16\eta + 25\eta^2 \right.$$

$$+ \quad (30 - 96\eta - 90\eta^2)\theta^2 + (105 + 144\eta + 25\eta^2)\theta^4 \;] \qquad (2.5)$$

$$+ \quad \frac{15}{16}\gamma_4 \eta e''^2[3 - 30\theta^2 + 35\theta^4 \;] \quad + \quad I''_0 \Big\}$$

g'' = mean argument of perigee

$$= \quad n_0 t \left\{ \frac{3}{2}\gamma_2(-1 + 5\theta^2) + \frac{-3}{3^2}\gamma_2^2[-35 + 24\eta + 25\eta^2 \right.$$

$$+ \quad (90 + 192\eta - 126\eta^2)\theta^2 + (3385 + 360\eta + 45\eta^2)\theta^4 \;] \qquad (2.6)$$

$$+ \quad \frac{5}{16}\gamma_4[21 - 9\eta^2 + (-270 + 126\eta^2)\theta^2 + (385 - 189\eta^2)\theta^4] \; \} + g''_0$$

h'' = mean longitude of ascending node

$$= \quad n_0 t \left\{ -3\gamma_2\theta + \frac{3}{2}\gamma_2^2[(-5 + 12\eta + 9\eta^2)\theta + (-35 - 36\eta - 5\eta^2)\theta^3] \right.$$

$$+ \quad \frac{5}{4}\gamma_4(5 - 3\eta^2)\theta(3 - 7\theta^2) \; \} \quad + \quad h''_0 \qquad (2.7)$$

Where: $\eta = \sqrt{(1 - e''^2)}$ and $\theta = \cos I''$

$$\gamma_2 = \frac{k_2}{a''^2} \qquad \gamma_3 = \frac{A_{3,0}}{a''^3} \qquad \gamma_4 = \frac{k_4}{a''^4}$$

$$k_2 = \frac{1}{2} J_2 a_e^2 \qquad A_{3,0} = -J_3 a_e^3 \qquad k_4 = -\frac{3}{8} J_4 a_e^4$$

a_e = equatorial radius of the earth

$$\gamma'_2 = \gamma_2 \eta^{-4} \qquad \gamma'_3 = \gamma_3 \eta^{-6} \qquad \gamma'_4 = \gamma_4 \eta^{-8}$$

All single primed variables denote (secular + long periodic) terms. All double primed variables denote secular terms only.

(NOTE: In Brouwer's original equations,

n_0 = Brouwer mean motion at epoch, however; within the GP4 equations [5], Brouwer's mean motion is denoted by n''_o.

These formulas differ significantly with those of reference [40], however; the GP4 formulas can be obtained from Brouwer if:

1. Terms of $\gamma'_4 e''^2$ are set to zero.
2. Polynomials appearing in the γ'^2_2 and γ'_4 terms are evaluated with η set equal to one.

Specifically, the truncated Brouwer equations are:

$$l'' = n_0 t \left\{ 1 + \frac{3}{2}\gamma_2(-1+3\theta^2) + \frac{1}{3}\gamma_2^2[26 - 156\theta^2 + 274\theta^4] \right\} + l''_0 \quad (2.8)$$

$$g'' = n_0 t \left\{ \frac{3}{2}\gamma_2(-1+5\theta^2) - \frac{1}{3}\gamma_2^2[14 - 228\theta^2 + 790\theta^4] \right.$$

$$\left. + \frac{15}{16}\gamma_4[12 - 144\theta^2 + 196\theta^4] \right\} + g''_0 \quad (2.9)$$

$$h'' = n_0 t \left\{ -3\gamma_2\theta + \frac{3}{8}\gamma_2[16\theta - 76\theta^3] + \frac{5}{4}\gamma_4 2\theta(3 - 7\theta^2) + h''_0 \right\} \quad (2.10)$$

The accuracy of these equations depends directly upon the smallness of the orbital eccentricity. For example, if $e'' = .02$, then $e''^2 = .0004$, and $\eta = .9998$. Thus, for the typical low altitude satellite, the approximation that $\eta = 1$ is valid. However, these approximations are applied to all satellite element sets that are generated by the GP4 theory. As another example, the Soviet Molniya satellite with an eccentricity of .7, yields, $e''^2 = .49$, and η would be approximately .71. In this case, the approximations do not look quite as desirable [12]. This development has shown that GP4 produces optimum results only for low eccentricity orbits[4].

Of additional interest are the GP4 equations which are used to recover the GP4 mean motion n''_0 and semi-major axis a''_0; from the

---

[4] Comparison with Brouwer [42] indicates that the GP4 J_2 short-periodic expressions are also truncated on eccentricity.

SGP element sets which are distributed by NORAD to the user community[5] [5] :

$$a_1 = \left(\frac{k_e}{n_0^*}\right)^{\frac{2}{3}} \tag{2.11}$$

$$\delta_1 = \left(\frac{3}{2}\right)\left(\frac{k_2}{a_1^2}\right) \frac{(3 - \cos^2 i_0 - 1)}{(1 - e_0^2)^{\frac{3}{2}}} \tag{2.12}$$

$$a_0^* = a_1 \left(1 - (\frac{1}{3})\, \delta_1 - \delta_1^2 - (\frac{134}{81})\, \delta_1^3\right) \tag{2.13}$$

$$\delta_0 = \left(\frac{3}{2}\right)\left(\frac{k_2}{a_0^2}\right) \frac{(3 \cos^2 i_0 - 1)}{(1 - e_0^2)^{\frac{3}{2}}} \tag{2.14}$$

Finally[6], $$n''_0 = \frac{n_0^*}{1 + \delta_0} \quad \text{and} \tag{2.15}$$

$$a''_0 = \frac{a_0^*}{1 - \delta_0} \tag{2.16}$$

Where: $k_e = \sqrt{GM}$ and G = Newton's gravitational constant

M = mass of the earth

---

5 In equations (2.11 through 2.14) a * denotes an SGP element.

6 Equations (2.15) and (2.16) are of the Brouwer form, i.e., short and long periodics are removed [41].

The relations just presented are very important because the SGP "a" to "n" conversion algorithm, given in Spacetrack Report #5 [43], is not the same algorithm used in the SPADOC subroutine SGPINT.

2.1.3 DP4 Satellite Theory

DP4 or SDP4 is an extension of the GP4 theory and is used for deep space satellites [5]. This theory was developed by Mr. Richard S. Hujsak (1977) [44, 45]. DP4 incorporates all of the geopotential and most of the drag representation of GP4. Additionally, doubly-averaged, first order, lunar and solar gravitational terms are added to the geopotential and drag effects [17]. DP4 also accounts for tesseral and sectoral resonances for twelve hour high eccentricity and twenty-four hour period near circular orbits [45]. A complete listing of the DP4 equations is available in reference [44]. The following synopsis of that paper will provide some insight with regard to these additional gravitational effects.

First, it is important to note that Hujsak utilizes the generalized method of averaging in his development of the deep space equations. The objective of the generalized method of averaging is to eliminate fast variables, or high frequency components from the equations of motion[7] [46]. This elimination is

---

[7] Note: Any function containing a fast variable will contribute short periodics to its system [47].

desirable because the maximum step size which can be used in the integration of a set of differential equations is constrained by the highest frequency within those equations. The resulting averaged equations of motion can be integrated numerically or analytically with a much greater step size than with the original equations [44, 48]. (See Appendix E for a more complete review of the generalized method of averaging.)

Hujsak's paper analyzes two problems. The first problem is the four body: moon, sun, oblate Earth and satellite problem. The second is a resonance analysis of twelve hour and twenty-four hour period orbits. Throughout the entire development, the first order harmonic J_2, and the second order harmonics, J_3 and J_4, are included in the Earth's geopotential. In the four body oblate earth problem Hujsak applies three transformations to eliminate fast variables and obtain an analytic solution.

In the first transformation, the dynamical system is a function of two fast variables, mean anomaly, M, and Greenwich sidereal time, θ. These variables satisfy the conditions for the application of the method of averaging. (See Appendix E for a discussion of these conditions.) This transformation averages the potential, R, for the four body oblate earth problem. Where[8]:

$$R = R_Z + R_V + R_L + R_S \tag{2.17}$$

---

8 The DP4 theory considers all perturbations as being uncoupled.

R_z = zonal potential (truncated after J_4)

R_v = tesseral harmonics

R_L = lunar potential

R_s = solar potential and,

averaging, "< >," is defined as:

$$\langle g \rangle_x = \frac{1}{2\pi} \int_0^{2\pi} (g) dx \tag{2.18}$$

At this point, the singly averaged potential, $\langle R \rangle_{M,\theta}$ is transformed twice more to remove the mean anomaly of the moon, γ_L, and the mean anomaly of the sun, γ_S. The resulting triply transformed four body oblate Earth dynamical system is solely a function of variables which vary slowly with time. The solution of this non-resonant system is obtained through analytical integration.

The resonance analysis investigates both twelve and twenty-four hour period orbits. The resonance condition exists when $\dot{M} \cong 2\dot{\theta}$, or $\dot{M} \cong \dot{\theta}$. Again, the dynamical system is a function of two fast variables, M and θ, however; this system does not satisfy the conditions for using the method of averaging. Therefore, Hujsak introduces two new variables, λ_1 and λ_2, which results in a new dynamical system that is a function of one fast variable, θ, and is in a form which satisfies the conditions to apply the method of averaging. This change of variable is dependent upon the resonance conditions. Specifically:

when $\dot{M} \cong 2\dot{\theta}$, $\lambda_1 = M - 2(\Omega - \theta)$ (2.19)

when $\dot{M} \cong \dot{\theta}$, $\lambda_2 = \omega + M + \Omega - \theta$ (2.20)

As in the four body problem, Hujsak averages the potential, R, three successive times, to eliminate the fast variables, θ, γ_L, and γ_S. The final dynamical system is a function of slow variables with the exception of n and λ, which vary more rapidly. The final solutions are all obtained analytically except for the solutions of $\dot{n}$ and $\dot{\lambda}$, which are obtained by numerical integration of the resulting equations [44].

2.1.4 HANDE Satellite Theory

The HANDE model was developed by Felix R. Hoots (1983), Directorate of Astrodynamics, Space Command, Colorado Springs, Colorado, for both near earth and deep space satellites. The gravitational model includes the zonal harmonics J_2, of first order, and J_3 and J_4, of second order [49]. Additionally, HANDE includes the DP4 model for twelve hour and twenty-four hour resonances, as well as lunar and solar gravitational effects. A significant improvement within this theory is found in the drag model which includes the effects of a dynamic atmosphere [9]. Hoots and France (1987) define a dynamical atmosphere as any modern empirical

model which uses various observed solar and geopotential parameters as inputs to produce a varying atmospheric model [50]. While the HANDE theory does include a dynamic atmosphere model, it uses average values of A_p and $F_{10.7}$ throughout its intervals [50]. Therefore, HANDE does not actually model the short periodic variations in atmospheric density. Nonetheless, HANDE uses the Jacchia 1970 atmospheric tables for its dynamic atmosphere. These tables account for diurnal bulge as well as solar and geomagnetic effects. Additionally, the HANDE atmospheric drag forces account for atmospheric rotation and atmospheric oblateness [51]. For a complete list of HANDE equations, see references [49] and [50]. The most current description of the HANDE theory is the 1987 article written by Hoots and France [50]. The following discussion is a brief overview of the most significant developments within that article.

Within their paper, Hoots and France obtain an analytical solution for the motion of an artificial earth satellite under the combined influence of gravity and any dynamic atmosphere. The most significant development is the incorporation of a dynamic atmosphere, which includes dynamic variation due to solar activity, into the HANDE theory. The motivation for developing an analytical solution instead of a semianalytical solution, is that semianalytical methods solve the equations of motion by numerical integration. Therefore, an analytical method goes through an initialization section only one time, whereas a semianalytical method must reinitialize at each integration step.

The analytic theory begins with the equations of motion which include the gravitational harmonics J_2, J_3, and J_4 and drag perturbations. The drag forces incorporate the rotational velocity of the Earth. Next, the generalized method of averaging is applied to obtain a transformation of variables which eliminates the dependence on mean anomaly, the fast variable. As in DP4, Hoots and France average the gravitational and drag components of these differential equations. To do so, it is necessary to assume that drag effects, derived from a tabular atmosphere, are both continuous and periodic in the fast variable. This assumption is based upon the idea that since tabular data closely resembles analytical models, such as the exponential or power function, and since these analytical models satisfy the prerequisite conditions, so does the tabular data. The resulting integrals of the drag functions give the average drag effect over one period of mean anomaly. To facilitate the actual integration, they introduce a change of variable:

$$dM = \frac{\left(\sqrt{(1-e^2)}\right)^3}{(1+e\cos f)^2}\, df \qquad (2.21)$$

where e = eccentricity

f = true anomaly

At this point, Hoots and France choose a Gauss Legendre quadrature to evaluate the drag integrals rather than an analytical integration.

This choice is significant because the algebraic formulation is independent of the density model chosen. Therefore, the HANDE theory maintains the flexibility to select both geopotential coefficients and a density model. Furthermore, the integration can be accomplished without using series expansions and consequently is valid for any eccentricity. Lastly, the quadrature evaluation is required only during initialization. The actual Gauss-Legendre formula used is:

$$I \cong \frac{1}{2\pi} \int_{-b}^{b} g(f)df \qquad (2.22)$$

where:

b = the value of true anomaly where density has decreased by a factor of 100 from its value at perigee

The value of b is determined as follows:

$$\cos b = \frac{ae(1-e) - \Delta r}{ae(1-e) + e\,\Delta r}, \quad \text{for} \quad \Delta r < 2ae \qquad (2.23)$$

$$\cos b = -1 \quad \text{for} \quad \Delta r \geq 2ae \qquad (2.24)$$

where a = semi-major axis

e = eccentricity

$$\Delta r = q\left[A_0 + A_1 q + A_2 q^2 + A_3 q^3 + A_4 q^4 + A_5 q^5 + A_6 q^6\right] \quad (2.25)$$

and,

Δr = altitude change from perigee required for a drop in density by a factor of 100

q = perigee height above the flattened earth (km)

The A_i coefficients were obtained by a polynomial fit to the Jacchia (1970) atmospheric tables. This fit was done for 882 degrees Kelvin exospheric temperature since Slowey (1979)[52] has shown this to be the mean temperature over the entire atmosphere during an average eleven year solar cycle.

It is of further interest to note that the most dominant effects of drag and J_2 coupling can be included in the drag integrals. This is accomplished by using the osculating altitude, r', at each step in the quadrature. Where $r' = r - \delta r$, and r is the osculating geocentric radial distance, and δr is the geocentric distance to the flattened earth surface.

Given this background on how to solve the drag functions, Hoots and France provide the results of an analytical solution to the transformed differential equations of motion. This analytical solution was obtained by treating the long-period gravitational terms separately from the remaining terms. Additionally, the resulting equations contain higher order derivatives, which are

obtained using a numerical technique that involves the use of a Chebyshev min-max polynomial.

Hoots and France emphasize that the numerical differentiation, the quadrature, and the required atmospheric density values all occur during the initialization of HANDE. Predictions at later times are made with totally analytic formulas.

The article concludes with an extensive orbit analysis between HANDE, SGP and an orbit based on an eighth order Cowell numerical integrator with a one minute step size. The atmospheric model used was the Jacchia (1970) model with a constant solar flux value of 150 and a constant geomagnetic index of $A_p = 4$. The gravitational model included zonals through J_4. A comparison of eighteen test cases, representing a wide range of altitudes and orbital geometries, indicated that the HANDE model had very good accuracy with an average RMS of 40 meters over a one day fit span.

Their real data analysis analysis utilized five operational satellites and predictions were made over a twenty day span prior to their decays. Including all predictions, HANDE had an average prediction RMS (kilometers) of 49.306, SP had 53.750, and SGP had 191.047. The results presented indicated that in a real world environment HANDE provides a significant improvement over SGP and is very competitive with special perturbations. Lastly, in the prediction mode, the theory is totally analytical and requires about one thousand words of computer storage space [50].

2.2. The Goddard Trajectory Determination System

The NORAD GP theories will be hosted in the Draper Laboratory modified Goddard Trajectory Determination System (GTDS) computer program. This incorporation will not degrade the operational performance of the GTDS program within the laboratory.

2.2.1 Overall GTDS Capabilities

The Goddard Trajectory Determination System (GTDS) is a multipurpose computer system designed "...to provide operational support for individual Earth, lunar and planetary space missions and for the research and development requirements of the various projects of the NASA/Goddard Space Flight Center (GSFC) scientific community [53]." A version of GTDS is the operational orbit determination system of the NASA/GSFC, at Greenbelt, Maryland. Also, the GTDS algorithms form the basis for the operational orbit systems in the Global Positioning System Operational Control Center and the Air Force Satellite Control Facility Data System Modernization. The Charles Stark Draper Laboratory (CSDL) received an export Research and Development version of GTDS in 1978 [54]. Since that time, Draper Laboratory has modified and created additional capabilities within the GTDS framework. The current capabilities of Draper Laboratory's version of GTDS can be described in three parts. The initial capabilities, originating from NASA/GSFC

are described in the GTDS math specifications (1976). Additional capabilities are described in the GTDS Research and Development User's Guide for the Averaged Orbit Generator (1978) [55]. This document describes the capabilities which were developed at the Computer Sciences Corporation. Capabilities resulting from Draper Laboratory initiatives are described in section 2.2.3. Throughout these descriptions it is of special interest to note the inherent flexibility of the GTDS architecture.

As of 1978, GTDS was partitioned into the following programs:

1. Ephemeris Generation Program (EPHEM)

This program propagates the vehicle state and, optionally, the state partial derivatives from prescribed initial conditions over a given time span. Also, this program can selectively choose an orbital theory, ranging from a first-order analytic theory[9] to a high-precision Cowell-type numerical integration [53, 56]. The user selects the appropriate model and then inputs the following: the initial elements at epoch; coordinate system type; desired atmospheric model and; satellite area and mass parameters [57]. Furthermore, the state transition matrix can be generated by numerical integration of the variational equations or by a two-body analytic approximation. Ephemeris output is generated as the satellite state (position and velocity) referenced to an indicated

---

9 This program has the option to select from either the Brouwer or Vinti analytic theories.

central body or to specified noncentral bodies. Additionally, satellite ephemeris files can be generated for subsequent use.

2. Ephemeris Compare Program (COMPARE)

This program compares two input satellite ephemeris files. The comparison can be specified over a particular arc including an arc of overlap between the ephemerides. The radial, along-track, and cross-track errors are output in tabular form to the printer [53,56]. The unit vectors for these errors are defined as follows [57]:

Radial $$\hat{H} = \frac{\vec{r}}{|\vec{r}|} \qquad (2.26)$$

Cross-Track $$\hat{C} = \frac{\vec{r} \times \vec{v}}{|\vec{r} \times \vec{v}|} \qquad (2.27)$$

Along-Track $$\hat{L} = \frac{(\vec{r} \times \vec{v}) \times \vec{r}}{|(\vec{r} \times \vec{v}) \times \vec{r}|} \qquad (2.28)$$

Printer plots of these differences and, Keplerian and equinoctial element histories and differences can be produced.

3. Differential Correction Program (DC)

This program estimates the satellite orbit and solve-for parameters. There are two types of solve-for parameters, dynamic and local. The dynamic solve-for parameters are those which are implicit in the equations of motion, such as the drag parameter or

the gravitational harmonic coefficients. The local solve-for variables are those which are implicit in the observation models such as the tracking station locations and observation or timing biases. Within this program all parameters are determined so as to minimize (in a Bayesian weighted least-squares sense) the sum of the squares of the differences between the observed and computed tracking data. Simultaneously, the solve-for variables are constrained to satisfy a priori conditions to within a specified uncertainty. Specifically, the user must supply these a priori conditions for a given solve-for parameter at a specified epoch. Both mean and covariance matrices are determined for the estimated parameters. Optional printer plots of observation residuals can be obtained.

4. Filter Program (FILTER)

This program provides an alternative to the Differential Correction Program. This FILTER program incorporates two sequential estimation algorithms as opposed to the batch processing method used in the DC program. These two algorithms, the Linear Kalman Filter (LKF) and the Extended Kalman Filter (EKF) process each observation to recursively update the state at each observation time.

5. Early Orbit Determination Program (EARLYORB)

This program is specifically designed to calculate an initial estimate of an Earth orbit when there is no a priori estimate available to start a differential correction. This initial estimate is obtained with as few as six measurements from selected station observations.

6. Data Simulation Program (DATASIM)

This program computes a simulated observation file at a specified frequency for given sets of ground tracking sites and observation intervals. Optionally, random and bias errors can be applied to the observations. Additionally, the observations can be modified to account for the effects of atmospheric refraction, antenna mount errors, transponder delays and light time delays.

7. Error Analysis Program (ANALYSIS)

This program provides the capability to determine satellite state uncertainties about a given orbit as a function of observation data uncertainties, epoch state uncertainties, and uncertainties in other system parameters. This program has functions similar to the DC and DATASIM programs. Accordingly, they share common mathematical processing subroutines, input processors, and data management options.

8. Data Management Program (DATAMGT)

The primary function of this program is to retrieve data from the GTDS on-line data base to create temporary working files that will be used in other programs within GTDS. In performing this function the DATAMGT program operates as part of the program that will use the working files. This program can also function as a stand alone program to create working files for a future program execution. It is of interest to note that all programs within GTDS, with the exception of the COMPARE and FILERPT programs, require the use of the Data Management Program.

9. Permanent File Report Generation Program (FILERPT)

This program produces summary and/or complete printer reports of the data and models existing in the GTDS permanent data base files. A typical use of the FILERPT program is to determine which permanent file data may be appropriate for later use in another GTDS program. For example, FILERPT could be utilized to examine the Earth Potential Fields File, and then you could apply a specific geopotential model from that file [53,56].

In addition to the improvements of the Semianalytical Satellite Theory, Draper Laboratory has also created a data interface which allows GTDS to use the following tracking sources: NORAD Historical Data System, radar observations, optical observations (Fieger 1987), European Space Agency Exosat data, TELESAT (Synch-

X) and other satellite data. Also, as a result of this thesis, Draper Laboratory will have the capability to evaluate the NORAD General Perturbation Satellite Theories.

2.2.2 GTDS Cowell Special Perturbations Orbit Generator

For this thesis, the Cowell generator will be used to create highly accurate reference files to be used both as the 'truth' in both the PCE fits and real data analyses of Chapter Five. The Cowell equations of motion are expressed as follows:

$$\frac{d^2\bar{r}}{dt^2} = -\frac{\mu\bar{r}}{|\bar{r}|^3} + \bar{P} \qquad (2.29)$$

Where: $\bar{r}$ = the position vector in an inertial Cartesian coordinate system

t = time

μ = the gravitational constant

$\bar{P}$ = the total perturbing acceleration

The actual accelerations which comprise $\bar{P}$ can include all or any subset of the following options [53]:

1. Gravitational acceleration due to n-point masses.
2. Gravitational acceleration due to nonsphericity of the central body gravitational potential. (21 x 21 harmonic coefficient capability)
3. Acceleration due to the mutual nonspherical gravitational attraction of the Earth and moon.
4. Acceleration due to aerodynamic forces. (Such as drag.)
5 Acceleration due to solar radiation pressure.
6. Acceleration due to thrusting spacecraft engines.
7. Acceleration due to attitude control system corrections.
8. Model replacement acceleration. This acceleration is obtained when accelerometer data is obtained from a spacecraft. This data may be used to replace all non-potential accelerations for a given spacecraft [53].

For the purposes of this analysis, $\bar{P}$ includes the first five types of acceleration including four point masses (Earth, sun, moon and satellite), with the harmonic coefficients tailored to the specific satellite of interest.

Within GTDS there are several options to select from to numerically integrate the equations of motion. The first option is to select the type of formulation of the equations of motion. There are two basic types of formulations, Class I and Class II. The set of Cowell equations (2.29) are solved directly for the vector $\bar{r}$, using the Stormer-Cowell numerical integration formulas. This method,

which solves second order systems directly, is known as a Class II formula. Alternately, the slightly modified Cowell equations (2.30)

$$\frac{d\bar{v}}{dt} = -\frac{\mu\bar{r}}{|\bar{r}|^3} + \bar{p} \tag{2.30}$$

are solved for the velocity vector, $\bar{v}$, using the Adams numerical integration formulas. This formulation is known as a Class I formula and it is necessary for the case of velocity dependent perturbations, such as atmospheric drag.

The second option to evaluate is the type of algorithm to utilize. Although there are various algorithms to choose from, pseudo-evaluate algorithms significantly increase the stability regions of predictor-corrector schemes at little or no cost in efficiency. These algorithms are used in this analysis.

A third option to consider is the order of the process. Various order formulas may be selected for use in the algorithm, recognizing that higher order formulas are more accurate but less stable. With this point in mind, this analysis uses a twelfth order predictor-corrector.

Finally, one must consider stepsize control. Since the orbit dynamics may undergo large variations during a revolution, such as a high eccentricity orbit, an algorithm must be selected to allow stepsize variations. Therefore, efficiency dictates the use of stepsize control for moderate and high eccentricity orbits.

Furthermore, within GTDS analytic stepsize control is more efficient and reliable than numerical stepsize control [53]. Throughout this analysis, a stepsize is used which allows for at least 100 steps per orbital revolution.

2.2.3 Draper Semianalytical Satellite Theory (DSST)

One of the early reasons for developing the DSST as described by McClain [48], was to make more efficient use of computer time, specifically in terms of decreasing runtime and storage space requirements. The goal was to devise a low cost, long-term orbit prediction capability for the following applications: mission feasibility studies, mission analysis (lifetime and geometry constraints), tracking station acquisition schedules, dynamic modeling where extended data gaps are encountered, and dynamic modeling required for differential correction procedures. A look at the method of DSST provides some insight to evaluate both the computational efficiency and accuracy of DSST.

The method of DSST is a combination of the strengths of special and general perturbation methods. Perturbations that can be expressed in terms of a disturbing potential have that potential expressed in the nearly singularity-free equinoctial elements [58], as opposed to the classical Keplerian or Delaunay variables. These perturbations are then put into Lagrangian Variation of Parameters (VOP) form, so that only small perturbations from two-body motion

can be considered. Those perturbations which cannot be expressed in terms of a potential, such as solar radiation pressure and drag, are expressed in Gaussian VOP equations. The small magnitudes that these perturbing forces have allows formal application of asymptotic methods [57,59] that are based on the method of averaging. (See Appendix E for details.) This particular method of averaging removes the short-periodic content from the VOP equations of motion. This allows numerical integration of the equations of motion with much larger step sizes [48]. Then interpolators are used to produce accurate mean orbital elements for any time of interest. Reverse transformations use the mean elements at the time of interest to evaluate the short-periodic motion. Interpolation concepts are developed to make the short-periodic calculations more efficient. These short-periodic components are then added to the mean motion to obtain the total satellite osculating state. It is significant to note that having the knowledge of the mean motion allows recovery of the short-periodics and hence of the full satellite dynamics. Therefore, the averaged or mean motion may be considered an expression of the total satellite dynamics [59]. This efficient recovery of the short periodics makes DSST as accurate as Special Perturbations, but without the significant increase in computational runtime [60]. This significant observation is further supported by the efforts of Green (1979) and Wagner (1983) [59,61].

Another major advantage of DSST is its inherent flexibility. First, the equations of motion can be either singly or doubly averaged. Second, the recursive formulation for the gravitational expansions, both in the averaged equations and in the short-periodic corrections, eliminates the need for separate analytic and software development for each harmonic term [8]. Also, this formulation allows tailoring of the geopotential by selecting specific zonals, tesserals, solar radiation pressures, atmospheric drag effects, lunar-solar effects, coupling effects, or resonance effects. Additionally, DSST represents atmospheric drag as definite integrals to be evaluated by numerical quadratures. This means that the same density routines that are used in SP models can be used in DSST. Furthermore, since the quadrature process of DSST is independent of the density model, there is great freedom to upgrade the density models without tremendous analysis or developmental efforts [8]. The overall impact of DSST's flexibility is a resulting increase in efficiency and a minimization of computer runtime. In short, force models and other physical models can be tailored to meet specific accuracy requirements with a resulting net savings in computational costs.

Since 1978, Draper Laboratory has significantly enhanced the original export version of the Semianalytical Satellite Theory and their GTDS program. These improvements are the result of the combined efforts of the CSDL Space Systems Analysis section and MIT graduate students under the guidance and leadership of Dr. Paul

J. Cefola. These enhancements encompass three general areas: mean element orbit determination, short-periodic variations and sequential and batch estimation.

There have been numerous improvements to mean orbit generation capabilities which include the following [62]:

1. Development of a J_2 squared model which uses explicit formulas constructed with the MACSYMA symbolic algebra system. These formulas include terms proportional to the zero-th and first powers of the eccentricity [15,63].
2. Development of a tesseral resonance model which is based on the recursive formulation of the averaged disturbing potential and its associated partial derivatives [64]. This model allows for a large number of resonant coefficients. The model employs the high eccentricity Hansen coefficient formulation [65] and two files of modified Newcomb operators. (One file is used for low to moderate eccentricity cases and one file for high eccentricity cases.)
3. Development of a recursive double averaged third-body point mass model that is applicable to high altitude orbits over long time intervals [66].
4. Development of second order averaging methods for the J_2/ drag problem [61].
5. Development of a semianalytical approach to the state transition matrix [61].

6. Development of a mean element interpolation concept coupled to the single step integrators of interest in short arc orbit determination applications [67].

Draper Laboratory's development of the short-periodic models includes the following:

1. Development of a recursive, short-periodic, zonal harmonic model by Slutsky [68].
2. Development of a recursive, tesseral m-daily model. These perturbations are due to the C and S coefficients in the gravity field, apply to low altitude satellites and are periodic over twenty-four hours or some fraction of a day [14].
3. Development of a recursive model for the tesseral short-periodic linear combination terms [14].
4. Development of a J_2 squared short-periodic model [15,63].
5. Development of J_2 and drag secular/tesseral m-daily coupling model [69].
6. Development of short-periodic models for atmospheric drag and solar radiation pressure based on numerical averaging [61].
7. Development of a weak time dependent third body short-periodic model based on numerical averaging [61].
8. Development of recursive short-periodic Lunar-Solar perturbation models by Slutsky [97] and Collins [66].
9. Development of interpolation concepts for the short-periodic calculations [67].

The efforts of Green (1979), Taylor (1981) and Wagner (1983) have developed both the sequential and batch estimations for DSST. Specifically, their developments include: the Semianalytical Kalman Filter, the Extended Semianalytical Kalman Filter and a Semianalytical Differential Corrections batch estimator [54,59,60,61].

2.3 Pertinent Coordinate Systems

Although both the NORAD GP theories and GTDS utilize numerous coordinate frames, this discussion will focus on one particular coordinate frame, the mean equinox and true equator of date. This frame is of capital interest since the element sets which NORAD supplies to the user community are referenced to this frame [17,78]. Also, for implementation into GTDS, it is assumed that the NORAD GP theories' outputs of position, velocity and partial derivatives are in this frame. Before examining the details of this unique coordinate frame, a review of some pertinent concepts is necessary.

A clear understanding of the ecliptic is essential for a precise analysis of coordinate systems. The ecliptic is the fundamental circle of the ecliptic system of celestial coordinates. The plane of the ecliptic is determined by the orbital motion of the earth around the sun. Specifically, the radius vector and velocity vector of the

Earth intersect the celestial sphere in a great circle along which the sun, if viewed from the center of the earth, would appear to be moving at that instant. In other words, the plane of the ecliptic, as viewed from the origin of a geocentric coordinate frame, is established by the apparent motion of the sun in the celestial sphere. The orientation of this plane is always changing due to the gravitational attractions of the other planets and the moon. As is the case with all satellites, the orbit of the Earth may be represented as a very slow, steady, progressive or secular motion upon which are superimposed a large number of small periodic variations with various periods and amplitudes. At any instant, the position of the plane due to the secular component alone is defined to be the instantaneous mean orbital plane, and the moving great circle in which this mean plane intersects the celestial sphere is the ecliptic. Given this precise definition of the ecliptic, other terms may now be defined relative to this plane.

First, the angle between the ecliptic and the celestial equator is called the obliquity of the ecliptic, ε. See Figure 2-1. The celestial equator is defined as the normal to the Earth's polar axis, and is always moving due to the luni-solar gravitational torques applied to the Earth's equatorial bulge. Furthermore, the two points where the equator intersects the ecliptic are the equinoctial points, or equinoxes. The equinox at which the sun, in its apparent annual motion, crosses the equator from south to north is called the vernal equinox, or the First Point of Aries, Υ. See Figure 2-1 [71].

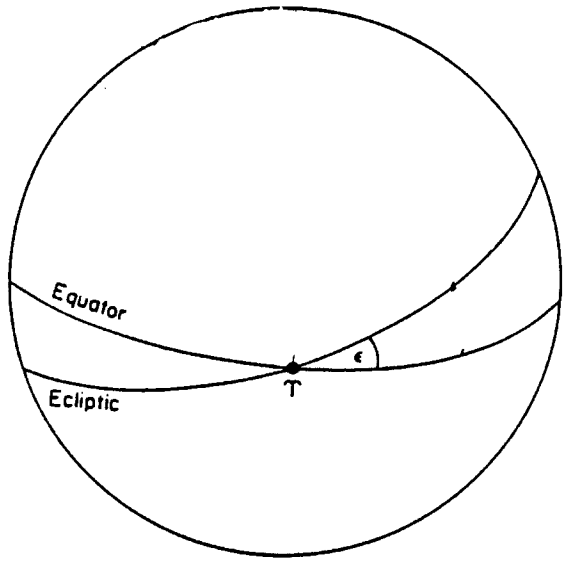

Figure 2-1. The Celestial Sphere

The position of the vernal equinox at a specific time is another key concept since it is commonly used as a reference point. An exact time must be specified because the position of the vernal equinox moves due to the combined motion of both the ecliptic and equatorial planes. This motion is further categorized as either general precession or nutation.

General precession is defined as the combined effects of planetary precession and lunisolar precession. Planetary precession is the slow rotation of the ecliptic plane, which is by definition a mean plane, (i.e. with only secular variations) due to the planets' gravitational attraction on the Earth. This precession consists of an

eastward movement of the equinox of approximately twelve seconds of arc per century and a decrease of obliquity of approximately forty-seven seconds of arc per century. Lunisolar precession is part of the motion of the equatorial plane which moves due to the gravitational attraction of the sun and the moon on the Earth's equatorial bulge. This precession is the smooth long period westward motion of the Earth's polar axis around the ecliptic pole. The period of this motion is 26,000 years, and the amplitude of the oscillations is 23.5 degrees. Furthermore, it is very important to recognize that the term, mean, when referenced to the equator or equinox, implies that only precession is taken into account [53].

Nutation describes the short periodic motion superimposed upon the lunisolar precession [72]. The dominating nutation term is due to the regression of the line of nodes of the moon's orbital plane, which has a period of 18.6 years. The elliptical motion of the sun and moon relative to the Earth produce other periodic terms, the most significant being half-month and half-year nutations. Nutation consists of corrections of the celestial longitude and corrections of the obliquity. These corrections are known as the nutation in longitude ($\Delta\varphi$) and the nutation in obliquity ($\Delta\varepsilon$) [17]. Respectively, these motions are the periodic oscillation of the apparent (true) vernal equinox relative to the mean vernal equinox (along the ecliptic); and the periodic oscillation of the true celestial equator relative to the mean celestial equator [70]. See Figure 2-2 [72].

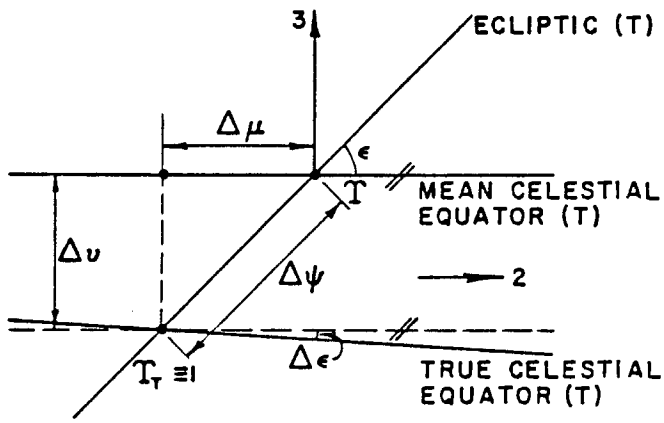

Figure 2-2. Nutation

Two other expressions play a key role in this coordinate system analysis, and they are:

$$\Delta\upsilon = \Delta\varphi \sin \varepsilon \tag{2.31}$$

and

$$\Delta\mu = \Delta\varphi \cos \varepsilon \tag{2.32}$$

The $\Delta\mu$ term is also known as the equation of the equinoxes [17], which is defined as the right ascension of the mean equinox referred to the true equator and equinox. This is equal to the difference between the mean and true right ascensions of a body on the equator [71].

The final key concept to review is the definition of the mean equator and mean equinox of 1950.0, or mean 1950.0 inertial coordinate frame. Both GTDS and NORAD theories use this frame as their basic inertial reference coordinate frame. It is an Earth-centered equatorial inertial frame frozen at 1950.0, which is 31 December 1949, at 2209 zulu time [17,53].

This completes the review of the appropriate concepts necessary for further analysis. The following development will describe both the GTDS and NORAD coordinate frame transformations.

The GTDS coordinate frame transformations utilize a **C** matrix. This **C** matrix provides the transformation from the mean 1950.0 inertial coordinate frame to the true of date inertial frame for a specified date [70]. As an example, where $\underline{R}$, is referred to the mean 1950.0 inertial frame,

$$\underline{r} = \mathbf{C}\underline{R} \qquad (2.33)$$

and where $\underline{r}$, is a vector referred to the true of date inertial frame [53]. This transformation occurs in two steps. First, it is necessary to note that the **C** matrix is a composite of two other matrices,

$$\mathbf{C} = \mathbf{NP} \qquad (2.34)$$

where **P** is the precession matrix and **N** is the nutation matrix. For both GTDS and NORAD theories, the precession matrix transforms the coordinate frame from the mean 1950.0 frame to the mean of date frame, and accounts for general precession. The GTDS nutation matrix transforms the coordinate frame from the mean of date frame, to the true of date frame. However, NORAD's nutation matrix transforms the coordinate frame from the mean of date to the mean equinox and true equator of date [70].

In order to describe these nutation transformations, it is necessary to define the following rotations, assuming a right-hand coordinate frame:

1. A rotation about the $\hat{x}$ axis:

$$R_1(\theta) = \begin{bmatrix} 1 & 0 & 0 \\ 0 & \cos(\theta) & \sin(\theta) \\ 0 & -\sin(\theta) & \cos(\theta) \end{bmatrix} \qquad (2.35)$$

2. A rotation about the $\hat{y}$ axis:

$$R_2(\theta) = \begin{bmatrix} \cos(\theta) & 1 & -\sin(\theta) \\ 0 & 1 & 0 \\ \sin(\theta) & 0 & \cos(\theta) \end{bmatrix} \qquad (2.36)$$

3. A rotation about the $\hat{z}$ axis:

$$R_3(\theta) = \begin{bmatrix} \cos(\theta) & \sin(\theta) & 0 \\ -\sin(\theta) & \cos(\theta) & 0 \\ 0 & 0 & 1 \end{bmatrix} \qquad (2.37)$$

GTDS uses a rigorous nutation transformation defined as the composite of three rotations:

$$\mathbf{N} = R_1(-\varepsilon - \Delta\varepsilon)\, R_3(-\Delta\varphi)\, R_1(\varepsilon) \qquad (2.38)$$

It is at this point that the NORAD transformations differ from the GTDS development [70].

The NORAD nutation matrix is based upon a modified approximate transformation. First, the rigorous transformation is replaced with an approximate transformation (developed by Mueller [72]) which is motivated by Figure 2-2. The transformation follows:

$$\mathbf{N} = R_1(-\Delta\varepsilon)\, R_2(\Delta\upsilon)\, R_3(\Delta\mu) \qquad (2.39)$$

When this transformation is taken to first order in $\Delta\upsilon$, or $\Delta\mu$, the resulting matrix takes the form:

$$\mathbf{N} \cong \begin{bmatrix} 1 & -\Delta\mu & -\Delta\upsilon \\ \Delta\mu & 1 & -\Delta\varepsilon \\ \Delta\upsilon & \Delta\varepsilon & 1 \end{bmatrix} + \text{second order terms} \qquad (2.40)$$

(Note: The maximum value of any second order term is $\cong 4 \times 10^{-9}$ radians)

Given this transformation, NORAD now modifies the nutation matrix by using only part of Mueller's matrix. The NORAD matrix is simplified by letting $\Delta\mu$ equal zero [17,70]. The resulting matrix is:

$$N_{NORAD} = \begin{bmatrix} 1 & 0 & -\Delta\upsilon \\ 0 & 1 & -\Delta\varepsilon \\ \Delta\upsilon & \Delta\varepsilon & 1 \end{bmatrix} \qquad (2.41)$$

There is another pertinent distinction between GTDS and NORAD coordinate transformations, and that relates to the GTDS **B** matrix. This matrix is the composite of an R_3 rotation through the Greenwich Hour Angle, θ_g, which is the right ascension of the Greenwich Meridian. This transformation relates the true of date coordinates to body-fixed coordinates. Specifically:

$$\mathbf{B} = R_3(\theta_g) \qquad (2.42)$$

NORAD has a similar transformation, except that the Mean Greenwich Hour Angle, $\tilde{\theta}_g$, is used in place of θ_g. The difference of these two terms, $\theta_g - \tilde{\theta}_g$, is also equal to the equation of the equinoxes, $\Delta\mu$ [70].

Chapter 3

INCORPORATION of the NORAD THEORIES into GTDS

3.1 Overview

The overall approach for implementing the NORAD GP theories in GTDS follows the existing GTDS ephemeris generation architecture. This architecture is reflected in Figure 3-1. All the GTDS main programs (Ephemeris Generation, Differential Correction, etc.) interface with the GTDS orbit generators through subroutine ORBIT which is the orbit generator driver. Below subroutine ORBIT, there are three major branches: Initialize, Restart, and Output. The Initialize branch functions are performed one time only. These include time initialization, calculation of reference values for various coordinate system transformations, force model initialization, and initial element set and coordinate conversions. The Restart branch is also an initialization, but it depends on the exact values of the epoch orbital element set. This branch directly supports differential correction (DC) runs and is executed prior to each DC iteration. In an ephemeris generation run, the Restart branch is executed one time only. This particular design is intentional and reflects an architecture which uses the same structure for both the DC and ephemeris generation runs. The Output branch evaluates the position, velocity and partial derivatives at the desired request time. After obtaining the position, velocity and

partial derivatives, the data flow returns to the Executive and Driver subroutines.

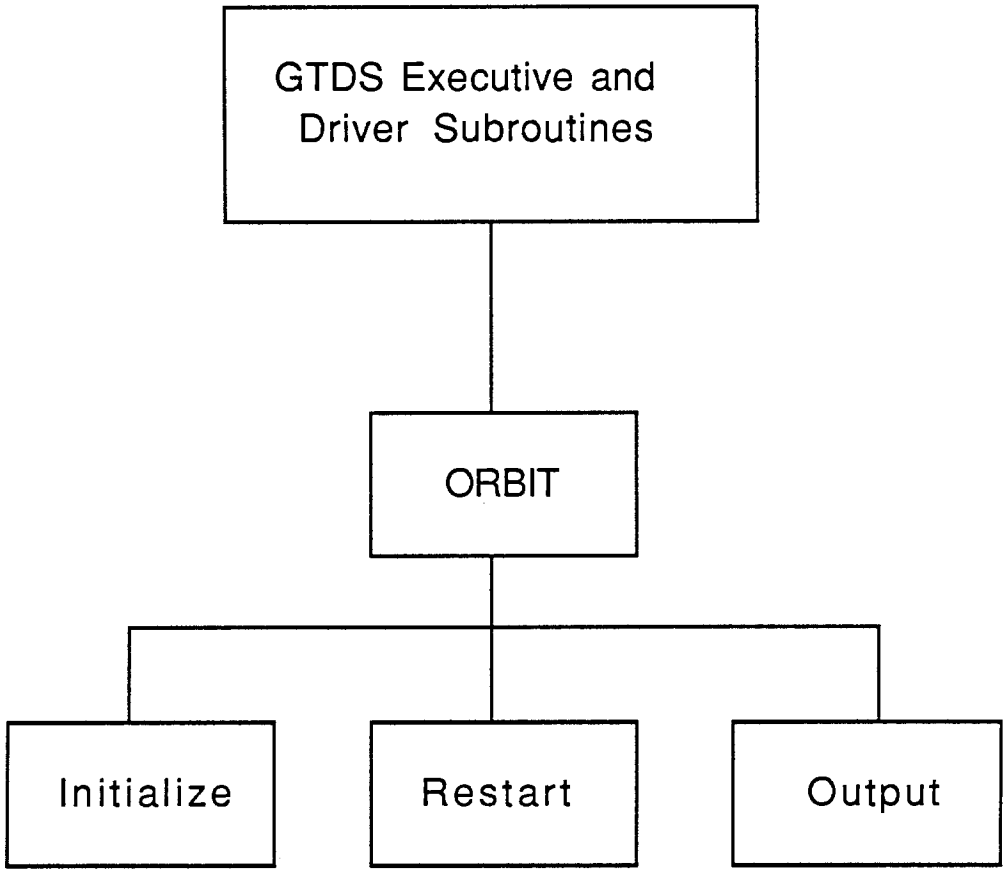

Figure 3-1 Basic GTDS Orbit Generator Architecture

Two other factors played significant roles in the design process. One consideration was to minimize the negative impact on the operation of any existing facility in the GTDS program. Similarly, another factor was to minimize the maintenance cost associated with updating any affected facility. These considerations were motivated directly by Draper Laboratory's previous experience in implementing the DSST in its version of

GTDS. This led to a design which makes the incorporation of the NORAD GP theories into GTDS independent of and yet accessible to other GTDS facilities. Specific aspects of the software design which followed from these two considerations include the establishment of a separate integration coordinate system (NORAD true equator and mean equinox of epoch) to support the NORAD GP theories and the establishment of new common blocks for the storage of the input NORAD element sets and drag parameters. In both of these design choices, the desire was to avoid variables and arrays with multiple meanings.

A major consideration is that the actual SPADOC 4B Fortran 77 source code was used to the maximum extent possible. One advantage of using this code is that we were able to easily reproduce the SPADOC benchmark test runs with a high degree of accuracy (See Chapter Four) and thereby gain confidence in the accuracy of our implementation. Additionally, any corrections or improvements to the NORAD GP theories that are made at Draper Laboratory will be in a form that is easy to evaluate in the government's SPADOC system. Finally, it was recognized that there were very significant developmental and testing economies to be achieved by following this approach.

A more detailed diagram of the overall design for the incorporation of the NORAD theories in GTDS is given in Figure 3-2. At the top, Figure 3-2 provides a brief schematic of the existing GTDS program. The module ODSEXEC is the overall main program. Subroutine SETRUN drives the input data processing. Subroutines

CREF – 1950 to GTDS True of Ref – TOD

CNREF – 1970 to NTOR

CNCREF – GTDS TOD to NTOR

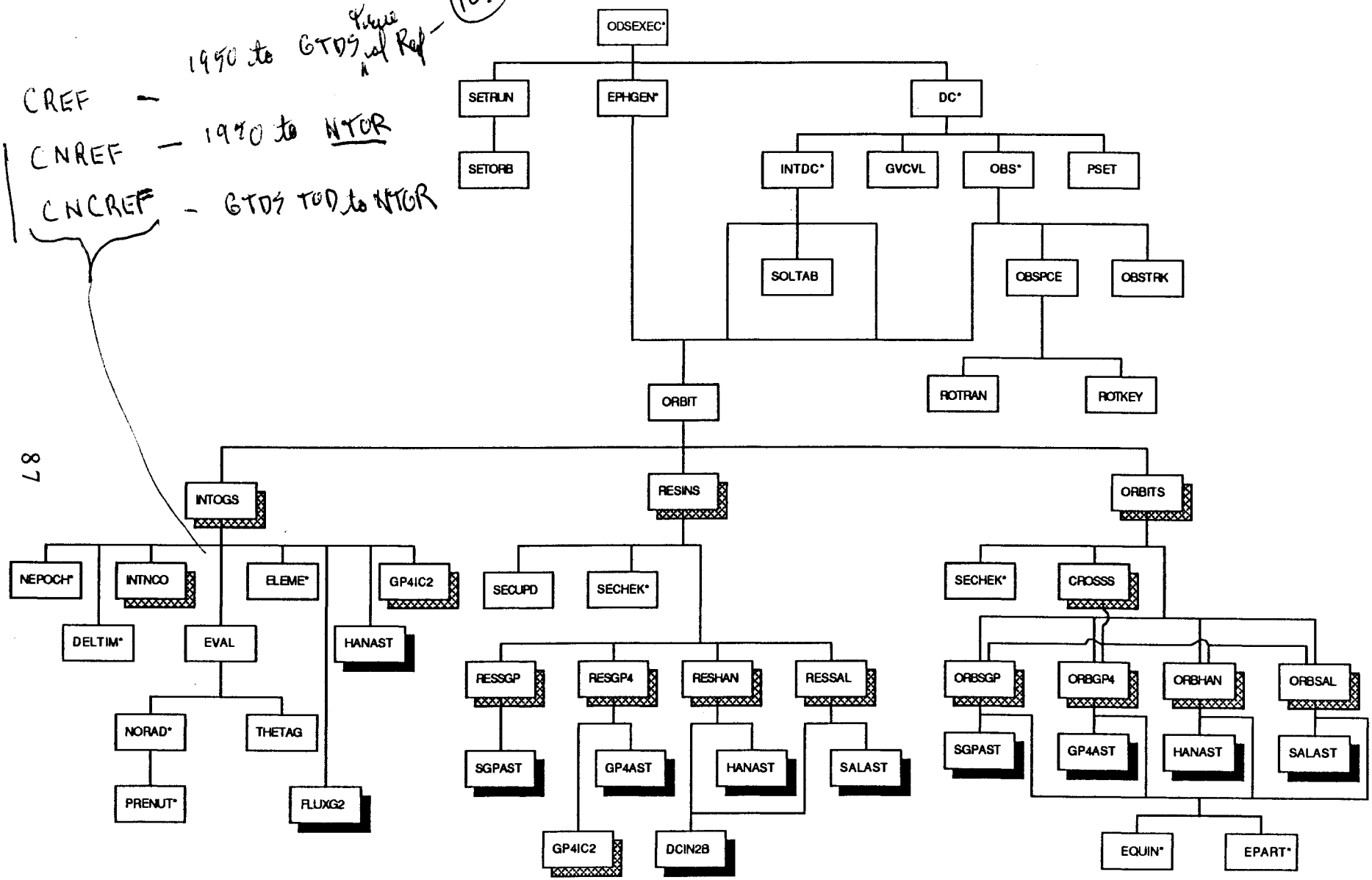

Figure 3-2 Overview of GTDS Implementation of NORAD/SPADOC GP Satellite Theories

new GTDS subroutine | SPADOC subroutine | previously existing GTDS subroutine that was modified (* means that subroutine was not modified)

EPHGEN and DC are the main drivers for the ephemeris generation and differential correction functions, respectively. For the Differential Correction capability, the mean equinoctial element solve-for logic developed earlier [59,60] for the DSST was employed. Subroutine ORBIT is the driver for both orbit and partial derivative generation. As discussed previously, the details of the orbit generation are then partitioned into 'one-time' initialization, initialization at the start of a DC iteration, and output at a request time. For the NORAD theory implementation, these functions will be handled in new subroutines INTOGS, RESINS, and ORBITS, respectively. The RESINS routine also calls new subroutine RESSGP, or RESGP4, or RESHAN to allow for 'restart' functionality specific to the SGP, GP4, or HANDE theories, respectively. Routines RESSGP, RESGP4, and RESHAN then call the appropriate SPADOC top level drivers subroutines[1]. For the output at request time functionality, ORBITS calls ORBSGP or ORBGP4 or ORBHAN which again calls the appropriate SPADOC top level driver. Figure 3-2 also depicts other new subroutines and other modified and unmodified GTDS subroutines. While the above software design makes very efficient usage of existing GTDS and SPADOC capabilities, it also requires strict attention to the communication of data between the several functions. The element set is the main format for communication and various definitions of the element set are employed. Some of these definitions are given

---

1 The drivers for the SGP, GP4, and HANDE theories are SGPAST, GP4AST, and HANAST, respectively. Provision for the NORAD Semianalytical Theory, SALT [73], is also made in Figure 3-2.

in Table 3-1 and their usage is discussed below. The input element set is the Keplerian elements. The input element set must be

Table 3-1. Element Set Definitions[2]									
1.		Input Element Set for GP Theories [External units]							
	n,a	e	i	W	w	M	$\dot{n}/2$	$\ddot{n}/6$	B*,B
2.		Input Element Set for GP Theories [Internal Units]							
	n,a	e	i	W	w	M	$\dot{n}/2$	$\ddot{n}/6$	B*,B
3.		GTDS Solve-Vector [Internal Units]							
		a	h	k	p	q	l	$\dot{n}/2$	
4.		SPADOC Solve-Vector [Internal Units]							
		k	h	n	l	p	q	$\dot{n}/2$	

converted to internal units and both GTDS and SPADOC internal unit conventions need to be considered. The GTDS GP differential correction (DC) capability uses the mean equinoctial elements as the solve parameters.[3] Thus, the Keplerian to equinoctial transformations are employed. For the internal GTDS drag solve-for parameter, the SPADOC drag solve-for parameter $\dot{n}/2$ is used. For the GP4 and HANDE theories, the input drag parameter (B* or B,

---

2 All of the element sets are understood to be epoch values.

3 This is a key design choice because the GTDS solve-for vector is very similar to the NORAD internal solve-for vector. Also, it allows the use of existing GTDS Variation of Parameter capabilities.

respectively) must be converted to $\dot{n}/2$. The SPADOC partial derivative routines return a state transition matrix employing the SPADOC solve-for parameter format. This must be converted to the GTDS format. After each DC iteration, the current values of the GTDS solve parameters must be converted to Keplerian elements for input to the GP theories. The current value of $\dot{n}/2$ also must be converted to B* or B if the GP4 or HANDE theories are being used.

The remainder of Chapter Three provides a detailed discussion of the NORAD GP implementation in GTDS. This discussion outlines the inputs, processing, and outputs. Section 3.2 describes the input options. Section 3.3 describes the processing. Within this section, the functions are presented primarily in the order that they would occur in a GP DC run. The presentation is limited to those GTDS functions that were modified and to the new functions that were developed. Section 3.4 reviews the output data. Finally, section 3.5 provides a brief commentary on the key SPADOC routines.

3.2 Input Data

3.2.1 Orbit Generator Input Data

Possible inputs include the following:

1. Pseudo-SGP elements from the NORAD Historical Data System (HDS).

2. Orbital elements from an earlier GTDS DC execution (SGP, GP4/DP4, 7 parameter HANDE or 18 parameter HANDE).

3. Orbital elements from a SPADOC benchmark execution (SGP, GP4/DP4, 7 parameter HANDE or 18 parameter HANDE).

Element sets are identified both by source and theory to allow appropriate preprocessing and to ensure correct usage in GTDS. SGP elements from the Historical Data System (HDS) include: the epoch mean motion time derivative divided by two, $\dot{n}_0 / 2$, (which is also the SGP theory drag parameter), the epoch mean motion second time derivative divided by six, $\ddot{n}_0 / 6$, and the drag parameter for GP4/DP4 theory, B*. With SGP elements from the HDS, either of the propagators, SGP and GP4/DP4, can be correctly executed. For several years, however, the GP4 theory has been used in the NORAD orbit determination processing for the low altitude cases and the DP4 theory has been used for the deep space orbits. The element sets resulting from the NORAD OD processing are converted to pseudo-SGP element sets before distribution to the overall user community. This conversion is accomplished for user convenience, but it should be undone before using the transmitted element sets for GP4 or DP4 orbit propagation. It is also possible to approximately convert SGP elements to HANDE elements [43] but that capability was not implemented in this effort.

The GTDS and SPADOC formats for the Keplerian element sets differ only in that the mean semi-major axis (km) is used in the GTDS format and the mean mean motion (revs/day) is used in the SPADOC format. And, of course, the element sets must be used in a consistent manner. SGP elements computed in a GTDS DC using the SGP orbit propagator should only be propagated subsequently using the SGP theory. Similarly, GP4/DP4, and HANDE element sets determined with a GTDS DC should only be propagated with the same orbit generators, respectively.

Element sets obtained from a previous GTDS DC execution or from a SPADOC benchmark may also include a drag solve-for parameter. For the SGP theory, the drag parameter is the epoch mean motion time derivative divided by two ($\dot{n}_0 / 2$). For the GP4/DP4 theories, B* is the drag solve for parameter. For the HANDE theory, the ballistic coefficient B is the additional solve-for parameter.

There are two options for the input to the HANDE theory. HANDE can be exercised with the standard seven parameter input; in this case, the eleven extra HANDE time derivatives $\dot{n} / 2$, $\ddot{n} / 6$, $(d^3n / dt^3) / 24$, $(d^4n / dt^4) / 120$, $\dot{e}$, $\ddot{e} / 2$, $(d^3e / dt^3) / 6$, di / dt, $\dot{\Omega}$, $\dot{\omega}$, and $\dot{M}$ will be computed as part of the 'one time' initialization process. Alternatively, the full eighteen parameter HANDE element set can be input.

In a HANDE DC, the extra time derivatives are also computed in the RESTART process.

For NORAD GP orbit generator runs in GTDS, all of the input element sets are currently assumed to be in the NORAD true equator and mean equinox of epoch coordinate system. Also, the user must currently request the WGS-72 gravity potential constants if the

NORAD GP orbit generators are being employed. Output in various coordinate systems including the NORAD true equator and mean equinox of epoch and Mean of 1950.0 is available.

Input of the element set epoch time follows the current GTDS convention (UTC) without modification.

3.2.2 Differential Correction Input Data

The choice of satellite theory and the allowable input element sets is the same as for the Orbit Generation function. The only additional inputs are that the user must request the mean equinoctial element solve-for parameter set and (optionally) the drag parameter solve-for functionality. The currently available drag parameter solve-for options[4] are the following:

1. SGP - Solve for $\dot{n}_0 / 2$.
2. GP4/DP4 - Solve for B*.
3. HANDE - Solve for B.

Also, the user may input an a priori standard deviation for the drag solve-for parameter. Existing GTDS DC inputs that are independent of the satellite theory are supported.

---

4 This refers to the drag solve-for parameter used in the input/output. As noted earlier, both SPADOC and GTDS internally always solve for the epoch mean motion time derivative divided by two.

3.3 Processing

This section describes the processing. Within this section, the functions are presented primarily in the order that they would occur in a GTDS GP DC run. The presentation is limited to those GTDS functions that were modified and to the new functions that were developed.

3.3.1 Key Common Blocks

Common blocks play an essential role in implementing the communication between the several subroutines. In this development, some existing GTDS common blocks were modified, three new common blocks were developed, and several SPADOC common blocks were employed. Most importantly, the SPADOC common blocks were accessed in the new interface routines (INTOGS, RESSGP, RESGP4, RESHAN, ORBSGP, ORBGP4, and ORBHAN) to support either the transfer of data into the SPADOC routines or the retrieval of data from the SPADOC routines. The key common blocks are listed in Table 3-2 along with brief comments on their usage. More detailed descriptions are provided as the common blocks are applied.

Table 3-2. Key Common Blocks

1.	Modified GTDS Common Blocks /FRC/ integration parameters /MATRIX/ current time and reference values of coordinate system transformations and related data
2.	New Common Blocks /GPELS/ input flags and values of the epoch NORAD element sets and simple transformations thereof /NORCON/ time and angle conversion factors /NORINT/ drag solve-for parameters and variances
3.	SPADOC Common Blocks /ACONVC/ units conversion constants /ACPHYS/ physical constants /ADCELT/ DC element set; used to input data to DCIN2B /ADCIRQ/ DC input/control data; used to input data to DCIN2B /AELSET/ standardized element set records; used to input data to the top level drivers (SGPAST, GP4AST, or HANAST) /AEPHOT/ standardized ephemeris records; used to retrieve data from the top level drivers (SGPAST, GP4AST, or HANAST) /AG2MAT/ used to retrieve state transition matrix from G2M CPC /AMATHC/ mathematical constants

3.3.2 Input Data Processing (SETRUN, SETORB)

This section describes the modifications to the GTDS input data processing function that were made to support the NORAD GP theories. There are modifications to processing of the GTDS mandatory cards[5] and these are implemented in subroutine SETRUN. The modifications to the processing of the Orbit Generator Optional (OGOPT) subdeck cards are implemented in subroutine SETORB.

3.3.2.1 SETRUN

There are two sets of modifications to be discussed. The first describes the processing of the mandatory cards in a Differential Correction (DC) or Ephemeris Generation (EPHEM) run when that program is the first job step. The second set of modications supports the passing of an element set to a second job step. This second capability is used when an EPHEM step is used to create an ORB1 file following a DC.

For the first capability, modifications were made to the processing of the ELEMENTi(i=1,2), EPOCH, ORBTYPE, and OUTPUT mandatory keyword cards. For the GP theories, new keyword cards ELEMENT3, ELEMENT4, ELEMENT5, and ELEMENT6 were introduced (see Appendix F). The ELEMENT3 card is mandatory for all the GP theories (SGP, GP4/DP4, and HANDE). The ELEMENT4, ELEMENT5, and ELEMENT6 cards are mandatory only for the HANDE eighteen parameter input

---

5 See the R & D GTDS User Guide for a discussion of the mandatory cards and the optional subdecks.

option. The processing in SETRUN is organized on a card by card basis and the discussion here follows that organization.

For the ELEMENT1 card, the initial error checking is modified to allow for the NORAD true equator and mean equinox of epoch input coordinate system orientation. The flow then branches to a NORAD-specific section. The input coordinate system type (see the description of the ELEMENT1 card in Appendix F) is stored in new common block /GPELS/. Based on this value, either the mean motion or the semimajor axis is stored in /GPELS/. If the mean motion is input, it is converted from NORAD external units (rev/day) to NORAD internal units (rad/min) prior to being stored in /GPELS/. The conversion factors are passed into SETRUN via the new common block /NORCON/. Next, eccentricity and inclination are stored in /GPELS/. Again, the inclination is converted from NORAD external units (deg) to NORAD internal units (rad).

The ELEMENT2 card supports the input of the longitude of ascending node, argument of perigee, and Mean anomaly. These are converted to internal units and then stored in /GPELS/.

The implementation of new mandatory cards required a increase in the number of mandatory keywords, NMAND, and new mandatory keywords in array MANCRD. The ELEMENT3 card supports the input of $\dot{n}_0 / 2$, $\ddot{n}_0 / 6$, and B* (or B for HANDE). The quantities $\dot{n}_0 / 2$ and $\ddot{n}_0 / 6$ are converted to NORAD internal units and all three quantities are stored in /GPELS/.

The ELEMENT4 card supports the input of the HANDE parameters $(d^3n / dt^3)_0 / 24$, $(d^4n / dt^4)_0 / 120$, and $\dot{e}$. All three quantities are converted to internal units and stored in /GPELS/.

The ELEMENT5 card supports the input of the HANDE parameters $(d^2e / dt^2)_0 / 2$, $(d^3e / dt^3)_0 / 6$, and $(di / dt)_0$. All three quantities are converted to internal units and stored in /GPELS/.

The ELEMENT6 card supports the input of the HANDE parameters $(d\Omega / dt)_0$, $(d\omega / dt)_0$, and $(dM / dt)_0$. All three quantities are converted to internal units and stored in /GPELS/.

The format of the EPOCH card is unchanged. The time initialization function is unchanged except that a NORAD reference time is computed. This reference time is the number of minutes from January 0.0, 1970 to the input epoch. The reference time is stored in /GPELS/. This calculation employs the GTDS module TIMREL and is based solely on Julian date.

For the ORBTYPE card, a new processing branch was implemented for the NORAD GP theories. The processing is similar in scope to that for the Brouwer and Vinti theories. The GP output type (osculating or mean) and the reference time computation method flag IGTIME are stored in /GPELS/. The integration coordinate system (NORAD true equator and mean equinox of epoch) flag in /FRC/ is set. The SLP working file parameter NWSLP in /FILES/ is set to true of date.

The OUTPUT card processing is unchanged except that the range of allowable output coordinate system orientations is expanded to include NORAD true equator and mean equinox of epoch frame.

After all the mandatory cards are read, there is additional initialization and consistency checking. For the NORAD GP theories, the following additional checks are performed:

- If one of the GP theories is requested and no ELEMENT3 card was read, an error is declared.

- If the HANDE theory with eighteen parameter input is requested and one of the ELEMENT4 or ELEMENT5 or ELEMENT6 cards was not read, an error is declared.

- If a GP theory other than HANDE with eighteen parameter input is requested and one of the ELEMENT4 or ELEMENT5 or ELEMENT6 cards was read, an error is declared.

At this point, the previously existing SETRUN data flow resumes and the various optional subdecks including the orbit generator subdeck OGOPT are read. The OGOPT cards are processed in subroutine SETORB. Modifications of SETORB to support the NORAD GP theories are described in the following section 3.3.2.2. Finally, several miscellaneous parameters are set. This includes the conversion of the specific orbit generator type to a 'general' type. The general types are numerical and analytical. The NORAD GP theories are included with the numerical theories (Cowell, SST, etc.) because this simplifies the subsequent treatment of the partial derivatives. After completion of SETRUN processing, control returns to the ODSEXEC level (see Figure 3-2).

The initialization by SETRUN of a second GTDS job step based on a state vector computed in the first job is straightforward. The ELEMENTi and EPOCH cards are not used in the input deck for the

second job step. For the NORAD GP theories, an additional branch was implemented. The input coordinate system type is set in /GPELS/ based on the type of GP theory employed in the first job step. The input coordinate system type is always one of the GTDS formats (see the ELEMENT1 card description in Appendix F). The Keplerian elements are copied from /DCINT/ to /GPELS/. If the first job step was a DC, these Keplerian elements will be the last DC iteration values. Similarly, the last iteration values of $\dot{n}_0 / 2$ and B^* (or B) are copied from common block /NORINT/ to /GPELS/. At this point, the previous SETRUN data flow resumes.

3.3.2.2 SETORB

Subroutine SETORB is called by SETRUN to process the OGOPT subdeck. The primary modification is to the processing of the DRAGPAR card. The general function of this card is to update drag solve-for parameters. For the GP theories, a separate branch is implemented. If the drag solve for capability is requested in a DC (or drag partials in an EPHEM), the drag partial derivative flag in /SWITCH/ is turned on and the a priori variance of the solve-for parameter is computed from the input standard deviation of that parameter (see Appendix F). The a priori variance of the drag solve-for parameter is then set in /GPELS/.

The processing of the POTFIELD card is also slightly modified. Specifically, the potential field number is also stored in /GPELS/. NORAD GP runs (both EPHEM and DC) may also use the STATEPAR and

STATETAB cards. However, the processing of those cards is not modified.

3.3.3 Initialization

Both the GTDS DC and EPHEM programs interface with the orbit generator through subroutine ORBIT. When ORBIT is requested to perform the one time initialization of a NORAD GP theory, new subroutine INTOGS is called. The general architecture for INTOGS follows the initialization of the numerical theories as implemented in GTDS routine INTOGN. The functions implemented in INTOGS include:

- initialization of time and coordinate systems
- initialization of semimajor axis
- initialization of element set arrays
- initialization of HANDE time derivatives
- initialization of drag solve-for parameters and partial derivative flags

These are described in the following paragraphs in more detail.

3.3.3.1 Initialization of Time and Coordinate Systems

This function starts with calls to NEPOCH and EVAL to compute time parameters including TZERO which is the number of A.1 seconds from 1950.0 to the input epoch. If the A.1 - UTC corrections are to be considered in computing the minutes from January 0.0, 1970 to

This number was reviewed in detail in 1992. Ken Seidelmann computed a number which is about 0.07 seconds less. W. McClain's number can be reconstructed by using the A.1-UTC time polynomial in the GTDS math spec with a time difference of 115 days and a $(A.1-UTC)_{1950} = -3.0$ seconds. Seidelmann argues that the -3.07 should be -3.034 (29.15 - 32.184). The genesis of the GTDS 3.07 value is unknown.

the epoch, this NORAD reference time is recomputed via the formula:

$$REFM70 = (TZERO - 631072263.899438\ D0) / 60 \tag{3.1}$$

and stored in /GPELS/. The constant in equation (3.1) is the number of seconds from 1950.0 to January 0.0, 1970.[6]

Next, a call to EVAL is made to compute the reference time coordinate transformation matrices. In INTOGN, this call provides the mean equator and mean equinox of 1950.0 to True of Date coordinate transformation (**C** matrix). For this implementation, EVAL was modified to additionally compute the rotation matrix which provides the transformation from the GTDS **C** matrix to the NORAD **C** matrix[7]. This rotation matrix is denoted as CNC, and is calculated in subroutine EVAL by the following equation:

$$CNC = CN\,C^T \tag{3.2}$$

The term CN in equation (3.2) is the NORAD **C** matrix and it is computed by calling the subroutine NORAD which in turn calls subroutine PRENUT (see Figure 3-2). The quantity C is the GTDS **C** matrix, which subroutine EVAL computes from the GTDS Solar Lunar Planetary (SLP) ephemeris files. The new variables CN and CNC were added to the GTDS common /MATRIX/ [70]. Subroutine INTOGS saves

6 This calculation was supplied by W. McClain.

7 The NORAD C matrix is the transformation from mean equator and mean equinox of 1950.0 frame to the NORAD true equator, mean equinox of date frame.

CNC, also in /MATRIX/. Subroutine INTOGS also computes some coordinate transformations to support the ephemeris generation print output options and these are also stored in /MATRIX/.

Additional modifications were made to EVAL. These are employed later in the overall data flow but discussed here for convenience. To allow EVAL to compute the NORAD **B** matrix[8], designated BN, the subroutine THETAG was modified to load the mean Greenwich Hour Angle into the variable GHAM. Subroutine THETAG already calculated this value as part of an equation to compute the Greenwich Hour Angle value. Specifically:

$$\theta_g = \tilde{\theta}_g + \Delta\mu \tag{3.3}$$

where

θ_g = Greenwich Hour Angle
$\tilde{\theta}_g$ = Mean Greenwich Hour Angle
$\Delta\mu$ = Equation of the Equinoxes.

To accommodate these changes, the new variables GHAM and BN were added to /MATRIX/.

8 The NORAD B matrix is the transformation from the NORAD true equator, mean equinox of date frame to the body fixed frame.

3.3.3.2 Initialization of Semimajor Axis

Several of the GP input options (see the ELEMENT1 card description in Appendix F) allow the input of the mean mean motion instead of the mean semimajor axis. This was done purposely to facilitate the direct usage of NORAD format element sets in GTDS. However, the input mean motion must be converted to semimajor axis to initialize the GTDS mean element solve-for vector. The conversions employ constants from the SPADOC common block modules /ACPHYS/ and /ACONVC/ which are 'included' in INTOGS. The options considered are the following:

- If SGP elements (SPADOC format) are input and the orbit generator is SGP, then the mean motion is converted to semimajor axis via an iterative algorithm taken from the SPADOC subroutine SGPINT.

- If GP4/DP4 elements (SPADOC format) are input and the orbit generator is GP4/DP4 or DP4, then the mean motion is converted to semimajor axis via the two body equation:

$$a = \sqrt[3]{\mu / n^2} \tag{3.4}$$

- If HANDE elements (SPADOC format) are input and the orbit generator is HANDE (either 7 or 18 parameter

input), then the mean motion is converted to semimajor axis via the two body equation (3.4).

- If SGP elements from the Historical Data System (SPADOC format) are input and the orbit generator is SGP, then the mean motion is converted to semimajor axis via the non-iterative algorithm given in the SGP portion of Spacetrack Report #3 [5].

- If SGP elements from the Historical Data System (SPADOC format) are input and the orbit generator is GP4/DP4 or DP4, then the mean motion is converted to semimajor axis via the non-iterative algorithm given in the SGP4 and SDP4 portions of Spacetrack Report #3 [5].

The computed value of semimajor axis (km) is stored in /GPELS/.

3.3.3.3 Initialization of Element Set Arrays

The Keplerian elements $a, e, i, \Omega, \omega, M$ now stored in /GPELS/ are converted to position and velocity, spherical elements, and equinoctial elements via the GTDS subroutine ELEME. The position and velocity, Keplerian elements, and spherical elements appear in the orbit generator initial condition reports. The epoch position and velocity, Keplerian elements, and equinoctial elements are stored in

GTDS common block /DCINT/ for subsequent use in the DC processing.

3.3.3.4 Initialization of HANDE

First, the SPADOC routine FLUXG2 is called to initialize the solar activity and geomagnetic index data.

For both HANDE input options (7 and 18 parameters), the Keplerian elements (including both mean motion and semimajor axis), B term (area to mass ratio), and reference time from /GPELS/ all are loaded into the SPADOC common block /AELSET/. For the 7 parameter input option, the HANDE top level driver routine HANAST is then called to initialize the extra eleven HANDE time derivatives $\dot{n}/2$, $\ddot{n}/6$, $(d^3n/dt^3)/24$, $(d^4n/dt^4)/120$, $\dot{e}$, $\ddot{e}/2$, $(d^3e/dt^3)/6$, di/dt, $\dot{\Omega}$, $\dot{\omega}$, and $\dot{M}$. The initialization process employs the Jacchia 1970 atmospheric density model as do all GTDS HANDE capabilities at present. The extra time derivatives are then stored in /GPELS/. For the eighteen parameter input option, the extra time derivatives are simply copied from /GPELS/ to /AELSET/.

HANDE can now accept Jacchia 64 & MSIS 83

3.3.3.5 Initialization of Drag Solve-for Parameters and Flags

This functionality supports the DC process by initializing the internal GP drag solve parameter $\dot{n}_0/2$ and its variance. Both the internal and external drag parameters (and their variances) are stored in common block /NORINT/. This common block provides locations for the current iteration, previous iteration, and initial

values. INTOGS puts the initial values of the respective parameters (and variances) into all three locations (current, previous, and initial). The theory specific details follow:

- For the SGP theory, the input values of $\dot{n}_0 / 2$ and its variance are copied from /GPELS/ to /NORINT/.

- For the GP4/DP4 theories, the internal solve-for parameter $\dot{n}_0 / 2$ is computed from the input B* value via the equation

This eqn is exact if eval at $t = t_0$ & use GP4 eqns.

$$\dot{n} / 2 = (3 / 2) n C_2 B^* \tag{3.5}$$

This approximate equation is derived from the GP4 theory. The C_2 coefficient is one of the parameters in the GP4 theory and is computed via the new subroutine GP4IC2. The algorithm in GP4IC2 is taken from SPADOC subroutine GP4INT. The variance of $\dot{n}_0 / 2$ is computed via the similar relation:

$$Var_{\dot{n}/2} = [(3 / 2) n C_2]^2 Var_{B^*} \tag{3.6}$$

- For the HANDE theory, the internal solve parameter $\dot{n}_0 / 2$ was either input (18 parameter option) or computed earlier (7 parameter option) via the

INTOGS call to HANAST (see above). The variance of $\dot{n}_0 / 2$ is computed via the equation

$$Var_{\dot{n}/2} = [(\dot{n} / 2) / B]^2 Var_B \tag{3.7}$$

This equation assumes that there is a linear relation between $\dot{n} / 2$ and B in the HANDE theory [50].

Finally, INTOGS sets the partial derivative flags INDY and INDX in common /FRC/ based on the data stored earlier in common /SWITCH/. These flags are used to control the DC logic. This last functionality is similar to that in INTOGN.

At this point, the one-time initialization is complete and the flow returns from INTOGS to ORBIT and in turn to either INTDC (the DC initialization driver in GTDS) or EPHGEN (the top level ephemeris generation driver in GTDS) (see Figure 3-2).

3.3.4 Solve Table Set-Up (SOLTAB)

In a DC run, subroutine SOLTAB is called by INTDC to set up the dynamic solve-for parameter tables and to set various program switches consistent with the requested solve-for parameters. The NORAD GP DC's employ the mean equinoctial element solve-for parameters and this set of solve-for parameters is already supported by SOLTAB. The initial cartesian, Keplerian, and equinoctial elements stored in common /DCINT/ earlier by subroutine INTOGS are copied into arrays of past and present element values stored in common /DCFL/. Then the present equinoctial elements are copied into the a priori and current estimation arrays. The a priori and current arrays are stored in /DCFL/ and /DCINT/, respectively. For the GP drag solve-for parameters, minor modifications were made to SOLTAB. If drag solve-for is requested, the initial value of $\dot{n}_0 / 2$ from common /NORINT/ is copied into the a priori and current estimation arrays. The code also tests the initial value of the $\dot{n}_0 / 2$ variance; if the value is nonzero, the initial variance is set in /DCFL/. From this point, SOLTAB checks other solve-for flags (which will be off in a GP DC) and then returns to the driver INTDC.

3.3.5 Restart (ORBIT, RESINS)

When ORBIT is requested to perform the start of DC initialization for a NORAD GP theory, the new subroutine RESINS is called. RESINS initializes standard GTDS parameters needed to start

another integration span beginning at epoch time. The routine checks for sectioning and then functions as a driver for calls to the GP satellite theory specific routines RESSGP, RESGP4, and RESHAN (see Figure 3-2):

3.3.5.1 Restart for SGP (RESSGP, SGPAST)

Subroutine RESSGP performs the following functions:

- The current iteration values of semimajor axis, eccentricity, and inclination are used to compute the SGP mean motion.

- The current iteration Keplerian elements and mean motion, the initial values of $\dot{n}_0 / 2$ and $\ddot{n}_0 / 6$, and the reference time REFM70 are loaded into the SPADOC standardized element set record common block, /AELSET/.

- For an EPHEM run without partial derivatives, the SPADOC top level driver for SGP, SGPAST, is called to perform the SGP initialization function.

- For a DC run or an EPHEM run with partial derivatives, the current iteration value of $\dot{n}_0 / 2$ is loaded into /AELSET/ and the SPADOC top level driver for SGP,

SGPAST, is called to perform the SGP initialization function with partial derivatives.

The current iteration values of the Keplerian elements come from array AEINT in GTDS common block /DCINT/. The iterative conversion from semimajor axis to mean motion uses a modified form of the mean motion to semimajor axis conversion found in SPADOC routine SGPINT. The conversions employ constants from SPADOC modules /ACPHYS/ and /ACONVC/ which are 'included' in RESSGP. The current iteration value of $\dot{n}_0 / 2$ comes from /NORINT/. The initial values of $\dot{n}_0 / 2$ and $\ddot{n}_0 / 6$, and the reference time REFM70 come from /GPELS/. The details of the SGP flow below the driver SGPAST are given in Figure 3-3.

3.3.5.2 Restart for GP4/DP4 (RESGP4, GP4IC2, GP4AST)

Subroutine RESGP4 performs the following functions:

- The current iteration value of semimajor axis is used to compute the GP4 mean motion via the two body formula.

- The current iteration Keplerian elements and mean motion, the initial value of B*, and the reference time REFM70 are loaded into the SPADOC common block /AELSET/.

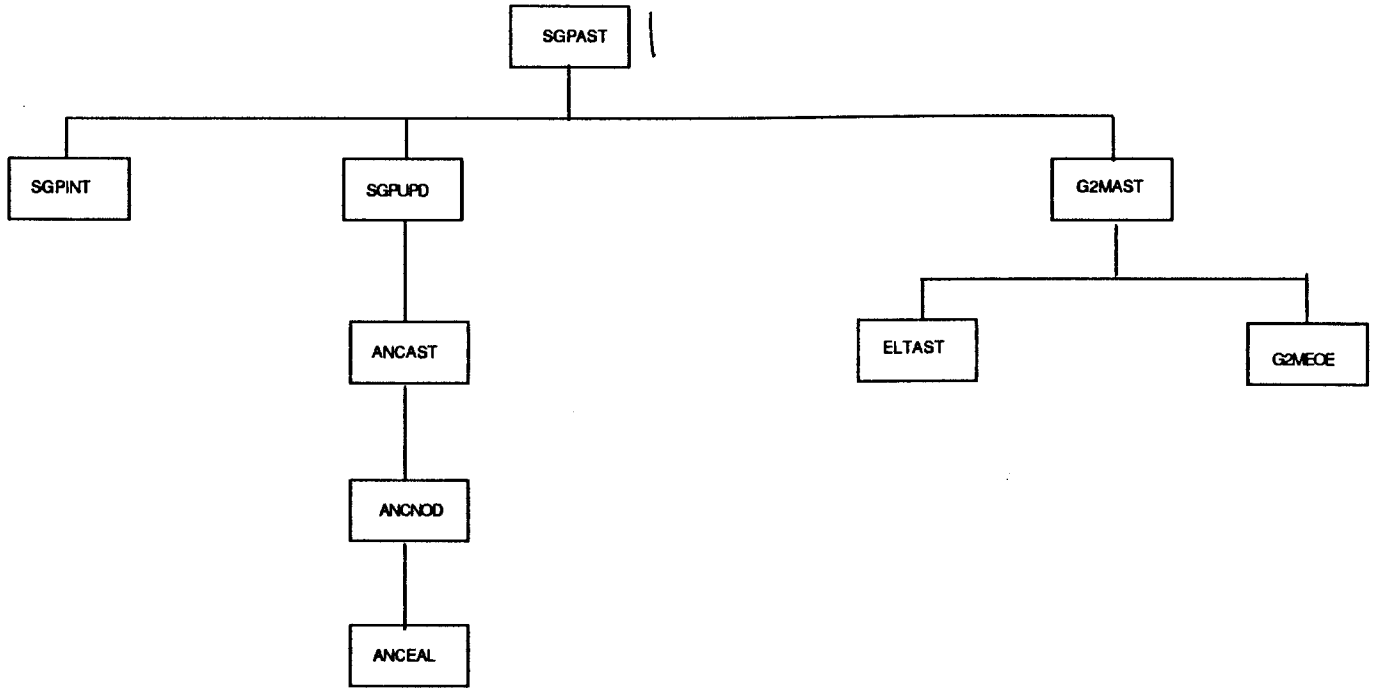

Figure 3-3 Overview of SGP Software

- For an EPHEM run without partial derivatives, the SPADOC top level driver for GP4/DP4, GP4AST, is called to perform the GP4/DP4 initialization function.

- For a DC run or an EPHEM run with partial derivatives, the current iteration value of $\dot{n}_0 / 2$ is converted to B^* via a call to GP4IC2, both $\dot{n}_0 / 2$ and B^* are loaded into /AELSET/, and the SPADOC top level driver for GP4/DP4, GP4AST, is called to perform the GP4/DP4 initialization function with partial derivatives.

The common block usage to support RESGP4 is similar to that for RESSGP. The details of the GP4 flow below the driver GP4AST are given in Figure 3-4.

3.3.5.3 Restart for HANDE (RESHAN, DCIN2B, HANAST)

For an EPHEM run, subroutine RESHAN calls the SPADOC top level driver for HANDE, HANAST, to perform the pre-update function if no partial derivatives are required. For an EPHEM run with partial derivatives, HANAST is called to perform the pre-update function with the G_2 partials.

For a DC run, the RESHAN performs the following functions:

init
init w/part
upd
upd w/part

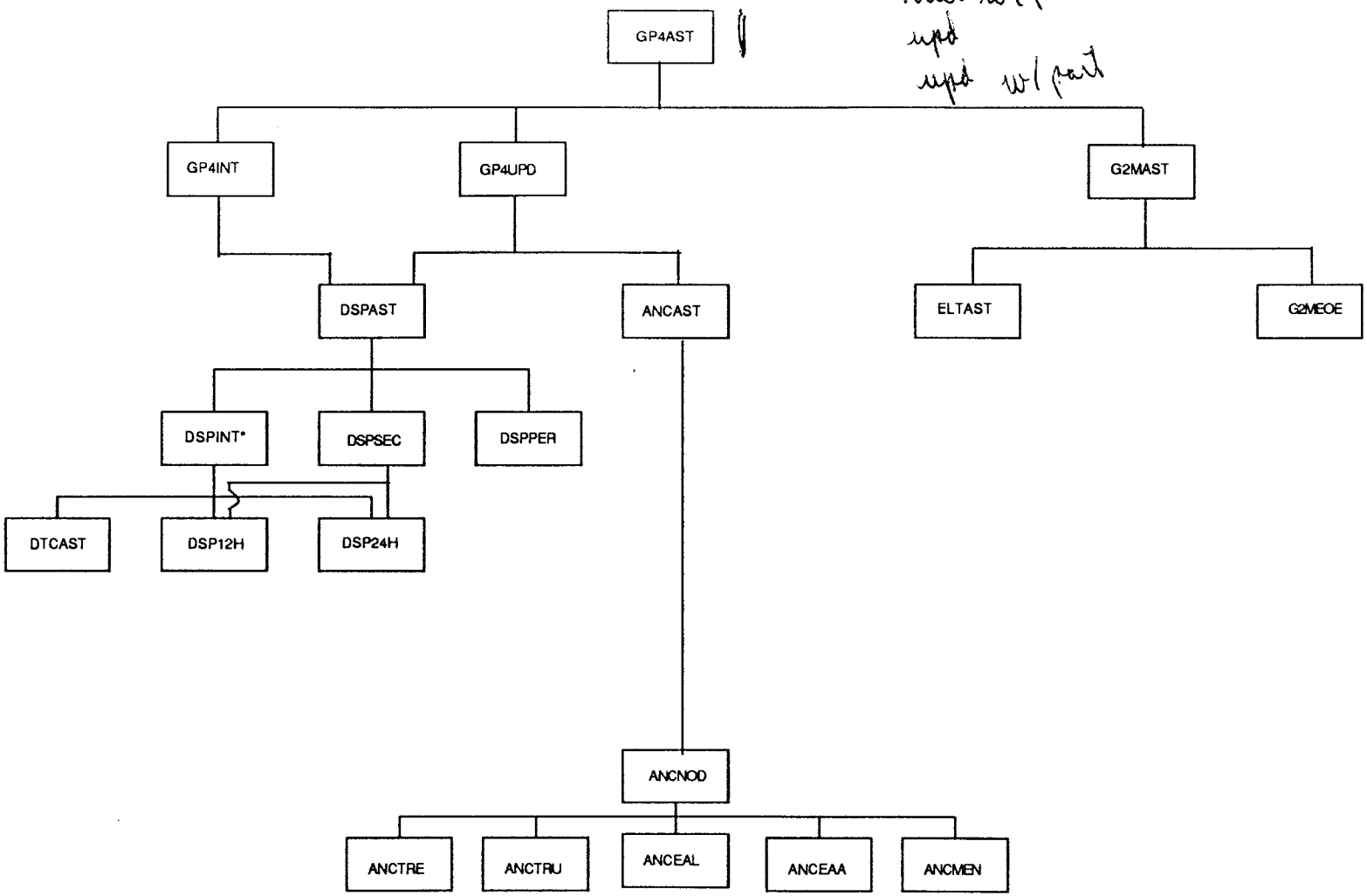

Figure 3-4 Overview of GP4/DP4 Software

(*The name DSPINT was changed to DP4INT)

- The current iteration value of semimajor axis is used to compute the HANDE mean motion via the two body formula.

- The current iteration Keplerian elements and mean motion, the initial value of B, and the reference time REFM70 are loaded into the SPADOC common block /AELSET/.

- If the drag solve-for capability is requested, the current iteration value of $\dot{n}_0 / 2$ is converted to B via a call to the SPADOC subroutine DCIN2B[9] and the B value is loaded into /AELSET/. This step requires the involvement of the SPADOC common blocks /ADCELT/ and /ADCIRQ/.

---

9 The SPADOC DCIN2B routine was modified as follows:

1. The representation time, LRPTIM, was changed from the value stored in ARLDCL (APLEPT, APLNEW), to the value stored in AOMGRM. (This change was coordinated and directed by Jon Kolb of FACC.)
2. Write statements which output data into File 7 were eliminated to avoid the possibility of writing data into GTDS files.
3. Debug write statements were eliminated.

- HANDE initialization is performed via a call to the driver HANAST to update the extra time derivatives $\dot{n}/2$, $\ddot{n}/6$, $(d^3n/dt^3)/24$, $(d^4n/dt^4)/120$, $\dot{e}$, $\ddot{e}/2$, $(d^3e/dt^3)/6$, di/dt, $\dot{\Omega}$, $\dot{\omega}$, and $\dot{M}$.

- HANDE pre-update with the G_2 partials is performed via a call to HANAST.

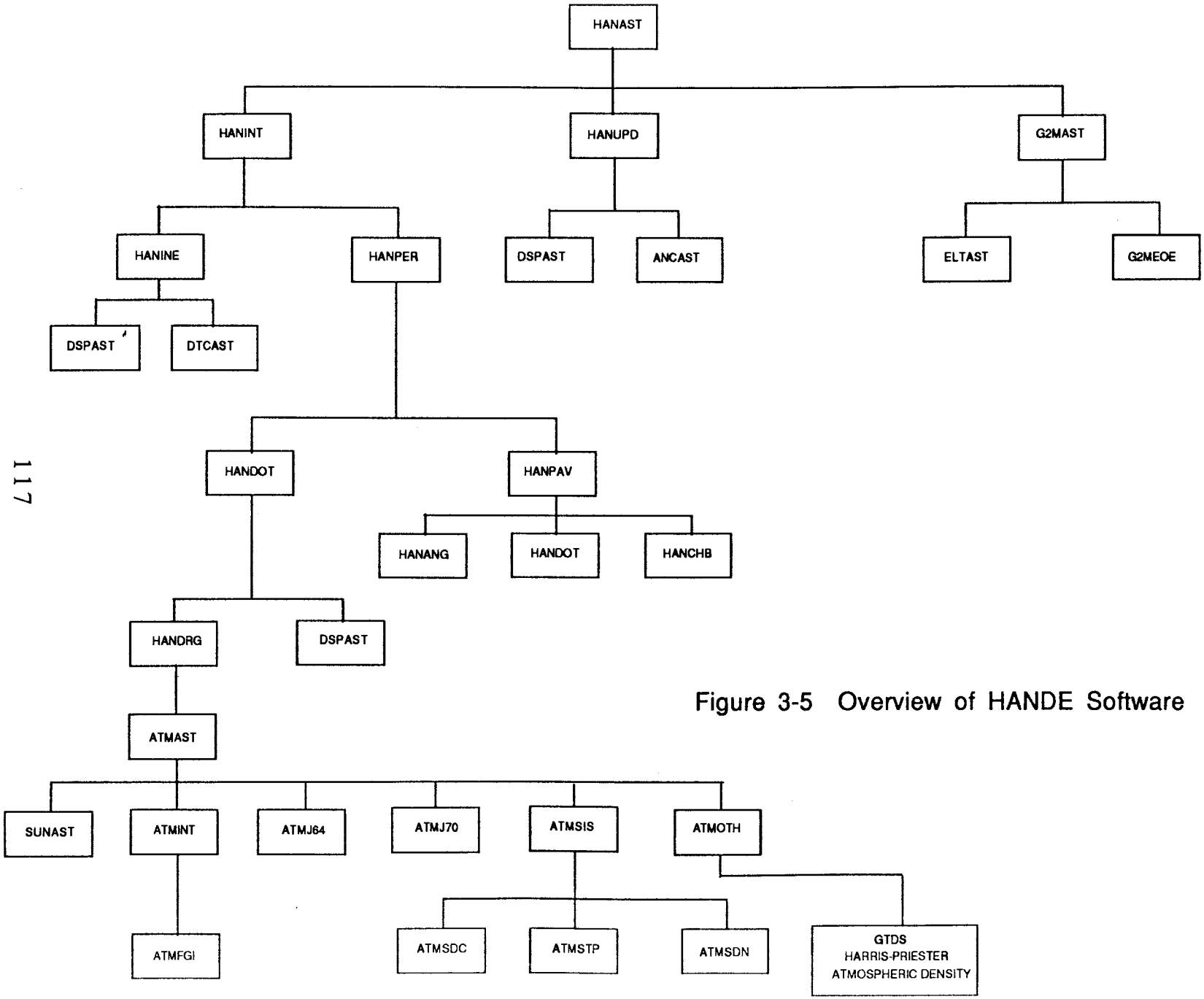

Figure 3-5 Overview of HANDE Software

The subroutine structure below HANAST is described in Figure 3-5.

3.3.6 Solve Parameter Titles (GVCVL)

Subroutine GVCVL is called by subroutine DC during the first DC iteration to generate output title arrays The title 'NDOT/2' and associated logic were added to support the NORAD GP theories drag solve-for option. Titles for the mean equinoctial elements were already implemented and did not require modification.

3.3.7 Output at Request Time (ORBIT, ORBITS, ORBSGP, ORBGP4, ORBHAN)

When ORBIT is to provide the position, velocity, and partial derivatives at a request time using one of the NORAD GP theories, ORBIT calls the new subroutine ORBITS. Subroutine ORBITS checks for sectioning and then makes calls to the appropriate intermediate driver ORBSGP, ORBGP4, or ORBHAN, which in turn calls the appropriate top level SPADOC GP theory driver SGPAST, GP4AST, or HANAST. Subroutines ORBSGP, ORBGP4, and ORBHAN are quite similar and are discussed jointly.

3.3.7.1 Position and Velocity

The processing starts with the conversion of the GTDS request time which is seconds from epoch (TTO) to the corresponding

SPADOC time which is the number of minutes since January 0.0, 1970. The conversion is implemented via the equation:

$$TIMREQ = REFM70 + (TTO/60) \tag{3.8}$$

In this expression, the SPADOC reference time REFM70 comes from common /GPELS/. The TTO parameter is passed into ORBSGP, ORBGP4, and ORBHAN via the /DCINT/ common. Next, the respective SPADOC top level driver (either SGPAST, GP4AST, or HANAST) is called to perform the update function. The update function returns position and velocity coordinates in the SPADOC internal units (earth radii, etc.) via the SPADOC ephemeris record common block /AEPHOT/. The coordinate frame is the NORAD true equator mean equinox of epoch. These coordinates are converted in ORBSGP, ORBGP4, and ORBHAN to km and km/sec using conversion constants from /AMATHC/ and /ACONVC/. The converted positions and velocities are stored in the GTDS arrays XTO and XDTO in common /DCINT/. At this point, the data flow returns to ORBITS and in turn to ORBIT if partial derivatives are not required.

3.3.7.2 Partial Derivatives

The SPADOC satellite theories return partial derivatives to ORBSGP, ORBGP4, and ORBHAN via the 6 x 7 array AG2STM in SPADOC common block /AG2MAT/. However, this array cannot be used directly in GTDS because of differences in the definition of the mean equinoctial element solve vectors between GTDS and SPADOC.

Review of Table 3-1 shows that the differences are the usage of the semimajor axis in the GTDS set versus the use of the mean motion in the SPADOC set and the mismatching sequence of elements. Also, the internal SPADOC units do not match the GTDS internal units. These differences dictate the interface operations which are applied to the SPADOC partial derivative matrix.

The SPADOC subroutines G2MAST and G2MEOE calculate the partial derivative matrix that is stored as the 6 x 7 array AG2STM in the SPADOC common block /AG2MAT/. Figure 3-6 gives the exact form of the AG2STM array:

$$\begin{bmatrix}
\frac{\partial k}{\partial k_0} & \frac{\partial k}{\partial h_0} & \frac{\partial k}{\partial p_0} & \frac{\partial k}{\partial q_0} & n_0(\frac{\partial k}{\partial n_0}) & \frac{\partial k}{\partial \lambda_0} & \frac{\partial k}{\partial (\dot{n}_0 / 2)} \\
\frac{\partial h}{\partial k_0} & \frac{\partial h}{\partial h_0} & \frac{\partial h}{\partial p_0} & \frac{\partial h}{\partial q_0} & n_0(\frac{\partial h}{\partial n_0}) & \frac{\partial h}{\partial \lambda_0} & \frac{\partial h}{\partial (\dot{n}_0 / 2)} \\
\frac{\partial p}{\partial k_0} & \frac{\partial p}{\partial h_0} & \frac{\partial p}{\partial p_0} & \frac{\partial p}{\partial q_0} & n_0(\frac{\partial p}{\partial n_0}) & \frac{\partial p}{\partial \lambda_0} & \frac{\partial p}{\partial (\dot{n}_0 / 2)} \\
\frac{\partial q}{\partial k_0} & \frac{\partial q}{\partial h_0} & \frac{\partial q}{\partial p_0} & \frac{\partial q}{\partial q_0} & n_0(\frac{\partial q}{\partial n_0}) & \frac{\partial q}{\partial \lambda_0} & \frac{\partial q}{\partial (\dot{n}_0 / 2)} \\
\frac{\partial n}{\partial k_0} & \frac{\partial n}{\partial h_0} & \frac{\partial n}{\partial p_0} & \frac{\partial n}{\partial q_0} & n_0(\frac{\partial n}{\partial n_0}) & \frac{\partial n}{\partial \lambda_0} & \frac{\partial n}{\partial (\dot{n}_0 / 2)} \\
\frac{\partial \lambda}{\partial k_0} & \frac{\partial \lambda}{\partial h_0} & \frac{\partial \lambda}{\partial p_0} & \frac{\partial \lambda}{\partial q_0} & n_0(\frac{\partial \lambda}{\partial n_0}) & \frac{\partial \lambda}{\partial \lambda_0} & \frac{\partial \lambda}{\partial (\dot{n}_0 / 2)}
\end{bmatrix}$$

Figure 3-6 Members of the AG2STM Array from Subroutine G2MEOE

The final form of the partials required by GTDS can be expressed:

$$\frac{\partial\, \underline{r}(t)\,,\, \underline{v}(t)\ (\text{ osculating })}{\partial\, \bar{a}_i\,(o)}\,.$$

$$= \left(\frac{\partial\, \underline{r}(t)\,,\ \underline{v}(t)\ (\text{ osc})}{\partial\, a_i(t)\ (\text{ osc})}\right)\left(\frac{\partial\, a_i\,(t)}{\partial\, \bar{a}_i\,(t)}\right)\ \frac{\partial\, \bar{a}_i\,(t)}{\partial\, \bar{a}_i\,(o)} \tag{3.9}$$

where the AG2STM array will be transformed to be the third matrix in the RHS of equation (3.9).

The first modification is necessary because the sequence of the partial derivatives in the SPADOC AG2STM array does not match the sequence required by GTDS. Therefore, the SPADOC sequence of $(k, h, p, q, n, \lambda, \dot{n}_0 / 2)$ must be changed to $(a, h, k, p, q, \lambda, \dot{n}_0 / 2)$. This reordered set of partial derivatives is stored in the array AGRSTM and its members are depicted in Figure 3-7.

$$\begin{bmatrix}
n_0(\frac{\partial n}{\partial n_0}) & \frac{\partial n}{\partial h_0} & \frac{\partial n}{\partial k_0} & \frac{\partial n}{\partial p_0} & \frac{\partial n}{\partial q_0} & \frac{\partial n}{\partial \lambda_0} & \frac{\partial n}{\partial (\dot{n}_0 / 2)} \\
n_0(\frac{\partial h}{\partial n_0}) & \frac{\partial h}{\partial h_0} & \frac{\partial h}{\partial k_0} & \frac{\partial h}{\partial p_0} & \frac{\partial h}{\partial q_0} & \frac{\partial h}{\partial \lambda_0} & \frac{\partial h}{\partial (\dot{n}_0 / 2)} \\
n_0(\frac{\partial k}{\partial n_0}) & \frac{\partial k}{\partial h_0} & \frac{\partial k}{\partial k_0} & \frac{\partial k}{\partial p_0} & \frac{\partial k}{\partial q_0} & \frac{\partial k}{\partial \lambda_0} & \frac{\partial k}{\partial (\dot{n}_0 / 2)} \\
n_0(\frac{\partial p}{\partial n_0}) & \frac{\partial p}{\partial h_0} & \frac{\partial p}{\partial k_0} & \frac{\partial p}{\partial p_0} & \frac{\partial p}{\partial q_0} & \frac{\partial p}{\partial \lambda_0} & \frac{\partial p}{\partial (\dot{n}_0 / 2)} \\
n_0(\frac{\partial q}{\partial n_0}) & \frac{\partial q}{\partial h_0} & \frac{\partial q}{\partial k_0} & \frac{\partial q}{\partial p_0} & \frac{\partial q}{\partial q_0} & \frac{\partial q}{\partial \lambda_0} & \frac{\partial q}{\partial (\dot{n}_0 / 2)} \\
n_0(\frac{\partial \lambda}{\partial n_0}) & \frac{\partial \lambda}{\partial h_0} & \frac{\partial \lambda}{\partial k_0} & \frac{\partial \lambda}{\partial p_0} & \frac{\partial \lambda}{\partial q_0} & \frac{\partial \lambda}{\partial \lambda_0} & \frac{\partial \lambda}{\partial (\dot{n}_0 / 2)}
\end{bmatrix}$$

Figure 3-7 Reordered AG2STM Matrix, AGRSTM

Another problem stems from the difference between the SPADOC and GTDS equinoctial element sets. The GTDS program DC logic expects the partial derivatives to be taken with respect to the semimajor axis at epoch, a_0, whereas the AGRSTM partial derivatives are taken with respect to mean motion at epoch, n_0. Additionally, the first row of the AGRSTM matrix takes the partial deviatives of the mean motion instead of the semimajor axis. To alleviate these differences, the chain rule of partial differentiation can be used as follows:

For the first column of array AGRSTM,

$$\frac{\partial a_i}{\partial a_0} = \frac{\partial a_i}{\partial n_0}\left(\frac{\partial n_0}{\partial a_0}\right) \tag{3.10}$$

Differentiation of the two body relation

$$n^2 a^3 = \mu \tag{3.11}$$

yields

$$\frac{\partial n_0}{\partial a_0} = -\frac{3}{2}\left(\frac{n_0}{a_0}\right) \tag{3.12}$$

Similarly, for the first row of AGRSTM,

$$\frac{\partial a}{\partial a_i} = \left(\frac{\partial a}{\partial n}\right)\frac{\partial n}{\partial a_i} \tag{3.13}$$

where:

$$\left(\frac{\partial a}{\partial n}\right) = -\frac{2}{3}\left(\frac{a}{n}\right) \tag{3.14}$$

Therefore, it is necessary to multiply the first column of the AGRSTM array by the factor $-\left(\frac{3}{2}\frac{n_0}{a_0}\right)$ and the first row by the factor $-\left(\frac{2}{3}\frac{a}{n}\right)$.

Additionally, the semi-major axis used in both the AG2STM and AGRSTM arrays is in NORAD internal units. All GTDS and NORAD distance and angle units are precisely the same with the exception of NORAD's semimajor axis, which is measured in Earth radii. To convert the members of the SPADOC derived arrays from NORAD units into GTDS units, divide column one by the conversion constant AKMPER (km/Earth radius) and multiply row one by AKMPER. Lastly, since any partial derivative taken with respect to mean motion at epoch is multiplied by mean motion at epoch, divide column one by n_0.

These operations are summarized as follows:

1. Multiply column 1 of AGRSTM by $\left(-\frac{3}{2}\frac{n_0}{a_0}\frac{1}{\text{AKMPER}}\frac{1}{n_0}\right)$
2. Multiply row 1 of AGRSTM by $\left(-\frac{2}{3}\frac{a}{n}\ (\text{AKMPER})\right)$

and are implemented in subroutines ORBSGP, ORBGP4, and ORBHAN. After these operations on AGRSTM are performed, the members of the first six rows and columns of the modified AGRSTM array will be equivalent to the members of the GTDS B_2 matrix as depicted in Figure 3-8.

$$\begin{bmatrix} \left(\frac{\partial a}{\partial a_0}\right) & \frac{\partial a}{\partial h_0} & \frac{\partial a}{\partial k_0} & \frac{\partial a}{\partial p_0} & \frac{\partial a}{\partial q_0} & \frac{\partial a}{\partial \lambda_0} \\ \left(\frac{\partial h}{\partial a_0}\right) & \frac{\partial h}{\partial h_0} & \frac{\partial h}{\partial k_0} & \frac{\partial h}{\partial p_0} & \frac{\partial h}{\partial q_0} & \frac{\partial h}{\partial \lambda_0} \\ \left(\frac{\partial k}{\partial a_0}\right) & \frac{\partial k}{\partial h_0} & \frac{\partial k}{\partial k_0} & \frac{\partial k}{\partial p_0} & \frac{\partial k}{\partial q_0} & \frac{\partial k}{\partial \lambda_0} \\ \left(\frac{\partial p}{\partial a_0}\right) & \frac{\partial p}{\partial h_0} & \frac{\partial p}{\partial k_0} & \frac{\partial p}{\partial p_0} & \frac{\partial p}{\partial q_0} & \frac{\partial p}{\partial \lambda_0} \\ \left(\frac{\partial q}{\partial a_0}\right) & \frac{\partial q}{\partial h_0} & \frac{\partial q}{\partial k_0} & \frac{\partial q}{\partial p_0} & \frac{\partial q}{\partial q_0} & \frac{\partial q}{\partial \lambda_0} \\ \left(\frac{\partial \lambda}{\partial a_0}\right) & \frac{\partial \lambda}{\partial h_0} & \frac{\partial \lambda}{\partial k_0} & \frac{\partial \lambda}{\partial p_0} & \frac{\partial \lambda}{\partial q_0} & \frac{\partial \lambda}{\partial \lambda_0} \end{bmatrix}$$

Figure 3-8 GTDS B_2 Matrix

This concludes the required operations necessary to make the SPADOC AG2STM array compatible with the GTDS convention.

There is one more issue to address before calculating the required 6 x 7 array:

$$\frac{\partial \underline{r}(t), \underline{v}(t) \text{ (osculating)}}{\partial \bar{a}_i (o)}$$

This issue is the calculation of the two body partial derivatives:

$$\left(\frac{\partial \underline{r}(t), \underline{v}(t) \text{ (osc)}}{\partial a_i(t) \text{ (osc)}}\right)$$

There are two required sets of input data which the subroutine EPART must have to calculate this partial derivative array. First,

the subroutine must have the osculating equinoctial elements, since these values are required inputs for the calls to subroutines AUXPAR and ECLONG. Additionally, EPART must have the position and velocity vectors. The position and velocity were obtained earlier. Given the position and velocity as input data, a call is made to the GTDS subroutine EQUIN, which calculates the osculating equinoctial orbital elements. Now, with the required position and velocity and osculating equinoctial elements, a call is made to subroutine EPART which yields the required two body partial derivatives.

Finally, the partial derivatives required by GTDS can be obtained by evaluating:

$$\left(\frac{\partial\, \underline{r}(t)\,,\, \underline{v}(t)\ (osc)}{\partial\, \bar{a}_i\ (o)}\right)$$

$$= \left(\frac{\partial\, \underline{r}(t)\,,\ \underline{v}(t)\ (\ osc)}{\partial\ a_i(t)\ (\ osc)}\right) \quad x \quad \left(\frac{\partial\, a_i\ (t)}{\partial\, \bar{a}_i\ (t)}\right) \quad x \quad \left(\frac{\partial\, \bar{a}_i\ (t)}{\partial\, \bar{a}_i\ (o)}\right) \qquad (3.15)^{10}$$

The resulting values are stored in the GTDS common block /DCINT/ for further processing within GTDS. This partial derivative implementation is a key interface which allows the GTDS software to calculate partial derivatives that use SPADOC position, velocity and partial derivatives as inputs.

---

10 Equation 3.15 is evaluated assuming that

$$\left(\frac{\partial\, a_i\ (t)}{\partial\, \bar{a}_i\ (t)}\right) = I_{6x6}$$

The SPADOC equations used to calculate the partial derivatives of the current mean equinoctial elements with respect to the mean equinoctial elements at epoch are very similar to the analytical GTDS (B_2 Matrix) for the J_2 terms. This comparison is further explored in appendices B and C. Appendix B presents the equations used in subroutine G2MEOE by theory type. Appendix C gives a mathematical comparison of the partial derivative equations of GTDS [74] and SPADOC [17].

3.3.8 Observation Modelling

3.3.8.1 Position and Velocity Data (OBSPCE, ROTKEY, ROTRAN)

Subroutine OBSPCE computes the PCE (Inertial Coordinates) observables. At a given observation time, the state is computed via a call to ORBIT. Subroutine OBSPCE transforms the computed state to the same reference frame as the actual observations. [In terms of the Residual Equation, O - C = Residuals, this routine generates the "C" which represents the calculated position or velocity. The "O" represents the actual observation.] Subroutine OBSPCE was modified to support the NORAD true equator and mean equinox of epoch integration coordinate system used by the GP theories. GTDS subroutines ROTKEY and ROTRAN were also modified to support this function.

It would be interesting to review OBSTRK to see if the mods support the OSB obs type. We could then use the LANDSAT data in live exper.

3.3.8.2 Tracking Data (OBSTRK)

Subroutine OBSTRK computes the tracking data observations for use in the DC program. This subroutine also was modified to support the NORAD true equator and mean equinox of epoch integration coordinate system used by the GP theories. This also required modification of GTDS subroutines TRANF and TRKPRT.

3.3.9 Parameter Reset (PSET)

GTDS subroutine PSET resets the dynamic parameters based on the adjusted values from the estimation array. In particular, this routine computes new Keplerian elements from the adjusted mean equinoctial elements. These new Keplerian elements subsequently are used in subroutines RESSGP, RESGP4, and RESHAN to restart the DC. PSET required a minor modification to support the NORAD GP drag solve-for option.

3.3.10 Output Report Modifications

Several GTDS output report routines were modified including CRDLBL, OUTCRD, OUTDC2, OUTDC4, OUTDC6, OUTDC7, OUTDC8, OUTGEN, OUTOG1, OUTOUT, OUTPAR, OUTSEC, OUTSLV, OUTWSD, and PRINT.

3.4 Output Data

Standard GTDS orbit generator print outputs and coordinate systems are supported. In particular, the capability exists to generate Mean of 1950.0 ORB1 files with the NORAD GP theories. This capability is possible because the output routines have access to the NORAD true equator and mean equinox of epoch to Mean of 1950.0 coordinate frame transformation matrix.

The Differential Correction Summary Report provides the following converged DC epoch element set data:

1. Mean equinoctial elements: $\bar{a}, \bar{h}, \bar{k}, \bar{p}, \bar{q}, \bar{\lambda}$ (The internal DC solve parameters).
2. Mean Keplerian elements: $\bar{a}, \bar{e}, \bar{i}, \bar{\Omega}, \bar{\omega}, \bar{M}$.
3. Mean motion and $\dot{n}_0 / 2$.

All of the element sets are supplied in the integrator coordinate system. These output requirements are designed to allow a subsequent Ephemeris Generation run with the same satellite theory as was used in the DC.

3.5 SPADOC Subroutines

As a result of the cooperation of the USAF Electronic Systems Division (ESD) and Ford Aerospace and Communication Corporation (FACC), this implementation presently includes forty-.seven SPADOC subroutines and block data modules. The SPADOC 4B Fortran source code for the SGP, GP4/DP4, and HANDE theories, along with the supporting utilities comprise on the order of several thousand

Fortran 77 source instructions. This section provides a brief description of the key subroutines:

SGPAST: Driver for the SGP theory (CPC[11] ASTSGP). See Figure 3-3. If the initialization control item is set, the routine SGPINT is called to compute initialization factors. The routine SGPUPD is always called to calculate ephemeris data at the requested time.

GP4AST: Driver for the GP4 and DP4 general perturbation theories (CPC ASTGP4). See Figure 3-4. If the initialization control item is set, the routine GP4INT is called to compute initialization factors. The routine GP4UPD is always called to calculate ephemeris data at the requested time.

HANAST: Driver for the HANDE general perturbation theory (CPC ASTHAN). See Figure 3-5. If the specific request type is INITIALIZE, the eleven HANDE time derivatives are computed and returned in the common AELSET to complete the element set record. If the request type is PRE-UPDATE, the only initialization completed is the part that is needed by the update and this initialization is not saved in the element set record. Then, an update follows. Where as if the request type is for an UPDATE ONLY, input elements and pre-update factors are used to compute position and velocity vectors, and mean

---

11 A Computer Program Component (CPC) consists of a functional or logically distinct part of a computer software configuration item (CSCI). A CSCI is a computer program that satisfies an end-use function and is contractually designated for configuration management. CPC's may be given additional designations (e.g., modules, routines) as desired by the project [75,76].

and osculating elements at the input request time. Results are available in the common AEPHOT.

G2MAST: This subroutine is part of a FACC Block B modification to the SPADOC code. This subroutine creates the capability for SGPAST, GP4AST and HANAST to access G_2 partial derivative data. G2MAST is an executive routine. This routine makes the appropriate calls for element set transformations and G_2 matrix computations.

G2MEOE: Calculates the G_2 partial derivatives of the satellite current mean equinoctial elements with respect to the epoch mean orbital elements and $\left(\frac{\dot{n}_0}{2}\right)$. In equation form these derivatives are:

$$\left(\frac{\partial \bar{a}_i(t)}{\partial \bar{a}_i(o)}\right). \tag{3.16}$$

Appendix B gives the equations used in this subroutine.

DSPAST: See Figures 3-4 and 3-5. An executive routine which is the driver for deep space modeling (CPC ASTDSP). This routine always calls the subroutine DP4INT[12] to compute initialization terms. Optionally, this routine can call DSPSEC, which computes deep space secular effects or DSPPER, which computes lunar-solar periodic effects on deep space orbits and updates the mean longitude, ascending node, argument of perigee, eccentricity and inclination.

---

12 The SPADOC routine DSPINT was renamed DP4INT since GTDS had previously employed the name DSPINT in its data simulation program.

HANPER: An executive routine which acts as a driver for HANDE initialization perturbations effects. The modeling includes drag and a deep space geopotential gravity field.

HANPAV: Computes averages for HANDE initialization perturbations effects on the mean motion and eccentricity. The modeling includes drag and a deep space geopotential gravity field.

HANDOT: This routine determines if the ballistic coefficient, B, is non-zero, and if so, it sets appropriate parameters and calls the subroutine HANDRG to incorporate atmospheric effects.

HANDRG: Computes the effects of atmospheric drag using a thirteen point Gauss-Legendre quadrature for each step in the integration. This routine calls the subroutine ATMAST to determine solar flux data and geomagnetic indices based on a specified atmospheric density model.

ATMAST: An executive routine for the dynamic atmospheric density modelling which calls the following:

1. Position of the sun (SUNAST).
2. Atmospheric data initialization (ATMINT).
3. Three atmospheric density models: ATMJ64 - Jacchia 1964, ATMJ70 - Jacchia 1970 and ATMSIS - Mass Spectrometer and Incoherent Scatter.
4. One other atmospheric density model stub (ATMOTH - A Government furnished model). Draper Laboratory intends

to add an additional capability to their orbit determination system by incorporating a modified Harris-Priester atmospheric density model into this subroutine. See Figure 3-5.

Chapter 4

ORBIT GENERATOR TEST CASES

The primary purpose of this chapter is to establish credibility in the accuracy with which the NORAD theory orbit generators have been incorporated into the Draper Laboratory's version of GTDS. As mentioned in Chapter Three, throughout this incorporation an intentional effort has been made to use the actual SPADOC Fortran source code to the maximum extent possible. This ground rule has proven to be the key to obtaining the excellent results of this chapter which establish strong benchmarks for this incorporation.

The first three sections present a comparison of externally generated GP orbit generator test cases and those same test cases run with the NORAD theories incorporated into GTDS. The SGP test case is taken from Spacetrack Report # 3 [5]. Test cases for GP4/DP4 and HANDE were provided by the Ford Aerospace Corporation (FACC). These test cases include the following orbit types: low Earth orbit, geosynchronous, a low Earth orbit near decay, and an eccentric high altitude orbit. A summary of the satellite orbital elements used in the orbit generator test cases is presented in Table 4-1. Aside from the SGP comparison, which had a maximum error of 3.3 meters, the GP4/DP4 and HANDE comparisons had a maximum error of 15.34 centimeters. This error occurred in the HANDE test case after ten days for a low Earth orbit.

Table 4-1. Characteristics of the Satellites Used in the Orbit Generator Test Cases

	Spacetrack #3	LEO #4282	Geosynchronous #7250	Near Decay #9494	Molniya #10455
n_0 (Revs/Day)	16.05824	15.772666	1.0026656	16.063255	2.005933
a_0 (Km)	6637.685619	6716.32803	42,166.20857	6635.0814	26,557.7272
e_0	0,0086731	0.030651	0.00021009	0.0020164	0.73913
i_0 (Degrees)	72.8435	49.4666	0.0099	64.9567	63.178
Ω_0 (Degrees)	115.9689	256.4375	249.2067	228.6393	315.2519
ω_0 (Degrees)	52.6987	262.1979	276.0882	271.2229	282.1774
M_0 (Degrees)	110.5714	128.473	194.66939	88.7752	10.6252
Period (Minutes)	89.69837	91.297184	1436.171697	89.164558	717.87014
Epoch Time					
(Yr/Mo/Day	80/10/1	84/06/221	84/0601	84/06/281	84/07/06
Hr/Min/Secs)	23/41/24.114	18/30/18.849	7/22/10.765	3/56/9.677	3/7/14.226

The last section of Chapter Four presents an analysis of the accuracy achieved in the incorporation of the orbit generator partial derivatives for each NORAD theory into GTDS. There were no externally generated partial derivative test cases available for this analysis. Nonetheless, an investigation of the elements of the state transition matrix for each NORAD theory indicates that the NORAD orbit generator partial derivatives have been accurately incorporated. Additionally this section points out some of the differences in the equations which generate the partial derivatives for each theory type. These differences are depicted in Appendix B in which the partial derivative equations for each NORAD theory have been decoded from the SPADOC software.

The results of the test cases used in this analysis are limited to point comparisons from other similar test cases. However, with the use of the NORAD theory test drivers[1], additional comparisons could include statistics and graphs. (See section 6.3 for details.)

---

[1] FACC has supplied the NORAD theory stand alone orbit generator test drivers to Draper Laboratory.

4.1 SGP Orbit Generator

The test case used for this comparison was taken from Spacetrack Report # 3 [5] and the results are shown in Table 4-2. In this table, a maximum error of 3.32 meters is indicated in the z-component of position at twelve hours past epoch. The errors in this orbit generator test case are approximately one order of magnitude greater, relative to the GP4/DP4 and the HANDE test cases. This discrepancy is most likely due to the fact that the results given in [5] were generated on the Honeywell 6080 with a mix of single and double precision arithmetic; however, both the SPADOC software and GTDS are coded exclusively in double precision on the IBM. One other observation worth noting is that Table 4-2 shows that the position errors are not monotonically increasing in magnitude. With the exception of the twelve hour z-component, six significant digits were matched throughout the comparison thereby establishing a very good SGP orbit generator benchmark.

Ref. 5 states that the results are only accurate to 5 or 6 digits after a 1 day prediction

Table 4-2. Benchmark of Spacetrack Report #3 SGP Test Case

TSINCE Epoch (Hrs)	Position Component	Spacetrack #3 (Kilometers)	GTDS (Kilometers)	Difference |(Meters)|
0	X	2328.96594238	2328.966084	0.14162
	Y	-5995.21600342	-5995.216040	0.03658
	Z	1719.97894287	1719.978736	0.20687
6	X	2456.00610352	2456.006670	0.56648
	Y	-6071.94232177	-6071.942438	0.11623
	Z	1222.95977784	1222.958812	0.96584
12	X	2567.39477539	2567.396198	1.42261
	Y	-6112.49725342	-6112.497355	0.08158
	Z	713.97710419	713.9737757	3.32849
18	X	2663.03179932	2663.032~~9~~7~~8~~98	0.9~~7~~9868
	Y	-6115.37414551	-6115.373847	0.29851
	Z	195.73919105	195.7363780	2.81305
24	X	2742.85470581	2742.855361	0.65519
	Y	-6099.13580322	-6099.135509	0.29422
	Z	-328.86091614	-328.8628486	1.93246

4.2 GP4/DP4 Orbit Generator

The Ford Aerospace Corporation supplied four test cases for this orbit generator which include the following orbits: NSSC 4282 - low Earth orbit, NSSC 7250 - geosynchronous, NSSC 9494 - low Earth orbit near decay, NSSC 10455 - Molniya (high eccentricity). Table 4-1 summarizes the characteristics of these orbits. Tables 4-3 through 4-6 present the outstanding results of the position comparisons. As in the SGP test case, all of the GP4/DP4 results indicate that there is no secular growth in the errors. It should be noted that the block data PHYSBD0 was used to generate the results of this section and in all the GTDS data twelve significant digits were used.

In the low Earth orbit (4282) test case (Table 4-3), a maximum error of 0.043 millimeters occurred in the z-component of the position vector after eighteen hours. In general, all the results show that the errors can be attributed to roundoff errors. Throughout the comparison the position components matched to eleven significant digits with only two exceptions.

The geosynchronous orbit (7250) test case results (Table 4-4) indicate a maximum error of 6.19 millimeters in the y-component of the position vector after twenty-four hours. An accuracy of at least eight significant digits was obtained for this case.

The results of the low Earth orbit (9494) near decay (Table 4-5) indicate a maximum error of 0.058 millimeters in the x-component of position after twelve hours. These results are

comparable to the results of the low Earth orbit (4282). Throughout this comparison an accuracy of eleven significant digits of accuracy was obtained with three exceptions.

The high eccentricity test case (10455) results (Table 4-6) indicate a maximum error of 10.34 millimeters in the z-component of position after twenty-four hours. With two exceptions, at least nine significant digits of accuracy were obtained throughout the entire comparison.

Overall, the results of the GP4/DP4 comparisons establish an excellent set of benchmarks. The comparison results have a maximum position error of 10.34 millimeters and in general, these results indicate that nine significant digit accuracy was obtained in the geosynchronous and Molniya cases, and an eleven digit accuracy in the low altitude case.

Table 4-3. Benchmark of FACC GP4/DP4 Test Case for Satellite #4282 (Low Earth Orbit)

TSINCE Epoch (Hrs)	Position Component	FACC (Earth radii)	FACC (Kilometers)	GTDS (Kilometers)	Difference |(Millimeters)|
0	X	0.161774617934	1031.8203527	1031.82035275	0.02
	Y	-0.961838779516	-6134.737584	-6134.73758398	0.03
	Z	0.447368026043	2853.3736648	2853.37366418	0.01
6	X	$-0.920145368523 \times 10^{-1}$	-586.88113799	-586.881138006	0.01
	Y	$-0.103889077286 \times 10^{1}$	6626.1855996	-6626.18559958	0.02
	Z	0.208631155884	1330.6776774	1330.67767743	0.02
12	X	-0.334409454982	-2132.9086491	-2132.90864915	0.01
	Y	-0.99727460390	-6360.7520557	-6360.75205574	0.006
	Z	$-0.485602199737 \times 10^{-1}$	-309.7236386	-309.723638621	0.02
18	X	-0.535177137495	-3413.4320318	-3413.43203185	0.03
	Y	-0.843535895042	-5380.1858159	-5380.18581592	0.009
	Z	-0.297487105318	-1897.4129184	-1897.41291847	0.043
24	X	-0.669190791127	-4268.1892065	-4268.18920656	0.04
	Y	-0.597153076274	-3808.7229361	-3808.72293614	0.02
	Z	-0.512437089011	-3268.3929327	-3268.39293272	0.007

Table 4-4. Benchmark of FACC GP4/DP4 Test Case for Satellite #7250 (Geosynchronous)

TSINCE Epoch (Hrs)	Position Component	FACC (Earth radii)	FACC (Kilometers)	GTDS (Kilometers)	Difference |(Millimeters)|
0	X	$0.661214394109 \times 10^{1}$	42173.146695	42173.1466656	0.10
	Y	$-0.635386758987 \times 10^{-2}$	-40.52582526	-40.5258252576	0.06
	Z	$0.159957206443 \times 10^{-2}$	10.202286569	10.2022865705	0.03
6	X	$-0.200184702687 \times 10^{-1}$	-127.68050581	-127.680506256	0.44
	Y	$0.661042407104 \times 10^{1}$	42162.177132	42162.1771320	0.34
	Z	$0.868146992809 \times 10^{-3}$	5.5371587021	5.53715871976	0.02
12	X	$-0.660927039255 \times 10^{1}$	-42154.818815	-42154.8188145	0.69
	Y	$-0.517543340474 \times 10^{-1}$	-330.09612934	-330.096130933	1.55
	Z	$-0.131313307985 \times 10^{-2}$	-8.3753399934	-8.37534005762	0.022
18	X	$0.820746321453 \times 10^{-1}$	523.48308386	523.483087368	3.47
	Y	$-0.661066187570 \times 10^{1}$	-42163.693883	-42163.6938815	2.47
	Z	$-0.826162282119 \times 10^{-3}$	-5.2693745537	-5.26937456658	0.0006
24	X	$0.661126734454 \times 10^{1}$	42167.555645	42167.5556431	1.47
	Y	0.107052137824	682.79298705	682.792993249	6.19
	Z	$0.104710850004 \times 10^{-2}$	6.6785993726	6.67859937459	0.002

Table 4-5. Benchmark of FACC GP4/DP4 Test Case for Satellite #9494 (Near Decay)

TSINCE Epoch (Hrs)	Position Component	FACC (Dimensionless)	FACC (Kilometers)	GTDS (Kilometers)	Difference |(Millimeters)|
0	X	-0.687119006419	-4382.5377839	-4382.53778400	0.05
	Y	-0.781768800324	-4986.2269472	-4986.22694725	0.02
	Z	$0.184675162429 \times 10^{-2}$	11.778831144	11.7788311711	0.03
6	X	-0.667858041046	-4259.6887466	-4259.68874662	0.03
	Y	-0.793838033395	-5063.2061451	-5063.20614512	0.02
	Z	$0.853045788077 \times 10^{-1}$	544.0841197	544.084119853	0.05
12	X	-0.643815752589	-4106.3437851	-4106.34378514	0.058
	Y	-0.800568137397	-5106.131657	-5106.13165701	0.04
	Z	0.168104144987	1072.1909307	1072.19093078	0.0016
18	X	-0.615005646980	-3922.5890422	-3922.58904220	0.0027
	Y	-0.802059641786	-5115.6446733	-5115.64467336	0.04
	Z	0.249593209221	1591.9391835	1591.93918349	0.0016
24	X	-0.581481613572	-3708.7682314	-3708.76823137	0.0027
	Y	-0.798452249411	-5092.6362378	-5092.63623779	0.0007
	Z	0.329129952129	2099.2352672	2099.23526722	0.055

Table 4-6. Benchmark of FACC GP4/DP4 Test Case for Satellite #10455 (Molniya)

TSINCE Epoch (Hrs)	Position Component	FACC (Dimensionless)	FACC (Kilometers)	GTDS (Kilometers)	Difference |(Millimeters)|
0	X	$0.115286773337 \times 10^{1}$	7353.1460406	7353.14604055	0.03
	Y	$-0.1159243821 \times 10^{1}$	-7393.8135883	-7393.81358823	0.02
	Z	$-0.190629924024 \times 10^{-1}$	-121.58633904	-121.586339043	0.01
6	X	0.916204871837	5843.6783602	5843.67836006	0.13
	Y	$0.352520453626 \times 10^{1}$	22484.230434	22484.2304347	0.18
	Z	$0.622392867309 \times 10^{1}$	39697.057307	39697.0573170	0.34
12	X	$0.124827859414 \times 10^{1}$	7961.6893908	7961.68939302	2.24
	Y	$-0.117434234091 \times 10^{1}$	-7490.1139865	-7490.11398665	0.11
	Z	$0.974114386133 \times 10^{-1}$	621.303306	621.303308616	2.60
18	X	0.897349428439	5723.4157967	5723.41579546	1.24
	Y	$0.354020047093 \times 10^{1}$	22579.87653	22579.8765309	0.25
	Z	$0.621376717934 \times 10^{1}$	39632.245928	39632.2459271	1.24
24	X	$0.133759001734 \times 10^{1}$	8531.3297052	8531.32971288	7.63
	Y	$-0.118404254923 \times 10^{1}$	-7551.9832245	-7551.98322500	0.27
	Z	0.213383228395	1360.9870374	1360.98704775	

4.3 HANDE Orbit Generator

One test case was available from FACC and was exercised using the eighteen parameter HANDE input option. However, the extra time derivative terms, which are required in the eighteen parameter input for the HANDE orbit generator, were computed on a calculator with only eight digit accuracy. Also, this set of data is different from the other test cases in that it covers a ten day time span wheras all the other test cases are for one day. This test utilized data from the low Earth orbit (4282) and the comparison results are indicated in Table 4-7. This table shows a maximum error of 15.34 centimeters which occurs in the z-component of position after ten days. Throughout this ten day period an accuracy of at least seven significant digits was obtained in all position components. The HANDE results are comparable to the GP4/DP4 results of section 4.2 and establish an excellent benchmark for the HANDE orbit generator.

Although this test did establish an outstanding numerical benchmark for HANDE, it did not test the complete functionality of the HANDE theory. For this application, only the pre-update and update functions are tested and not the initialization functionality.

Table 4-7. Benchmark of FACC Hande Test Case for Satellite #4282 (Low Earth Orbit)

TSINCE Epoch (Hrs)	Position Component	FACC (Dimensionless)	FACC (Kilometers)	GTDS (Kilometers)	Difference (Millimeters)
0	X	0.161738467798483	1031.5897823	1031.589782	0.25777165
	Y	-0.961828956752921	-6134.6749331	-6134.674933	0.06066125
	Z	0.447408218797824	2853.6300196	2853.630020	0.4478433
10	X	0.894397013370494	5704.5848949	5704.584874	20.870665
	Y	0.533423985035906	3402.2501888	3402.250284	95.24068
	Z	-0.189409785858578	1208.0811845	-1208.081031	153.47239

4.4 State Transition Matrix Analysis

This section analyzes the accuracy of the results attained for the incorporation of the SPADOC orbit generator partial derivatives into Draper Laboratory's GTDS. Precisely, these are the partial derivatives of current mean equinoctial orbital elements with respect to the epoch mean equinoctial elements, and are represented as follows:

$$\frac{\partial \bar{a}_i(t)}{\partial \bar{a}_i(o)} \qquad (3.16)$$

These partial derivatives are members of both the "Modified" AGRSTM matrix[2] and the GTDS B_2 matrix. See Figures 3-7 and 3-8 for an exact description of the two arrays.

This analysis did not have access to externally generated partial derivative test cases. Therefore, to establish confidence in the accuracy of the GP theory partial derivatives, a three step approach was utilized. This included the following:

1. A initial comparison of DSST partials to SGP partials to get a preliminary accuracy estimate.

---

2 For the purposes of this analysis the state transition matrix will be defined to include only the first six rows and columns of the AGRSTM matrix.

2. Use of a single-sided finite differencing technique to ensure that the correct partials were being generated. (See Appendix D.)
3. Additional comparisons of SGP, DP4/DP4, and HANDE partial derivatives to the DSST partial derivatives. The DSST orbit generator was configured to include only the J_2, J_3, and J_4 zonal harmonics in its geopotential model and the test case used for comparisons is the Spacetrack SGP test case as described in Table 4-1.

The initial step was to compare partial derivatives generated by the DSST orbit generator with a geopotential model designed to replicate the behavior of the SGP orbit generator. The partial derivatives, and the differences between the DSST and SGP partials are presented in Tables 4-10 and 4-11 respectively. The initial comparison produced promising results. Thirty-four of thirty-six partial derivatives were within 1.28% agreement between DSST and SGP. Considering the differences between the DSST and SGP orbit generators, and the fact that a single-sided finite differencing technique was utilized for the analysis, the 1.28% agreement seems quite reasonable. However, two of the partial derivatives, $\frac{\partial \lambda}{\partial h_o}$ and $\frac{\partial \lambda}{\partial k_o}$, were in disagreement by more than 30%. These larger errors caused some concern since they suggested a possible error. In order to ensure that the two partial derivatives of concern

were being generated correctly, it was necessary to accomplish a finite differencing analysis.

4.4.1 Finite Differencing

A single-sided finite differencing technique was used to analyze two partial derivatives, $\frac{\partial \lambda}{\partial h_o}$ and $\frac{\partial \lambda}{\partial k_o}$. The specific equation used in this analysis is given in Appendix D and is as follows:

$$\frac{f(x_o + \Delta x) - f(x_o)}{\Delta x} \cong \left[\frac{\partial f(x)}{\partial x}\right]_{x = x_o} \qquad (D.3)$$

Using equation (D.3), the necessary forms of the partial derivative equations are as follows:

$$\frac{\lambda\,(\text{perturbed}) - \lambda\,(\text{unperturbed})}{\Delta k_o} \cong \frac{\partial \lambda}{\partial k_o} \qquad (4.1)$$

and,

$$\frac{\lambda\,(\text{perturbed}) - \lambda\,(\text{unperturbed})}{\Delta h_o} \cong \frac{\partial \lambda}{\partial h_o}. \qquad (4.2)$$

The NORAD orbit generators in GTDS assume Keplerian element input (See Chapter Three). Therefore, further specification of the test case was required. Since,

$$k = e \cos(\Omega + \omega) = e \cos \pi \tag{4.3}$$

and,

$$h = e \sin(\Omega + \omega) = e \sin \pi \tag{4.4}$$

the eccentricity was chosen as the parameter to be perturbed, while setting π equal to zero and then to ninety degrees. With these given constraints, k is equal to e when π is zero and h is equal to e when π is ninety degrees. Now equations (4.1) and (4.2) can be modified as follows:

$$(\text{For } \pi = 0^\circ) \qquad \frac{\lambda\,(\text{perturbed}) - \lambda\,(\text{unperturbed})}{\Delta e_o} \cong \frac{\partial \lambda}{\partial k_o} \tag{4.5}$$

$$(\text{For } \pi = 90^\circ) \qquad \frac{\lambda\,(\text{perturbed}) - \lambda\,(\text{unperturbed})}{\Delta e_o} \cong \frac{\partial \lambda}{\partial h_o} \tag{4.6}$$

Given equations (4.5) and (4.6) it was necessary to make four SGP orbit generator runs to complete the analysis. Again, all runs utilized the Spacetrack test case as described in Table 4-1 with the exception that π was set to zero degrees for two of the runs and to

ninety degrees for the others. The Δe was .0002, and for the purposes of this analysis, the eccentricity value listed in Table 4-1 was designated as the perturbed value. The partial derivatives that were obtained from finite differencing were compared to both the SGP partials and the DSST partials that were generated with the modified geopotential model as previously described. A summary of all of these results is presented in Tables 4-8 and 4-9. Both tables indicate that the partial derivatives computed by finite differencing the SGP theory compare to within 1 - 2% of the SGP analytic partials. Additionally, the results indicate that the DSST partials do not compare favorably with the finite difference calculated partials. The combination of these two observations indicates that the SGP orbit generator was propagating the appropriate partial derivatives based on the "SGP mean" elements.

Table 4-8. Finite Differencing Analysis for $\frac{\partial \lambda}{\partial k_0}$

	SGP Analytic vs SGP Finite Differencing			
	T I M E			
	Epoch	1 Day	3 Days	5 Days
SGP Analytic	$-2.961452285747845 \times 10^{-3}$	$-5.922904571495689 \times 10^{-3}$	$-1.184580914299138 \times 10^{-2}$	$-1.776871371448707 \times 10^{-2}$
SGP Finite Diff	-2.995×10^{-3}	-5.99×10^{-3}	-1.1985×10^{-2}	-1.797×10^{-2}
Δ % Error	1.1328	1.1328	1.17502	2.01286

	DSST vs SGP Finite Differencing			
	T I M E			
	Epoch	1 Day	3 Days	5 Days
DSST	0	$-4.369445765706 \times 10^{-3}$	$-1.303698034099 \times 10^{-2}$	$-2.160983331011 \times 10^{-2}$
SGP Finite Diff	-2.995×10^{-3}	-5.99×10^{-3}	-1.1985×10^{-2}	-1.797×10^{-2}
Δ % Error	N/A	37.08833	8.0692	16.84341

Table 4-9. Finite Differencing Analysis for $\frac{\partial \lambda}{\partial h_0}$

	SGP Analytic vs SGP Finite Differencing			
	TIME			
	Epoch	1 Day	3 Day	5 Day
SGP Analytic	$-2.961452285747845 \times 10^{-3}$	$-5.922904571495689 \times 10^{-3}$	$-1.184580914299138 \times 10^{-2}$	$-1.776871371448707 \times 10^{-2}$
SGP Finite Diff	-2.995×10^{-3}	-5.99×10^{-3}	-1.198×10^{-2}	-1.7975×10^{-2}
Δ % Error	1.1328	1.1328	1.1328	-1.1609

	DSST vs SGP Finite Differencing			
	TIME			
	Epoch	1 Day	3 Day	5 Day
DSST	$-2.168404344971 \times 10^{-19}$	$-4.372782553122 \times 10^{-3}$	$-1.306479060579 \times 10^{-2}$	$-2.168083327141 \times 10^{-2}$
SGP Finite Diff	-2.995×10^{-3}	-5.99×10^{-3}	-1.198×10^{-2}	-1.7975×10^{-2}
Δ % Error	N/A	36.98371	8.30316	17.0926

4.4.2 SGP State Transition Matrix

Tables 4-10 and 4-11 present both the DSST and SGP state transition matrices at one day past epoch. An initial observation of Table 4-11 indicates that only $\frac{\partial \lambda}{\partial h_o}$ and $\frac{\partial \lambda}{\partial k_o}$ are significantly different from the DSST values. Except for these, the SGP partial derivatives are within 1.28% of the DSST partial derivatives. However, studying the equations which are unique to the SGP theory, as listed in Appendix B, reveals a possible explanation for these discrepancies.

There are three partial derivative equations that differ from the DSST equations[3] and they correspond to the following partials:

$$\frac{\partial \lambda}{\partial a_o}, \quad \frac{\partial \lambda}{\partial h_o}, \text{ and } \frac{\partial \lambda}{\partial k_o} \tag{4.7}$$

After examining the applicable equations, the only difference is found in the definition of the first time derivative of the mean longitude at epoch, $\dot{L}_o$. The SGP theory uses the following definition:

$$\dot{L}_o \equiv \dot{\pi}_o \tag{4.8}$$

---

3 It should be noted that Appendix C establishes that the DSST and SGP equations are equivalent with the exception of the partial derivatives listed in equation (4.7).

while DSST uses a different definition:

$$\dot{L}_o \equiv \dot{\pi}_o + \dot{M}_o \tag{4.9}$$

This algorithmic difference is directly related to the unique properties of the Kozai mean motion used in the SGP theory. Thus the difference in the partial derivatives can be attributed to the difference in the "DSST mean" elements versus the "SGP mean" elements.

Table 4-10. DSST B_2 Matrix vs SGP "Modified" AGRSTM Array At Epoch + 1 Day

	1	7	13	19	25	31
DSST	1.000	0	0	0	0	0
SGP	0.99980619	0	0	0	0	0
	2	8	14	20	26	32
DSST	$-3.829448979\ D^{-7}$	$9.96192463\ D^{-1}$	$-8.72617836\ D^{-2}$	$6.64434462\ D^{-4}$	$-3.23670195\ D^{-4}$	0
SGP	$-3.80024955\ D^{-7}$	$9.96190373\ D^{-1}$	$-8.72857837\ D^{-2}$	$6.59378864\ D^{-4}$	$-3.21157628\ D^{-4}$	0
	3	9	15	21	27	33
DSST	$-1.11352531\ D^{-7}$	$8.72385292\ D^{-2}$	$9.96180397\ D^{-1}$	$1.93201851\ D^{-4}$	$-9.41156133\ D^{-5}$	0
SGP	$-1.11140333\ D^{-7}$	$8.72627065\ D^{-2}$	$9.96178273\ D^{-1}$	$1.93295290\ D^{-3}$	$-9.41465680\ D^{-4}$	0
	4	10	16	22	28	34
DSST	$-6.89903301\ D^{-6}$	$8.80930579\ D^{-5}$	$-4.44556613\ D^{-4}$	$9.49664730\ D^{-1}$	$-2.05709117\ D^{-2}$	0
SGP	-6.89976339	$8.92092790\ D^{-5}$	$-4.45142679\ D^{-4}$	$9.49657500\ D^{-1}$	$-2.05837484\ D^{-2}$	0
	5	11	17	23	29	35
DSST	$-1.59306668\ D^{-5}$	$2.03417215\ D^{-4}$	$1.02653282\ D^{-3}$	$-6.93254087\ D^{-2}$	1.05450487	0
SGP	$-1.59355625\ D^{-5}$	$2.06036056\ D^{-4}$	$-1.02809307\ D^{-3}$	$-6.93514190\ D^{-2}$	1.05451440	0
	6	12	18	24	30	36
DSST	$-2.27190945\ D^{-2}$	$-8.70324152\ D^{-4}$	$4.39204055\ D^{-3}$	$-2.28815524\ D^{-1}$	$1.11464369\ D^{-1}$	1.0
SGP	$-2.27548577\ D^{-2}$	$-5.95664077\ D^{-4}$	$2.97228613\ D^{-3}$	$-2.28885378\ D^{-1}$	$1.11481106\ D^{-1}$	1.0

Table 4-11. DSST B_2 Matrix - SGP "Modified" AGRSTM Array At Epoch + 1 Day

% ERROR

1 0.01948	7 0.0	13 0.0	19 0.0	25 0.0	31 0.0
2 -0.76355	8 0.0002097	14 0.027503	20 0.760887	26 -0.7762738	32 0.0
3 -0.1905641	9 -0.027714	15 0.0002132	21 -0.048363	27 0.03289	33 0.0
4 0.010586	10 -1.267093	16 0.1318315	22 0.0007613	28 0.062402	34 0.0
5 0.030731	11 -1.287423	17 0.1519922	23 0.037519	29 -0.0009037	35 0.0
6 0.1574147	12 -31.558365	18 32.32562	24 0.030528	30 -0.015015	36 0.0

4.4.3 GP4/DP4 State Transition Matrix

Tables 4-12 and 4-13 present both the DSST and GP4/DP4 state transition matrices at one day past epoch. An initial observation of Table 4-13 indicates that the GP4/DP4 partial derivatives compare extremely well with the DSST partial derivatives. The worst comparison is for $\frac{\partial \lambda}{\partial h_o}$, which is within 1.32% of the DSST value. Again, looking at the applicable equations in Appendix B reveals that GP4/DP4 has a unique definition of $\dot{L}_o$ which follows:

$$\dot{L}_o \equiv \dot{\pi}_o + \dot{M}_o - n_o \tag{4.10}$$

As in SGP, this different definition affects $\frac{\partial \lambda}{\partial a_o}$, $\frac{\partial \lambda}{\partial h_o}$, and $\frac{\partial \lambda}{\partial k_o}$. A comparison of elements (6), (12) and (18) for Tables 4-9, 4-13 and 4-15 indicates that the corresponding GP4/DP4 partial derivatives are much closer to the DSST partial derivatives than SGP, but not quite as good as the HANDE partials. This is a consistent observation since the HANDE equations for these partials are equivalent to the DSST equations for these partials.

Table 4-12. DSST B_2 Matrix vs GP4/DP4 "Modified" AGRSTM Array At Epoch + 1 Day

1 1.000	7 0	13 0	19 0	25 0	31 0
0.99984296	0	0	0	0	0
2 $-3.829448979\ D^{-7}$	8 $9.96192463\ D^{-1}$	14 $-8.72617836\ D^{-2}$	20 $6.64434462\ D^{-4}$	26 $-3.23670195\ D^{-4}$	32 0
$-3.82187303\ D^{-7}$	$9.96189674\ D^{-1}$	$-8.72941820\ D^{-2}$	$6.58236154\ D^{-4}$	$-3.20601058\ D^{-4}$	0
3 $-1.11352531\ D^{-7}$	9 $8.72385292\ D^{-2}$	15 $9.96180397\ D^{-1}$	21 $1.93201851\ D^{-4}$	27 $-9.41156133\ D^{-5}$	33 0
$-1.12042753\ D^{-7}$	8.72709864	$9.96177511\ D^{-1}$	$1.92969756\ D^{-4}$	$-9.39880131\ D^{-5}$	0
4 $-6.89903301\ D^{-6}$	10 $8.80930579\ D^{-5}$	16 $-4.44556613\ D^{-4}$	22 $9.49664730\ D^{-1}$	28 $-2.05709117\ D^{-2}$	34 0
$-6.89705916\ D^{-6}$	$8.91249345\ D^{-5}$	$-4.44721811\ D^{-4}$	$9.49572744\ D^{-1}$	$-2.04950242\ D^{-2}$	0
5 $-1.59306668\ D^{-5}$	11 $2.03417215\ D^{-4}$	17 $1.02653282\ D^{-3}$	23 $-6.93254087\ D^{-2}$	29 1.05450487	35 0
$-1.59275011\ D^{-5}$	$2.05817793\ D^{-4}$	$-1.02700397\ D^{-3}$	$-6.95853765\ D^{-2}$	1.05460781	0
6 $-2.27190945\ D^{-2}$	12 $-8.70324152\ D^{-4}$	18 $4.39204055\ D^{-3}$	24 $-2.28815524\ D^{-1}$	30 $1.11464369\ D^{-1}$	36 1.0
-2.27505835	$-8.81860787\ D^{-4}$	$4.40037043\ D^{-3}$	$-2.28191759\ D^{-1}$	1.111432710^{-1}	1.0

Table 4-13. DSST B_2 Matrix - GP4/DP4 "Modified" AGRSTM Array At Epoch + 1 Day

% ERROR

1 0.015704	7 0.0	13 0.0	19 0.0	25 0.0	31 0.0
2 -0.19889	8 0.0002799	14 0.03712	20 0.93286	26 -0.948229	32 0.0
3 0.61985	9 -0.037205	15 0.0002897	21 0.1201308	27 -0.135578	33 0.0
4 -0.02861	10 -1.17134	16 0.0371601	22 0.0099567	28 -0.3689068	34 0.0
5 -0.0198717	11 -1.1801252	17 0.045897	23 0.374996	29 -0.0097619	35 0.0
6 0.138601	12 1.325556	18 -0.189658	24 -0.272606	30 0.28807	36 0.0

Further analysis of the equations which are unique to the GP4/DP4 theory indicates that four more partial derivatives are affected. These partials are all a function of the variable PAR3, which in turn is a function of the GP4/DP4 drag parameter, BSTAR. The following partial derivatives are affected:

$$\frac{\partial h}{\partial h_o}, \quad \frac{\partial k}{\partial h_o}, \quad \frac{\partial h}{\partial k_o}, \text{ and } \frac{\partial k}{\partial k_o} \tag{4.11}$$

Respectively, these partials correspond to elements (8), (9), (14) and (15) of the state transition matrix. A comparison of these elements in Tables 4-9, 4-13 and 4-15 indicates a large error between the GP4/DP4 values and the HANDE values, but a relatively small error between the GP4/DP4 and SGP values. Both of these observations are consistent, but for different reasons. The comparison of Tables 4-9 and 4-13 is consistent because of a software design that defines the R3 field of the ELEMENT3 input card in the GTDS Ephemeris Generation Program. For these test cases, that field contains a value[4] of 0.66816×10^{-4}. In order to generate the results for the SGP comparison (Table 4-9), this R3 value is not applicable because there are no drag dependent partials in the state transition matrix for SGP. However, when generating the GP4/DP4 results, this value represents the parameter BSTAR with the units (1/Earth Radius). Therefore, BSTAR is properly utilized by the GP4/DP4 orbit generator and, accordingly, the drag dependent partial

[4] This value is from the Spacetrack SGP test case as previously described.

derivatives are calculated correctly. Another reason for better agreement between the GP4/DP4 and SGP elements is that the DSST geopotential model utilized is very compatible with the SGP theory and with the GP4/DP4 theory, for this low altitude test case.

The reason that the comparison of Tables 4-13 and 4-15 is consistent is a bit more complicated. An initial analysis indicated that an input data error may have caused the errors. By design, the R3 field of the ELEMENT3 card becomes the drag parameter, B, for a HANDE theory type. In the HANDE run that generated the results of Table 4-15, the R3 value is the same as for the GP4/DP4 test case, but it represents a drag parameter with the units of (meters^2 / kilogram) because the theory type is designated as HANDE. To find out how much this anomaly would affect the results, the applicable equations in Appendix B were investigated. The HANDE equations for

$$\frac{\partial h}{\partial h_o}, \quad \frac{\partial k}{\partial h_o}, \quad \frac{\partial h}{\partial k_o}, \text{ and } \frac{\partial k}{\partial k_o} \tag{4.11}$$

are functions of the drag parameter and other HANDE time derivative terms that were not input into the DSST run. Since the DSST run did not input the extra drag terms and the R3 value was not changed to the appropriate B value, the comparison of the values for the (8), (9), (14) and (15) elements in Tables 4-13 and 4-15 is consistent. Another factor which would cause errors in these elements is the fact that the DSST geopotential model used in this test case is not an optimum selection for the HANDE model.

4.4.4 HANDE State Transition Matrix

Tables 4-14 and 4-15 tabulate both the DSST and HANDE state transition matrices at one day past epoch. The values of Table 4-15 compare very well with the DSST values with the exception of elements (8), (9), (14) and (15), which correspond to the drag dependent partials. An inconsistency is expected for these elements in Table 4-15 for the reasons discussed in section 4.4.3. In contrast, relative to SGP and GP4/DP4, Table 4-15 shows the smallest errors when compared to the following DSST partial derivatives:

$$\frac{\partial \lambda}{\partial a_o}, \quad \frac{\partial \lambda}{\partial h_o}, \text{ and } \frac{\partial \lambda}{\partial k_o}. \tag{4.7}$$

This observation is supported by the equations in Appendix B which show that the HANDE equations use the same definition of the first time derivative of the mean longitude at epoch as do the DSST equations. (See equation 4.9). Therefore, the DSST and HANDE partial derivative equations are equivalent for these terms.

Table 4-14. DSST B_2 Matrix vs HANDE "Modified" AGRSTM Array At Epoch + 1 Day

1 1.000 0.99999223	7 0 0	13 0 0	19 0 0	25 0 0	31 0 0
2 $-3.829448979\ D^{-7}$ $-3.82153892\ D^{-7}$	8 $9.96192463\ D^{-1}$ $9.96365423\ D^{-1}$	14 $-8.72617836\ D^{-2}$ $-8.30710448\ D^{-2}$	20 $6.64434462\ D^{-4}$ $6.58460467\ D^{-4}$	26 $-3.23670195\ D^{-4}$ $-3.20710312\ D^{-4}$	32 0 0
3 $-1.11352531\ D^{-7}$ -1.11025843	9 $8.72385292\ D^{-2}$ $8.29557343\ D^{-2}$	15 $9.96180397\ D^{-1}$ $9.96530824\ D^{-1}$	21 $1.93201851\ D^{-4}$ $1.89977962\ D^{-4}$	27 $-9.41156133\ D^{-5}$ $-9.25308274\ D^{-5}$	33 0 0
4 $-6.89903301\ D^{-6}$ $-6.88663600\ D^{-6}$	10 $8.80930579\ D^{-5}$ $8.90231305\ D^{-5}$	16 $-4.44556613\ D^{-4}$ $-4.44421382\ D^{-4}$	22 $9.49664730\ D^{-1}$ $9.49631949\ D^{-1}$	28 $-2.05709117\ D^{-2}$ -2.04633706	34 0 0
5 $-1.59306668\ D^{-5}$ $-1.59006322\ D^{-5}$	11 $2.03417215\ D^{-4}$ $2.05546519\ D^{-4}$	17 $-1.02653282\ D^{-3}$ $-1.02565034\ D^{-3}$	23 $-6.93254087\ D^{-2}$ $-6.94938869\ D^{-2}$	29 1.05450487 1.05453705	35 0 0
6 $-2.27190945\ D^{-2}$ -2.27296973	12 $-8.70324152\ D^{-4}$ $-8.80104491\ D^{-4}$	18 $4.39204055\ D^{-3}$ $4.39160674\ D^{-3}$	24 $-2.28815524\ D^{-1}$ $-2.27897663\ D^{-1}$	30 $1.11464369\ D^{-1}$ $1.11000028\ D^{-1}$	36 1.0 1.0

Note: The top element in each numbered cell is the DSST value and bottom value is the HANDE value

Table 4-15. DSST B_2 Matrix - HANDE "Modified" AGRSTM Array At Epoch + 1 Day

	1 0.000767	7 0.0	13 0.0	19 0.0	25 0.0	31 0.0
%	2 -0.20762	8 -0.01736	14 -4.80248	20 0.899109	26 -0.91447	32 0.0
E	3 -0.29338	9 4.90929	15 -0.035177	21 1.66866	27 -1.68387	33 0.0
R O	4 -0.17969	10 -1.05578	16 -0.030419	22 0.00345	28 -0.52278	34 0.0
R	5 -0.188533	11 -1.04676	17 -0.085967	23 0.24302	29 -0.003051	35 0.0
	6 0.046669	12 1.123758	18 0.0098771	24 -0.40113	30 0.416582	36 0.0

Excluding the drag partials, the HANDE partial derivatives are within 1.68% of the DSST partial derivatives. Again, in this low altitude test case, with a modified DSST geopotential model, these errors can be attributed to the differences between "DSST mean" and "HANDE mean" elements.

Chapter 5

DIFFERENTIAL CORRECTION TEST CASES

The purpose of this chapter is two fold. First, the results of this chapter demonstrate that the incorporated NORAD theories provide the appropriate data flows to accomplish differential correction fits to both simulated and real data. Therefore, these results demonstrate part of the analysis capability which exists as a result of incorporating the NORAD theories into Draper Laboratory's GTDS computer program. Additionally, this chapter presents an analysis of both low altitude and geosynchronous test cases to develop preliminary insight to the accuracy performance of the NORAD theories. This chapter first describes the methodology used in these analyses. The approach includes a Precise Conversion of Elements (PCE) test with the simulated data, and another deterministic analysis employing real tracking data.

5.1 Test Methodology

Deterministic methods are applied to both simulated and real data error analyses within this chapter. The simulated data analysis applies the GTDS Precise Conversion of Elements (PCE) initialization procedure [56]. This procedure is a least squares differential correction algorithm that solves for epoch mean elements based on

the fit of the specified satellite theory to the ephemeris of a reference or "truth" position and velocity file. The PCE procedure has multiple applications. If the reference file is produced by a high precision Cowell integration, using a comprehensive force model, then the procedure can illustrate some of the mathematical limitations of the specified perturbation theory. Collins (1979) utilized the PCE procedure to test his semianalytical satellite theory for the long term motion of very high altitude orbits [66].

The primary advantage of this PCE application is that the availability of noise-free observations, (the reference position and velocity coordinates) with arbitrary time distribution, allows for a strong test of the inherent accuracy characteristics of a given satellite theory.

A more limited objective for the PCE procedure is to test a specified GP theory against the corresponding physical model for the given GP satellite theory. The current GP theories include J_2, J_3, J_4 and drag. This procedure has been exercised.

Another application for the PCE procedure is software validation. Taylor (1981) used the procedure to verify software for both the Semianalytical Kalman Filter (SKF) and Extended Semianalytical Kalman Filter (EKF) [60]. The specific PCE application for this thesis is to verify the differential correction software for each NORAD GP theory. The following discussion presents a synopsis of the PCE procedure:

1. An ORB1 file is produced, for the specific NORAD theory, using a set of 'truth' epoch orbital elements as input to the GTDS EPHEM program. At fixed time intervals the inertial rectangular components of the position and velocity are output to the ORB1 file to represent "actual" observations.

2. For the specified NORAD theory, the perturbed position and velocity histories are computed over the same time span as the ORB1 file in step one. This computation is based upon a set of a priori elements at epoch that are different from the 'truth' elements used in step 1.

3. At each observation time, the observation residuals are obtained by subtracting the position and velocity computed with the NORAD theory, in step two, from the "actual" observations. The vector of observation residuals, $\delta \underline{b}$, is used in the least squares equations for corrections to the mean elements at epoch as follows:

$$\delta \bar{a}_i \ (o) = \left(A^T W A\right)^{-1} A^T W \delta \underline{b} \qquad (5.1)$$

where $\bar{a}_i(o)$ = mean equinoctial elements at epoch

W = a weighting matrix

A = the partial derivative of the observations with respect to the element set at epoch, i.e.:

$$\left[\frac{\partial \underline{r}(t), \underline{v}(t)}{\partial \bar{a}_i(o)}\right] \tag{5.2}$$

For this analysis, the evaluation of the **A** matrix assumes that the partial derivatives of the osculating elements at time, t, with respect to the mean elements also at time, t, are given by:

$$\left[\frac{\partial a_i(t)}{\partial \bar{a}_i(t)}\right] = I \tag{5.3}$$

Therefore, the **A** matrix evaluated at the observation times is composed of sub-matrices of the form:

$$\left[\frac{\partial \underline{r}(t), \underline{v}(t)}{\partial \bar{a}_i(t)}\right]\left[\frac{\partial \bar{a}_i(t)}{\partial \bar{a}_i(o)}\right] \tag{5.4}$$

The term, $\left[\frac{\partial \bar{a}_i(t)}{\partial \bar{a}_i(o)}\right]$, is just the state transition matrix for the NORAD theory at time t.

4. After all observations have been processed, the revised estimate of the mean equinoctial elements at epoch is obtained from the following equation:

$$\hat{a}_i\ (o) = \bar{a}_i\,(o) + \delta\, a_i\,(o) \tag{5.5}$$

All of the elements are assumed to be mean and $\bar{a}_i\,(o)$ represents the a priori estimate of the mean equinoctial elements at epoch. The element set $\hat{a}_i\,(o)$ is the new estimate and it replaces the $\bar{a}_i\,(o)$ employed in step two.

5. Steps two through four are repeated until a designated convergence criterion is met.

At the end of the PCE procedure, the specified NORAD GP theory will have been least squares fit to the reference ephemeris in the designated fit span. Given this best fit, the converged set of epoch mean elements is obtained and used as input to the GTDS EPHEM program to generate another ORB1 file corresponding to the "best fit" GP trajectory. Both the reference and "best fit" ORB1 files are then analyzed with the GTDS COMPARE program [56].

The real data analysis employs a deterministic approach that uses the actual tracking data in the orbit determination process in order to evaluate the relative impact of a given NORAD GP theory on that process. The differences in the resulting orbit determination processes as described by the estimated state and other solve-for

parameters and the corresponding predicted ephemerides provide an indication of the effect on the process of the specific NORAD GP theory [77]. The steps that will be employed in this real data analysis are as follows:

1. Generate a "truth" ephemeris by orbit determination processing of the best available actual observations using a very accurate DSST model.

2. Process real observations with a given NORAD GP theory.

3. Generate an ephemeris that is based on the converged Differential Correction solve-for parameters obtained in step two.

4. Compare the NORAD GP ephemeris with the DSST "truth" ephemeris in the fit span. This comparison reveals the differences between the "truth" satellite theory (in this case the DSST) and the specified satellite theory.

Throughout both the PCE and real data analyses, the dimensionless term, weighted RMS, will be used as a measure of fit quality. Within this thesis, weighted RMS will be defined as [54]:

$$\sqrt{\frac{1}{m} \sum_i \left(\frac{\Delta y_i}{\sigma_i} \right)^2} \tag{5.6}$$

Where Δy_i = i^{th} residual

σ_i = standard deviation associated with the sensor and observations

m = number of observations

5.2 Low Altitude Case

The simulated test case used in this low altitude PCE analysis demonstrates that the NORAD GP differential correction software functions as intended. Table 5-1 provides the characteristics of the specific orbit used in the simulated data analysis.

Table 5-1. Initial Parameters of the low altitude orbit for PCE.

Element	Value
a	6789.00 km
e	0.001
i	65.0°
Ω	357.99°
ω	37.76°
M	299.5°
Perigee Height	404.076 km
Apogee Height	417.654 km
Area	2.00 m^2
Mass	200.0 kg
Epoch 1979 4 November	12 hours 0 minutes 0.000 seconds

The real data low altitude analysis uses nine days of NORAD tracking data (30 August 77 - 7 September 77). This data represents a portion of the tracking history for NSSC 10299 in the Historical Data System (HDS) catalog. NORAD provided Draper Laboratory with the observation data, a tracking network description, and a history of geomagnetic and solar activity for use in orbit determination studies [60]. It is important to note that neither the satellite initial conditions nor a satellite description were provided for this test case. However, Taylor's (1981) study established that NSSC 10299 is the Cosmos 947 satellite [60]. This fact is important because it establishes a priori estimates of the satellite's mass and area parameters which are very important in the low altitude orbit determination process.

This section is organized into two parts. The first part presents results from a comparison of the specified NORAD GP theory and the reference or "truth" file using the Precise Conversion of Elements procedure described in Section 5.1. These tests are run with data that simulates a static atmosphere. The second part of this section describes the real data comparison results from NSSC 10299 which reflect an active atmosphere. The real data comparison statistics between the NORAD theories and a very accurate DSST during a three day fit span, reveal the sensitivity of the DC solutions to the differences between the specified NORAD GP theory and the DSST.

5.2.1 PCE Fits to a Specified NORAD Reference Ephemeris

These tests are a real plus because they demonstrate the correct working of the DC including

a) analysis in 3.3.7.

b) 3.3.8.1 (PCE obs)

c) DC software interface

The characteristics of the low altitude orbit used in this Precise Conversion of Elements (PCE) are detailed in Table 5-1. This orbit is used in all the NORAD GP theory test cases. A summary of the measurement standard deviations employed in the differential correction process is presented in Table 5-2. The relative weighting between the position and velocity measurements is based on the propagation of errors in circular orbits. The "truth" data used in this PCE was produced with the GTDS EPHEM Program and the corresponding NORAD theory using the WGS-72 parameters. The ephemeris of the reference run is stored as an ORB1 file and was compared to each NORAD GP theory "best fit" trajectory in a one day fit span as described in section 5.1. Again, it is important to note that these comparisons were for ideal data in a stable atmosphere.

Table 5-2. Differential Correction Parameters Used in Low Altitude PCE

Measurement Type		Measurement Standard Deviation		
		Sigma Value	Sigma Units	Theory Integration Coordinate System
NORAD Theories	X	1500.0	Meters	NORAD True of Reference
	Y	1500.0	Meters	
	Z	1500.0	Meters	
	XDOT	150.0	cm/sec	
	YDOT	150.0	cm/sec	
	ZDOT	150.0	cm/sec	

5.2.1.1 SGP Low Altitude DC Comparison

The SGP ephemeris comparison results during the one day fit span are summarized in Table 5-3. The only perturbed a priori element in the differential correction run was a two kilometer increase in the semimajor axis. The converged final position error RMS of 7.194×10^{-5} meters indicates that the SGP differential correction processing was very effective when measured against a SGP "truth" file. The actual compare plots reveal extremely small secular drifts in various parameters as would be expected without exact matching orbit files.

Table 5-3. SGP Low Altitude PCE Results

Initial weighted RMS	76.021
Final weighted RMS	2.513×10^{-8}
Initial Position Error RMS(m)	185247.12
Final Position Error RMS(m)	7.194×10^{-5}
Number of Iterations	5
Converged?	YES
Residual Standard Deviation and (% Observations Accepted)	
x (m)	2.593×10^{-5} (100%)
y (m)	1.113×10^{-5} (100%)
z (m)	2.360×10^{-5} (100%)
x (cm/sec)	4.079×10^{-6} (100%)
y (cm/sec)	1.758×10^{-6} (100%)
z (cm/sec)	3.7115×10^{-6} (100%)

5.2.1.2 GP4 Low Altitude DC Comparison

The GP4 PCE results during the one day fit span are presented in Table 5-4. Four Keplerian elements were perturbed in this analysis and they are as follows: semi-major axis (+2.0km), eccentricity (+.001), inclination (+.1 degrees) and longitude of

ascending node (-0.44 degrees). As in the SGP case, the converged final position error RMS of 2.946×10^{-5} meters indicates that the GP4 DC software is correctly functioning with a GP4 "truth" file. The actual COMPARE plots do not reveal any significant trends other than normal iteration patterns.

Table 5-4. GP4 Low Altitude PCE Results

Initial weighted RMS	81.051
Final weighted RMS	1.209×10^{-8}
Initial Position Error RMS(m)	197658.64
Final Position Error RMS(m)	2.946×10^{-5}
Number of Iterations	5
Converged?	YES

Residual Standard Deviation and (% Observations Accepted)	
x (m)	2.07×10^{-5} (100%)
y (m)	8.97×10^{-6} (100%)
z (m)	1.89×10^{-5} (100%)
x (cm/sec)	2.35×10^{-6} (100%)
y (cm/sec)	9.96×10^{-7} (100%)
z (cm/sec)	2.12×10^{-6} (100%)

5.2.1.3 HANDE Low Altitude D.C. Comparison.

The HANDE PCE results during the one day fit span are summarized in Table 5-5. Four Keplerian elements were perturbed exactly as in the GP4 analysis. After five iterations, the converged final position error RMS was 2.952×10^{-5} meters. Again, this performance is very similar to the SGP and GP4 results, and indicates that the HANDE DC processing is very effective with a HANDE "truth" file. Actual COMPARE plots are very similar to the SGP and GP4 results.

Table 5-5. HANDE Low Altitude PCE Results

Initial weighted RMS	81.118
Final weighted RMS	1.211×10^{-8}
Initial Position Error RMS(m)	197819.07
Final Position Error RMS(m)	2.952×10^{-5}
Number of Iterations	5
Converged?	YES

Residual Standard Deviation and (% Observations Accepted)	
x (m)	2.070×10^{-5} (100%)
y (m)	8.974×10^{-6} (100%)
z (m)	1.890×10^{-5} (100%)
x (cm/sec)	2.350×10^{-6} (100%)
y (cm/sec)	9.962×10^{-7} (100%)
z (cm/sec)	2.122×10^{-6} (100%)

5.2.2 Fits to Real Data (NSSC 10299)

As described in section 5.2, this differential correction test case uses data which represents six days of tracking history of NSSC 10299. Table 5-6 describes the initial parameters that were used in this application. Throughout this analysis a DSST orbit

generator which incorporated a full force model was used to establish a reference ephemeris for the fit span comparisons. Table 5-7 depicts the DSST force model used in this case. The reference ephemeris, obtained with a differential correction fit over days four through six, was generated by using a priori epoch mean elements that were obtained from a differential correction fit to real observations over the first three day period. After eight iterations the fit over days four through six converged to a weighted RMS of 2.24. The results of the observation processing are presented in Figure 5-1. This DSST ephemeris was used as a reference to compare with a DSST prediction over days four and five. The initial conditions for this prediction were obtained from the DSST fit over the first three days. Additionally, both the GP4 and HANDE theories were used to fit the NSSC 10299 tracking data over both three day fit spans. The converged DSST reference ephemeris was compared to the GP4 and HANDE differential correction fits over days four through six.

Table 5-6. Initial Parameters of NSSC 10299

Element	Value
a Kilometers	6635.805
e	0.0098
i Degrees	72.97
Ω Degrees	125.77
ω Degrees	65.44
M Degrees	103.14
Perigee height (Km)	192.634
Apogee height (Km)	322.696
Epoch 30 August, 1977 $0^h\ 0^m\ 0.000^s$	

Table 5-7. Force Model Used in the DSST 'Truth' Model for the Low Altitude Case (NSSC 10299)

AOG Model	SPG Model
Zonals: (8x0) GEM9	Zonals: (8x0), e^3
Tesseral Resonance: None	M-Dailies: (8x8), e^3
Second Order J_2: On	Tesserals (8x8), e^2
Lunar-Solar Point Mass:	J_2 + Drag/M-Daily Coupling (8x8), e^2
Moon: $(a/r)^4$, e^2	Lunar-Solar-Point Mass: Analytical Model
Sun: $(a/r)^2$, e^2	Solar Radiation Pressure: Off
Solar Radiation Pressure: Off	$J_2{}^2$-Second Order
Drag: On	Drag Short Periodics: On
C_D = 2.0	
Satellite Mass: 5700 kg	
Satellite Area: 6.1 m^2	

OBSERVATION SUMMARY BY TYPE

TYPE	RANG	AZ	EL	RRAT
TOTAL NO.	275	275	275	239
NO. ACCEPTED	238 (86%)	265 (96%)	265 (96%)	223 (93%)
WEIGHTED RMS	3.112	1.892	1.584	2.175
MEAN RESDUAL	464.1	-4.003	35.67	-160.4
STANDARD DEV	1144.	178.6	138.5	778.9

OBSERVATION SUMMARY BY STATION

STATION	PARO	CBDF	CBDF	CBDF	CBDF	CBDF	ASCO	ASCO	ASCO	ASCO
TYPE	ALL	ALL	RANG	AZ	EL	RRAT	ALL	RANG	AZ	EL
TOTAL NO.	0	72	18	18	18	18	80	20	20	20
NO. ACCEPTED	0 (0%)	67 (93%)	17 (94%)	18 (100%)	16 (88%)	16 (88%)	80 (100%)	20 (100%)	20 (100%)	20 (100%)
WEIGHTED RMS	0.0000E+00	2.883	3.656	2.222	3.086	2.351	2.024	2.780	2.738	0.8907
STANDARD DEV	0.0000E+00	0.0000E+00	69.24	176.8	172.1	467.0	0.0000E+00	209.5	259.8	82.81

STATION	ASCO	EGLO	EGLO	EGLO	EGLO	NAVO	NAVO	NAVO	NAVO	CLEF
TYPE	RRAT	ALL	RANG	AZ	EL	ALL	RANG	AZ	EL	ALL
TOTAL NO.	20	45	15	15	15	63	21	21	21	0
NO. ACCEPTED	20 (100%)	42 (93%)	12 (80%)	15 (100%)	15 (100%)	44 (69%)	16 (76%)	13 (61%)	15 (71%)	0 (0%)
WEIGHTED RMS	0.6118	1.833	2.909	1.133	1.164	1.800	0.2169	3.169	0.8673	0.0000E+00
STANDARD DEV	718.5	0.0000E+00	163.5	70.95	55.86	0.0000E+00	416.8	203.9	106.1	0.0000E+00

STATION	CLET	CLET	CLET	CLET	CLET	FYLO	FYLO	FYLO	FYLO	FYLO
TYPE	ALL	RANG	AZ	EL	RRAT	ALL	RANG	AZ	EL	RRAT
TOTAL NO.	428	107	107	107	107	36	9	9	9	9
NO. ACCEPTED	398 (92%)	80 (74%)	106 (99%)	106 (99%)	106 (99%)	35 (97%)	9 (100%)	9 (100%)	8 (88%)	9 (100%)
WEIGHTED RMS	2.011	3.854	0.8609	1.115	1.411	2.334	0.4959	2.421	3.141	2.512
STANDARD DEV	0.0000E+00	124.2	90.03	104.5	769.8	0.0000E+00	711.3	348.5	155.2	500.3

STATION	FYLF	FYLF	FYLF	FYLF	FYLF	FYLT	FYLT	FYLT	FYLT	FYLT
TYPE	ALL	RANG	AZ	EL	RRAT	ALL	RANG	AZ	EL	RRAT
TOTAL NO.	20	5	5	5	5	72	18	18	18	18
NO. ACCEPTED	18 (90%)	4 (80%)	5 (100%)	5 (100%)	4 (80%)	59 (81%)	18 (100%)	17 (94%)	18 (100%)	6 (33%)
WEIGHTED RMS	2.174	1.756	1.953	2.331	2.575	2.501	1.497	2.724	1.290	5.365
STANDARD DEV	0.0000E+00	4277.	193.0	162.5	246.6	0.0000E+00	1232.	250.9	134.4	107.7

STATION	DYBF	DYBT	THUF	THUF	THUF	THUF	THUF	ANTO	ANTO	ANTO
TYPE	ALL	ALL	ALL	RANG	AZ	EL	RRAT	ALL	RANG	AZ
TOTAL NO.	0	0	164	41	41	41	41	84	21	21
NO. ACCEPTED	0 (0%)	0 (0%)	164 (100%)	41 (100%)	41 (100%)	41 (100%)	41 (100%)	84 (100%)	21 (100%)	21 (100%)
WEIGHTED RMS	0.0000E+00	0.0000E+00	2.402	2.526	2.104	1.222	3.284	2.680	3.882	2.200
STANDARD DEV	0.0000E+00	0.0000E+00	0.0000E+00	904.4	187.9	201.1	408.5	0.0000E+00	104.4	44.71

STATION	ANTO	ANTO
TYPE	EL	RRAT
TOTAL NO.	21	21
NO. ACCEPTED	21 (100%)	21 (100%)
WEIGHTED RMS	2.543	1.531
STANDARD DEV	54.21	152.2

Figure 5-1. DSST Low Altitude Observation Processing Summary

5.2.2.1 Fit Span Comparisons

This section presents a comparison of the DSST results from the first and second differential correction fit spans. This section also provides the results of a comparison between the converged DSST reference ephemeris and both the GP4 and HANDE DC fit ephemerides over days four and five.

5.2.2.1.1 DSST Analysis

A comparison of the two three day fit spans in this particular analysis presents an interesting example of the effects of a dynamic atmosphere. The results of the first three day fit span are given in Table 5-8 which presents a 1230.9 meter RMS position error, over three days of tracking data. Table 5-9 depicts the second three day fit span results and indicates a 1554.0 meter RMS position error. There is also an increase in the weighted RMS from 1.39 to 2.24. These significant differences prompted a comparison of the stability of the atmosphere during the second three day fit span relative to the first three days. A study of the solar and geomagnetic activity of days four through six revealed an increase in the average geomagnetic index from 4.3 to 6.7, and a simultaneous increase in the average solar flux value from 82.86 to 83.73 [54]. The increase in both of these factors indicates a "hotter" or more dynamic atmosphere existed over days four through six. The

tracking data analysis suggests that unmodeled atmospheric variations can cause an increase in both position and weighted RMS. The significance of these increases is highlighted by the fact that this particular DSST model approaches the accuracy of a special perturbations model, and the differential correction process did not eliminate these RMS differences. This analysis suggests that further studies be undertaken to understand more clearly the impact of both geomagnetic and solar flux variations. It may be desirable to incorporate these effects into the orbit determination process in order to improve the accuracy.

Table 5-8. Results of DSST DC for NSSC 10299, Days 1-3

Residual	Standard Deviation
Range	1051 meters
Azimuth	113.1 seconds of arc
Elevation	134.2 seconds of arc
Range-Rate	378.0 cm/sec
Position RMS error over 3 day fit span 1230.9 meters	
Number of Iterations: 8	
Weighted RMS 1.39	σ_a = 14.76 cm

Table 5-9. Results of DSST DC for NSSC 10299, Days 4-6

Residual	Standard Deviation
Range	1144 meters
Azimuth	178.6 seconds of arc
Elevation	138.5 seconds of arc
Range-Rate	778.9 cm/sec
Position RMS error over 3 day fit span 1554.0 meters	
Number of Iterations: 8	
Weighted RMS 2.24	σ_a = 34.68 cm

5.2.2.1.2 GP4 Analysis

The GP4 theory was used to fit the same tracking data as in the DSST reference fit. Figure 5-2 presents the observation summary for the GP4 fit. These results are comparable to the converged DSST results given in Figure 5-1 except that the GP4 model did not accept as many range observations. It is also of interest to note that the GP4 range sigma of 1124 meters almost matches the DSST value of 1144 meters. Table 5-10 presents a summary of the results of the GP4 differential correction, which are very comparable to the DSST fit. However, a careful study of Figures 5-3 through 5-8, which display comparisons in position and mean longitude, reveals some significant findings about the sensitivity of the DC solution to the differences between the GP4 and DSST theories. In particular, the along-track differences of days four and five, as seen in Figures 5-5 and 5-6, reveal a small cubic signature with a distinctive twelve hour periodicity superimposed. The same pattern is also present in Figures 5-7 and 5-8, the mean longitude differences for days four and five. The twelve hour periodicity may be explained by the fact that the GP4 and DSST theories are based on different treatments of the m-daily geopotential terms as explained in Chapter 2. These observations support the suggestion that the differential correction process does not remove the periodic characteristics of the GP4 orbit determination results in this particular low altitude test case.

OBSERVATION SUMMARY BY TYPE

TYPE	RANG	AZ	EL	RRAT
TOTAL NO.	275	275	275	239
NO. ACCEPTED	185 (67%)	259 (94%)	264 (96%)	222 (92%)
WEIGHTED RMS	2.556	2.172	1.670	2.207
MEAN RESDUAL	544.9	30.45	43.28	-343.5
STANDARD DEV	1124.	197.1	151.9	817.6

OBSERVATION SUMMARY BY STATION

STATION	PARQ	CBDF	CBDF	CBDF	CBDF	CBDF	ASCQ	ASCQ	ASCQ	ASCQ
TYPE	ALL	ALL	RANG	AZ	EL	RRAT	ALL	RANG	AZ	EL
TOTAL NO.	0	72	18	18	18	18	80	20	20	20
NO. ACCEPTED	0 (0%)	62 (86%)	10 (55%)	18 (100%)	16 (88%)	18 (100%)	76 (95%)	16 (80%)	20 (100%)	20 (100%)
WEIGHTED RMS	0.0000E+00	2.785	3.844	1.941	2.843	2.750	1.896	2.627	2.515	1.185
STANDARD DEV	0.0000E+00	0.0000E+00	130.7	146.2	146.4	499.0	0.0000E+00	157.6	244.3	140.4

STATION	ASCQ	EGLQ	EGLQ	EGLQ	EGLQ	NAVQ	NAVQ	NAVQ	NAVQ	CLEF
TYPE	RRAT	ALL	RANG	AZ	EL	ALL	RANG	AZ	EL	ALL
TOTAL NO.	20	45	15	15	15	63	21	21	21	0
NO. ACCEPTED	20 (100%)	39 (86%)	9 (60%)	15 (100%)	15 (100%)	43 (68%)	16 (76%)	12 (57%)	15 (71%)	0 (0%)
WEIGHTED RMS	0.6337	2.512	3.497	2.745	1.239	1.477	0.2101	2.630	0.8228	0.0000E+00
STANDARD DEV	709.1	0.0000E+00	204.5	105.6	66.87	0.0000E+00	409.0	174.1	98.72	0.0000E+00

STATION	CLET	CLET	CLET	CLET	CLET	FYLQ	FYLQ	FYLQ	FYLQ	FYLQ
TYPE	ALL	RANG	AZ	EL	RRAT	ALL	RANG	AZ	EL	RRAT
TOTAL NO.	428	107	107	107	107	36	9	9	9	9
NO. ACCEPTED	369 (86%)	51 (47%)	106 (99%)	106 (99%)	106 (99%)	35 (97%)	9 (100%)	9 (100%)	8 (88%)	9 (100%)
WEIGHTED RMS	1.812	3.279	1.430	1.227	1.646	2.428	0.6914	2.444	3.451	2.428
STANDARD DEV	0.0000E+00	101.1	144.9	101.5	925.7	0.0000E+00	1005.	329.3	143.6	328.4

STATION	FYLF	FYLF	FYLF	FYLF	FYLF	FYLT	FYLT	FYLT	FYLT	FYLT
TYPE	ALL	RANG	AZ	EL	RRAT	ALL	RANG	AZ	EL	RRAT
TOTAL NO.	20	5	5	5	5	72	18	18	18	18
NO. ACCEPTED	19 (95%)	4 (80%)	5 (100%)	5 (100%)	5 (100%)	53 (73%)	18 (100%)	15 (83%)	18 (100%)	2 (11%)
WEIGHTED RMS	1.998	1.560	2.613	0.9018	2.363	2.256	1.857	2.551	1.545	5.792
STANDARD DEV	0.0000E+00	3475.	182.0	74.56	406.8	0.0000E+00	1463.	230.9	85.46	77.15

STATION	DYBF	DYBT	THUF	THUF	THUF	THUF	THUF	ANTQ	ANTQ	ANTQ
TYPE	ALL	ALL	ALL	RANG	AZ	EL	RRAT	ALL	RANG	AZ
TOTAL NO.	0	0	164	41	41	41	41	84	21	21
NO. ACCEPTED	0 (0%)	0 (0%)	164 (100%)	41 (100%)	41 (100%)	41 (100%)	41 (100%)	70 (83%)	11 (52%)	18 (85%)
WEIGHTED RMS	0.0000E+00	0.0000E+00	2.100	1.902	2.344	1.429	2.546	3.089	2.466	3.371
STANDARD DEV	0.0000E+00	0.0000E+00	0.0000E+00	815.9	201.6	220.3	505.6	0.0000E+00	59.35	83.79

STATION	ANTQ	ANTQ
TYPE	EL	RRAT
TOTAL NO.	21	21
NO. ACCEPTED	20 (95%)	21 (100%)
WEIGHTED RMS	2.827	3.357
STANDARD DEV	60.82	290.8

Figure 5-2. GP4 Low Altitude Observation Processing Summary

Table 5-10. Results of the GP4 DC for NSSC 10299 Days 4-6

Residual	Standard Deviation
Range	1124 meters
Azimuth	197.1 seconds of arc
Elevation	151.9 seconds of arc
Range-Rate	817.6 cm/sec
Position RMS error over 3 day fit span 1551.1 meters	
Number of Iterations: 12	
Weighted RMS 2.13	σ_a = 41.93 cm

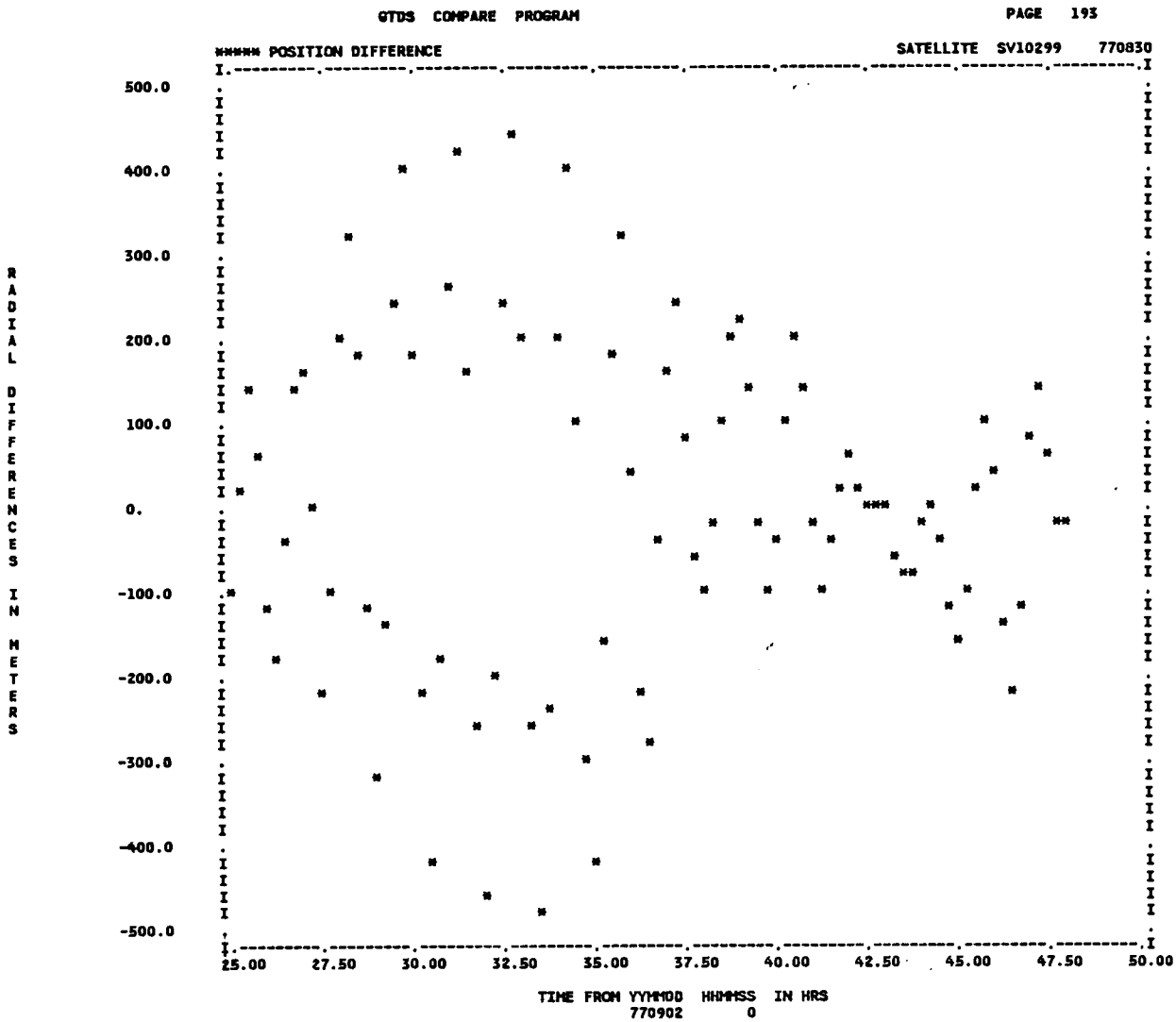

Figure 5-3. GP4-DSST Radial Differences Day 5

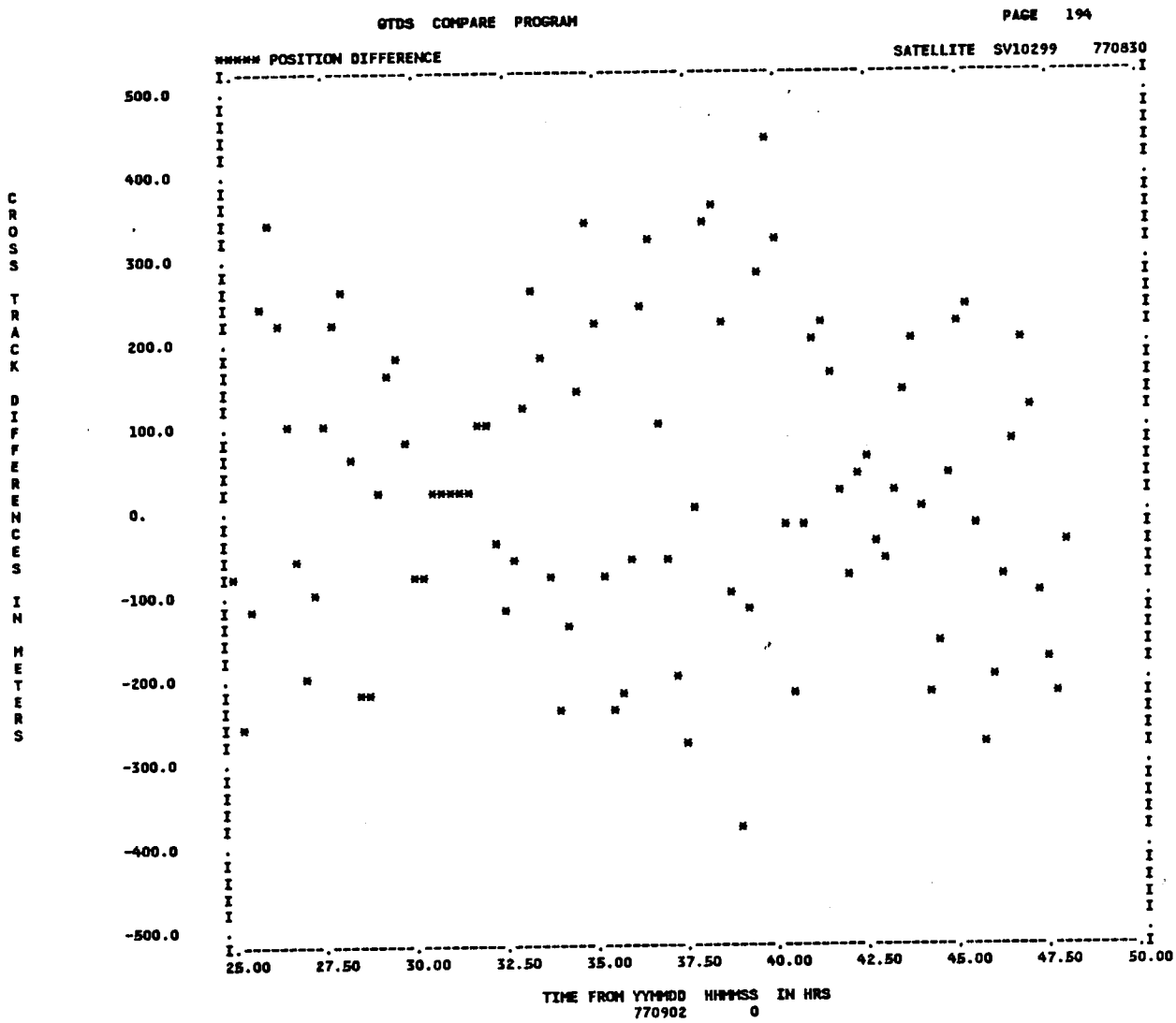

Figure 5-4. GP4-DSST Cross-Track Differences Day 5

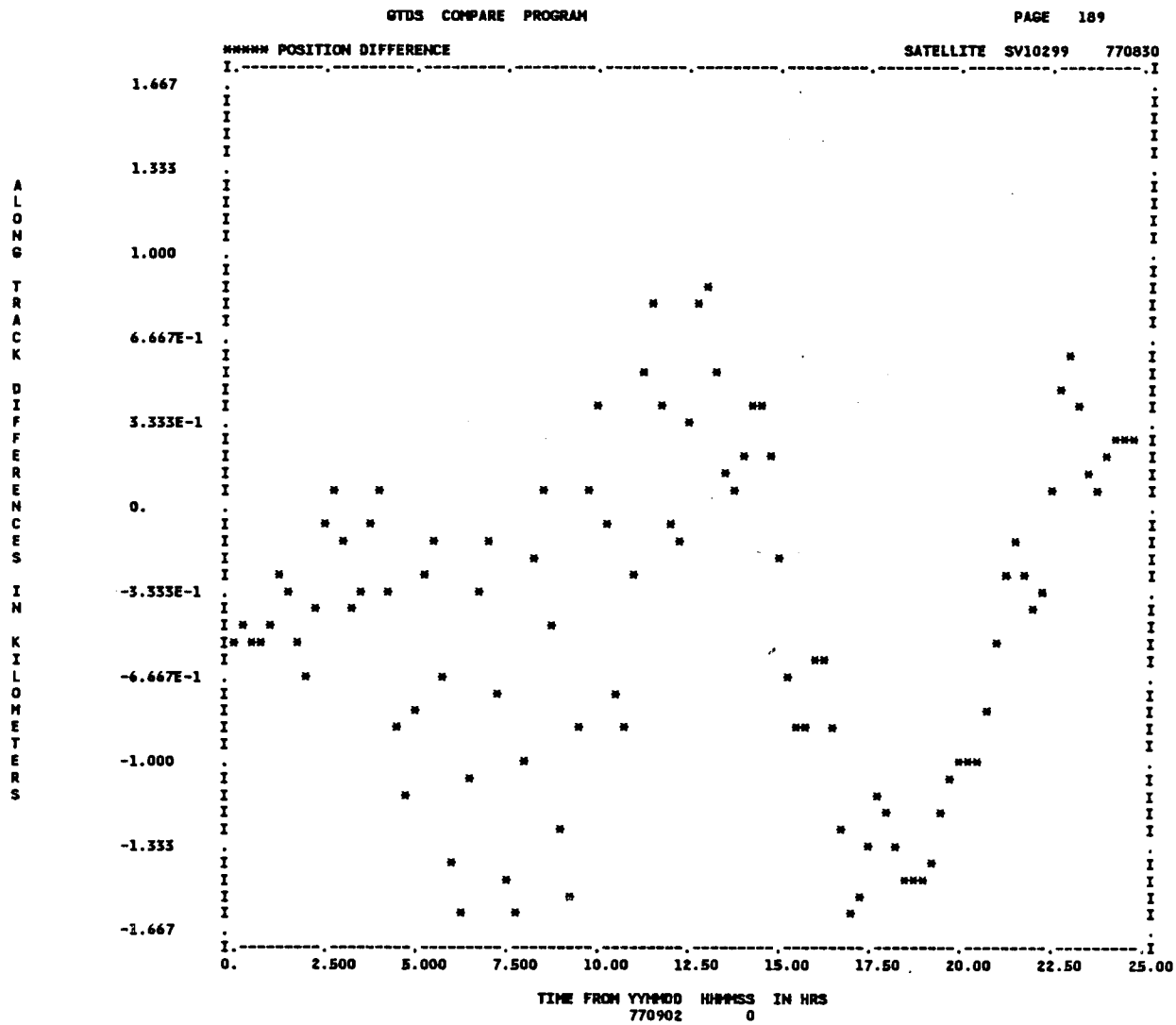

Figure 5-5. GP4-DSST Along-Track Differences Day 4

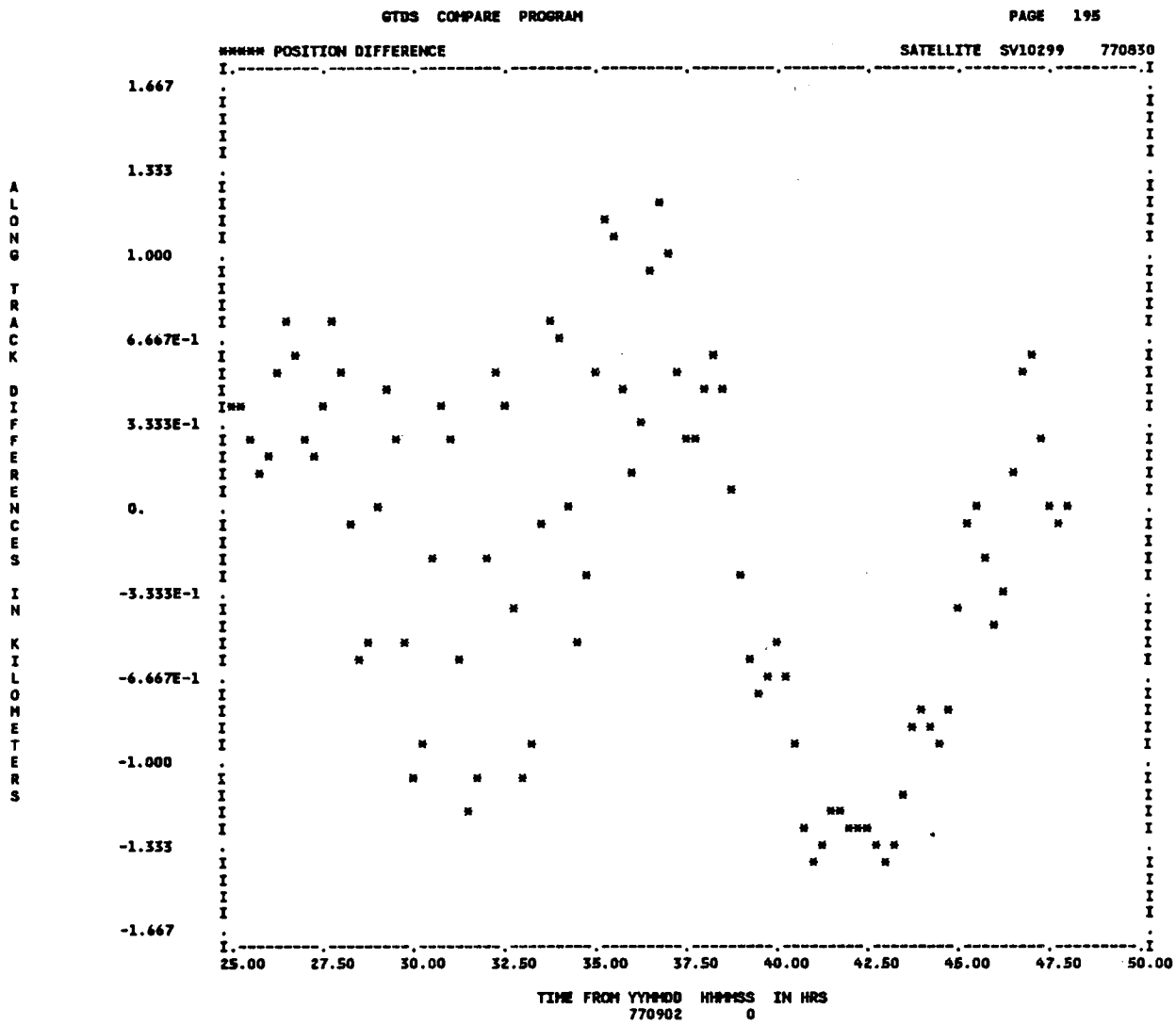

Figure 5-6. GP4-DSST Along-Track Differences Day 5

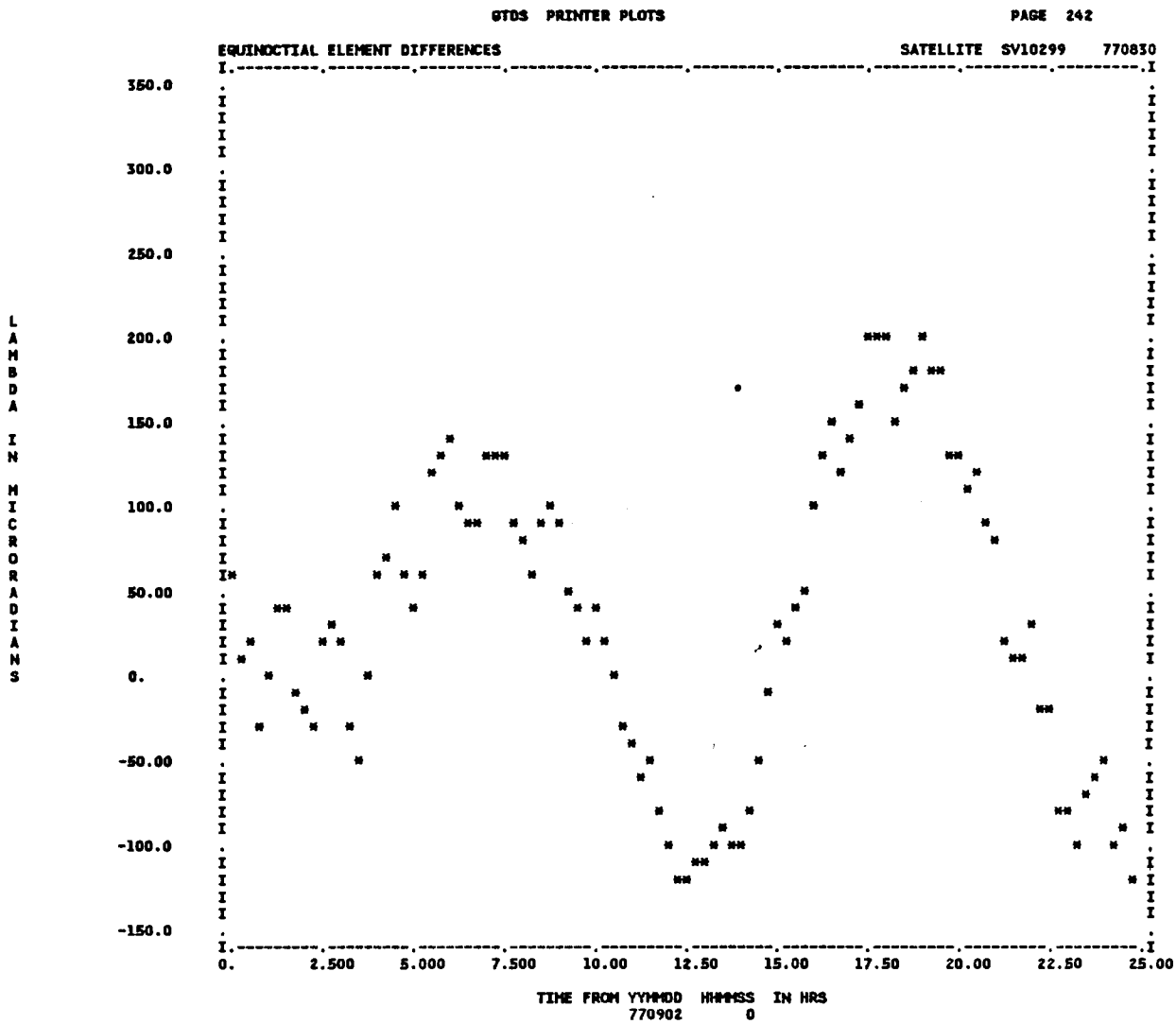

Figure 5-7. GP4-DSST Mean Longitude Differences Day 4

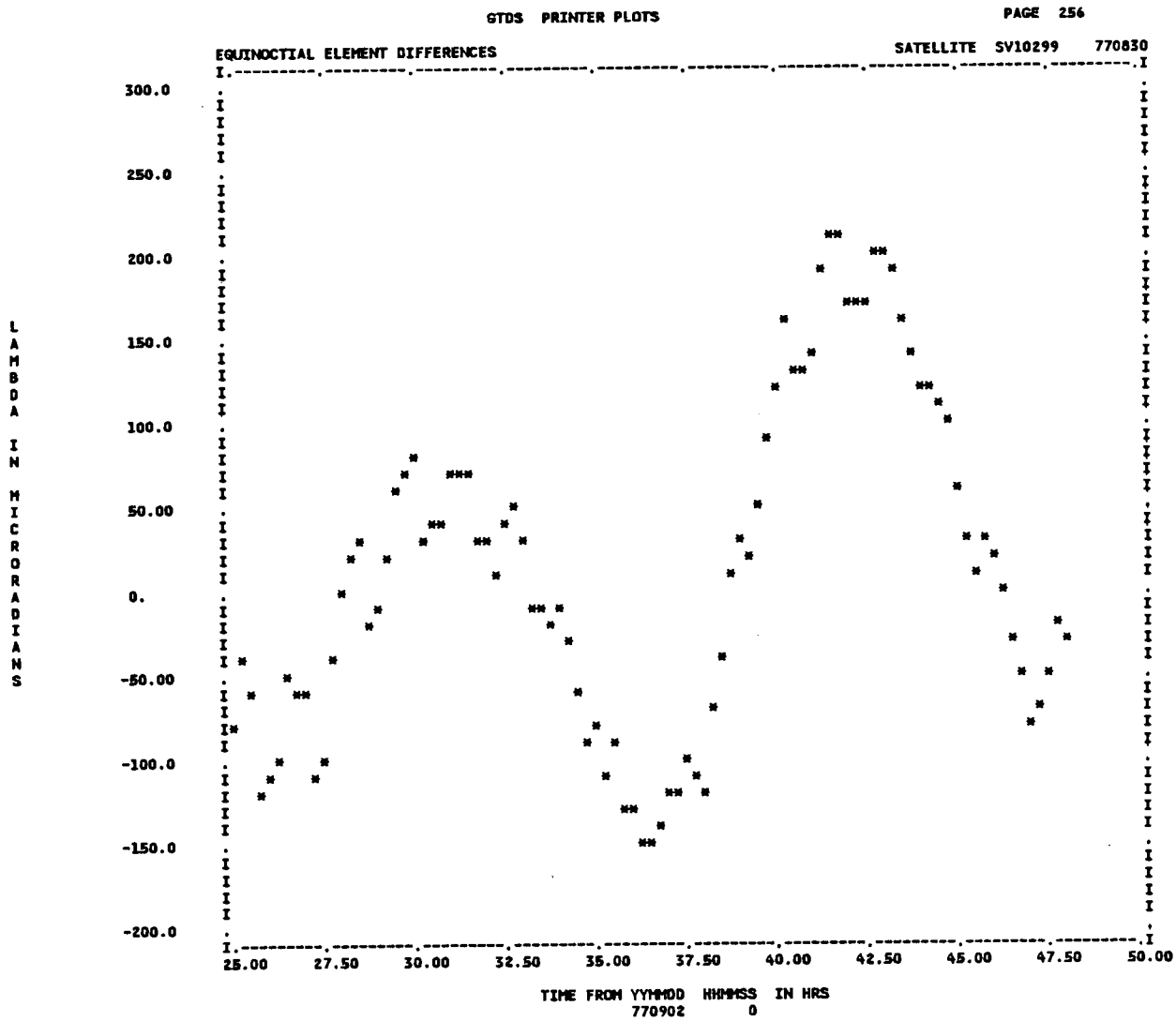

Figure 5-8. GP4-DSST Mean Longitude Differences Day 5

5.2.2.1.3 HANDE Analysis

As in the GP4 analysis, the HANDE theory was used to fit the tracking data over days four through six. The observation summary in Figure 5-9 is almost identical to the GP4 results with the exception that 3% less range observations and 1% more range rate observations are accepted. Similarly, the results of Table 5-11 are very comparable to the GP4 results of Table 5-10. Also, in this low altitude, high drag analysis, Figures 5-10 through 5-15 are nearly identical to the GP4 results of Figures 5-3 through 5-8. The combination of these observations, in conjunction with the similarity between the GP4 and DSST results, indicates that all three theories provide similar sensitivities to the DC solution process as seen by the similar values of total position RMS, weighted RMS and range sigmas. Since all three theories provide very similar results, this tends to indicate that none of the theories correctly account for atmospheric variations in the DC solution process. This conclusion is based upon a comparison of the results of the original three day DSST differential correction fit (Table 5-8), with the corresponding values in each theory over days four through six.

OBSERVATION SUMMARY BY TYPE

TYPE	RANG	AZ	EL	RRAT
TOTAL NO.	275	275	275	239
NO. ACCEPTED	176 (64%)	261 (94%)	265 (96%)	223 (93%)
WEIGHTED RMS	2.598	2.127	1.699	2.227
MEAN RESIDUAL	569.0	22.43	55.69	-327.4
STANDARD DEV	1152.	200.8	151.1	810.6

OBSERVATION SUMMARY BY STATION

STATION	PARQ	CBDF	CBDF	CBOF	CBOF	CBOF	ASCQ	ASCQ	ASCQ	ASCQ
TYPE	ALL	ALL	RANG	AZ	EL	RRAT	ALL	RANG	AZ	EL
TOTAL NO.	0	72	18	18	18	18	80	20	20	20
NO. ACCEPTED	0 (0%)	61 (84%)	9 (50%)	18 (100%)	16 (88%)	18 (100%)	76 (95%)	16 (80%)	20 (100%)	20 (100%)
WEIGHTED RMS	0.0000E+00	2.772	4.036	1.861	2.997	2.540	2.094	3.680	2.112	1.051
STANDARD DEV	0.0000E+00	0.0000E+00	126.4	132.1	151.6	446.4	0.0000E+00	243.9	208.2	124.3

STATION	ASCQ	EGLQ	EGLQ	EGLQ	EGLQ	NAVQ	NAVQ	NAVQ	NAVQ	CLEF
TYPE	RRAT	ALL	RANG	AZ	EL	ALL	RANG	AZ	EL	ALL
TOTAL NO.	20	45	15	15	15	63	21	21	21	0
NO. ACCEPTED	20 (100%)	39 (86%)	9 (60%)	15 (100%)	15 (100%)	43 (68%)	16 (76%)	12 (57%)	15 (71%)	0 (0%)
WEIGHTED RMS	0.5232	2.393	3.552	2.395	1.258	1.397	0.2315	2.500	0.7317	0.0000E+00
STANDARD DEV	601.0	0.0000E+00	231.3	85.44	65.37	0.0000E+00	453.6	164.2	89.07	0.0000E+00

STATION	CLET	CLET	CLET	CLET	CLET	FYLQ	FYLQ	FYLQ	FYLQ	FYLQ
TYPE	ALL	RANG	AZ	EL	RRAT	ALL	RANG	AZ	EL	RRAT
TOTAL NO.	428	107	107	107	107	36	9	9	9	9
NO. ACCEPTED	362 (84%)	44 (41%)	106 (99%)	106 (99%)	106 (99%)	35 (97%)	9 (100%)	9 (100%)	8 (88%)	9 (100%)
WEIGHTED RMS	1.700	2.876	1.404	1.324	1.645	2.437	0.6938	2.493	3.268	2.627
STANDARD DEV	0.0000E+00	83.58	140.0	100.7	933.1	0.0000E+00	1013.	334.2	144.3	345.0

STATION	FYLF	FYLF	FYLF	FYLF	FYLF	FYLT	FYLT	FYLT	FYLT	FYLT
TYPE	ALL	RANG	AZ	EL	RRAT	ALL	RANG	AZ	EL	RRAT
TOTAL NO.	20	5	5	5	5	72	18	18	18	18
NO. ACCEPTED	19 (95%)	4 (80%)	5 (100%)	5 (100%)	5 (100%)	56 (77%)	18 (100%)	17 (94%)	18 (100%)	3 (16%)
WEIGHTED RMS	2.002	1.557	2.641	0.9770	2.316	2.667	1.910	3.355	1.386	5.967
STANDARD DEV	0.0000E+00	3466.	171.3	79.08	372.5	0.0000E+00	1504.	281.9	80.73	66.33

STATION	DYBF	DYBT	THUF	THUF	THUF	THUF	THUF	ANTQ	ANTQ	ANTQ
TYPE	ALL	ALL	ALL	RANG	AZ	EL	RRAT	ALL	RANG	AZ
TOTAL NO.	0	0	164	41	41	41	41	84	21	21
NO. ACCEPTED	0 (0%)	0 (0%)	164 (100%)	41 (100%)	41 (100%)	41 (100%)	41 (100%)	70 (83%)	10 (47%)	18 (85%)
WEIGHTED RMS	0.0000E+00	0.0000E+00	2.074	1.872	2.305	1.465	2.497	3.155	3.508	2.977
STANDARD DEV	0.0000E+00	0.0000E+00	0.0000E+00	822.1	196.3	219.6	493.6	0.0000E+00	94.41	68.72

STATION	ANTQ	ANTQ
TYPE	EL	RRAT
TOTAL NO.	21	21
NO. ACCEPTED	21 (100%)	21 (100%)
WEIGHTED RMS	2.834	3.420
STANDARD DEV	60.35	281.0

Figure5-9. HANDE Low Altitude Observation Processing Summary

Table 5-11. Results of HANDE DC for NSSC 10299 Days 4-6

Residual	Standard Deviation
Range	1152 meters
Azimuth	200.8 seconds of arc
Elevation	151.1 seconds of arc
Range-Rate	810.6 cm/sec
Distance RMS error over 3 day fit span 1565.585 meters	
Number of Iterations: 12	
Weighted RMS 2.14	σ_a = 42.106

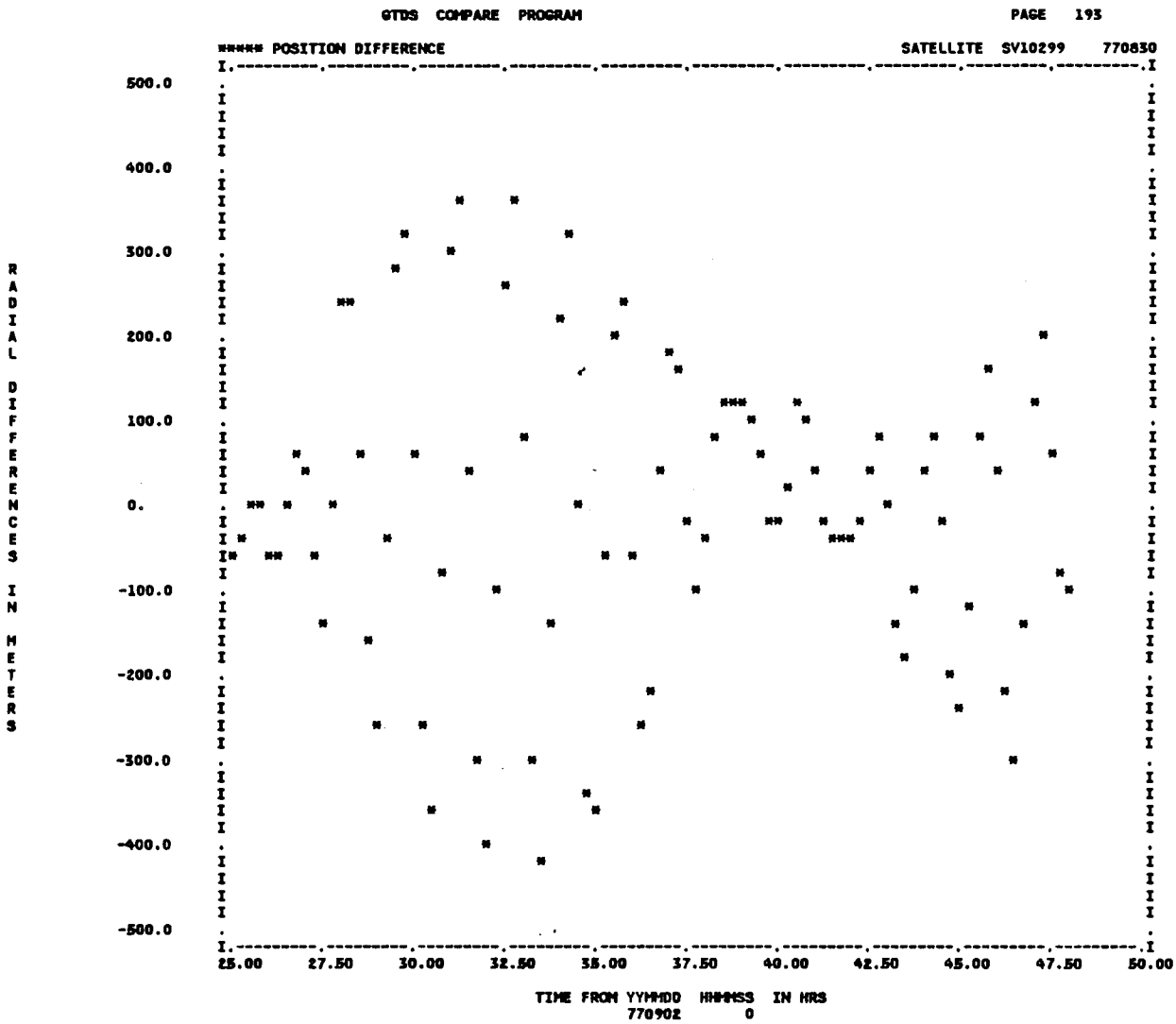

Figure 5-10. HANDE-DSST Radial Differences Day 5

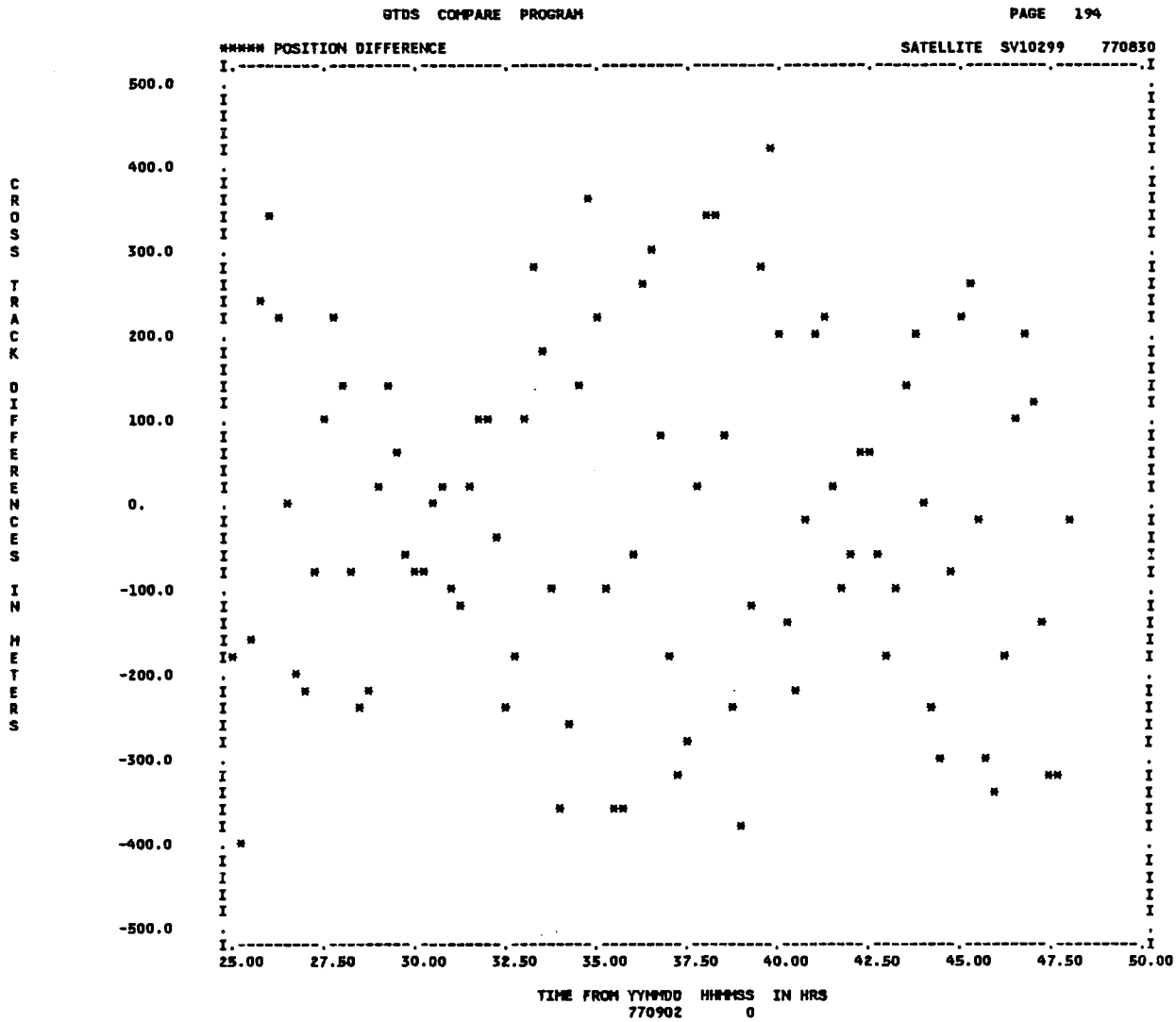

Figure 5-11. HANDE-DSST Cross-Track Differences Day 5

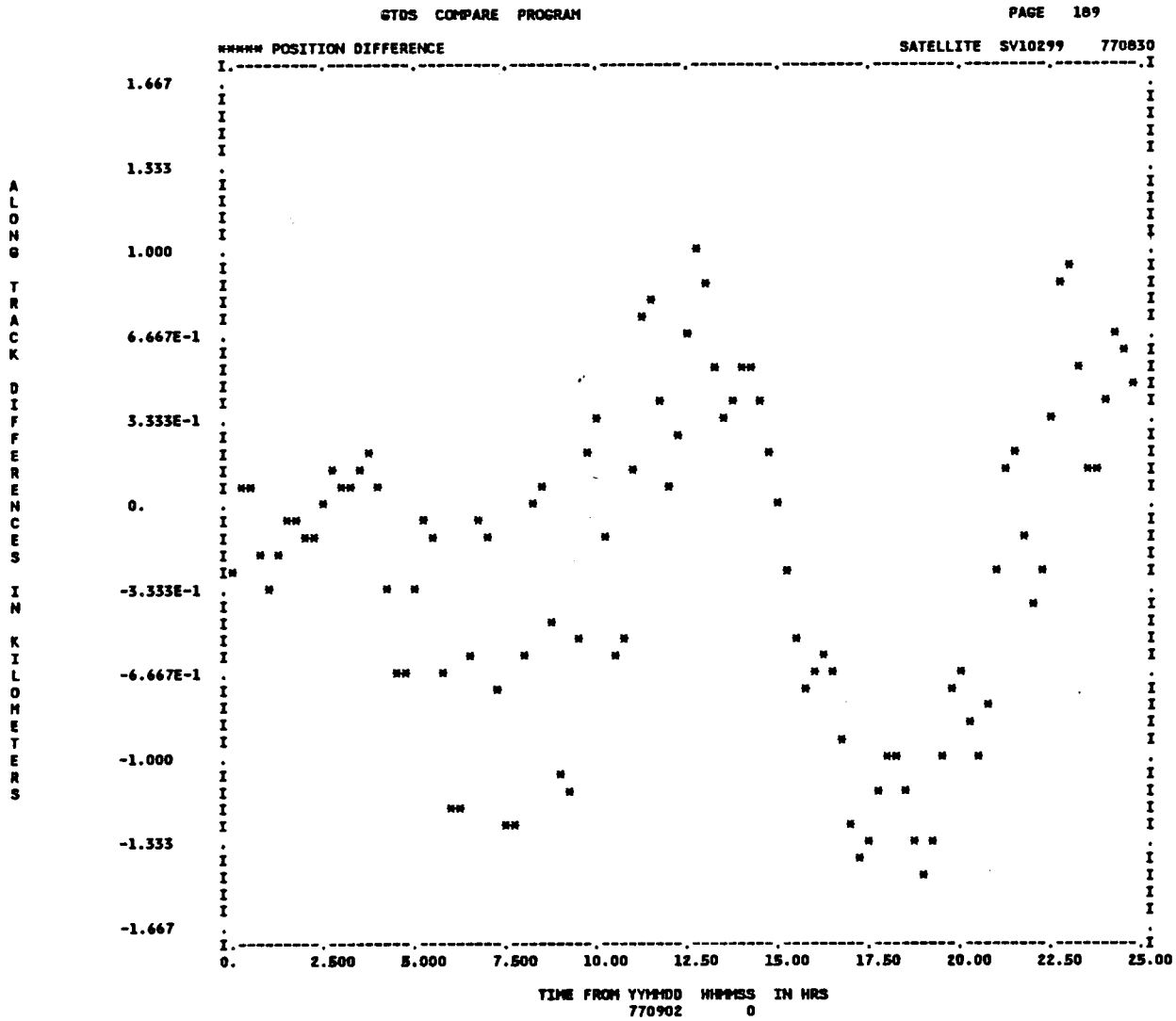

Figure 5-12. HANDE-DSST Along-Track Differences Day 4

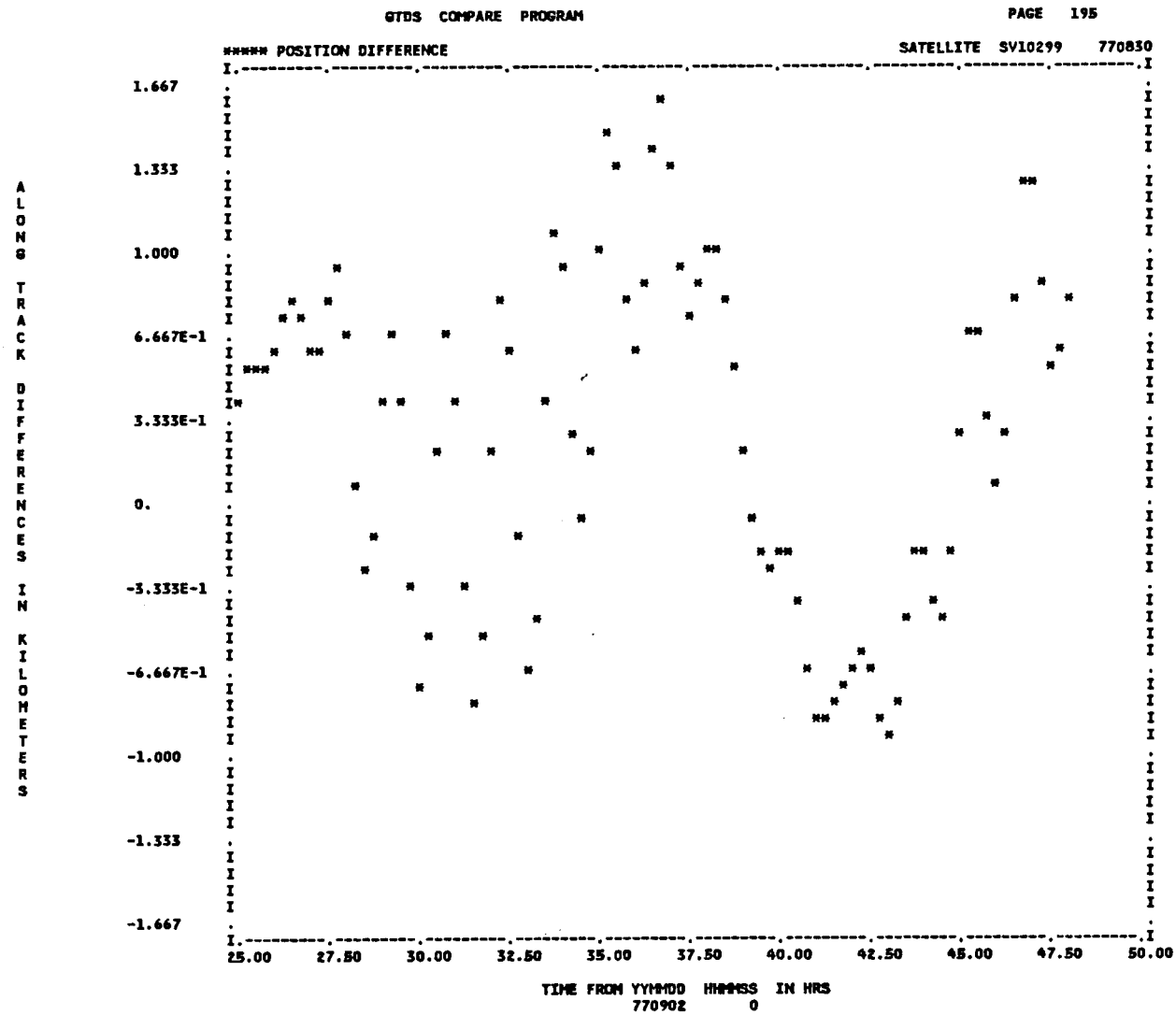

Figure 5-13. HANDE-DSST Along-Track Differences Day 5

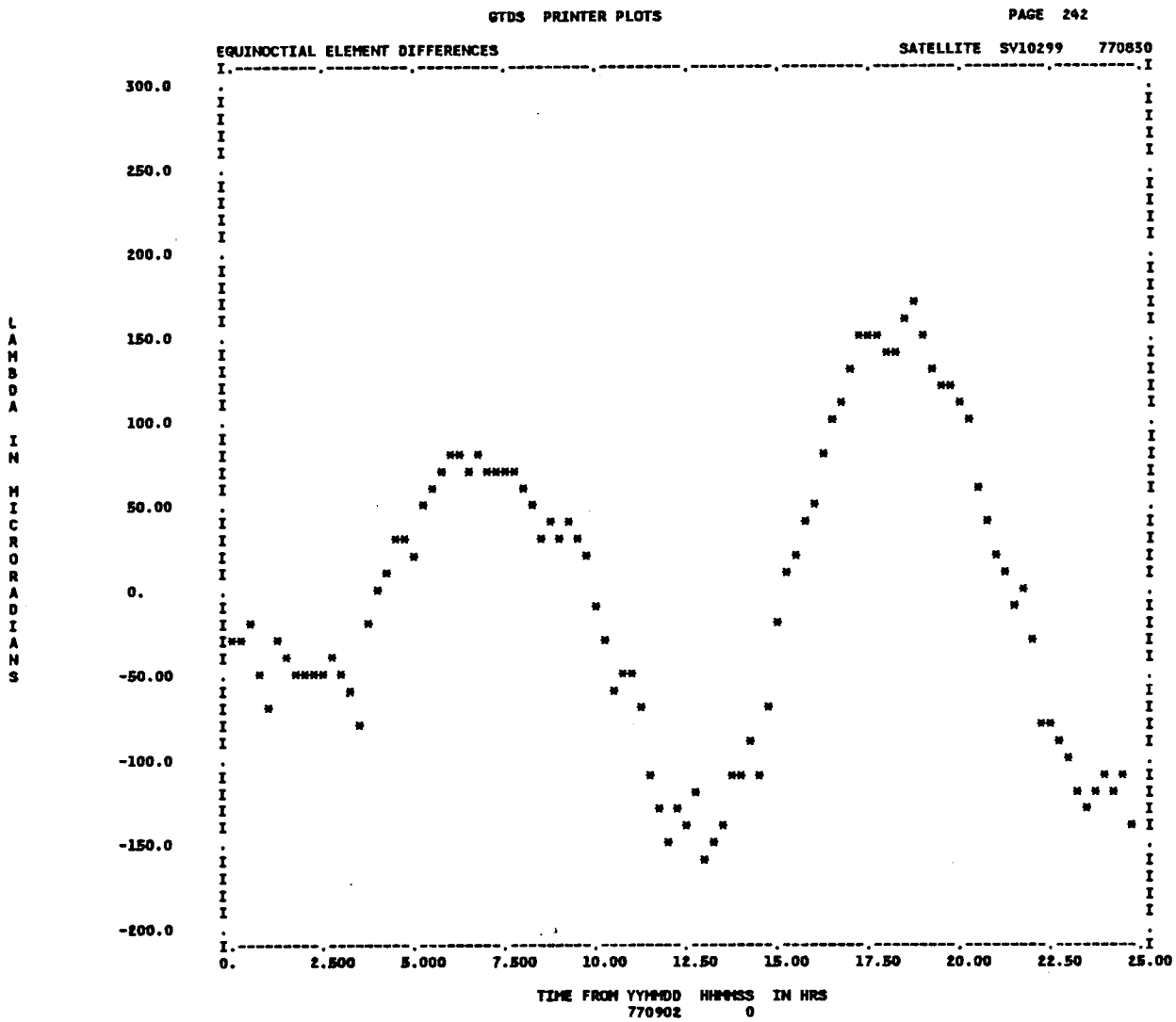

Figure 5-14. HANDE-DSST Mean Longitude Differences Day 4

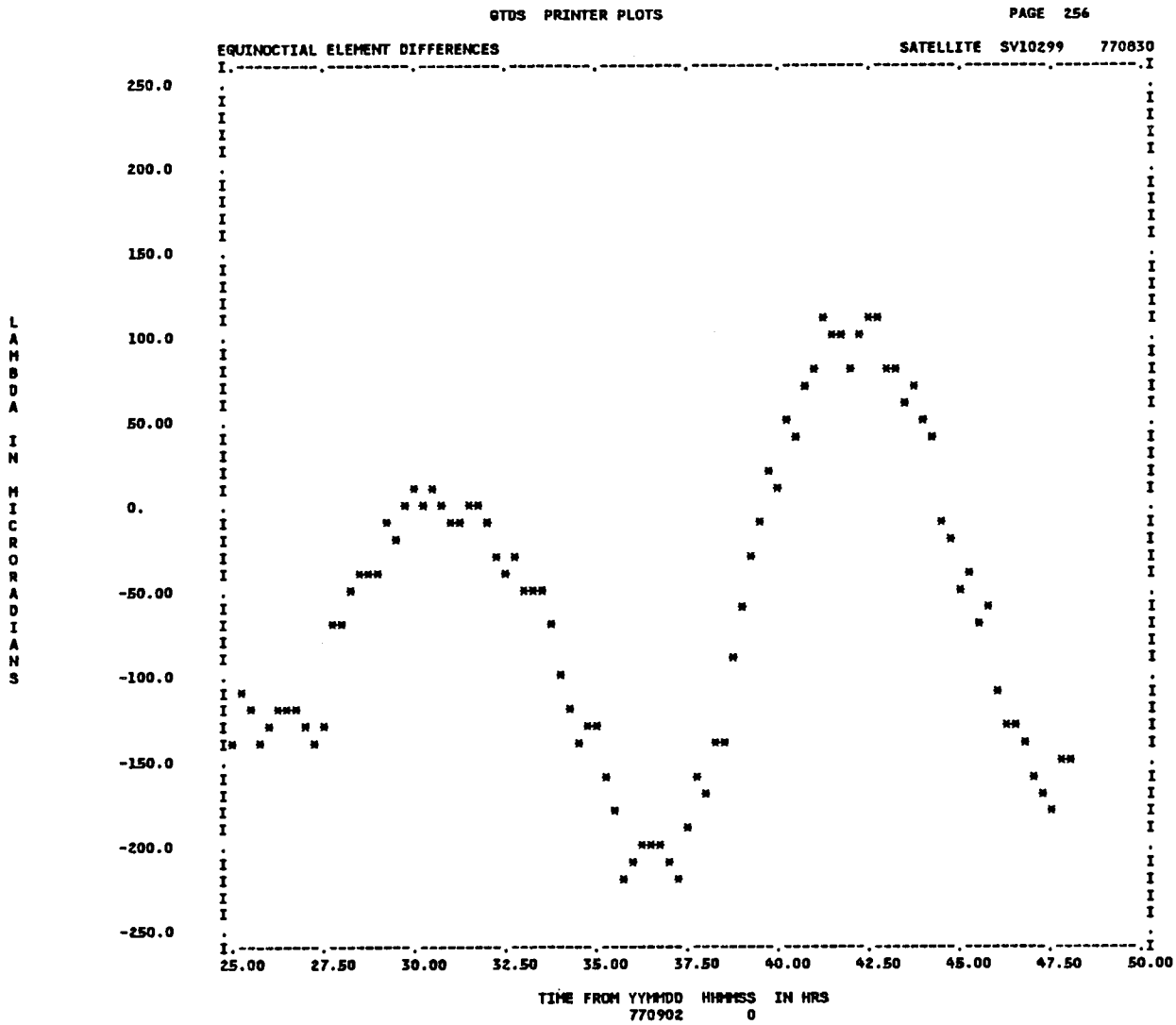

Figure 5-15. HANDE -DSST Mean Longitude Differences Day 5

5.3 Geosynchronous Case

The importance of geosynchronous orbit analysis is well established for both civilian and military communications satellites and their applications. Today, the number of satellites within the geosynchronous ring is increasing to the point where it is useful to better understand the details of the NORAD geosynchronous orbit determination process. Both the simulated data Precise Conversion of Elements analysis and the real data case will provide insight into the orbit determination performance of NORAD's DP4 theory and a "Modified DP4" theory.

The real data analysis will utilize actual tracking data for the Canadian ANIK D2 satellite. The ANIK D2 is a twenty-four channel communications satellite in the 6/4 GHz band [79]. This satellite was designed to replace original ANIKs in the same band which are used for voice and data transmission [80]. The ANIK D2 was launched from the Orbiter Discovery during Mission 51A on 9 November 1984, and after geosynchronous transfer, it assumed a position at 111.5 degrees West longitude. The ANIK D2 was then put into an orbital storage status until 1 January 1986 when it came into full service [79]. The tracking data utilized in this analysis represents the D2 tracking history during the storage time frame. The specific data used for this case was taken from a maneuver-free period and therefore this data creates an optimum test environment for a geosynchronous analysis. An added feature of this analysis is that tracking data from two independent sources, TELESAT (Canada) and

the NORAD Historical Data System, were merged to form a comprehensive data base.

As in the low altitude case, this section first presents the results of the PCE analysis for the DP4 theory. In general, this theory is shown to neglect some lunar-solar and resonance effects, as is expected due to the mathematical explanation presented in chapter two. The real data results carry significant impact because of the optimum test case environment provided by the ANIK D2 tracking data, including 134 precision observations over a twenty-six day arc.

5.3.1 PCE Fit to the DP4 Propagation Trajectory

This PCE analysis used an ephemeris based on a DP4 trajectory produced by the GTDS EPHEM program as the "truth" model or reference trajectory. The force model used in this model is the DP4 force model using WGS-72 parameters. This "truth" model was compared with a DC "Best Fit" ephemerides over a thirty day fit span. The characteristics of the geosynchronous orbit used as initial conditions in this analysis are presented in Table 5-12.

Table 5-12. Initial Parameters of Geosynchronous Orbit for PCE

Element	Value
a	42,164.09 km
e	0.001
i	1.50°
Ω	166.00°
ω	144.99°
M	25.4129°
Perigee height	35,828.12 km
Apogee height	35,743.8 km
Diameter	1.67365 meters
Mass	200.0 Kg
Epoch 1988 6 Oct 6 hrs 43 min 51.670 sec Input Coordinate System NORAD True of Date - Earth Equator	

5.3.1.1 DP4 Geosynchronous DC Comparison

The DP4 ephemeris comparison results during a thirty day fit span are summarized in Table 5-13. Three Keplerian elements were perturbed as follows: semimajor axis (+2km), inclination (+0.5 degrees), and longitude of ascending mode (+0.5 degrees). The converged final position error was 1.325×10^{-5} meters after six iterations. These results indicate that the DP4 DC processing is very effective when compared to a DP4 "truth" file. As in the low altitude PCE results, the actual COMPARE plots reveal extremely small secular drifts in various parameters as is expected.

Table 5-13 DP4 Geosynchronous PCE Results

Initial weighted RMS	86.842
Final weighted RMS	3.616×10^{-9}
Initial Position Error RMS(m)	318226.64
Final Position Error RMS(m)	1.325×10^{-5}
Number of Iterations	6
Converged?	YES

Residual Standard Deviation and (% Observations Accepted)	
x (m)	9.498×10^{-6}
y (m)	8.728×10^{-6}
z (m)	2.931×10^{-6}
x (cm/sec)	6.378×10^{-8}
y (cm/sec)	6.917×10^{-8}
z (cm/sec)	2.152×10^{-8}

5.3.2 Fits to TELESAT ANIK D2 Tracking Data

This analysis is the first step of a larger, more comprehensive study. This comprehensive analysis will study the fundamental characteristics of the general perturbation orbit determination and prediction error budgets with an overall goal to improve the operational DP4 theory. The main focus of this study will be to understand how the truncations and approximations associated with a perturbation theory, in general, and with the DP4 theory in particular, impact the orbit determination process for high altitude orbits. The plan for this study begins with DSST orbit determination runs with various truncations of the mean element equations of motion and the short-periodic models. Initially, the DSST model will be truncated to closely approximate the DP4 General Perturbation model. The DSST theory will then incorporate various modifications to the satellite theory. This analysis will also evaluate the impact on computer run time as modifications are incorporated. The resulting performance data will provide useful guidance for the future enhancement of DP4, or any other NORAD GP theories used for deep space.

The role of the geosynchronous analysis presented in this thesis is to provide some initial estimate of the relative errors due to the DP4 algorithm. In order to provide this estimate, Draper Laboratory's Semi-Analytical Satellite theory was used to fit the merged NORAD and TELESAT tracking data. Table 5-14 provides a summary of the force model used for this analysis. The observation

weights used in the differential correction process were taken from references [82] and [83]. Epoch mean elements were taken from the converged best DSST fit, and used to generate a "truth" ephemeris with which to compare the DP4 theory. The approximate characteristics of the ANIK D2 Reference orbit are given in Table 5-15. The DP4 comparison ephemeris will be generated with epoch mean elements taken from the DP4 theory's best fit to the same data fit by the DSST model. For this particular case, the procedure will isolate the effects of the satellite theory differences. An additional test will utilize the "Modified DP4" theory, in the same manner as the DP4 theory. The "Modified DP4" theory is the net result of an analysis by Dr. Paul Cefola, Wayne McClain (CSDL) and Bruce Baxter (The Aerospace Corporation) [81]. The original DP4 theory was modified to correct an error which truncated the lunar solar contribution to the secular rates whenever the inclination was less than three degrees. Specifically, the ascending node rate, due to lunar solar perturbations was set to zero for all orbits with less than three degree inclination.

Table 5-14. Force Model Used in the DSST 'Truth' Model for the Geosynchronous (ANIK D2) Case

AOG Model	SPG Model
Zonals: (8x0) GEML2	Zonals: (4x0)
Tesseral Resonance: (8x8)	M-Dailies: (4x4), e^2
Second Order J_2 effect: On	Tesserals: (2x2)
Lunar-Solar Point Mass:	J_2 + Drag/M-Daily Coupling: Off
Moon: $(a/r)^8$, e^2	Lunar-Solar-Point Mass: On
Sun: $(a/r)^3$, e^2	Solar Radiation Pressure: On
Solar Radiation Pressure: On	$J_2{}^2$ Second Order: Off
Drag: Off	Drag Short Periodics: Off

Table 5-15. Initial Parameters of ANIK D2 Reference Orbit

Element	Value
a	42,166.215 Km
e	0.0002198
i	1.77°
Ω	277.00°
ω	71.51°
M	288.164°
Perigee height	35,778.80 km
Apogee height	35,797.34 km
Satellite Area	12 m^2
Satellite Mass	640.5 kg
Epoch 1985, April 5, 12 hrs 59 min 28.623 sec Input Coordinate System Mean of 1950.0 Earth Equator	

5.3.2.1 DSST Analysis

It is necessary to explain in detail how the DSST "truth" ephemeris was established in order to provide a valid foundation for comparison to the DP4 ephemeris. First of all, the DSST force model employed (Table 5-14) is essentially equivalent to a special perturbations model. This model requires more computer run time, but it is extremely accurate. The real data in this analysis was fit over twenty-six days. Figure 5-16 is a summary of the observation processing during the twenty-six day time span. It is significant to note that 121 of 134 range observations were accepted, as was 97% of all azimuth, elevation and right ascension observations and 100% of the declinations. A three sigma editing feature was part of the observation processing design. As previously mentioned, the observation data includes both NORAD tracking data from the Historical Data System and TELESAT tracking data. The final residual statistics are presented in Table 5-16 which shows a 1.94 weighted RMS over the twenty-six day fit span. Overall, the DSST fit provides an excellent basis from which to generate a "truth" ephemeris.

OBSERVATION SUMMARY BY TYPE

TYPE	RANG	AZ	EL	RA	DEC	RRAT
TOTAL NO.	134	134	134	40	40	10
NO. ACCEPTED	121 (90%)	131 (97%)	130 (97%)	39 (97%)	40 (100%)	10 (100%)
WEIGHTED RMS	1.407	2.008	2.344	1.852	1.923	1.271
MEAN RESDUAL	0.4978	-3.343	-1.080	-14.81	18.71	1.241
STANDARD DEV	7.018	57.42	66.28	34.91	32.95	0.2752

OBSERVATION SUMMARY BY STATION

STATION	EGLQ	PRKQ	ALTQ	MILQ	MILQ	MILQ	MILQ	MILQ	TTAF	TTAF
TYPE	ALL	ALL	ALL	ALL	RANG	AZ	EL	RRAT	ALL	RANG
TOTAL NO.	0	0	0	40	10	10	10	10	372	124
NO. ACCEPTED	0 (0%)	0 (0%)	0 (0%)	27 (67%)	0 (0%)	7 (70%)	10 (100%)	10 (100%)	365 (98%)	121 (97%)
WEIGHTED RMS	0.0000E+00	0.0000E+00	0.0000E+00	2.542	0.0000E+00	3.983	2.173	1.271	1.904	1.407
STANDARD DEV	0.0000E+00	0.0000E+00	0.0000E+00	0.0000E+00	0.0000E+00	11.99	31.94	0.2752	0.0000E+00	7.018

STATION	TTAF	TTAF	MAGC	MBGC	MBGC	MBGC	MCGC	KAGC	KBGC	KCGC
TYPE	AZ	EL	ALL	ALL	RA	DEC	ALL	ALL	ALL	ALL
TOTAL NO.	124	124	0	32	16	16	0	0	0	0
NO. ACCEPTED	124 (100%)	120 (96%)	0 (0%)	32 (100%)	16 (100%)	16 (100%)	0 (0%)	0 (0%)	0 (0%)	0 (0%)
WEIGHTED RMS	1.835	2.358	0.0000E+00	1.375	1.519	1.214	0.0000E+00	0.0000E+00	0.0000E+00	0.0000E+00
STANDARD DEV	57.57	68.35	0.0000E+00	0.0000E+00	13.36	13.61	0.0000E+00	0.0000E+00	0.0000E+00	0.0000E+00

STATION	CAGC	CBGC	CCGC	CCGC	CCGC	STMC	STMC	STMC
TYPE	ALL	ALL	ALL	RA	DEC	ALL	RA	DEC
TOTAL NO.	0	0	24	12	12	24	12	12
NO. ACCEPTED	0 (0%)	0 (0%)	23 (95%)	11 (91%)	12 (100%)	24 (100%)	12 (100%)	12 (100%)
WEIGHTED RMS	0.0000E+00	0.0000E+00	3.092	2.954	3.212	0.2383	0.2579	0.2169
STANDARD DEV	0.0000E+00	0.0000E+00	0.0000E+00	53.33	18.46	0.0000E+00	30.94	21.27

Figure 5-16. DSST Geosynchronous Observation Processing Summary

Table 5-16. Results of DSST DC for Merged Telesat Data

Residual	Standard Deviation
Range	7.018 meters
Azimuth	57.42 seconds of arc
Elevation	66.28 seconds of arc
Range-Rate	27.52 cm/sec
Weighted RMS error over 26 day fit span 1.94	
Number of Iterations: 10	

5.3.2.2 DP4 Analysis

The DP4 model was used to fit the same data as in the DSST case. The observation processing summary is presented in Figure 5-17. In general, this summary suggests that the processing provided a good basis for the differential correction since the data is over a long arc, with good quality observations. However, it is important to note that only 9% of the range data was accepted, 13 of 134 observations. This indicates that for this particular case, the DP4 model had problems with the precision range data being outside of the three sigma tolerance. Obviously, the DP4 range standard deviation was much greater than the DSST range standard deviation. The results of Table 5-17 support this observation as the DP4 range standard deviation was 14.73 meters, which is approximately twice the 7.018 meter standard deviation for the DSST range residual (Table 5-16). The twenty-six day fit span results of Table 5-18 show a position difference of 6.66 kilometers RMS for the converged DP4 ephemeris when compared to the converged DSST reference ephemeris. Although the magnitude of the position error is significant, it is perhaps more important to study Figures 5-18 through 5-22 which present comparisons in position, longitude of the ascending node and mean longitude. Specifically, Figure 5-20, the along track differences, Figure 5-21, the longitude of the ascending node histories, and Figure 5-22, the mean longitude differences, present indications of a periodic or cubic signature that could indicate mismodeling of resonance or lunar-solar

perturbations. The significance of this analysis is that even with an excellent data base, from two independent sources which use a long arc of actual tracking observations, the differential correction process does not compensate for neglected effects. Further analysis is necessary to investigate this finding which compares a DSST fit to the DP4 fit.

DIFFERENTIAL CORRECTION SUMMARY PAGE 2 OF 2 PAGE 44

OBSERVATION SUMMARY BY TYPE

TYPE	RANG	AZ	EL	RA	DEC	RRAT
TOTAL NO.	134	134	134	40	40	10
NO. ACCEPTED	13 (9%)	130 (97%)	131 (97%)	39 (97%)	40 (100%)	0 (0%)
WEIGHTED RMS	3.002	2.242	2.558	2.646	1.723	0.0000E+00
MEAN RESDUAL	-1.400	-4.321	-0.1654	13.24	1.766	0.0000E+00
STANDARD DEV	14.73	59.63	72.70	47.33	29.94	0.0000E+00

OBSERVATION SUMMARY BY STATION

STATION	EGLQ	PRKQ	ALTQ	MILQ	MILQ	MILQ	MILQ	MILQ	TTAF	TTAF
TYPE	ALL	ALL	ALL	ALL	RANG	AZ	EL	RRAT	ALL	RANG
TOTAL NO.	0	0	0	40	10	10	10	10	372	124
NO. ACCEPTED	0 (0%)	0 (0%)	0 (0%)	17 (42%)	1 (10%)	6 (60%)	10 (100%)	0 (0%)	257 (69%)	12 (9%)
WEIGHTED RMS	0.0000E+00	0.0000E+00	0.0000E+00	4.039	2.022	6.149	2.151	0.0000E+00	2.292	3.070
STANDARD DEV	0.0000E+00	0.0000E+00	0.0000E+00	0.0000E+00	0.0000E+00	10.36	31.77	0.0000E+00	0.0000E+00	15.23

STATION	TTAF	TTAF	MAGC	MBGC	MBGC	MBGC	MCGC	KAGC	KBGC	KCGC
TYPE	AZ	EL	ALL	ALL	RA	DEC	ALL	ALL	ALL	ALL
TOTAL NO.	124	124	0	32	16	16	0	0	0	0
NO. ACCEPTED	124 (100%)	121 (97%)	0 (0%)	32 (100%)	16 (100%)	16 (100%)	0 (0%)	0 (0%)	0 (0%)	0 (0%)
WEIGHTED RMS	1.854	2.589	0.0000E+00	1.874	1.724	2.014	0.0000E+00	0.0000E+00	0.0000E+00	0.0000E+00
STANDARD DEV	58.14	75.09	0.0000E+00	0.0000E+00	25.19	20.71	0.0000E+00	0.0000E+00	0.0000E+00	0.0000E+00

STATION	CAGC	CBGC	CCGC	CCGC	CCGC	STMC	STMC	STMC
TYPE	ALL	ALL	ALL	RA	DEC	ALL	RA	DEC
TOTAL NO.	0	0	24	12	12	24	12	12
NO. ACCEPTED	0 (0%)	0 (0%)	23 (95%)	11 (91%)	12 (100%)	24 (100%)	12 (100%)	12 (100%)
WEIGHTED RMS	0.0000E+00	0.0000E+00	3.481	4.523	2.114	0.1693	0.2010	0.1301
STANDARD DEV	0.0000E+00	0.0000E+00	0.0000E+00	73.88	18.79	0.0000E+00	28.44	18.70

Figure 5-17. DP4 Geosynchronous Observation Processing Summary

Table 5-17. Results of DP4 DC for Merged Telesat Data

Residual	Standard Deviation
Range	14.73 meters
Azimuth	59.63 seconds of arc
Elevation	72.70 seconds of arc
Range-Rate	0% accepted
Weighted RMS error over 26 day fit span 2.391	
Number of Iterations: 19	

This is based on very small number accepted.

Table 5-18. Comparison of DP4 Theory with Converged DSST

	26 Day Fit Span	
	Position RMS (km)	Velocity RMS (cm/sec)
Radial	1.071	36.59
Cross-Track	3.176	23.96
Along-Track	5.757	10.09
Total	6.666	44.89

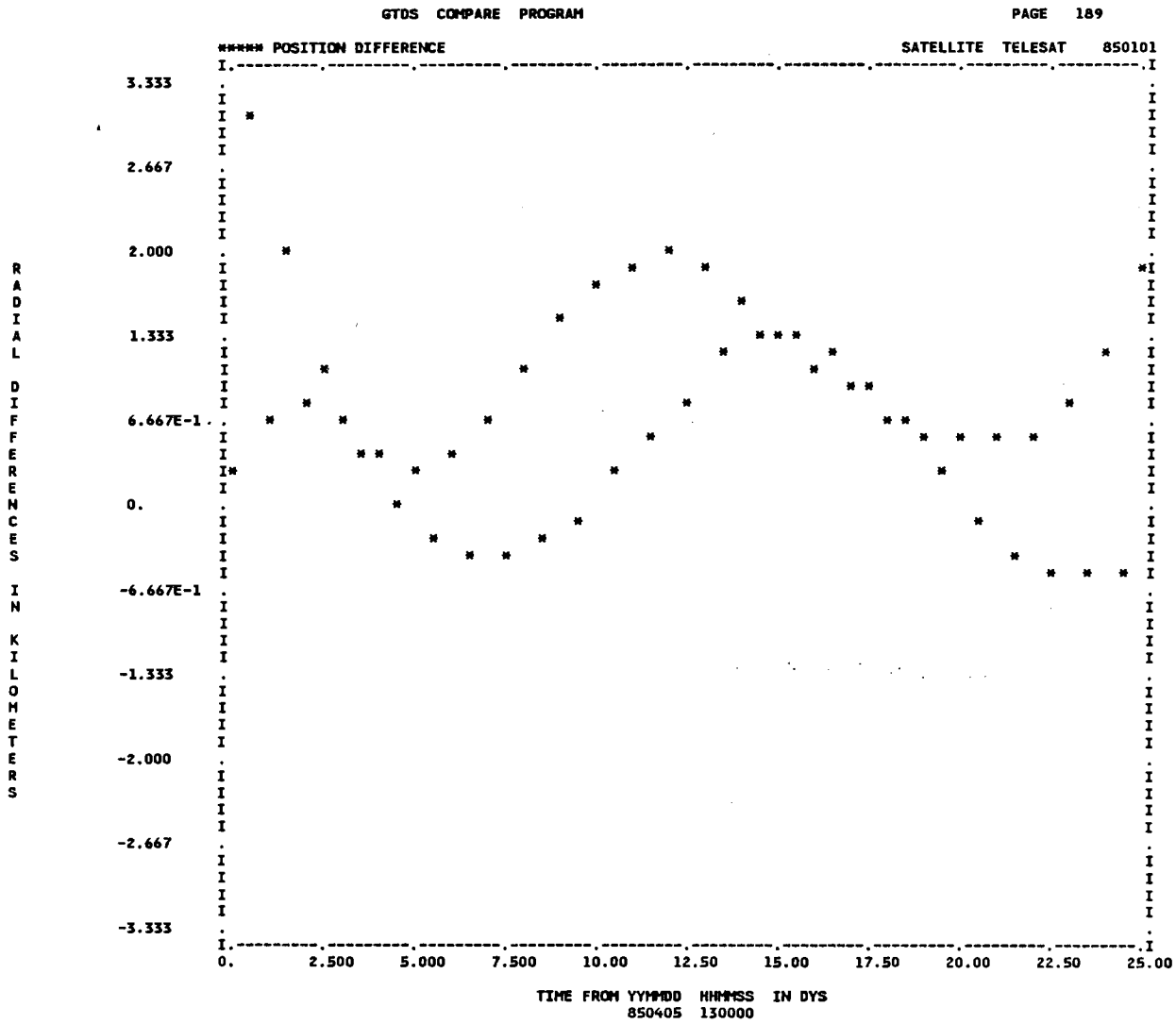

Figure 5-18. DP4-DSST Fit Span Radial Differences

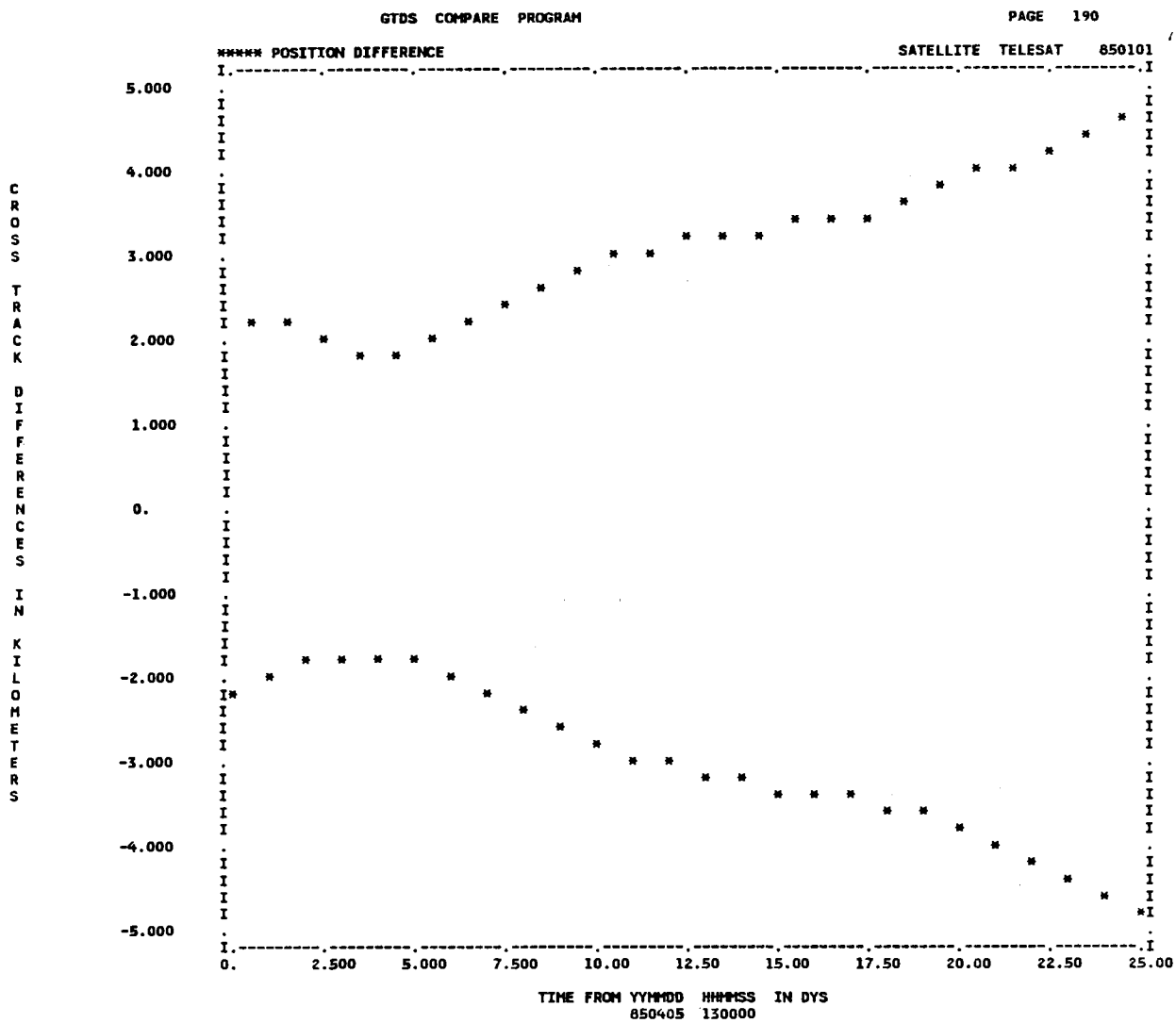

Figure 5-19. DP4-DSST Fit Span Cross-Track Differences

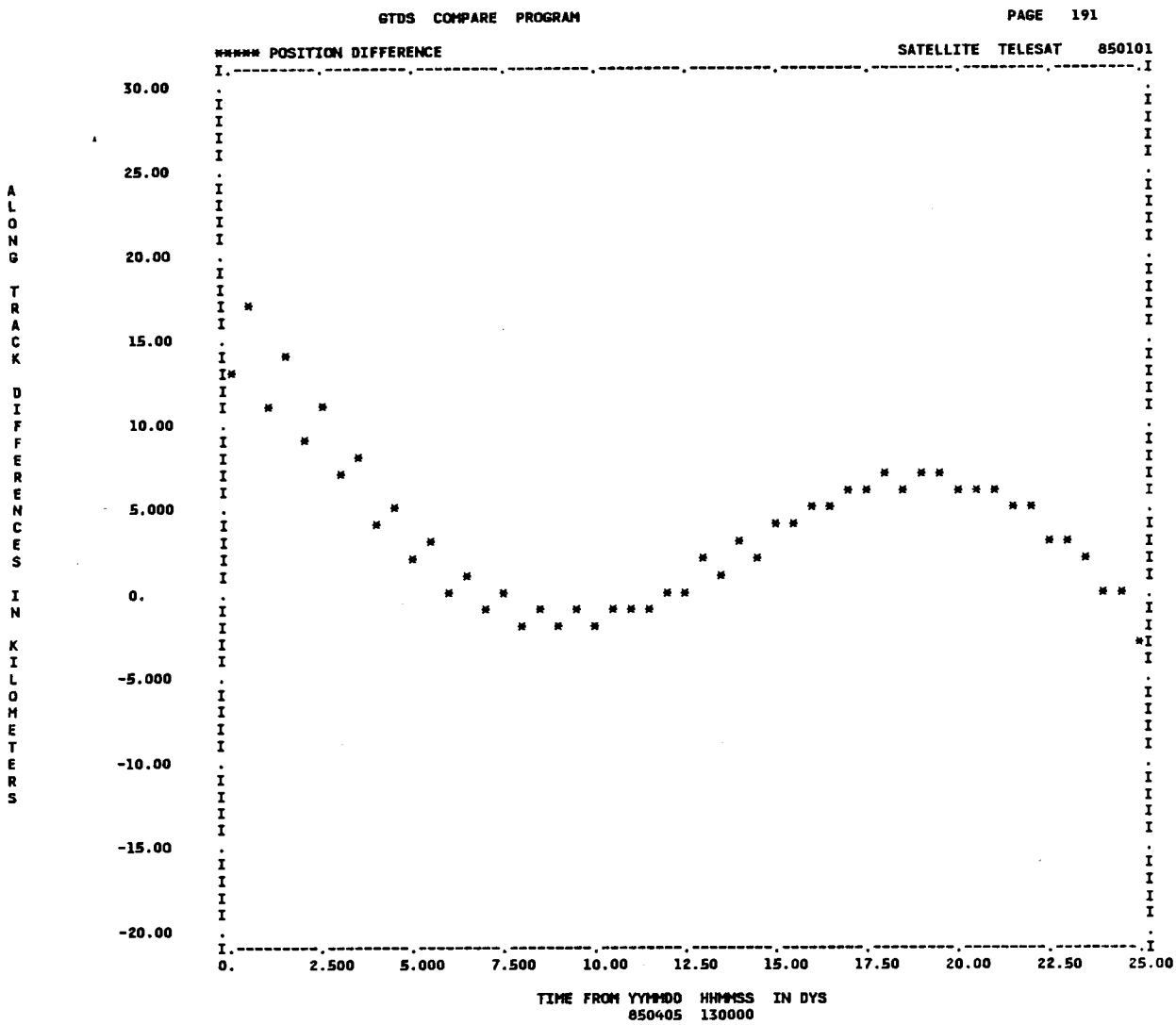

Figure 5-20. DP4-DSST Fit Span Along-Track Differences

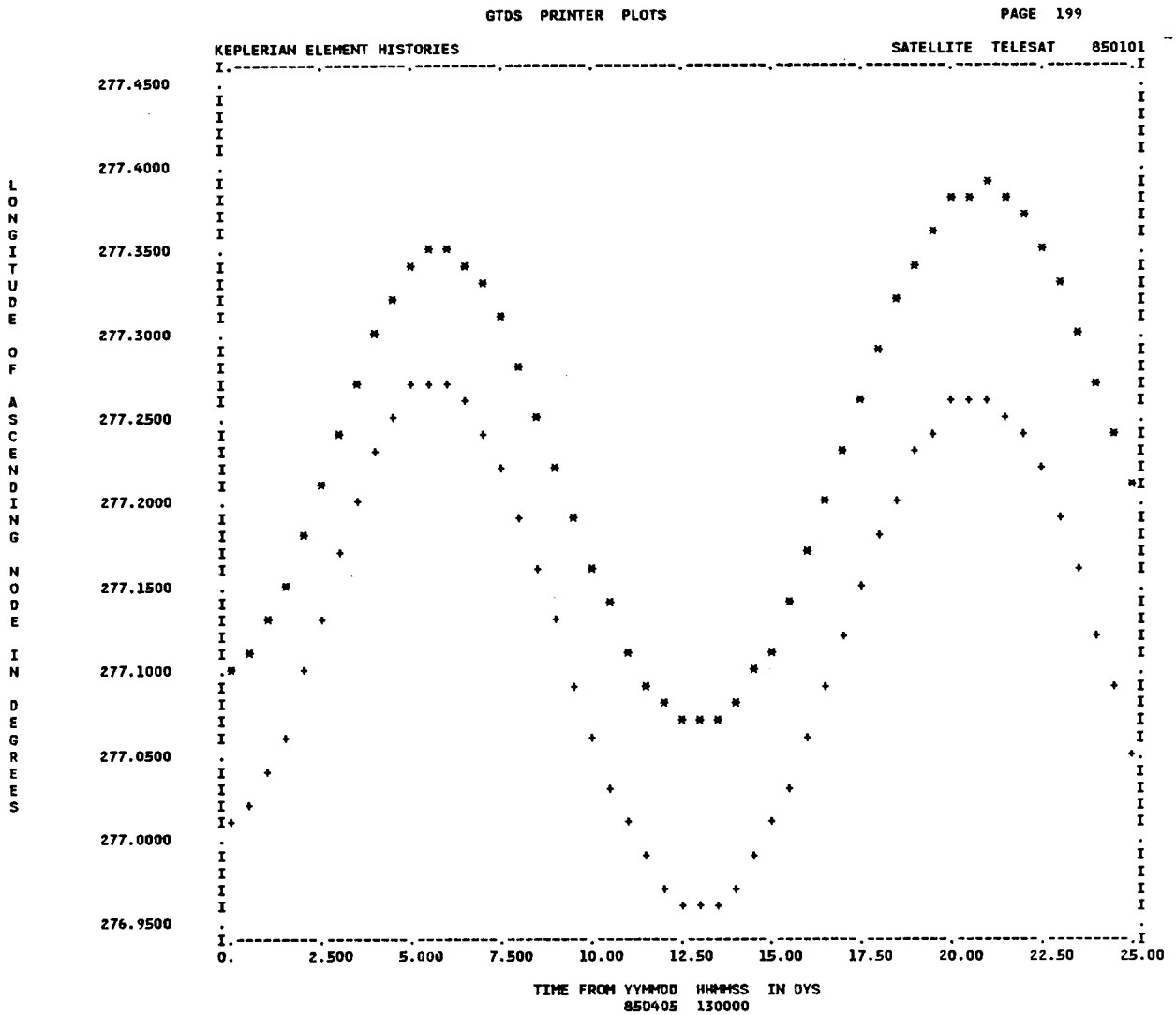

Figure 5-21. DP4 and DSST Fit Span Longitude of Ascending Node Histories

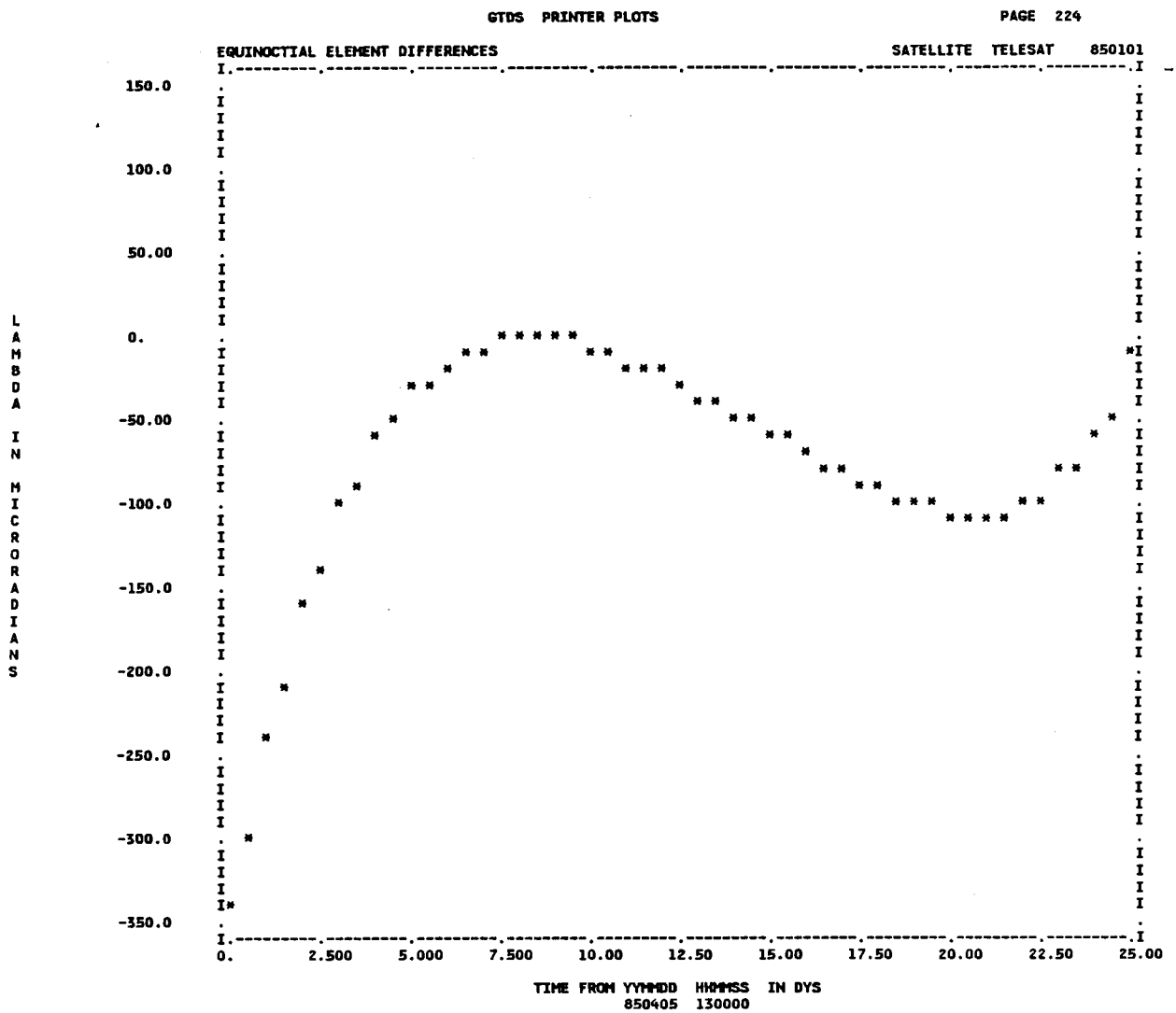

Figure 5-22. DP4-DSST Fit Span Mean Longitude Differences

The "Modified DP4" model also processed the same merged observations with results that were very similar to the DP4 processing. See Figure 5-23. The only significant difference in the fit span results, as depicted in Tables 5-19 and 5-20 is a decrease in the cross-track RMS values from 3.176 kilometers to 0.681 kilometers. Figures 5-24 through 5-28 support this analysis. Specifically, a comparison of Figure 5-27 and 5-21 graphically illustrates the noticeable improvement in the longitude of the ascending node histories from approximately 0.1 degrees in DP4 to 0.05 degrees in the "Modified DP4" model. All of the remaining "Modified DP4" figures remain essentially the same as the original DP4 results.

DIFFERENTIAL CORRECTION SUMMARY PAGE 2 OF 2 PAGE 44

OBSERVATION SUMMARY BY TYPE

TYPE	RANG	AZ	EL	RA	DEC	RRAT
TOTAL NO.	134	134	134	40	40	10
NO. ACCEPTED	13 (9%)	130 (97%)	131 (97%)	39 (97%)	40 (100%)	0 (0%)
WEIGHTED RMS	3.335	2.265	2.493	2.532	1.848	0.0000E+00
MEAN RESDUAL	2.400	-4.333	0.5063	14.06	7.127	0.0000E+00
STANDARD DEV	16.36	60.87	70.68	45.40	32.88	0.0000E+00

OBSERVATION SUMMARY BY STATION

STATION	EGLQ	PRKQ	ALTQ	MILQ	MILQ	MILQ	MILQ	MILQ	TTAF	TTAF
TYPE	ALL	ALL	ALL	ALL	RANG	AZ	EL	RRAT	ALL	RANG
TOTAL NO.	0	0	0	40	10	10	10	10	372	124
NO. ACCEPTED	0 (0%)	0 (0%)	0 (0%)	17 (42%)	1 (10%)	6 (60%)	10 (100%)	0 (0%)	257 (69%)	12 (9%)
WEIGHTED RMS	0.0000E+00	0.0000E+00	0.0000E+00	3.995	1.719	6.053	2.203	0.0000E+00	2.295	3.435
STANDARD DEV	0.0000E+00	0.0000E+00	0.0000E+00	0.0000E+00	0.0000E+00	10.32	31.93	0.0000E+00	0.0000E+00	16.93

STATION	TTAF	TTAF	MAGC	MBGC	MBGC	MBGC	MCGC	KAGC	KBGC	KCGC
TYPE	AZ	EL	ALL	ALL	RA	DEC	ALL	ALL	ALL	ALL
TOTAL NO.	124	124	0	32	16	16	0	0	0	0
NO. ACCEPTED	124 (100%)	121 (97%)	0 (0%)	32 (100%)	16 (100%)	16 (100%)	0 (0%)	0 (0%)	0 (0%)	0 (0%)
WEIGHTED RMS	1.898	2.516	0.0000E+00	1.708	1.556	1.847	0.0000E+00	0.0000E+00	0.0000E+00	0.0000E+00
STANDARD DEV	59.56	72.95	0.0000E+00	0.0000E+00	22.79	17.49	0.0000E+00	0.0000E+00	0.0000E+00	0.0000E+00

STATION	CAGC	CBGC	CCGC	CCGC	CCGC	STMC	STMC	STMC
TYPE	ALL	ALL	ALL	RA	DEC	ALL	RA	DEC
TOTAL NO.	0	0	24	12	12	24	12	12
NO. ACCEPTED	0 (0%)	0 (0%)	23 (95%)	11 (91%)	12 (100%)	24 (100%)	12 (100%)	12 (100%)
WEIGHTED RMS	0.0000E+00	0.0000E+00	3.567	4.378	2.610	0.1854	0.2061	0.1620
STANDARD DEV	0.0000E+00	0.0000E+00	0.0000E+00	71.47	19.84	0.0000E+00	27.95	21.57

Figure 5-23. "Modified" DP4 Geosynchronous Observation Processing Summary

Table 5-19. Results of "Modified" DP4 DC for Merged Telesat Data

Residual	Standard Deviation
Range	16.36 meters
Azimuth	60.87 seconds of arc
Elevation	70.68 seconds of arc
Range-Rate	0% accepted
Weighted RMS error over 26 day fit span 2.387	
Number of Iterations: 19	

Table 5-20. Comparison of "Modified" DP4 Theory with Converged DSST (D2)

	26 Day Fit Span	
	Position RMS (km)	Velocity RMS (cm/sec)
Radial	1.027	39.39
Cross-Track	0.681	16.57
Along-Track	6.073	9.851
Total	6.197	43.86

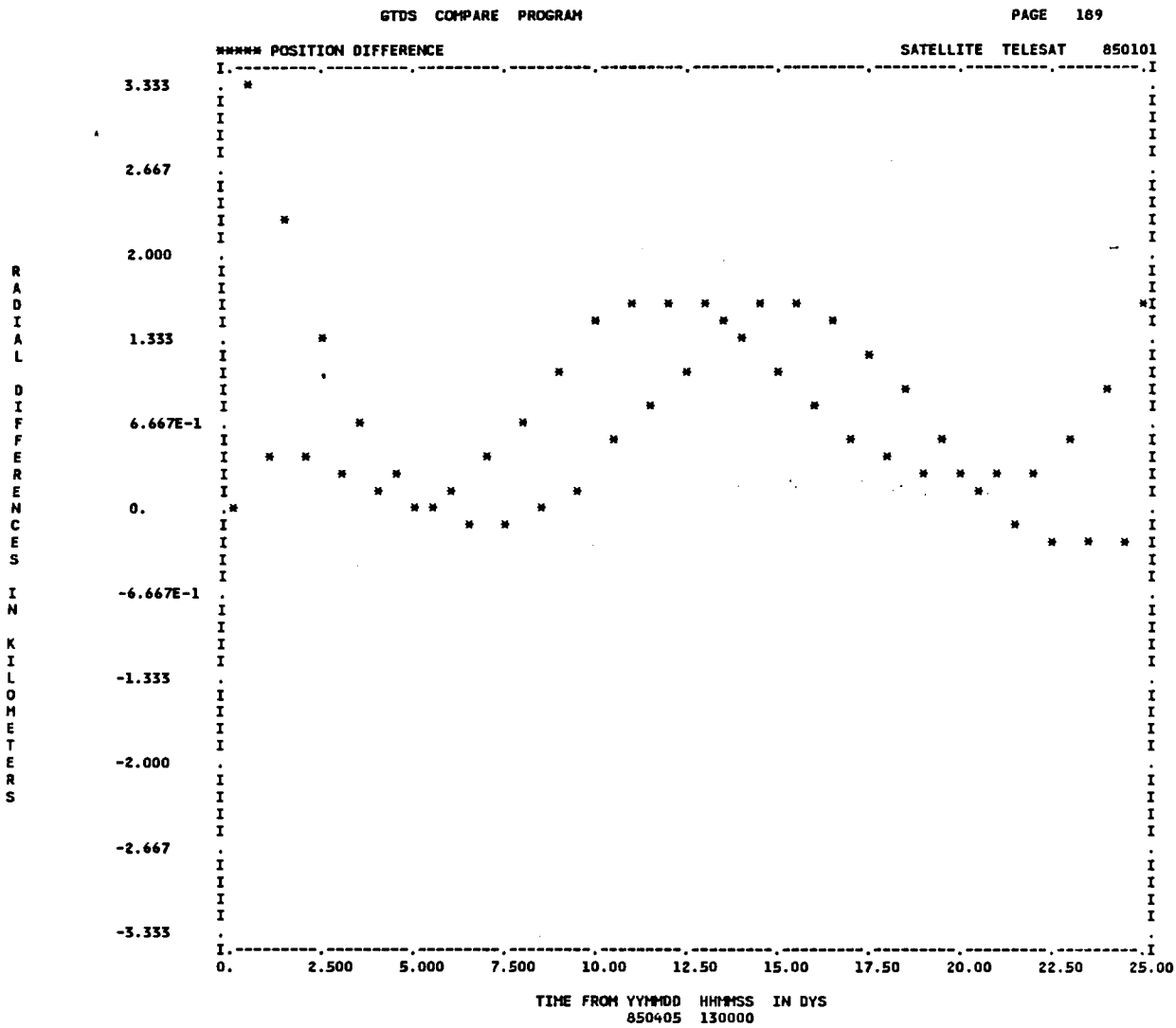

Figure 5-24. "Modified DP4" -DSST Fit Span Radial Differences

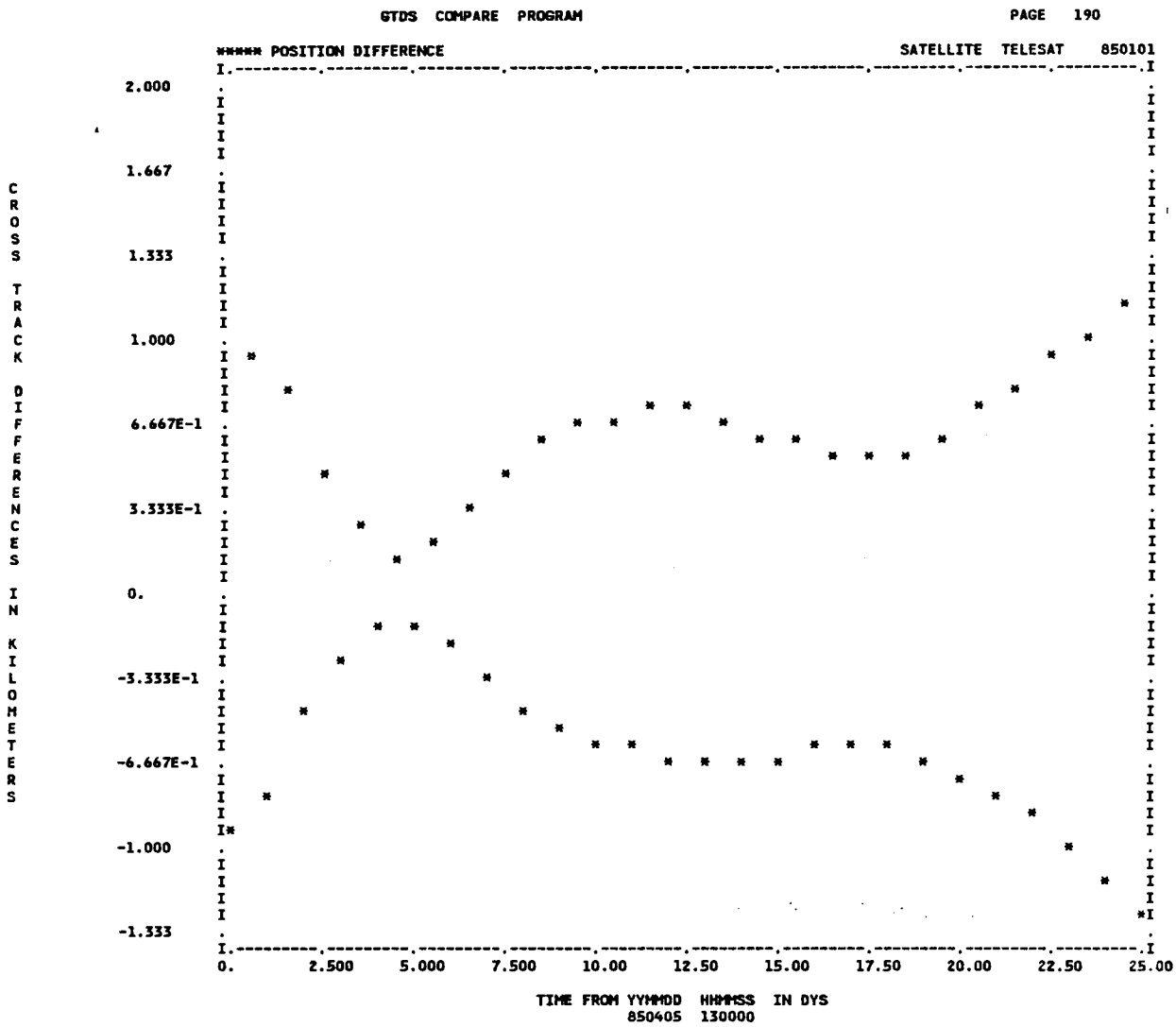

Figure 5-25. "Modified DP4" -DSST Fit Span Cross-Track Differences

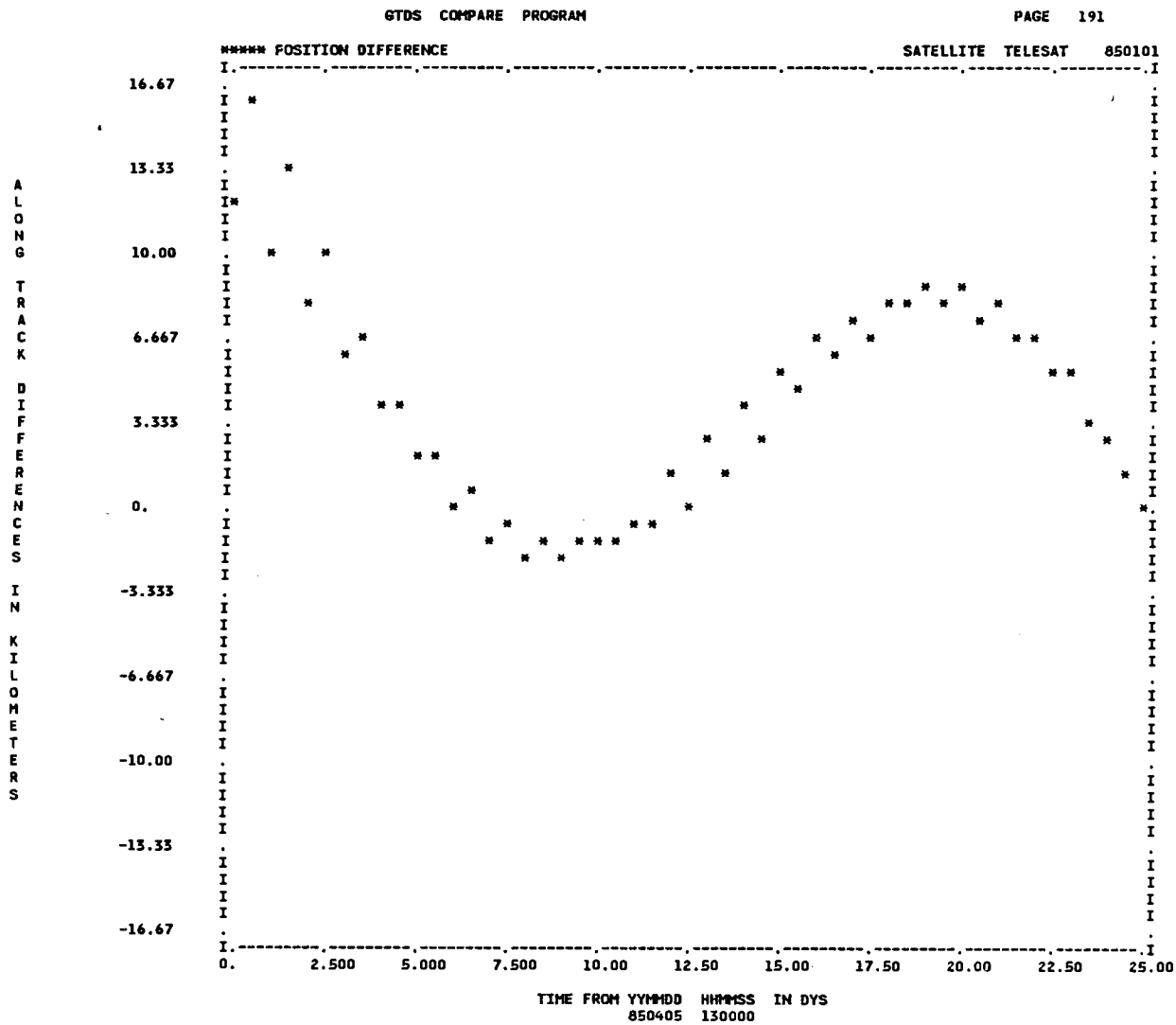

Figure 5-26. "Modified DP4" -DSST Fit Span Along-Track Differences

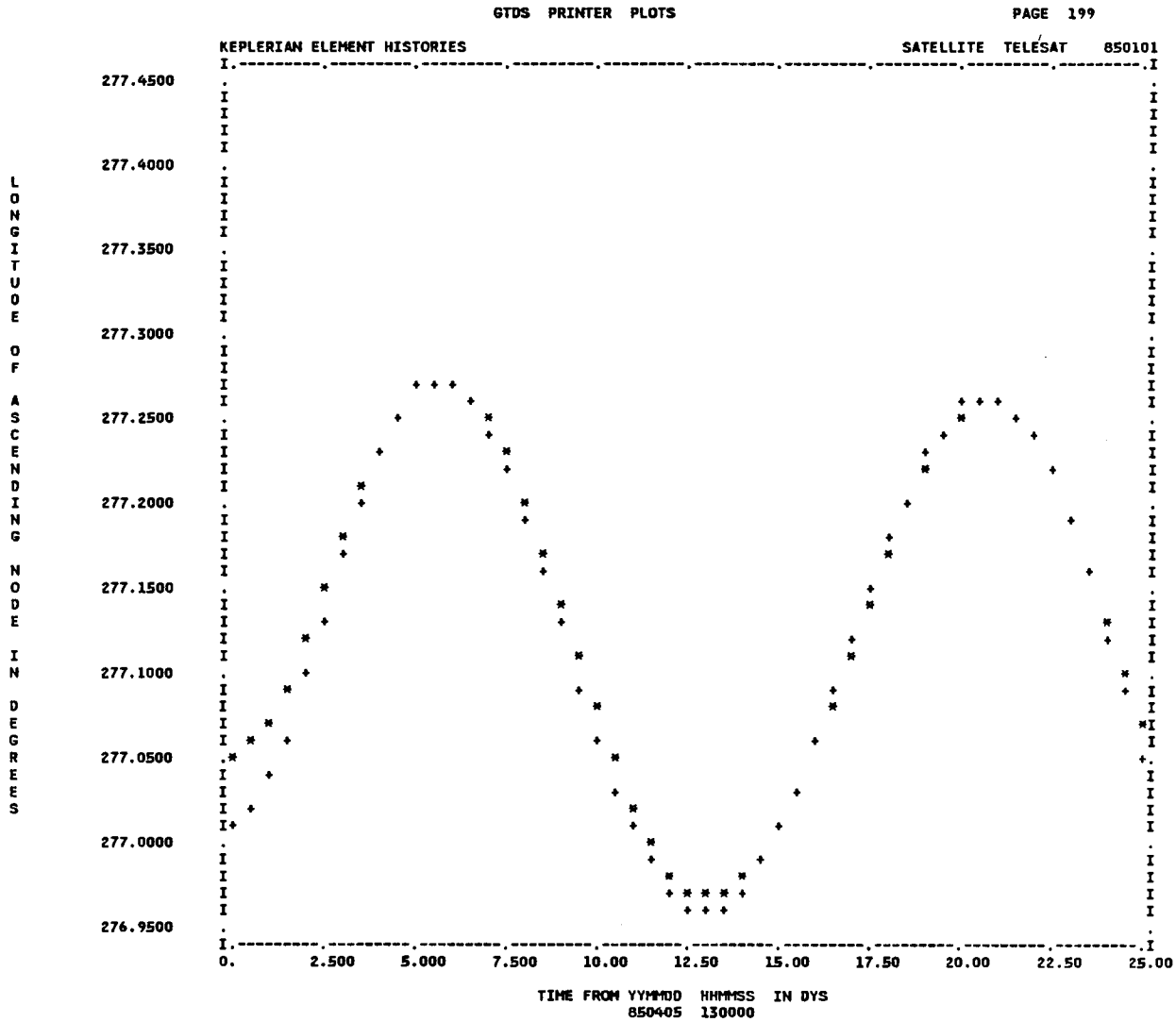

Figure 5-27. "Modified DP4" and DSST Fit Span Longitude of Ascending Node Histories

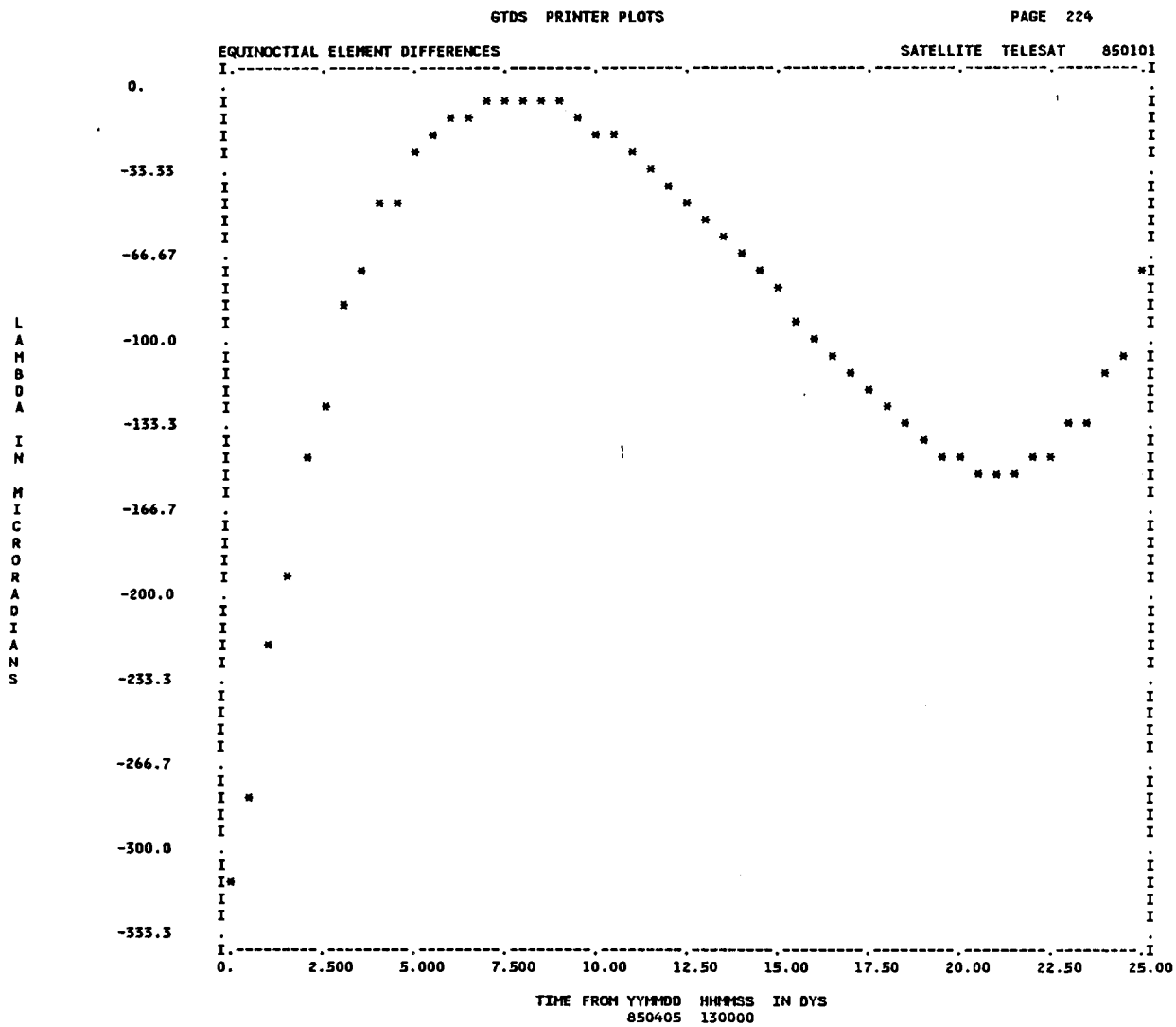

Figure 5-28. "Modified DP4" -DSST Fit Span Mean Longitude Differences

Chapter 6

CONCLUSIONS / FUTURE WORK

6.1 Summary

The primary objective of this thesis was to accurately incorporate the SGP, GP4/DP4 and HANDE general perturbation theories into the Draper Laboratory modified Goddard Trajectory Determination System orbit computation program. The Ford Aerospace & Communications Corporation supplied the SPADOC Fortran source code and test cases which made this implementation possible. The real tracking data used to demonstrate NORAD GP theory orbit determination using the Draper Laboratory orbit computation program consisted of the following:

1. NORAD tracking data for the low altitude NSSC 10299 for the period 30 August 77 - 7 September 77.

2. TELESAT tracking data for the ANIK D2 communication satellite for the period 1 January 85 - 31 December 85.

3. Tracking data from the NORAD Historical Data System for the ANIK D2 satellite covering the period 1 January 1985 to 31 December 1985.

Chapter Two provides a review of all the NORAD GP theories which were a part of this incorporation. This chapter also presents an overview of the Draper Laboratory's Goddard Trajectory Determination System and its capabilities. This review is significant because it presents the "new" tools which are now available to analyze the NORAD GP theories. Additionally, Chapter Two explains the differences between the coordinate systems most commonly used by NORAD and GTDS.

Chapter Three describes the implementation effort in a manner that matches the actual data flow. A key aspect of the incorporation was the ability to maintain an independent functionality between the NORAD software and the existing GTDS architecture. This feature also minimized required modifications to both the NORAD and GTDS software. Nonetheless, thirty-two GTDS subroutines and four SPADOC subroutines were modified and eleven new GTDS subroutines were created to complete the interface.

Chapter Four presents the results of testing the newly incorporated NORAD orbit generators. An SGP test case generated with mixed-mode arithmetic was taken from Spacetrack Report #3 [5] and the results of this case were regenerated to an accuracy of 3.32 meters. The Ford Aerospace Corporation supplied orbit generator test cases which served as benchmarks for the GP4/DP4 and HANDE theories. These test cases were regenerated to an accuracy of 10.34 millimeters for GP4/DP4 and to 15.34 centimeters for the HANDE theory. An analysis of the elements of the state transition matrix for each NORAD theory indicated that the

NORAD orbit generator partial derivatives were accurately incorporated.

Chapter Five discusses the differential correction results for a Precise Conversion of Elements analysis and for a real data test protocol for both the low altitude and geosynchronous flight regimes. The Precise Conversion of Elements analysis used a reference ephemeris that was based on a specific GP theory ephemeris. The same NORAD GP theory starting with a perturbed a priori element set was then fit to this reference. Each theory converged to a DC solution after five iterations thereby verifying the implementation and functionality of the DC software.

In the real data analyses, a high precision DSST model is fit to the tracking data in order to obtain mean elements which are subsequently used to generate a truth ephemeris. Then, a given NORAD GP theory was used to process the same tracking data through a differential correction process to obtain an epoch mean element set. This converged element set was used to generate a NORAD GP ephemeris. This GP ephemeris was then compared to the DSST reference orbit in the GP fit span. These low altitude and geosynchronous results are summarized in Tables 6-1 and 6-2 respectively.

Table 6-1. Summary of Real Data Low Altitude Results

	GP4 Days (4-6)	HANDE Days (4-6)	DSST Days (1-3)	DSST Days (4-6)
DC Results Position Error RMS (meters) Over 3 Day Fit Span	1551.1	1565.6	1230.9	1554.0

Table 6-2. Summary of Real Data Geosynchronous Results

	DP4	"Modified" DP4	DSST
DC Results Weighted RMS Error Over 26 Day Fit Span	2.39	2.39	1.94
Comparison Results with Converged DSST Over 26 Day Fit Span			
Position RMS (km)	6.67	6.20	N/A
Velocity RMS (cm/sec)	44.89	43.86	N/A

6.2 Conclusions

The NORAD General Perturbation theories have been accurately incorporated into the Draper Laboratory's Goddard Trajectory Determination System orbit computation program. The results of chapter Four provide strong confidence in the accuracy of this incorporation. As a result of this incorporation, Draper Laboratory has the capability to further analyze the NORAD GP theories. This capability is unique in that the NORAD GP theories can now be analyzed with the tools within Draper Laboratory's GTDS computer program as described in chapter Two. Similarly, Draper Laboratory can investigate error budgets for any specific satellite trajectory, using any of the incorporated NORAD GP theories. The design of this incorporation maintains the SPADOC software as an independent block interface which allows corrections and improvements to be easily communicated between Draper Laboratory and the government's SPADOC environment.

The analysis of the state transition matrix elements for each NORAD GP theory indicates that the differences which exist between the values of the partial derivatives are primarily due to the different definitions of each theory's "mean" elements. Further analysis of these differences would be valuable in understanding the partial derivatives and their particular contributions to the orbit determination process.

The results of the low altitude PCE analyses indicate that all NORAD GP differential correction processing was very effective when compared with each corresponding theory's "truth" file.

However it is significant to note that the differential correction process (based on the real observations) did not correct for the effects of neglecting a dynamic atmosphere with either the NORAD models nor even with the highly accurate DSST model. This observation suggests a need for satellite theories to better account for geomagnetic and solar flux variations within their density models. Further study of the impact of these effects is essential to improving orbit determination accuracy.

The low altitude case results revealed that the differences between the GP and DSST DC solutions contained m-daily periodic effects. This was to be expected based on the different assumptions used to build the GP and DSST satellite theories as described in Chapter two.

The results of the geosynchronous analysis carry significant impact due to the outstanding data provided by TELESAT [83] and the NORAD HDS; also, the ANIK D2 satellite was in a maneuver-free 'storage' mode during this analysis period. The real data results, for the case considered in this analysis, suggest that the DP4 theory does not incorporate some lunar-solar effects and resonance effects, as seen in the along-track and mean longitude differences, and longitude of ascending node differences. This observation also was valid for the "Modified DP4" theory results; however, the cross-track error was improved.

6.3 Future Work

This thesis has created a new and unique analysis capability at the Draper Laboratory. Accordingly, there is a tremendous opportunity for further studies. The tools for these further studies lie within the Draper Laboratory modified Goddard Trajectory Determination System computer program. Any of the newly incorporated NORAD GP theories may now be modified or improved in a research environment without impacting operational capabilities. Again, it cannot be over emphasized that this research effort would not have been possible without the cooperation and assistance of the AF Space Command Directorate of Operational Analysis (DOA), the AF Electronic System Division (ESD) and the Ford Aerospace & Communications Corporation (FACC). Future research efforts, and the impact of those efforts will be determined, in a large part by the continued cooperation of these agencies. The following research suggestions present only a partial list of ideas that may have an impact in the future enhancement of NORAD's GP orbit determination capabilities. These suggestions are presented in three general categories; Draper Laboratory implementation and verification, NORAD GP theory performance and NORAD GP theory enhancements.

The following activities are suggestions for further implementation and verification at Draper Laboratory:

1. As noted in chapter Four, it would be desirable to employ the SPADOC standalone test drivers (SGPDRV, GP4DRV, HANDRV) for the GP theories modified to write GTDS-format ORB1 files. These ORB1 files could then be systematically compared with ORB1 files produced by the NORAD GP theories operating in GTDS. The error time histories and statistics would give further verification of the GTDS implementation.

2. The performance of the HANDE time derivative initialization only has been investigated implicitly through its operation in the DC process. The capability to access the GTDS Harris-Priester atmosphere density model in a HANDE initialization run to allow the resulting mean element histories to be compared with those produced by the DSST should be developed. In this context, it would be desirable to implement the option for mean element output with the GTDS NORAD GP theories. done

3. Investigate the GP state transition matrix and the drag solve-for partials using a double-sided finite differencing technique.

4. Incorporate and analyze the NORAD Semianalytical Satellite Theory (SALT) in the Draper Laboratory GTDS computer program.

done

5. Develop the capability for the NORAD theories to access the GTDS physical models: geopotential coefficients, timing polynomials, density models, and solar activity/geomagnetic index data files. Develop the capability for the GTDS orbit generators (DSST and Cowell) to access the SPADOC atmospheric density models.

done

The performance of the NORAD GP theories could be analyzed with the following activities:

1. Modify the PCE test methodology to solve for epoch mean elements based on the fit of each NORAD GP theory to the ephemeris of a high precision Cowell integration. Exploit this idea further by comparing the NORAD and Cowell ephemerides over both fit and predict spans. Run extensive tests to get trends within each theory, against the Cowell integrator in both fit and predict spans.

2. Modify the real data analysis approach by comparing the NORAD GP ephemeris with a variety of different "truth"

models in a given predict span. Possible truth models include the following:

a. Use the same DSST "truth" model as was used in the fit span analysis in Chapter Five.

b. Create two "truth" models by sorting a given observation data set to form two independent batches. Then fit DSST to each of these batches to obtain an initial element set to propagate two "truth" ephemerides.

talk to Ron about how we would represent

c. Filter/smooth either the DSST or Cowell model to get another reference trajectory.

3. Utilize an orbit determination approach to measure the DSST accuracy by comparing specified solutions over numerous overlapping time periods. Such an approach was employed by the Computer Sciences Corporation for an orbit determination study of the HEAO-2 Spacecraft. In that study, orbit solution accuracies were estimated by calculating ephemeris position differences in the four to six hour overlap intervals.

This approach assumes that if two orbit solutions are accurate then the overlap differences will be small but that the converse is not true. Furthermore, if several consecutive overlap differences show a significant (fifty percent or more) reduction when a more precise set of orbit determination parameters is selected, then it is

reasonable to conclude that the error in the orbit solutions has been decreased. The HEAO-2 study also stated that the conclusion should also be partially based on the behavior of the RMS weighted residuals of the solutions [98].

Another approach that could be used to measure the accuracy of the DSST model is the technique that Lichten and Bertiger [99] use in a GPS orbit determination study. The key concept of their approach is to compare orbits that were determined independently without any common measurements and compare the RMS differences over a time interval during which no data were used for either of the two solutions.

* 4. Run extensive timing analysis for efficiency comparisons of DSST vs. any given GP theory.

* 5. Develop a systematic understanding of how the orbit determination process is impacted by varying levels of geomagnetic disturbance at various altitudes and mean solar activity levels. Develop a capability for including these effects in a given satellite theory, such as HANDE or DSST. (this could be in conjunction w/ Filter)

6. As described in chapter Five, study the NORAD DP4 theory by modifying the DSST geopotential model to match the DP4 model and then determine the impact of adding specific terms with regard to accuracy and computer run time. This analysis would have the overall goal of improving the operational capabilities of the DP4 general perturbation theory.

7. Analyze the GP performance in non-traditional flight regimes. High eccentricity orbits with periods of 24 hours or longer such as the EXOSAT are of interest.

8. Investigate the accurate conversion of element sets between Cowell, DSST, SGP, GP4/DP4, and HANDE.

The following two suggestions are activities that could directly enhance specified NORAD GP theories:

1. Incorporate m-daily effects into the GP4, HANDE, or SALT theories by using some of the recursive models from DSST.

2. Consider the development of an 'operational style' GP theory with fast computation speed based on non-singular, canonical elements, such as the Poincare second set. This development should include a formulation of the

state transition matrix. This satellite theory would allow the same variables to be used as the DC solve parameters and the satellite theory initial conditions. Low e and low i would not be special cases in this theory. Recursive models should be considered for this satellite theory. The transmission of elements to users should also be considered.

Appendix A

Overview of General and Special Perturbation Methods

This appendix provides an overview of perturbations, the methods which are employed to solve the perturbation problem, as well as the advantages and disadvantages of these methods. Following a brief introduction to perturbations, this appendix will discuss both general and special perturbation methods. This development includes the basic theory of each method, and the advantages and disadvantages for each given method. The motion of a satellite about a planet cannot be solved accurately with the two-body Keplerian theory. Although this theory is an integral part of any trajectory, the actual path will vary from this theoretical reference orbit due to the presence of other masses; solar radiation effects; the asphericity of the central planet, or other attracting masses; and atmospheric drag. These factors cause the satellite to deviate from a classical two-body orbit, and are known as perturbations. From a mathematical viewpoint, these perturbations fall into two general categories: secular - terms that grow monotonically with time, such as the precession of the vernal equinox which moves westward approximately fifty arc-seconds per year; [84] or periodic - any terms that are cyclic, such as the Earth's nutation which is caused by the moon creating a torque on the Earth's equatorial bulge [85]. A further distinction is often made between short and long periodic terms based upon a given boundary

frequency. Classically there are two types of perturbation methods: general and special. This review will begin with a look at general perturbation methods.

General Perturbation Methods

General perturbations (GP), include methods of generalizing the expressions for simple two-body motion, such as a planet about the sun, to include the disturbing effects of other planets by utilizing infinite trigonometric series expansions and term-by-term analytic integration. The resulting expressions are known as general perturbations [86]. The analysis of general perturbations has played a significant and key role in celestial mechanics. As early as 1665, Sir Issac Newton, at the age of twenty-three, conceived the law of gravitation, the laws of motion, and the fundamental concepts of the differential calculus. But, due to a flaw in his general perturbation theory[1], Newton tossed his papers aside, and the world would not learn of any of his discoveries until twenty years later [85]. In all fairness, Newton had explained most of the variations in the moon's orbit, except the motion of perigee. In 1749, Alexis-Claude Clairant found that the second order perturbation terms removed discrepancies between the observed and theoretical values, which apparently, had not been treated by Newton. Ironically, about 100 years later, the full explanation was found in an unpublished

[1] Newton only had a small discrepancy in his explanation of the moon's motion.

manuscript of Newton's. Nonetheless, Clairant was the first person to accurately predict the return of Hailey's Comet in 1759, based upon calculations of the perturbations due to Jupiter and Saturn. He correctly predicted a possible error of one month due to mass uncertainty and other more distant planets. In 1845, the presence of the planet Neptune was deduced analytically by John Couch Adams and Urbain-Jean-Joseph LeVerrier, from the analysis of the perturbed motion of Uranus. Furthermore, the shape of the Earth was deduced by an analyisis of long period perturbation terms in the eccentricity of the Earth's orbit [85]. These early developments were motivated by a desire to explain the motion of planets or heavenly bodies. A different era of motivation was launched on October 4th, 1957 - SPUTNIK! This single event was the beginning of a very serious analysis of artificial satellite motion about the earth. General perturbation theory played a fundamental role in this early development. Within two years, Dirk Brouwer, of the Yale University Observatory, working under a contract with the Air Force Cambridge Research Center, provided a solution to the trajectory of an artificial satellite without drag [42]. This initial solution is the foundation of present day general perturbation theories, including some of those used by NORAD.

Brouwer's Theory

Brouwer gives the solution for a spheroidal Earth with the gravitational potential limited to the principal term through the

fifth harmonic. The method is summarized as follows. Brouwer begins with the equations of motion of a small mass attracted by a spheroid:

$$\frac{d^2x}{dt^2} = \frac{\partial U}{\partial x}, \qquad \frac{d^2y}{dt^2} = \frac{\partial U}{\partial y}, \qquad \frac{d^2z}{dt^2} = \frac{\partial U}{\partial z} \tag{A.1}$$

With the potential,

$$U = \frac{\mu}{r} + \frac{\mu k_2}{r^3}(1 - 3\sin^2\beta) + \ldots \tag{A.2}$$

The equatorial plane is taken as the x-y plane; β is the latitude; r is the geocentric radial distance to the satellite, $\mu = k^2 m$;
where m is the mass of the spheroid, and k = G, which is the Gaussian Constant, or the universal gravitational constant. Specifically,

$$G = 6.670 \times 10^{-8} \text{ dyne } \frac{cm^2}{gm^2} \tag{A.3}$$

Now, let i be the inclination of the orbital plane; ω, the argument of pericenter, and f, the true anomaly. See Figure A-1.

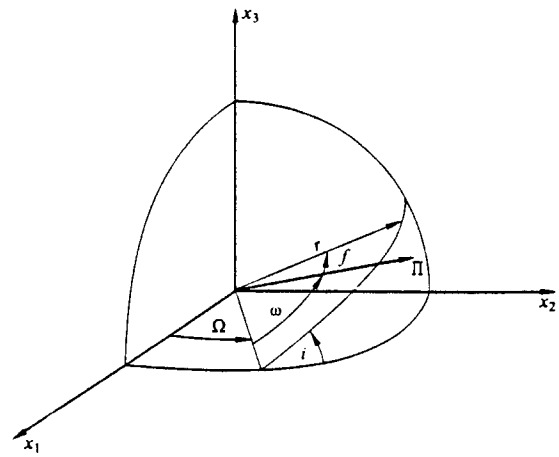

Figure A-1. Orbiting Mass in a Right-Handed Coordinate Frame

Then, by the law of sines for spherical triangles:

$$\sin \beta = \sin i \sin(\omega + f) \tag{A.4}$$

and $$2 \sin^2 \beta = \sin^2 i \,(1 - \cos(2\omega + 2f)) \tag{A.5}$$

Therefore, the disturbing function can be written in terms of orbital elements as:

$$U = \frac{\mu k_2}{a^3}\left[\left(-\frac{1}{2} + \frac{3}{2}\cos^2 i\right)\frac{a^3}{r^3} + \left(\frac{3}{2} - \frac{3}{2}\cos^2 i\right)\frac{a^3}{r^3}\cos(2\omega + 2f)\right] \tag{A.6}$$

Where a and e are the osculating semimajor axis and eccentricity respectively [42]. The term k_2, which Brouwer introduced in 1946, is equivalent to $J_2 \frac{R^2}{2}$, with R defined as the equatorial radius of the earth [42]. From this point, Brouwer derives his solution using canonical transformations, which is a method developed by H. Von Zeipel in 1916. (It is of interest to note that J. A. Morrison states that the Von Zeipel procedure is a particular case of the generalized method of averaging, corresponding to an appropriate choice of the arbitrary functions arising in the averaged equations [87].) These transformations are used to actually simplify the system into one of fewer unknowns. To gain some appreciation for this procedure, the following development will present a brief description of the canonical transformations.

First, Brouwer uses a new set of variables, the Delaunay variables, which are defined as follows:

$$L = (\mu a)^{\frac{1}{2}} \qquad l = \text{mean anomaly} \tag{A.7}$$

$$G = L(1-e^2)^{\frac{1}{2}} \qquad g = \text{argument of pericenter} \tag{A.8}$$

$$H = G \cos I \qquad h = \text{longitude of ascending node} \tag{A.9}$$

With these variables, the equations of motion become:

$$\frac{dL}{dt} = \frac{\partial F}{\partial l}, \quad \frac{dl}{dt} = -\frac{\partial F}{\partial L} \tag{A.10}$$

$$\frac{dG}{dt} = \frac{\partial F}{\partial g}, \quad \frac{dg}{dt} = -\frac{\partial F}{\partial G} \tag{A.11}$$

$$\frac{dH}{dt} = \frac{\partial F}{\partial h}, \quad \frac{dh}{dt} = -\frac{\partial F}{\partial H} \tag{A.12}$$

Where

$$F = \frac{\mu^2}{2L^2} + \frac{\mu^4 k_2}{L^6}\left[\left(-\frac{1}{2} + \frac{3}{2}\frac{H^2}{G^2}\right)\frac{a^3}{r^3} + \left(\frac{3}{2} - \frac{3}{2}\frac{H^2}{G^2}\right)\frac{a^3}{r^3}\cos(2g + 2f)\right] \tag{A.13}$$

This function F is also known as a Hamiltonian [42], which is defined as:

$$H(q, p, t) = \sum_k p_k \dot{q}_k - L(q, \dot{q}, t) \tag{A.14}$$

Where q = generalized coordinates

p = generalized momenta

$\dot{q}$ = generalized velocities

and, the function L is the Lagrangian [88],

L = (kinetic energy) - (potential energy) =

$$\sum_k \frac{1}{2} m_k \left(\dot{x}_k^2 + \dot{y}_k^2 + \dot{z}_k^2\right) - V(x, t) \tag{A.15}$$

Next, Brouwer transforms his Hamiltonian, F, which is a function of the original Delauney variables, through successive canonical transformations, with the aid of appropriate generating functions, into new Hamiltonians, $F^{\cdot}$, and finally, $F^{\cdot\cdot}$. This final Hamiltonian is a function of only three variables, and it is separated into secular and periodic parts. The secular motions are obtained to order k_2^2, and the periodic terms are developed to order k_2. At this point, Brouwer solves the equations of motion, and then transforms the variables back into Keplerian elements [42]. This completes the overview of Brouwer's general perturbation theory.

An alternative form of the geopotential was derived by Dr. John Vinti in which he used the definition of k_2, as defined by Brouwer, to obtain the following expression [42] :

$$U = V = F = \frac{\mu}{r}\left[1 - \sum_{p=2}^{\infty} J_p \left(\frac{R}{r}\right)^p P_p(\sin \beta)\right]. \tag{A.16}$$

This is the standard form of the geopotential which is the accepted form in use today.

General Perturbation Methods Continued

Also, by October of 1959, Yoshida Kozai, of the Smithsonian Astrophysical Observarory and Harvard College Observatory, derived the perturbations of the Keplerian elements of a close Earth

satellite without drag as functions of mean orbital elements and time [38]. In June of 1961, Brouwer and Gen-Ichiro Hori published, "Theoretical Evaluation of Atmospheric Drag Effects in the Motion of an Artificial Satellite." This theory was the first general perturbation theory to include the effects of atmospheric drag. It represents the atmosphere with an exponential density model, and neglects atmospheric rotation. It is interesting to note that although this model may seem quite simple, the resulting equations alone fill thirty pages in the Astronomical Journal [89]. The efforts of Brouwer and Kozai form the foundation the operational NORAD general perturbation theories.

Present day efforts in the theoretical development of analytical satellite theory are led by A. Deprit at the National Bureau of Standards.

Advantages and Disadvatages of General Perturbations

Since general perturbation models are solved analytically, you get exact answers. The result will apply to a general class of cases, and will reveal much information about the perturbed orbit. This is especially true for long duration calculations [85]. The most significant advantage of GP satellite theories is their ability to map position and velocity of an object from some initial time directly to a user-specified output time without costly step-by-step numerical integration [8].

Although these are significant advantages, there is a price to pay. The two major drawbacks are a loss of accuracy and flexibility. In order to solve the equations of motion analytically, many of these theories suffer from severely restricted perturbation models. Several are limited to lower degree zonal harmonics. Also, the third-body perurbation, when included, is usually restricted to the cases of very close earth satellites. Furthermore, in some models, there are problems for low eccentricity, low inclination or at critical inclination [48]. These anomalies are revealed by examining Brouwer's generating function for his second canonical transformation, and Kozai's differential equation representing the variation of eccentricity. For Brouwer, the expressions are [42]:

$$S_1^* =$$

$$G'' \gamma_2 \left(\frac{L'^2}{G''^2} - \frac{L'^4}{G''^4} \right) \left[\frac{1}{16} \left(1 - 11 \frac{H^2}{G''^2} \right) - \frac{5}{2} \frac{H^4}{G''^4} \left(1 - 5 \frac{H^2}{G''^2} \right)^{-1} \sin 2g'' \right] \quad \text{(A.17)}$$

Where $\frac{H^2}{G''^2} = \cos^2 i \quad \Rightarrow \quad \left(1 - 5 \frac{H^2}{G''^2} \right)^{-1} = \frac{1}{(1 - 5 \cos^2 i)}$ (A.18)

This yields the critical inclination, i (in degrees), singularity at:

$$1 - 5 \cos^2 i = 0; \quad \text{(A.19)}$$

when $i = 63^0$

For Kozai[38], $$\frac{de}{dt} = \frac{1-e^2}{na^2e}\frac{\partial R}{\partial M} - \frac{\sqrt{1-e^2}}{na^2e}\frac{\partial R}{\partial \omega} \qquad (A.20)$$

Where $e = 0$, creates a singularity[2].

In general, the current style of a first order GP theory can comprise tens of thousands of terms which require a prohibitive storage capacity. The only way to reduce the storage requirements is to restrict the theory itself. Additionally, whenever new terms or models are introduced, the GP theory software must accomodate these changes [48]. This is a very serious concern, for example, in atmospheric density models, where significant new work has been appearing each year since 1962. These new models are complex and do not necessarily follow existing algorithms or established software routines. Furthermore, the treatment of more complex gravitational fields and atmospheric density models with improved analytic expressions will result in a tremendous increase in algorithmic complexity. The use of such algorithms would be subject to [8]:

- -- increased analysis and software costs,
- -- reduced program speed and increased memory usage,
- -- difficulties in verifying program correctness,
- -- and program inflexibility.

---

[2] A singularity will exist only if $\frac{\partial R}{\partial M}$ and $\frac{\partial R}{\partial \omega}$ are not proportional to some power of the eccentricity.

It should be noted that some authors have tried to use a recursion concept with the GP theories. The use of recursions creates flexibility and reduces computer storage requirements.

Special Perturbation Methods

Special perturbations (SP) are techniques which deal with the direct numerical integration of the equations of motion including all necessary perturbing acceleratons [85]. In 1748, Euler developed the method of variation of parameters which at the time, was really a gerneral perturbation theory. However, as soon as direct numerical integration was used to solve the equations of motion, it became a special perturbation. The essence of variation of parameters is to find how the selected set of parameters vary with time due to the perturbations. The classical orbital element set variations are summarized in the Lagrange Planetary Equations which give the following orbital element derivatives [86]:

$$\left(\frac{da}{dt}, \quad \frac{de}{dt}, \quad \frac{di}{dt}, \quad \frac{d\Omega}{dt}, \quad \frac{d\omega}{dt}, \quad \frac{d\lambda}{dt}\right) \qquad (A.21)$$

where $\lambda = -n\tau$

n = mean motion

τ = Time of pericenter passage

The most straight forward and simplest of all special perturbation methods is known as Cowell's method. It is a direct numerical integration of the equations of motion in rectangular coordinates. Phillip H. Cowell developed the method in the early 20th century and he used it to determine the orbit of the eighth satellite of Jupiter. The application of Cowell's method is simply to write the equations of motion of the object being studied, including all the perturbations, and then to integrate them step-by-step numerically. Classically, Cowell's method has been applied in a Cartesian coordinate system, but improvements have been made by formulating the problem in polar and spherical coordinates [86].

Another SP theory, known as the method of Encke, is more complex than that of Cowell. It was actually proposed by William and George Bond in 1849, however; it became known as the work of Johann Franz Encke in 1851. In the Cowell method, the sum of all accelerations was integrated together. In Encke's method, the difference between the primary acceleration and all the perturbing accelerations is integrated. Therefore, all calculations and states are with respect to a reference, osculating orbit. This osculating orbit is the trajectory that would result if all perturbing accelerations could be removed at a particular time. One can integrate as long as the reference orbit and the true orbit do not deviate excessively. If so, a process of rectification, or realigning the reference and actual orbits, must occur to continue the integration [85].

Today these methods are in use with various numerical integration methods, including the Adams-Bashforth Multi-Method (GTDS) and the eighth order Gauss-Jackson or sum squared method (NORAD).

Advantages and Disadvantages of Special Perturbations

In general, special perturbations are very accurate, provided that the appropriate integration method is applied to the orbit of concern. Additionally, Cowell's method is simple in formulation and implementation, allowing any number of perturbations to be handled at the same time [85]. In Encke's method the determination of position and velocity in the osculating orbit is subject only to roundoff errors and is independent of the particular numerical technique used to perform the integration. The integrated quantities themselves are small, and when added to the osculating quantities, will have little effect on the determination of the true orbit. Before the errors in the deviations can grow in size sufficient to have a detrimental effect, a new osculating orbit is selected through rectification [86]. Due to the increased accuracy of special perturbations, NORAD uses the SP method for tracking objects of high interest when needed [17].

Nonetheless, there are also problems with special perturbation methods. First, they are computationally inefficient. For example, in order to get reasonably accurate data for a geosynchronous satellite orbit, with Cowell equations of motion, requires integration step sizes of less than 600 seconds in a high-order predictor-corrector integrator [59]. In other words, this requires a hundred or more steps per satellite orbit to give accurate results. Second, they are good for only one specific set of initial conditions, and therefore cannot be used to analyze a class of cases. Lastly, in

most cases, roundoff or truncation errors will be present to some degree. Roundoff errors result from the fact that a computer can carry only a finite number of digits of any given number. Therefore, the occurence of this roundoff many times in the integration process can result in significant errors [85]. Brouwer and Clemence [90] give a formula for the probable roundoff error after n steps as $\log\left(.1124\ n^{\frac{3}{2}}\right)$ in number of decimal places. As an example, for 300 integration steps, the probable error in decimal points would be 2.76. Now, if six places of accuracy are required, then nine places must be carried in the calculations. The point here is that the fewer integration steps taken, the smaller the accumulated roundoff error. The best inhibitor of the significant accumulation of roundoff error is the use of double precision arithmetic. Truncation error is a result of an inexact solution of the differential equations. Basically, this error results from not using all of the series expansion terms employed in the integration method. The larger the step size, the larger the truncation error, so the ideal here is to have small step sizes. This is in exact opposition to minimizing roundoff errors. Thus, errors are unavoidable in numerical integration, and the objective is to use a method that minimizes the sum of roundoff and truncation error. Roundoff error is a function of the machine and truncation error is a function of the integration method [85].

Appendix B

Subroutine G2MEOE Mathematics

This appendix presents the equations of each NORAD GP theory that correspond to the 6 x 6 GTDS state transition matrix. These partial derivatives are elements of the first six rows and columns of the 6 x 7 AG2STM array within subroutine G2MEOE as depicted in Figure 3-06. These are the partial derivatives of the current mean equinoctial elements with respect to the epoch mean equinoctial elements,

$$\frac{\partial \bar{a}_i(t)}{\partial \bar{a}_i(o)} . \qquad (3.16)$$

The equations presented in this appendix were derived from the SPADOC Fortran source code. As stated in chapter Three, the SPADOC equinoctial elements correspond to the GTDS equinoctial elements in the following manner:

$$(a_f, a_g, \chi, \varphi, n, L) \rightarrow (k, h, p, q, a, \lambda) \qquad (B.1)$$

However; in this appendix the terms, a_f and a_g will simply be denoted as f and g. The given equations are written in SPADOC equinoctial elements along with Keplerian elements and their derivatives, just as they are presented within the Fortran code.

These equations can be written in terms of Draper Laboratory's equinoctial element set by replacing the SPADOC equinoctial elements by the appropriate terms as given in equation (B.1). It was necessary to decode this subroutine to obtain the actual equations in use for a given theory because the available sources, [17] and [39], left some questions as to what the actual partial derivative equations were. Additionally, there was no source document available to provide the HANDE partial derivatives [50].

This appendix is divided into four major sections. The first section presents the equations which are common to all NORAD GP theories and includes twenty-nine partial derivatives. The remaining sections present equations which are unique to each NORAD theory by type. Throughout the appendix the following format is used to present the equations:

$$\left(\frac{\partial \bar{a}_i(t)}{\partial \bar{a}_i(o)}\right) = \left(\frac{\partial \bar{a}_i(t)}{\partial \bar{a}_i(o)}\right) =$$

(Draper equinoctial elements) (SPADOC equinoctial elements)

AG2STM (i,j) = RHS Equation
(i,j = 1,6)

Within the array AG2STM the order of the subscripts (rows and columns) is as follows:

subscript 1 $(\bar{f}(t), \bar{g}(t), \bar{\chi}(t), \bar{\psi}(t), \bar{n}(t), \bar{L}(t))$

subscript 2 $(\bar{f}_o, \bar{g}_o, \bar{\chi}_o, \bar{\psi}_o, \bar{n}_o, \bar{L}_o)$.

Additionally, any partial that is taken with respect to n_o is multiplied by n_o. The partial derivatives which are common to all three GP theories include the following:

$$\frac{\partial k}{\partial p_o} = \frac{\partial f}{\partial \chi_o} = \text{AG2STM}(1,3) =$$
$$-(\sin \Omega_o)(\sin i_o)(1+\cos i_o) \cdot \tag{B.2}$$
$$\left[5(\dot{\Omega}_o) + \frac{3}{2}\frac{J_2 n_o}{\left[a_o(1-e_o^2)\right]^2}\right] g(t)(t-t_o)$$

$$\frac{\partial k}{\partial q_o} = \frac{\partial f}{\partial \psi_o} = \text{AG2STM}(1,4) =$$
$$-(\cos \Omega_o)(\sin i_o)(1+\cos i_o) \cdot \tag{B.3}$$
$$\left[5(\dot{\Omega}_o) + \frac{3}{2}\frac{J_2 n_o}{\left[a_o(1-e_o^2)\right]^2}\right] g(t)(t-t_o)$$

$$n_o\frac{\partial k}{\partial n_o} = n_o\frac{\partial f}{\partial n_o} = \text{AG2STM}(1,5) =$$
$$-\frac{7}{3}(\dot{\Omega}_o + \dot{\omega}_o)\, g(t)(t-t_o) \tag{B.4}$$

$$\frac{\partial k}{\partial \lambda_o} = \frac{\partial f}{\partial L_o} = \text{AG2STM}(1,6) = 0 \tag{B.5}$$

$$\frac{\partial h}{\partial p_o} = \frac{\partial g}{\partial \chi_o} = \text{AG2STM}(2,3) =$$
$$(\sin \Omega_o)(\sin i_o)(1+\cos i_o) \cdot \tag{B.6}$$
$$\left[5(\dot{\Omega}_o) + \frac{3}{2}\frac{J_2 n_o}{\left[a_o(1-e_o^2)\right]^2}\right] f(t)\,(t-t_o)$$

$$\frac{\partial h}{\partial q_o} = \frac{\partial g}{\partial \psi_o} = \text{AG2STM}(2,4) =$$
$$(\cos \Omega_o)(\sin i_o)(1+\cos i_o) \cdot \tag{B.7}$$
$$\left[5(\dot{\Omega}_o) + \frac{3}{2}\frac{J_2 n_o}{\left[a_o(1-e_o^2)\right]^2}\right] f(t)\ (t-t_o)$$

$$n_o\frac{\partial h}{\partial n_o} = n_o\frac{\partial g}{\partial n_o} = \text{AG2STM}(2,5) =$$
$$\frac{7}{3}(\dot{\Omega}_o + \dot{\omega}_o)\, f(t)\,(t-t_o) \tag{B.8}$$

$$\frac{\partial h}{\partial \lambda_o} = \frac{\partial q}{\partial L_o} = \text{AG2STM}(2,6) = 0 \tag{B.9}$$

$$\frac{\partial p}{\partial k_o} = \frac{\partial \chi}{\partial f_o} = \text{AG2STM}(3,1) =$$
$$f_o\left(\frac{4\,\dot{\Omega}_o}{(1-e_o^2)}\right)(\cos \Omega(t) \sin i(t))\left[\frac{1}{(1+\cos i(t))}\right](t-t_o) \tag{B.10}$$

$$\frac{\partial p}{\partial h_o} = \frac{\partial \chi}{\partial g_o} = \text{AG2STM}(3,2) =$$
$$g_o\left(\frac{4\,\dot{\Omega}_o}{(1-e_o^2)}\right)(\cos \Omega(t) \sin i(t))\left[\frac{1}{(1+\cos i(t))}\right](t-t_o) \tag{B.11}$$

$$\frac{\partial p}{\partial p_o} = \frac{\partial \chi}{\partial \chi_o} = \text{AG2STM}(3,3) =$$
$$\cos(\dot{\Omega}_o(t-t_o)) - \left[(\sin \Omega_o)(\sin i_o)(1+\cos i_o)\left[-\frac{3J_2 n_o}{2\left[a_o(1-e_o^2)\right]^2}\right]\cdot\right.$$
$$\left.(\cos \Omega(t) \sin i(t))\left[\frac{1}{(1+\cos i(t))}\right](t-t_o)\right] \tag{B.12}$$

$$\frac{\partial p}{\partial q_o} = \frac{\partial \chi}{\partial \psi_o} = \text{AG2STM}(3, 4) =$$

$$\sin\left(\dot{\Omega}_o(t - t_o)\right) - \left[(\cos \Omega_o)(\sin i_o)(1 + \cos i_o)\left[-\frac{3J_2 n_o}{2\left[a_o(1 - e_o^2)\right]^2}\right]\cdot\right.$$

$$\left.(\cos \Omega(t)\ \sin i(t))\left[\frac{1}{(1 + \cos i(t))}\right](t - t_o)\right] \quad \text{(B.13)}$$

$$n_o\frac{\partial p}{\partial n_o} = n_o\frac{\partial \chi}{\partial n_o} = \text{AG2STM}(3, 5) =$$

$$\left(\frac{7\,\dot{\Omega}_o}{3}\right)\left((\cos \Omega(t)\ \sin i(t))\left[\frac{1}{(1 + \cos i(t))}\right](t - t_o)\right) \quad \text{(B.14)}$$

$$\frac{\partial p}{\partial \lambda_o} = \frac{\partial \chi}{\partial L_o} = \text{AG2STM}(3, 6) = 0 \quad \text{(B.15)}$$

$$\frac{\partial q}{\partial k_o} = \frac{\partial \psi}{\partial f_o} = \text{AG2STM}(4, 1) =$$

$$-f_o\left(\frac{4\,\dot{\Omega}_o}{(1 - e_o^2)}\right)\left((\sin \Omega(t)\ \sin i(t))\left[\frac{1}{(1 + \cos i(t))}\right](t - t_o)\right)$$

(B.16)

$$\frac{\partial q}{\partial h_o} = \frac{\partial \psi}{\partial g_o} = \text{AG2STM}(4, 2) =$$

$$-g_o\left(\frac{4\,\dot{\Omega}_o}{(1 - e_o^2)}\right)\left((\sin \Omega(t)\ \sin i(t))\left[\frac{1}{(1 + \cos i(t))}\right](t - t_o)\right)$$

(B.17)

$$\frac{\partial q}{\partial p_o} = \frac{\partial \psi}{\partial \chi_o} = \text{AG2STM}(4, 3) =$$

$$-\sin\left(\dot{\Omega}_o(t - t_o)\right) \quad +$$

$$\left([(\sin\ \Omega_o)\ (\sin\ i_o)]\ (1+\cos i_o)\ \left[-\frac{3J_2 n_o}{2[a_o\ (1-e_o^2)]^2}\right]\right) \cdot \left((\sin\ \Omega(t)\ \sin\ i\ (t))\ \left[\frac{1}{(1+\cos\ i\ (t))}\right]\ (t-t_o)\right) \tag{B.18}$$

$$\frac{\partial q}{\partial q_o} = \frac{\partial \psi}{\partial \psi_o} = \text{AG2STM}\,(4,\,4\,) = \cos\left(\dot{\Omega}_o(t-t_o)\right) + \left([(\cos\ \Omega_o)\ (\sin\ i_o)]\ (1+\cos i_o)\ \left[-\frac{3J_2 n_o}{2[a_o\ (1-e_o^2)]^2}\right]\right) \cdot \left((\sin\ \Omega(t)\ \sin\ i\ (t))\ \left[\frac{1}{(1+\cos\ i\ (t))}\right]\ (t-t_o)\right) \tag{B.19}$$

$$n_o\frac{\partial q}{\partial n_o} = n_o\frac{\partial \varphi}{\partial n_o} = \text{AG2STM}\,(4,\,5\,) = -\left(\frac{7\ \dot{\Omega}_o}{3}\right)\left((\sin\ \Omega(t)\ \sin\ i\ (t))\ \left[\frac{1}{(1+\cos\ i\ (t))}\right]\ (t-t_o)\right) \tag{B.20}$$

$$\frac{\partial q}{\partial \lambda_o} = \frac{\partial \psi}{\partial L_o} = \text{AG2STM}\,(4,6\,) = 0 \tag{B.21}$$

$$\frac{\partial n}{\partial k_o} = \frac{\partial a}{\partial f_o} = \text{AG2STM}\,(5,1\,) = 0 \tag{B.22}$$

$$\frac{\partial n}{\partial h_o} = \frac{\partial a}{\partial g_o} = \text{AG2STM}\,(5,\,2) = 0 \tag{B.23}$$

$$\frac{\partial n}{\partial p_o} = \frac{\partial a}{\partial \chi_o} = \text{AG2STM}\,(5,\,3) = 0 \tag{B.24}$$

$$\frac{\partial n}{\partial q_o} = \frac{\partial a}{\partial \psi_o} = \text{AG2STM}\,(5,\,4) = 0 \tag{B.25}$$

$$n_o \frac{\partial n}{\partial n_o} = n_o \frac{\partial n}{\partial n_o} = \text{AG2STM}(5, 5) = n_o \tag{B.26}$$

$$\frac{\partial n}{\partial \lambda_o} = \frac{\partial a}{\partial L_o} = \text{AG2STM}(5, 6) = 0 \tag{B.27}$$

$$\frac{\partial \lambda}{\partial p_o} = \frac{\partial L}{\partial \chi_o} = \text{AG2STM}(6, 3) = (t - t_o) \cdot \tag{B.28}$$

$$\left(\sin \Omega_o \sin i_o (1 + \cos i_o) \left[\dot{\Omega}_o \left(3 \sqrt{(1 - e_o^2)} + 5 \right) + \frac{3 J_2 n_o}{2 [a_o (1 - e_o^2)]^2} \right] \right)$$

$$\frac{\partial \lambda}{\partial q_o} = \frac{\partial L}{\partial \varphi_o} = \text{AG2STM}(6, 4) = (t - t_o) \cdot \tag{B.29}$$

$$\left(\cos \Omega_o \sin i_o (1 + \cos i_o) \left[\dot{\Omega}_o \left(3 \sqrt{(1 - e_o^2)} + 5 \right) + \frac{3 J_2 n_o}{2 [a_o (1 - e_o^2)]^2} \right] \right)$$

$$\frac{\partial \lambda}{\partial \lambda_o} = \frac{\partial L}{\partial L_o} = \text{AG2STM}(6, 6) = 1.0 \tag{B.30}$$

Equation (B.30) is the last equation which is common to all the NORAD GP theories. The equations which are unique to the SGP theory are as follows[1]:

$$\frac{\partial k}{\partial k_o} = \frac{\partial f}{\partial f_o} = \text{AG2STM}(1, 1) =$$

---

1 Throughout the remaining equations $\dot{\pi}_o = \dot{\Omega}_o + \dot{\omega}_o$.

$$\cos\left(\dot{\pi}_o\,(t-t_o)\right) - \left[\left[\frac{4\,(\dot{\Omega}_o+\dot{\omega}_0)}{(1-e_o^2)}\right] f_o\; g(t)\,(t-t_o)\right] \tag{B.31}$$

$$\frac{\partial k}{\partial h_o} = \frac{\partial f}{\partial g_o} = \text{AG2STM}(1,2) =$$

$$-\sin\left(\dot{\pi}_o\,(t-t_o)\right) - \left[\left[\frac{4\,(\dot{\Omega}_o+\dot{\omega}_0)}{(1-e_o^2)}\right] g_o\; g(t)\,(t-t_o)\right] \tag{B.32}$$

$$\frac{\partial h}{\partial k_o} = \frac{\partial g}{\partial f_o} = \text{AG2STM}(2,1) =$$

$$\sin\left(\dot{\pi}_o\,(t-t_o)\right) + \left[\frac{4\,(\dot{\Omega}_o+\dot{\omega}_0)}{(1-e_o^2)}\right] f_o\left[\,f(t)\,(t-t_o)\right] \tag{B.33}$$

$$\frac{\partial h}{\partial h_o} = \frac{\partial g}{\partial g_o} = \text{AG2STM}(2,2) =$$

$$\cos\left(\dot{\pi}_o\,(t-t_o)\right) + \left[\frac{4\,(\dot{\Omega}_o+\dot{\omega}_0)}{(1-e_o^2)}\right] g_o\left[\,f(t)\,(t-t_o)\right] \tag{B.34}$$

$$\frac{\partial \lambda}{\partial k_o} = \frac{\partial L}{\partial f_o} = \text{AG2STM}(6,1) =$$

$$f_o\left[\frac{(3\,(\dot{\pi}_o+\dot{\pi}_o))}{(1-e_o^2)}\right](t-t_o) \tag{B.35}$$

$$\frac{\partial \lambda}{\partial h_o} = \frac{\partial L}{\partial g_o} = \text{AG2STM}(6,2) =$$

$$g_o\left[\frac{(3\,(\dot{\pi}_o+\dot{\pi}_o))}{(1-e_o^2)}\right](t-t_o) \tag{B.36}$$

$$n_o\frac{\partial \lambda}{\partial n_o} = n_o\frac{\partial L}{\partial n_o} = \text{AG2STM}(6,5) =$$

$$\left(\frac{7}{3}\ \dot{\pi}_o + n_o\right)(t - t_o) \qquad \text{(B.37)}$$

The equations which are unique to the GP4/DP4 theory are as follows[2]:

$$\frac{\partial k}{\partial k_o} = \frac{\partial f}{\partial f_o} = \text{AG2STM}(1,1) = \text{AG2STM}(1,1)\Big|_{SGP} + \qquad \text{(B.38)}$$

$$(\text{PAR3})_o \left(\frac{1}{e_o}\right)^3 (t - t_o)\ g(t)\ g_o\,[(\cos\Omega_o)\,g_o - (\sin\Omega_o)\,f_o]$$

$$\frac{\partial k}{\partial h_o} = \frac{\partial f}{\partial g_o} = \text{AG2STM}(1,2) = \text{AG2STM}(1,2)\Big|_{SGP} + \qquad \text{(B.39)}$$

$$(\text{PAR3})_o \left(\frac{1}{e_o}\right)^3 (t - t_o)\ g(t) f_o\,[(\sin\Omega_o)\,f_o - (\cos\Omega_o)\,g_o]$$

$$\frac{\partial h}{\partial k_o} = \frac{\partial g}{\partial f_o} = \text{AG2STM}(2,1) = \text{AG2STM}(2,1)\Big|_{SGP} - \qquad \text{(B.40)}$$

$$(\text{PAR3})_o \left(\frac{1}{e_o}\right)^3 (t - t_o)\ f(t) g_o\,[(\cos\Omega_o)\,g_o - (\sin\Omega_o)\,f_o]$$

$$\frac{\partial h}{\partial h_o} = \frac{\partial g}{\partial g_o} = \text{AG2STM}(2,2) = \text{AG2STM}(2,2)\Big|_{SGP} - \qquad \text{(B.41)}$$

$$(\text{PAR3})_o \left(\frac{1}{e_o}\right)^3 (t - t_o)\ f(t) f_o\,[(\sin\Omega_o)\,f_o - (\cos\Omega_o)\,g_o]$$

---

2 The PAR3 term is a drag term which is unique to the GP4/DP4.

$$\frac{\partial \lambda}{\partial k_o} = \frac{\partial L}{\partial f_o} = \text{AG2STM}(6,1) =$$

$$\left[\frac{f_o(3(\dot{\pi}_o + \dot{M}_o - n_o) + \dot{\pi}_o)}{(1-e_o^2)}\right](t-t_o) \qquad \text{(B.42)}^3$$

$$\frac{\partial \lambda}{\partial h_o} = \frac{\partial L}{\partial g_o} = \text{AG2STM}(6,2) =$$

$$\left[\frac{g_o(3(\dot{\pi}_o + \dot{M}_o - n_o) + \dot{\pi}_o)}{(1-e_o^2)}\right](t-t_o) \qquad \text{(B.43)}$$

$$n_o \frac{\partial \lambda}{\partial n_o} = n_o \frac{\partial L}{\partial n_o} = \text{AG2STM}(6,5) =$$

$$\left(\frac{7}{3}(\dot{\pi}_o + \dot{M}_o - n_o) + n_o\right)(t-t_o) \qquad \text{(B.44)}$$

The equations which are unique to the HANDE theory are as follows:

$$\frac{\partial k}{\partial k_o} = \frac{\partial f}{\partial f_o} = \text{AG2STM}(1,1) = \text{AG2STM}(1,1)\Big|_{SGP} +$$

$$[(\sin\omega_o)(\cos\Omega_o) - (\cos\omega_o)(\sin\Omega_o)] \cdot [\sin(\omega(t) + \Omega(t))] \cdot$$

$$(t-t_o)\left[(\dot{e}_o) + (t-t_o)\left\{\left(\frac{\ddot{e}_o}{2}\right) + (t-t_o)\left(\frac{\dddot{e}_o}{6}\right)\right\}\right]\left(\frac{1}{e_o}\right) \qquad \text{(B.45)}$$

---

3 Throughout the remaining equations the term $\dot{M}_o$ is equivalent to the following:

$$\dot{M}_o = \frac{3}{2} J_2 \left(\frac{1}{a(1-e^2)}\right)^2 n_o \left(1 - \frac{3}{2}\sin^2 i\right)\sqrt{1-e^2}$$

$$\frac{\partial k}{\partial h_o} = \frac{\partial f}{\partial g_o} = \text{AG2STM}(1,2) = \text{AG2STM}(1,2)\Big|_{SGP} -$$

$$[(\cos\omega_o)(\cos\Omega_o) - (\sin\omega_o)(\sin\Omega_o)] \cdot [\sin(\omega(t) + \Omega(t))] \cdot$$

$$(t - t_o)\left[(\dot{e}_o) + (t - t_o)\left\{\left(\frac{\ddot{e}_o}{2}\right) + (t - t_o)\left(\frac{\dddot{e}_o}{6}\right)\right\}\right]\left(\frac{1}{e_o}\right) \quad \text{(B.46)}$$

$$\frac{\partial h}{\partial k_o} = \frac{\partial g}{\partial f_o} = \text{AG2STM}(2,1) = \text{AG2STM}(2,1)\Big|_{SGP} -$$

$$[(\sin\omega_o)(\cos\Omega_o) - (\cos\omega_o)(\sin\Omega_o)]\cos(\omega(t) + \Omega(t)) \cdot$$

$$(t - t_o)\left[(\dot{e}_o) + (t - t_o)\left\{\left(\frac{\ddot{e}_o}{2}\right) + (t - t_o)\left(\frac{\dddot{e}_o}{6}\right)\right\}\right]\left(\frac{1}{e_o}\right) \quad \text{(B.47)}$$

$$\frac{\partial h}{\partial h_o} = \frac{\partial g}{\partial g_o} = \text{AG2STM}(2,2) = \text{AG2STM}(2,2)\Big|_{SGP} +$$

$$[(\cos\omega_o)(\cos\Omega_o) - (\sin\omega_o)(\sin\Omega_o)]\cos(\omega(t) + \Omega(t)) \cdot$$

$$(t - t_o)\left[(\dot{e}_o) + (t - t_o)\left\{\left(\frac{\ddot{e}_o}{2}\right) + (t - t_o)\left(\frac{\dddot{e}_o}{6}\right)\right\}\right]\left(\frac{1}{e_o}\right) \quad \text{(B.48)}$$

$$\frac{\partial \lambda}{\partial k_o} = \frac{\partial L}{\partial f_o} = \text{AG2STM}(6,1) =$$

$$f_o\left[\frac{(3(\dot{\pi}_o + \dot{M}_o) + \dot{\pi}_o)}{(1 - e_o^2)}\right](t - t_o) \quad \text{(B.49)}$$

$$\frac{\partial \lambda}{\partial h_o} = \frac{\partial L}{\partial g_o} = \text{AG2STM}(6,2) =$$

$$g_o\left[\frac{(3(\dot{\pi}_o + \dot{M}_o) + \dot{\pi}_o)}{(1 - e_o^2)}\right](t - t_o) \quad \text{(B.50)}$$

$$n_o\frac{\partial \lambda}{\partial n_o} = n_o\frac{\partial L}{\partial n_o} = \text{AG2STM}(6,5) =$$

$$\left(\frac{7}{3}\,(\dot{\pi}_o + \dot{M}_o) + n_o\right)(t - t_o) \qquad \text{(B.51)}$$

It is interesting to note that the following three partial derivatives, $\frac{\partial \lambda}{\partial k_o}$, $\frac{\partial \lambda}{\partial h_o}$, and $n_o \frac{\partial \lambda}{\partial n_o}$, which correspond to the AG2STM (6,1),(6,2) and (6,5) members, are all functions of the first time derivative of the mean longitude $\dot{L}_o$, and this term is defined differently for SGP, SGP4 and HANDE. Hence, for these three theories, these partial derivatives will yield different results.

Appendix C

A COMPARISON OF GTDS AND SPADOC PARTIAL DERIVATIVE EQUATIONS

This appendix is a discussion of a mathematical comparison of the equations which calculate the partial derivatives of current mean equinoctial elements with respect to the mean equinoctial elements at epoch for both the GTDS and the SPADOC computer code. These partials are denoted as follows:

$$\frac{\partial \bar{a}_i(t)}{\partial \bar{a}_i(o)} \tag{3.16}$$

where $a_i = (a, h, k, p, q, \lambda)$

The GTDS partial derivatives include the secular variations due to J_2 only with no truncation of the orbital eccentricity. These partials are stored in the 6 x 6 GTDS B_2 matrix. The equations which are dicussed in this appendix are taken from Shaver (See [74], Tables 3.9 through 3.14). The SPADOC equations were taken from the SGP theory equations as shown in Appendix B. A comparison of these equations shows that the partial derivative equations, which are derived from the SGP theory computer code, after being modified as

described in Section 3.3.7.2, are equivalent[1] to the equations which generate the GTDS B_2 matrix. The comparison indicated that the members of the first six rows and columns of Figure 3-6 are equivalent to the members of Figure 3-8, the GTDS B_2 matrix with the exception listed in the footnote. This observation is supported by and explained within the analysis in Sections 4.4.2 - 4.4.4. This mathematical comparison did not address the partials that are taken with respect to the drag parameter nor did the analysis consider the NORAD SALT theory. SPADOC partial derivatives were modified, in the same manner as in section 3.3.7.2, to obtain the form of the GTDS partial derivatives. These modifications will include using one or more of the following factors:

1. $$\frac{\partial a_i}{\partial a_o} = \frac{\partial a_i}{\partial n_o}\left(\frac{\partial n_o}{\partial a_o}\right) \qquad \text{(C.1)}$$

where $$\left(\frac{\partial n_o}{\partial a_o}\right) = -\left(\frac{3}{2}\frac{n_o}{a_o}\right)$$

---

[1] The only exception to this equivalence is that the SGP theory defines the mean longitude derivative at epoch as follows:

$$\dot{L}_o = \dot{\pi}_o$$

wheras GTDS defines the same term as follows: $\dot{L}_o = \dot{\pi}_o + \dot{M}_o$

This difference affects only the following partial derivatives:

$\frac{\partial \lambda}{\partial k_o}$, $\frac{\partial \lambda}{\partial h_o}$, and $\frac{\partial \lambda}{\partial a_o}$.

2. $$\frac{\partial a}{\partial a_i} = \left(\frac{\partial a}{\partial n}\right)\frac{\partial n}{\partial a_i} \qquad \text{(C.2)}$$

where $\left(\frac{\partial a}{\partial n}\right) = -\left(\frac{2}{3}\frac{a}{n}\right)$

3. Divide by n_o where appropriate.

Following the necessary modifications, it can be shown that the SPADOC SGP theory equations and GTDS equations for the B_2 matrix elements are equivalent. The following relations were useful in this analysis:

$$\delta_1 = \frac{3}{2} J_2 \left(\frac{r_e}{a_o(1-e_o^2)}\right)^2 n_o \left(2 - \frac{5}{2}\sin^2 i_o - \cos i_o\right) = \dot{\pi}_o \qquad \text{(C.3)}$$

$$\delta_2 = -\frac{3}{2} J_2 \left(\frac{r_e}{a_o(1-e_o^2)}\right)^2 n_o \cos i_o = \dot{\Omega}_o \qquad \text{(C.4)}$$

where $r_e = 1$ for this implementation.

Also, given that

$$\left(\frac{1-C}{1+C}\right) = \cos i, \quad x = \left(\frac{1}{(1-e_o^2)}\right), \quad \mu = n_o^2 a_o^3, \qquad \text{(C.5 a,b,c)}$$

$$K \equiv \left(\frac{3}{2} J_2 r_e^2 \mu^{\frac{1}{2}}\right) = \left(\frac{3}{2} J_2 r_e^2 n_o a_o^{\frac{3}{2}}\right) \qquad \text{(C.6)}$$

Then it follows that

$$\delta_2 = -K a_o^{-\frac{7}{2}} x^2 \left[\frac{(1 - C)}{(1 + C)}\right] = \dot{\Omega}_o \qquad (C.7)$$

The equinoctial element $p = \dfrac{(\sin i)(\sin \Omega)}{(1 + \cos i)} = \chi$ (C.8)

$$\left(\frac{2}{1 + C}\right) = (1 + \cos i) \qquad (C.9)$$

The equinoctial element $q = \dfrac{(\sin i)(\cos \Omega)}{(1 + \cos i)} = \psi$ (C.10)

$$\delta_3 = \frac{3}{2} J_2 \left(\frac{r_e}{a_o (1 - e_o^2)}\right)^2 n_o \left(1 - \frac{3}{2} \sin^2 i_o\right) \sqrt{(1 - e_o^2)} = \dot{M}_o \qquad (C.11)$$

$$\dot{\Omega}_o = -K a_o^{-\frac{7}{2}} x^2 \left[\frac{(1 - C)}{(1 + C)}\right] \qquad (C.12)$$

$$K = \left(\frac{3}{2} J_2 r_e^2 n_o a_o^{\frac{3}{2}}\right) \qquad (C.13)$$

where $r_e = 1$ for this implementation.

The GTDS retrograde factor, I, was equal to one for this analysis.

Appendix D

Finite Differencing

A single-sided finite differencing technique was used in this research to obtain approximations to the partial derivatives of various quantities. These partial derivatives were then compared to the state transition matrix generated by each NORAD GP theory. This appendix develops this differencing technique and points out some of it's limitations.

One way to develop this single-sided finite differencing technique is to start with a Taylor series expansion of a scalar function of x, f(x):

$$f(x_0 + \Delta x) = f(x_0) + \Delta x \left[\frac{\partial f(x)}{\partial x}\right]_{x = x_0} + \frac{(\Delta x)^2}{2}\left[\frac{\partial^2 f(x)}{\partial x^2}\right]_{x = x_0} + \dots \quad \text{(D.1)}$$

Now, simply subtract $f(x_0)$ from the right hand side of equation (D.1) which yields:

$$f(x_0 + \Delta x) - f(x_0) \cong \Delta x \left[\frac{\partial f(x)}{\partial x}\right]_{x = x_0} \quad \text{(D.2)}$$

Finally, divide by Δx which yields the following single-sided finite differencing approximation [61]:

$$\frac{f(x_0 + \Delta x) - f(x_0)}{\Delta x} \cong \left[\frac{\partial f(x)}{\partial x}\right]_{x = x_0} \qquad \text{(D.3)}$$

This approximation is essentially equivalent to Euler's method, which is also known as the tangent method, whereby the derivative at a point (x_n, y_n) is approximated with the following difference quotient:

$$\frac{(y_{n+1} - y_n)}{h} = f'(x_n, y_n) \qquad \text{(D.4)}$$

Where h is the length of a subinterval on an interval [a,b] [91].

Dahlquist and Bjorck [91] point out that a weakness of the Euler method is that the step length or size must be chosen quite small in order to maintain acceptable accuracy.

Green (1979) explains that there are two sources of error for the single-sided finite differencing approach: neglect of higher order terms and roundoff. The error due to the neglect of higher order terms will be less than or equal to the following:

$$\text{Error} \leq \left\{\frac{\Delta x}{2}\left[\max\left|\frac{\partial^2 f(x)}{\partial x^2}\right|\right]\right\} \qquad \text{(D.5)}$$

Roundoff errors are due to the finite word length inherent in the computer being used. Varying the stepsize, (Δx), can significantly affect the roundoff error. Green (1979) states that with double

precision on the Amdahl 470 V6 (sixteen digits), he found that good results were obtained when:

$$(\Delta x) = 1 \times 10^{-5} \ (x)$$

With single precision (eight digits), a good stepsize was [61]:

$$(\Delta x) = 1 \times 10^{-3} \ (x)$$

A stepsize of 2×10^{-4} was used in the double precision finite difference analysis of Section 4.4.1.

Appendix E

Review of the Generalized Method of Averaging

The objective of the generalized method of averaging is to eliminate fast variables, or high frequency components, from differential equations. One reason for applying this technique is to eliminate terms that do not make important contributions to the solution, but that can cause difficulties in obtaining a numerical or analytical solution [46]. This idea is not new in the study of celestial mechanics. Although the history of this method appears to be somewhat controversial, this appendix will attempt to present an objective chronology.

This development begins with Euler's (1748) investigation of the mutual perturbations of Jupiter and Saturn. This study led to the first analytical development of the variation of parameters. Euler's treatment was not totally general since he did not consider the orbital elements as being simultaneously variable. Lagrange improved Euler's analysis, and by 1782 he had completely developed the variation of parameters yielding the Lagrange planetary equations. It is of further interest to note that Lagrange's variational equations were derived for the special case in which the disturbing acceleration was represented as the gradient of the disturbing function. Gauss pointed out that this is not completely necessary. Accordingly, he derived another set of variational equations which are appropriate for various component resolutions

of the disturbing acceleration vector [86]. Nonetheless, it is perhaps from a further analysis of Lagrange's planetary equations that the method of averaging, as applied to celestial mechanics, has its origins. McClain (1977) points out, given conservative perturbing forces, that the osculating element rates can be represented in terms of the partial derivatives of a disturbing function. For Lagrange's case, this function is simply the negative of the disturbing geopotential function. Furthermore, to obtain a formulation dependent only on the elements, the disturbing function can be developed in terms of the elements through a formal Fourier series expansion. (See Battin, (1987); and McClain (1977) for details.) The significance of this expansion is that it permits isolation of specific frequencies in the motion by inspection [48].

The "averaging," or removal of periodic terms, begins when one integrates this Fourier series expansion, either analytically or numerically. Danby (1964) develops Gauss' analytic method for the calculation of secular perturbations. The secular terms found in the first order solution to Lagrange's planetary equations arise from the constant term in the disturbing function when this function is expanded in a Fourier series in the mean anomalies of the disturbed and disturbing planets. Specifically, this term is found from the following integral:

$$\frac{1}{4\pi^2}\int_0^{2\pi}\int_0^{2\pi} R\, dM\, dM' \qquad \text{(E.1)}$$

Where the quantity R is gravitational potential

since all but the constant term vanishes [92]. Thus, it appears that Gauss' analytic method is the first application of the method of averaging to celestial mechanics.

Ensuing studies begin with Delaunay's (c. 1860) study of the moon's motion. He uses successive canonical transformations to solve the equations of motion. Furthermore, Delaunay recognized that the major difficulty in the avoidance of unbounded terms in the series solution of the equations of motion was the choice of a reference frequency, ω. The development of Delaunay's method of successive canonical transformations to a method utilizing a generating function, S, was first forseen by Tisserand in 1868 [47].

The next series of developments center on the work of Lindstedt, Poincare', and Von Zeipel. Their work begins with Lindstedt's (1882) problem of obtaining a series solution, free from secular and/or mixed secular terms, of the following equation:

$$\ddot{x} + \omega_0^2 x = \varepsilon f(x, \dot{x}, t) \tag{E.2}$$

where $0 < \varepsilon < 1$ is a small parameter.

Lindstedt notes the possibility of obtaining a solution to the following equations:

$$\begin{aligned} x &= x_0(t) + \varepsilon x_1(t) + \varepsilon^2 x_2(t) + \dots \\ \dot{x} &= \dot{x}_0(t) + \varepsilon \dot{x}_1(t) + \varepsilon^2 \dot{x}_2(t) + \dots \end{aligned} \tag{E.3}$$

with $x_j(t)$, and $\dot{x}_j(t)$ as bounded functions for all $t \in R$, was found to depend essentially on the nature of f and its derivatives up to some order. Furthermore, he introduced the following reference solution $(x_0(t), \dot{x}_0(t))$:

$$\begin{aligned} x_0 &= a\cos(\omega t + \sigma) \\ \dot{x}_0 &= -a\omega \sin(\omega t + \sigma) \end{aligned} \qquad \text{(E.4)}$$

where ω is a priori unknown but, by assumption, developable in a power series:

$$\omega = \omega_0 + \varepsilon\omega_1 + \varepsilon^2\omega_2 + \varepsilon^3\omega_3 + \dots \qquad \text{(E.5)}$$

where $\omega_1, \omega_2, \dots$ are constants depending on ω_0, a and f. In 1886, Poincare' reduced Lindstedt's work to a systematic averaging procedure for Hamiltonian, but not necessarily conservative, systems. Additionally, Poincare' studied related questions, including the problem of resonance in the nonlinear sense and the overall divergence of Linstedt's series. In 1911, Von Zeipel generalized the ideas of Poincare' in his analysis of the motion of asteroids [47]. This concludes the classical review of averaging in celestial mechanics.

Since 1929, similar problems and questions arose in nonlinear circuit theory leading to the averaging methods of Krylov and Bogoliubov (1937) [93]. These studies were made available, in 1942, to the western mathematicians thanks to the translation efforts of

Lefshetz [47]. Bogoliubov and Mitropolsky (1961), develop both the earlier methods of Krylov and Bogoliubov, and a specific application of those methods. Respectively, the first development begins with the problem of having secular terms on the right hand side of a series solution to the equations of motion. They further point out that, as a rule, power series are divergent [93]. As I have just described, both of these problems were also investigated by Poincare' in his studies in celestial mechanics. Nonetheless, Bogoliubov and Mitropolsky note that the approximate fomulae obtained by taking a limited number of terms of a power series, m = 1, 2, 3 ... are found to be extremely suitable for practical calculations. In fact, these series are asymptotic, since the mth approximation is proportional to the $(m+1)^{th}$ power of the small parameter, ε [93]. A very similar development is presented by Nayfeh (1973), whereby he truncates a series, which diverges for all values of x, after n terms, specifically:

$$y = \frac{1}{x} + \frac{1}{x^2} + \frac{2!}{x^3} + \frac{3!}{x^4} + \dots + \frac{(n-1)!}{x^n} + \dots \qquad \text{(E.6)}$$

He then investigates whether or not this series is of any value in finding a particular solution to a given equation. Nayfeh finds, that for a fixed value of n, the error committed in truncating the series is numerically less than the first neglected term, i. e., the $(n+1)^{th}$ term. Although the series does diverge, for a fixed n, the first n

terms in the series can represent y with an error which can be made arbitrarily small by taking $|x|$ sufficiently large. In fact, such a series is called an asymptotic series of the Poincare' type (Poincare' 1892) and is denoted by [94]:

$$y \sim \sum_{n=1}^{\infty} \frac{(n-1)!}{x^n} \quad \text{as } |x| \to \infty \tag{E.7}$$

In essence, Nayfeh (Poincare') establishes a bound on the error due to truncation of the power series. With this idea in mind, Bogolbiubov and Mitropolsky point out that series convergence is not the critical issue and proceed to develop Krylov's and Boglobiubov's asymptotic approximations for a differential equation of the form studied by Lindstedt and Poincare', specifically:

$$\ddot{x} + \omega^2 x = \varepsilon f(x, \dot{x}) \tag{E.8}$$

where ε is a small positive parameter.

The main difference in the corresponding analyses is that Lindstedt and Poincare' were modeling conservative dynamical systems, whereas Krylov and Bogliubov were considering non-conservative systems, containing sources and sinks of energy. Krylov and Boglobiubov's development continues by seeking a general solution in the following form:

$$x = a\cos\psi + \varepsilon u_1(a,\psi) + \varepsilon^2 u_2(a,\psi) + \varepsilon^3 u_3(a,\psi) + \dots \quad \text{(E.9)}$$

where $\psi = (\omega t + \theta)$

Also, where $u_1(a,\psi), u_2(a,\psi), \dots$ are 2π periodic functions of the angle ψ, and the quantities a and ψ are functions of time defined by the following differential equations:

$$\frac{da}{dt} = \varepsilon A_1(a) + \varepsilon^2 A_2(a) + \dots$$
$$\frac{d\psi}{dt} = \omega + \varepsilon B_1(a) + \varepsilon^2 B_2(a) + \dots \quad \text{(E.10)}$$

Thus, the original second-order equation (E.8), has been replaced by two first order differential equations (E.10). Therefore, Krylov and Bogoliubov conclude that the practical applicability of the method is not determined by the convergence of the series within equations (E.9) nor (E.10) as these series approach infinity, but rather by their asymptotic properties for a given fixed value of terms when $\varepsilon \to 0$ [93].

Bogoliubov and Mitropolsky also derive the generalized method of averaging in the case of a system with rapidly rotating phase. They begin with a dynamical system whose state is characterized by the rapidly rotating phase, or angular variable, α and the r variables $x_1, x_2, \dots x_r$. This system is represented by the following equations:

$$\frac{dx_k}{dt} = X_k\left(\alpha_1, x_1, \ldots x_r\right) \quad (k = 1, 2, \ldots r)$$
$$\frac{d\alpha}{dt} = \lambda\omega\left(x_1, \ldots x_r\right) + A\left(\alpha_1, x_1, \ldots x_r\right) \qquad \text{(E.11)}$$

Where λ is a large parameter, and $\lambda\omega$ is the frequency of the rotation α.

Also, X_k and A are 2π periodic functions of α; and $\varepsilon = \frac{1}{\lambda\omega}$.

At this point, the derivation shows how to eliminate α from the right hand side of equations (E.11) by averaging. First, they define a near identity transformation, or change of variables:

$$x_k = \bar{x}_k + \sum_{n=1}^{\infty} \frac{1}{\lambda_n} \xi_k^{(n)}\left(\bar{\alpha}, \bar{x}_1, \ldots \bar{x}_r\right) \quad (k = 1, 2, \ldots r)$$
$$\alpha = \bar{\alpha} + \sum_{n=1}^{\infty} \frac{1}{\lambda^n} U_n\left(\bar{\alpha}, \bar{x}_1, \ldots \bar{x}_r\right) \quad (k = 1, 2, \ldots r) \qquad \text{(E.12)}$$

Thus, equations (E.10) reduce to:

$$\frac{d\bar{x}_k}{dt} = \sum_{n=0}^{\infty} \frac{1}{\lambda^n} X_k^n\left(\bar{x}_1, \ldots \bar{x}_r\right)$$
$$\frac{d\bar{\alpha}}{dt} = \lambda\omega\left(\bar{x}_1, \ldots \bar{x}_r\right) + \sum_{n=0}^{\infty} \frac{1}{\lambda^n} \Omega_n\left(\bar{x}_1, \ldots \bar{x}_r\right) \qquad \text{(E.13)}$$

such that the coefficients in equation (E.13) do not depend on the angular variable, $\bar{\alpha}$ [93]. Another benefit of this procedure, is that the functions ξ_k and U_n need not be restricted to scalar functions [94].

Following the work of Krylov and Bogoliubov, there have been numerous applications that use the method of averaging in both celestial mechanics and nonlinear circuit theory. I will conclude this review of the generalized method of averaging with a most interesting mathematical analysis prepared for NASA, by Analytical and Computational Mathematics, Inc., (Nov 1977). This report states that the generalized method of averaging is based upon the following Main Theorem of Averaging, for the periodic case, (See Verhulst 1976 [95]).

Consider the the initial value problem:

$$\frac{d\vec{x}}{dt} = \varepsilon \vec{f}(\vec{x}, t, \varepsilon) \qquad \vec{x}(0, \varepsilon) = \vec{x}_0 \tag{E.14}$$

with $t \in [0, \infty]$, $\varepsilon \in [0, \varepsilon_0]$, $\vec{x} \in G$

where G is an open bounded set in R^n,

and the following conditions are satisfied [46]* :

(1) $\vec{f}$ is defined in a connected set G;

(2) $\vec{f}$ is continuous and uniformally bounded in G;

(3) $\vec{f}$ is Lipshitz**-continuous with respect to $\vec{x}$ in G;

**Note: (A Lipshitz condition is referenced to the Uniqueness Theorem, i.e. :

* Note: The first three conditions ensure that the solution to equation (E.13) exists and is unique.

If (x,y) and $\left(\frac{\partial f}{\partial y}\right)$ are continuous for all (x,y) in a rectangle R in the Euclidean Plane, and bounded by:

$$\text{(a)} \quad |f| \leq K \qquad \text{(b)} \quad \left(\frac{\partial f}{\partial y}\right) \leq M \qquad \text{for all } (x,y) \text{ in } R,$$

then the initial value problem, equation (E.14), has one solution, y(x), which is defined at least for all x in the interval $|x - x_0| < \alpha$. Where α is the smaller of the two numbers (a) and (b)/K. Furthermore, (a) and (b) are sufficient conditions rather than necessary, and can be lessened. From the mean value theorem of differential calculus,

$$f(x, y_2) - f(x, y_1) = (y_2 - y_1) \left.\frac{\partial f}{\partial y}\right|_{y = y^*} \qquad \text{(E.15)}$$

where (x, y_1) and (x, y_2) are assumed to be in R,

and y^* is a suitable value between y_1 and y_2.

From this fact, and condition (b), it follows that equation (E.16):

$$|f(x, y_2) - f(x, y_1)| \leq M|y_2 - y_1| \qquad \text{(E.16)}$$

can replace condition (b) and is known as a Lipshitz condition. The important point to gain from this immediate analysis is that the continuity of f(x,y) is not enough to guarantee the uniqueness of the solution [96].)

(4) $\lim_{\varepsilon \to 0} \vec{f}(\vec{x}, t, \varepsilon) = f(\vec{x}, t, 0)$ exists uniformly in G;

(5) $\vec{f}$ has a bounded derivative of ε in G;

(6) $\vec{f}$ is periodic in t with period T.

Appendix F

USER GUIDE DATA

This appendix provides user guide data for the implementation of the NORAD GP theories in GTDS. Additional options have been defined for several previously existing GTDS keyword cards (ELEMENT1, ELEMENT2, ORBTYPE, OUTPUT, POTFIELD, STATEPAR and DRAGPAR) and four new GTDS keyword cards (ELEMENT3, ELEMENT4, ELEMENT5, ELEMENT6) have been constructed. The following keyword descriptions describe the card usage for the NORAD GP theories. None of the modifications are intended to delete current capabilities. Therefore, the R & D GTDS User Guide should be consulted in conjunction with the card descriptions in this appendix. Finally, two sample input decks are provided. The first sample deck is for a HANDE differential correction run employing the seven parameter input option. The second sample deck is for a DP4 differential correction run processing tracking data for the Telesat D2 spacecraft.

ELEMENT1

- Card format: (A8, 3I3, 3G21.14)
- Applicable programs: EPHEM, DC
- Detailed Format:

Columns	Format	Description	
1-8	A8	ELEMENT1 - KEYWORD to set the first three components of the initial state vector and to identify the coordinate system and reference central body of the initial state	
9-11	I3	Input coordinate system orientation: =8, NORAD true equator, mean equinox of epoch	
12-14	I3	Input coordinate system type: =10, SGP elements (GTDS format) =11, GP4/DP4 elements (GTDS format) =12, HANDE elements (GTDS format) =13, SALT elements (GTDS format) =14, SGP elements (SPADOC format) =15, GP4/DP4 elements (SPADOC format) =16, HANDE elements (SPADOC format) =17, SALT elements (SPADOC format) =18, SGP elements (from the NORAD Historical Data System) (SPADOC format)	
15-17	I3	Input element set reference central body: =1, Earth	
		GTDS Format	SPADOC Format
18-38	G21.14	semimajor axis (km)	mean motion (revs/day)
39-59	G21.14	eccentricity	eccentricity
60-80	G21.14	inclination (deg)	inclination (deg)

ELEMENT2

- Card format: (A8, 3I3, 3G21.14)
- Applicable programs: EPHEM, DC
- Detailed Format:

Columns	Format	Description
1-8	A8	ELEMENT2 - KEYWORD to set the second three components of the initial state
9-17	3I3	Blank
		GTDS and SPADOC Formats
18-38	G21.14	longitude of ascending node (deg)
39-59	G21.14	argument of perigee (deg)
60-80	G21.14	Mean anomaly (deg)

ELEMENT3

- Card format: (A8, 3I3, 3G21.14)
- Applicable programs: EPHEM, DC
- Detailed Format:

Columns	Format	Description		GP Theory Application
1-8	A8	ELEMENT3 - KEYWORD to set the NORAD GP theory drag parameters		
9-17	3I3	Blank		
18-38	G21.14	$\dot{n}_0 / 2$,	(rev/day^2)	(SGP, HANDE[1])
39-59	G21.14	$\ddot{n}_0 / 6$,	(rev/day^3)	(SGP, HANDE)
60-80	G21.14	B* ,	(Earth Radii^{-1})	(GP4)
		B ,	(m^2/kg)	(HANDE)

1 For the HANDE theory, the $\dot{n}_0 / 2$ and $\ddot{n}_0 / 6$ parameters are required only if the 18 parameter input option is being employed.

ELEMENT4

- Card format: (A8, 3I3, 3G21.14)
- Applicable programs: EPHEM, DC
- Detailed Format:

Columns	Format	Description
1-8	A8	ELEMENT4 - KEYWORD to set the the first group of extra time derivatives required for the HANDE theory when the 18 parameter input option is being employed
9-17	3I3	Blank
18-38	G21.14	$(d^3n / dt^3)_0 / 24$, (rev/day^4)
39-59	G21.14	$(d^4n / dt^4)_0 / 120$, (rev/day^5)
60-80	G21.14	$\dot{e}$, (day^{-1})

ELEMENT5

- Card format: (A8, 3I3, 3G21.14)
- Applicable programs: EPHEM, DC
- Detailed Format:

Columns	Format	Description
1-8	A8	ELEMENT5 - KEYWORD to set the second group of extra time derivatives required for the HANDE theory when the 18 parameter input option is being employed
9-17	3I3	Blank
18-38	G21.14	$(d^2e / dt^2)_0 / 2$, (day^{-2})
39-59	G21.14	$(d^3e / dt^3)_0 / 6$, (day^{-3})
60-80	G21.14	$(di / dt)_0$, (rev/day)

ELEMENT6

- Card format: (A8, 3I3, 3G21.14)
- Applicable programs: EPHEM, DC
- Detailed Format:

Columns	Format	Description
1-8	A8	ELEMENT6 - KEYWORD to set the third group of extra time derivatives required for the HANDE theory when the 18 parameter input option is being employed
9-17	3I3	Blank
18-38	G21.14	$(d\Omega / dt)_0$, (rev/day)
39-59	G21.14	$(d\omega / dt)_0$, (rev/day)
60-80	G21.14	$(dM / dt)_0$, (rev/day)

ORBTYPE

- Card format: (A8, 3I3, 3G21.14)
- Applicable programs: EPHEM, DC
- Detailed Format:

Columns	Format	Description
1-8	A8	ORBTYPE - KEYWORD to select the orbit generator type
9-11	I3	NORAD Orbit Generator Type: =13, SGP =14, GP4/DP4 (automatic selection) =15, DP4 =16, HANDE (7 parameter input) =17, HANDE (18 parameter input) =18, SALT
12-14	I3	Osculating or Mean Output: =1, osculating =2, mean (not operational)
15-17	I3	Integration Coordinate System: =8, NORAD true equator and mean equinox of epoch
18-38	G21.14	Computation method for Minutes since Jan 0.0, 1970 (SPADOC Reference Time) =1, A.1 - UTC corrections are considered (uses GTDS TZERO parameter) =2, Based solely on Julian Date (corresponds to FACC 'zero time constants' option)

OUTPUT

- Card format: (A8, 3I3, 3G21.14)
- Applicable programs: EPHEM
- Detailed Format:

Columns	Format	Description
1-8	A8	OUTPUT - KEYWORD to select the orbit generator printer output
9-11	I3	Output Coordinate System Orientation: =1, mean Earth equator and equinox of 1950.0 =2, true of reference (inertial) =3, true of reference or date (body-fixed) =4, mean ecliptic and equinox of 1950.0 =5, true of date, ecliptic and equinox =6, NORAD true equator and mean equinox of output date =7, not used =8, NORAD true equator and mean equinox of epoch
12-14	I3	Output Reference System: =2, Cartesian, Keplerian, and spherical (default)
15-17	I3	Output Reference Body: =1, Earth
18-38	G21.14	Year, month, day of end of print arc (yymmdd)

OUTPUT (cont'd)

39-59	G21.14	Hours, minutes, seconds of end of print arc (hhmmss.ssss)
60-80	G21.14	Output print interval (seconds)

POTFIELD

- Card format: (A8, 3I3, 3G21.14)
- Applicable programs: DC, EPHEM
- Detailed Format:

Columns	Format	Description
1-8	A8	POTFIELD - KEYWORD to indicate if retrieval of potential field data is required
9-11	I3	Body for which field data is to be retrieved:
		=1, Earth
12-14	I3	Potential field model number
		=7, WGS-72[2]
		Note: This setting is mandatory for NORAD GP theory runs until subroutine INTNCO is completed.
15-17	I3	not used
18-38	G21.14	not used
39-59	G21.14	not used
60-80	G21.14	not used

2 The GTDS data set 'NEW.EARTHFLD.DATA' must be attached to FT08 via JCL.

STATEPAR

- Card format: (A8, 3I3, 3G21.14)
- Applicable programs: DC, EPHEM
- Detailed Format:

Columns	Format	Description
1-8	A8	STATEPAR - KEYWORD to set the state vector partial derivatives switch to compute state partial derivatives in an EPHEM Program run, or to indicate state solve-for parameters in a DC Program run
9-11	I3	State solve-for parameter component type: =3, mean equinoctial elements (a,h,k,p,q, λ) Note - This value applies to both the Semianalytical Satellite Theory and the NORAD GP theory implementations in GTDS
12-14	I3	not used for NORAD GP theories
15-17	I3	not used for NORAD GP theories
18-38	G21.14	not used for NORAD GP theories
39-59	G21.14	not used for NORAD GP theories
60-80	G21.14	not used for NORAD GP theories

DRAGPAR

- Card format: (A8, 3I3, 3G21.14)
- Applicable programs: DC
- Detailed Format:

Columns	Format	Description
1-8	A8	DRAGPAR - KEYWORD to update drag solve-for parameters
9-11	I3	Drag options: =0, no drag solve-for requested =6, solve for the appropriate drag parameter in a NORAD GP theory DC - $\dot{n}_0 / 2$ in SGP - B* in GP4/DP4 - B in HANDE/SALT
12-14	I3	not used for NORAD GP theories
15-17	I3	not used for NORAD GP theories
18-38	G21.14	not used for NORAD GP theories
39-59	G21.14	not used for NORAD GP theories
60-80	G21.14	A priori standard deviation of the drag solve-for parameter (optional) - $\sigma_{\dot{n}_0 / 2}$ in SGP - σ_{B^*} in GP4/DP4 - σ_B in HANDE/SALT

Sample Data Card Deck For HANDE Differential Correction Run

```
CONTROL    DC                                                    SV10299    770830
ELEMENT1   8 12   1   6635.805            .0098                   72.97
ELEMENT2              118.12              55.73                   164.08
ELEMENT3              0.0                 0.0                     1.07D-3
EPOCH                 770902              000000
OBSINPUT   5          770902 000000       770905 000000
ORBTYPE   16   1   8  1
DMOPT
/PARQ    100396   3  346.4107137          484329.0236        2620600.3352
/CBDF    100393   3   86.77134266         524414.1586        1740527.3512
/ASCQ    100354   3   51.74810742        - 75424.0547        3453550.4294
/EGLQ    100399   3   30.41996473         303420.7437        2734706.5524
/NAVQ    100745   3  325.6775670          333252.1124        2611349.5500
/CLEF    100349   3  208.9523966          641728.1775        2104825.2759
/CLET    100359   3  208.9523966          641728.1775        2104825.2759
/FYLQ    100341   3  294.8848220          542207.6106        3591953.1280
/FYLF    100342   3  296.4543978          542201.7699        3591959.4260
/FYLT    100343   3  293.1495292          542157.0336        3592003.7670
/DYBF    100337   3  886.2302620          375418.7758         395935.4601
/DYBT    100401   3  886.2302620          375418.7758         395935.4601
/THUF    100348   3  389.1741628          763404.1687        2914256.3160
/ANTQ    100363   3    0.4623641          170836.974048      2981226.378593
OBSDEV     9          300
OBSDEV    27           30
OBSDEV     4           72
OBSDEV     5           72
END
DCOPT
/PARQ    001004005    48.                  54.                46.8
/PARQ    009         100.
/CBDF    001004005    34.                  93.6               57.6
/CBDF    009         200.
/ASCQ    001004005    77.                  90.                118.8
/ASCQ    009        1200.
/EGLQ    001004005    67.                  61.2               54.
/NAVQ    001004005  1979.                  64.8               122.4
/CLEF    001004005  3044.                  190.8              140.4
/CLEF    009         600.
/CLET    001004005    33.                  111.6              118.8
/CLET    009         700.
/FYLQ    001004005  1460.                  144.               57.6
/FYLQ    009         200.
/FYLF    001004005  2764.                  104.4              86.4
/FYLF    009         200.
/FYLT    001004005  1174.                  104.4              115.2
/FYLT    009         100.
/DYBF    001004005    59.                  158.4              237.6
/DYBF    009         400.
/DYBT    001004005    54.                  219.6              144.
/DYBT    009         400.
/THUF    001004005   879.                  97.2               165.6
/THUF    009         200.
/ANTQ    001004005    27.                  25.2               21.6
/ANTQ    009         100.
PRINTOUT   1     4     11.
```

Sample Data Card Deck For HANDE Differential Correction Run (Cont'd)

```
CONVERG   12          1.D-3                                   1.0
ELLMODEL  1           6378.14              298.25
END
OGOPT
POTFIELD  1   7
DRAGPAR   6
STATEPAR  3
STATETAB  1   2   3   4                     5                  6
END
FIN
CONTROL   EPHEM                             OUTPUT             SV10299    770830
OUTPUT    1   2   1   770905                0.0                 900.
ORBTYPE   16  1   8   1
OGOPT
DRAGPAR   0
POTFIELD  1   7
OUTOPT    1           770902000000.         770905000000.       900.
END
FIN
CONTROL   COMPARE                                             SV10299    770830
COMPOPT
CMPEPHEM  1102102     770902000000.         770904000000.      15
CMPPLOT   3                                                    2.0
HISTPLOT  1102102     770902000000.         770904000000.      900.
END
FIN
```

Sample Data Card Deck For DP4 Differential Correction Run

```
CONTROL    DC                                                          TELESAT     850101
ELEMENT1   8 11   1   42164.464          0.0012822                     1.9714
ELEMENT2               277.7290          200.7923                      158.4946
ELEMENT3                 0.0              0.0                           0.0
EPOCH                  850405             125928.623
OBSINPUT   5           850405 130000      850501 000000
ORBTYPE   15   1   8   1
DMOPT
/EGLQ    100399   3    36.0               303420.6760          2734706.2880
/PRKQ    100404   3   889.974             375418.7730           395935.4700
/ALTQ    100334   3    63.380              92343.3990          1672844.8831
/MILQ    100369   3   123.100             423702.6530          2883032.2178
/TTAF    100602   3   260.714             441022.54384         2790348.05586
/MAGC    100231  13  3058.680             204228.8380          2034431.4260
/MBGC    100232  13  3058.670             204228.8420          2034432.5420
/MCGC    100233  13  3058.700             204230.5690          2034432.6400
/KAGC    100221  13   784.200             354438.5780          1283628.3260
/KBGC    100222  13   784.210             354438.5810          1283630.0780
/KCGC    100223  13   784.230             354437.7860          1283629.8310
/CAGC    100211  13  1510.210             334902.0474          2532022.9049
/CBGC    100212  13  1510.190             334902.0500          2532024.6167
/CCGC    100213  13  1510.200             334901.2554          2532024.4064
/STMC    100027  13    74.1               465357.948           2944723.28
END
DCOPT
EDIT          2      3.0
TRACKELV   3 13        5.                  5.
/EGLQ    001004005    67.                 61.2                  54.
/PRKQ    001004005    49.5                66.3                  125.5
/PRKQ    009          34.9
/ALTQ    001004005    17.0                30.1                  34.9
/ALTQ    009          5.3
/MILQ    001004005    2.1                 13.5                  14.8
/MILQ    009          1.
/TTAF    001004005     5.                 29.                   29.
/MAGC    006007       16.                 16.
/MBGC    006007       14.8                14.8
/MCGC    006007       16.3                16.3
/KAGC    006007       16.2                16.2
/KBGC    006007       16.7                16.7
/KCGC    006007       38.                 38.
/CAGC    006007       17.7                17.7
/CBGC    006007       17.1                17.1
/CCGC    006007       18.1                18.1
/STMC    006007      144.                144.
PRINTOUT   1      4     1.
CONVERG   20         1.D-3                                          1.0
ELLMODEL   1         6378.135            298.26
OBSCORR    1   1   0  2222.
/TTAF    600002004   2                    2
/TTAF    500004001   0.0
/TTAF    500005001   0.0
PASSTIME   1         10.D16
END
OGOPT
```

Sample Data Card Deck For DP4 Differential Correction Run (Cont'd)

```
POTFIELD  1  7
STATEPAR  3
STATETAB  1  2  3  4                    5                    6
END
FIN
CONTROL   EPHEM                          OUTPUT               TELESAT    850101
OUTPUT    1  2  1  850501.              125928.623           3600.
ORBTYPE  15  1  8  1
OGOPT
POTFIELD  1  7
OUTOPT    1        850405130000.        850501130000.        1800.
END
FIN
CONTROL   COMPARE                                             TELESAT    850101
COMPOPT
CMPEPHEM  1102102  850405130000.        850501000000.        720.
CMPPLOT   3                                                   2.0
HISTPLOT  1102102  850405130000.        850501000000.        43200.
END
FIN
```

List of References

1. Lemonick, Michael D., "Surging Ahead," Time, Vol. 130, No. 14, 5 October 1987.

2. Pesavento, Peter, "Sputnik's Heirs: What the Soviets are Doing in Space," Technlogy Review, 30 October 1987.

3. Stein, Charles, "Draper Labs: Searching for a Way to Launch a New Era," Boston Globe, 17 August 1987.

4. DeVere, G.T., and Johnson, N.L., "The NORAD Space Network," Spaceflight, Volume 27, Numbers 7 & 8, July/August 1985.

5. Hoots, Felix R., and Roehrich, Ronald L., Models for Propagation of NORAD Element Sets, Spacetrack Report No. 3, December 1980, Aerospace Defense Command, United States Air Force.

6. Roehrich, Ronald L. and Cranford, Kenneth, et al, "General Perturbations Mathematical Models for The Space Computation Center," Analysis Memorandum 71-12, Fourteenth Aerospace Force, Ent Air Force Base, Colorado, 16 August 1971.

7. Lane, Max H., "The Development of an Artificial Satellite Theory Using a Power-Law Atmosphere Density Representation," AIAA preprint 65-35, presented at the AIAA Second Aerospace Sciences Meeting, New York, New York, 25-27 January 1965.

8. Cefola, Paul J., "Demonstration of the Semianalytical Satellite Theory Approach to Improving Orbit Determination Software," Technical Proposal prepared for Headquarters Aerospace Defense Command, Peterson AFB, Colorado, from Charles Stark Draper Laboratory, Cambridge, Massachusetts, September 1977. (Copy available from Dr. Paul Cefola, CSDL.)

9. Hoots, Felix R., Models for Propagation of Space Command Element Sets, Spacetrack Report No. 6, July 1986, USAF Space Command, United States Air Force.

10. Kaula, W. M., Theory of Satellite Geodesy, Waltham, Massachusetts: Blaidell Publishing, 1966.

11. Harmonic Analysis Program (HAP) User's Guide, Wolf Research and Development, 1972.

12. Cefola, Paul J., Memorandum to Department of Astrodynamics, "Technical Comments on SST," Prepared as a response to comments received from the Department of Astrodynamics Headquarters Aerospsace Defense Command, Peterson AFB Colorado, regarding a September 1977 Technical Proposal (Reference [8]), 3 April 1978 . (Copy available from Dr. Paul Cefola, CSDL.)

13. Kaniecki, Jean-Patrick Rene', Short Periodic Variations in the First Order Semianalytical Satellite Theory, S.M. Thesis, Department of Aeronautics and Astronautics, Massachusetts Institute of Technology, August 1979.

14. Proulx, Ron, et al., "A Theory for the Short Periodic Motion Due to the Tesseral Harmonic Gravity Field," AIAA preprint 81-180, presented at the AIAA/AAS Astrodynamics Specialist Conference, Lake Tahoe, Nevada, 3-5 August, 1981.

15. Zeis, Eric G., A Computerized Algrebraic Utility for the Construction of Nonsingular Satellite Theories, S. M. Thesis, Department of Aeronautics and Astronautics, Massachusetts Institute of Technology, September 1978.

16. Mueller, A. C., "Recursive Analytical Solution Describing Artificial Satellite Motion Perturbed by an Arbitrary Number of Zonal Terms," presented at the AIAA/AAS Astrodynamics Conference, Jackson, Wyoming, September 1977.

17. Hilton, C.G., et al, Mathematical Foundation For SCC Astrodynamic Theory, SPADOC Computation Center Computer Program Product Specification, TP SCC 008, 6 April 1982.

18. Khan, M. A., "Accuracy of the Earth's Gravity Field Models," Physics of the Earth and Planetary Interiors, Vol. 31, March 1983.

19. Lerch, Francis J., Klosko, Steven M., et al, "Gravity Model Improvement Using GEOS-3 GEM 9 and GEM 10," results presented at the Spring Annual Meeting of the American Geophysical Union, Washington D. C., June 1977.

20. Wakker, K. F., Ambrosius, B. A. C., et al, "Precise Orbit Computation, Gravity Model Adjustment and Altimeter Data Processing for the ERS-1 Altimetry Mission," Technical Report under ESA contract 6140/84/D/IM, Delft University of Technology, Delft, Netherlands, February 1987.

21. Lerch, Francis J., Klosko, Steven M., et al, "A Gravity Model for Crustal Dynamics (GEM L2)," Journal of Geophysical Research, Vol. 90, No. B11, 30 September 1985.

22. Cefola, Paul J., Conversation with Carl Wagner NOAA, 1986.

23. Seppelin, Thomas O., "The Department of Defense World Geodetic System 1972," Presented at the International Symposium on Problems Related to the Redefinition of North American Geodetic Networks, Fredericton, New Brunswick, Canada, 20-25 May 1974.

24. The Report of the National Commission on Space, Pioneering the Space Frontier An Exciting Vision of our Next Fifty Years in Space, New York, New York: Bantam Books, May 1986.

25. Lawrence, Robert M., Strategic Defense Initiative, Bibliography and Research Guide, Ithaca, New York: Westview Press, 1987.

26. Sridharan, R., "Status of the Network," Vugraphs presented at The Space Surveillance Workshop, Hanscom Air Force Base, Massachusetts, 8-10 April 1986.

27. Stares, Paul B., The Militarization of Space US Policy, 1945-84, Ithaca, New York: Cornell University Press, 1985.

28. Sundberg, Eric, Lt Col, Headquarters, USAF Space Command, correspondence with Dr. Paul J. Cefola, 12 August 1987.

29. Sundberg, Eric, "SPACE 2000 A View From the Blue," AIAA/AAS preprint 87-452, presented at the AIAA/AAS Astrodynamics Specialist Conference, Kalispell, Montana, 10-13 August 1987.

30. Cooke, David G., "The SMART Catalog," AIAA/AAS preprint 87-450, presented at the AIAA/AAS Astrodynamics Specialist Conference, Kalispell, Montana, 10-13 August 1987.

31. Marshall, Eliot, "Solar Monitor Shot Down by ASAT," Science, 4 October 1985.

32. Covault, Craig, "SDI Delta Intercept Yields Data On Space Collision Shock Waves," Aviation Week and Space Technology, 8 June 1987.

33. U. S. Department of Defense Strategic Defense Initiative, and The U. S. Congress Office of Technology Assessment, and The Heritage Foundation, Anti-Missile and Anti-Satellite Technologies and Programs SDI and ASAT, Park Ridge, New Jersey: Noyes Publications, 1986.

34. Wackernagel, H.B., "Orbit Representation," SCC Development Division, Memorandum for Record, 2 October 1975. (Copy available from Dr. Paul Cefola, CSDL.)

35. Arsenault, Jeanine L., Chaffee, Lois and Kuhlman, James R., "General Ephemeris Routine Formulation Document," Technical Documentary Report ESD-TDR-64-522, 496L System Program Office, Electronic System Division, Hanscom Field, Bedford, Massachusetts, August 1964, Air Force Systems Command, United States Air Force. (Copy available from Dr. Paul Cefola, CSDL.)

36. Gabbard, John, of Aerospace Defense Command, correspondence with Dr. Paul J. Cefola, May 1977.

37. Arsenault, Jeanine, "General Ephemeris Routine Experimentation," Philco-Ford document, January 1965. (Copy available from Dr. Paul Cefola, CSDL.)

38. Kozai, Yoshida, "The Motion of a Close Earth Satellite," Astronomical Journal, Vol. 64, No. 1274, November 1959.

39. Koskela, Paul E., Astrodynamic Analysis for the Advanced Orbit/Ephemeris Subsystem, Prepared under DDI Subcontract No. 66-1 to AF 04 (695) - 976 for Data Dynamics, Inc., Monterey Division, Aeronutronic Publication No. U-4180, 1 September 1967.

40. Major, Paul E., and Hoots, Felix R., "Primary GP Theories used in the Space Defense Center," Analysis Memorandum 75-2, 7 May 1975, Office of Astrodynamic Applications, Ent Air Force Base, Colorado.

41. Lane, Max H. and Cranford, Kenneth H., "An Improved Analytical Drag Theory for the Artificial Satellite Problem," AIAA preprint 69-925, presented at the AIAA/AAS Astrodynamic Conference, Princeton, New Jersey, 20-22 August 1969.

42. Brouwer, Dirk, "Solution of the Problem of Artificial Satellite Theory Without Drag," Astronomical Journal, Vol. 64, No. 1274, November 1959.

43. Hoots, Felix R., and France Richard G., Transformations Between Element Sets, Spacetrack Report No. 5, June 1986, Space Command, United States Air Force.

44. Hujsak, Richard S., A Restricted Four Body Solution for Resonating Satellites Without Drag, Spacetrack Report No. 1, November 1979, Aerospace Defense Command, United States Air Force.

45. Hujsak, Richard S., "FORTRAN SGP/SGP4/DP4 Program Description," Aerospace Data Analysis Program Number 77-1, 6 April 1977, Office of Astrodynamics, Headquarters Aerospace Defense Command, Peterson Air Force Base, Colorado.

46. Graf, Otis F. Jr., Mueller, Alan and Starke, Stephen, "The Method of Averages Applied to the Kustaanheimo Steifel (KS) Differential Equations," Analytical and Computational Mathematics Technical Report, ACM-TR-109, prepared for the NASA/Johnson Space Center, November 1977, Analytical and Computational Mathematics, Inc., Houston, Texas.

47. Giacaglia, G.E.O., Perturbation Methods in Non-Linear Systems, New York, New York: Springer-Verlag, 1972.

48. McClain, Wayne D., A Recursively Formulated First Order Semianalytical Artificial Satellite Theory Based on the Generalized Method of Averaging, Volume 1, NASA CR-156782, N78-28147, November 1977.

49. Hoots, Felix R., "An Analytical Satellite Theory Using Gravity and a Dynamic Atmosphere," AIAA preprint 82-1409, presented at the AIAA/AAS Astrodynamics Conferernce, San Diego, California, 9-11 August 1982.

50. Hoots, Felix R., and France, Richard G., "An Analytic Satellite Theory Using Gravity and a Dynamic Atmosphere," Celestial Mechanics, Vol. 40 No. 1, 1987.

51. Hoots, Felix R., "New Orbit Models in SPADOC4," Vugraphs presented at the Deep Space Sensor and Surveillance Workshop, Lincoln Laboratory, Bedford, Massachusetts, 9-11 April 1985. (Note: This presentation was videotaped and is available at the Lincoln Laboratory library.)

52. Slowey, J. W., "Global Frequency Distribution of Exosphere Temperature," Technical Report, Air Force Geophysics Laboratory, Hanscom AFB, Massachusetts, AFGL-TR-79-0143, July 1979.

53. Cappellari, J. O., et al, Mathematical Theory of the Goddard Trajectory Determination System, X-582-76-77, Goddard Spaceflight Center, Greenbelt, Maryland, April 1976.

54. Cefola, Paul J., "Orbit Determination for Low Altitude Spacecraft," Draper Laboratory Document, PL-253-15Z -WDM, 10 June 1986.

55. Long, A.C. and Early, L.W., System Description and User's Guide for the GTDS R&D Averaged Orbit Generator, CSC ISD-7816020, Computer Science Corporation, November 1978.

56. Computer Sciences Corporation and Systems Development and Analysis Branch (GSFC), "Research and Development Goddard Trajectory Determination System User's Guide," July 1978.

57. Fieger, Martin E., An Evaluation of Semianalytical Satellite Theory Against Long Arcs of Real Data For Highly Eccentric Orbits, S. M. Thesis, Department of Aeronautics and Astronautics, Massachusetts Institute of Technology, January 1987.

58. Cefola, Paul J. and Broucke, R., "On the Formulation of the Gravitational Potential in Terms of Equinoctial Variables," presented at the AIAA 13th Aerospace Sciences Meeting, Pasadena, California, January 20-22 1975.

59. Wagner, Elaine A., Application of the Extended Semianalytical Kalman Filter to Synchronous Orbits, S.M. Thesis, Department of Aeronautics and Astronautics, Massachusetts Institute of Technology, February 1983.

60. Taylor, Stephen P., Semianalytical Satellite Theory and Sequential Estmiation, S. M. Thesis, Department of Aeronautics and Astronautics, Massachusetts Institute of Technology, September 1981.

61. Green, Andrew J., Orbit Determination and Prediction Processes for Low Altitude Satellites, S. M. Thesis, Department of Aeronautics and Astronautics, Massachusetts Institute of Technology, December 1979.

62. CSDL Technical Proposal No. 5-503, prepared for NORAD in 1984.

63. Bobick, A., J_2-Square MACSYMA Working Notes, Draper Laboratory, July 1981. (Copy available from Dr. Paul Cefola, CSDL.)

64. Proulx, Ron, "Mathematical Description of the Tesseral Resonance and Resonant Harmonic Coefficient Solve-For Capabilities," DRAPER IOC NSWC-001-15Z-RJP, 13 April 1982.

65. Proulx, Ron and McClain, Wayne, "Series Representation and Rational Approximations for Hansen Coefficient," Paper No. AIAA 82-0073, AIAA 20th Aerospace Sciences Meeting, Orlando, Florida, 11-14 January 1982.

66. Collins, Sean K., Long Term Predictions of High Altitude Orbits, Phd. Thesis, Department of Aeronautics and Astronautics, Massachusetts Institute of Technology, March 1981.

67. Early, Leo W., "A Portable Orbit Generator Using Semianalytical Satellite Theory," AIAA/AAS Astrodynamics Conference, Williamsburg, Virginia, 18-20 1986.

68. Slutsky, Mark, Zonal Harmonic Short-Periodic Model, Draper Laboratory, Division 15Z, IOC, PL-016-81-MS, 30 November 1981.

69. Cefola, Paul J., "Second Order Coupling of M-Daily Terms with J_2 Secular Rates," Charles Stark Draper Intralab Memorandum IRD-011-15Z-PJC, 7 July 1981.

70. McClain, Wayne D., Intralab Memorandum, "GTDS Implementation of the NORAD C and B Matrices," Charles Stark Draper Laboratory, Cambridge, Massachusetts, 14 September 1987.

71. Woolard, Edgar W. and Clemence, Gerald M., Spherical Astronomy, New York, New York: Academic Press Inc., 1966.

72. Mueller, Ivan I., Spherical and Practical Astronomy as Applied to Geodesy, New York, New York: Frederick Ungar Publishing Co., 1969.

73. Liu, J. J. F., and Alford, R. L., "A Semi-Analytic Thoery for the Motion of a Close-Earth Artificial Satellite with Drag," AIAA/AAS preprint 79-0123, presented at the 17th Aerospace Sciences Meeting, New Orleans, Louisiana, 15-17 January 1979.

74. Shaver, Jeffrey S., Formulation and Evaluation of Parallel Algorithms for the Orbit Determination Problem, Phd. Thesis, Department of Aeronautics and Astronautics, Massachusetts Institute of Technology, March 1980.

75. CSDL-C-5526, Software Development Policies and Guidelines, 15 April 1983.

76. Department of Defense, Military Standard Defense System Software Development, Washington D. C., DOD-STD-2167, 4 June 1985.

77. McClain, W., Cefola, P. and Carter, D., "Landsat Orbit Determination Study," Draper Laboratory Technical Report, CSDL-R-1952, March 1987.

78. Not Used

79. Groves, G. V., "Canadian Speaks to Canadian," Spaceflight, Volume 29, Number 2, February 1987.

80. Jedicke, Peter and Cunningham, Clifford, "Canada's Satellite System," Spaceflight, Volume 27, Numbers 7 & 8, July/August 1985.

81. Cefola, Paul J. and McClain, Wayne, "Accuracy of the NORAD DP4 Satellite Theory for Synchronous Equatorial Orbits," Draper Laboratory Intralab Memeorandum, NOR/PL-002-15Z-PJC, 6 May 1987.

82. Gaposchkin, E.M., Byers, R.M., and Conant, G.H., Deep Space Network Calibration 1985, MIT Lincoln Laboratory Project Report STK-144, 11 December 1986.

83. Cefola, Paul J., Correspondence with Mr. Frans C. Kez, Manager Flight Dynamics Group, TELESAT CANADA, letter dated 17 October 1987.

84. Geyling-Westerman, Introduction To Orbital Mechanics, Reading, Massachusetts: Addison-Wesley, 1971.

85. Bate, Mueller, and White, Fundamentals of Astrodynamics, New York, New York: Dover, 1971.

86. Battin, Richard H., An Introduction to the Mathematics and Methods of Astrodynamics, New York, New York: American Institute of Aeronautics and Astronautics, Inc., 1987.

87. Morrison, J.A., "Generalized Method of Averaging and the Von Zeipel Method," AIAA preprint 65-687, presented at the AIAA/ION Astrodynamics Specialist Conference, Monterey, California, 16-17 September 1965.

88. Vinti, J.P., Author's personal notes for Celestial Mechanics Course 16.491/.492, Massachusetts Institute of Technology, Cambridge, Massachusetts, 1986.

89. Brouwer, D. and Hori, G., "Theoretical Evaluation of Atmospheric Drag Effects in the Motion of an Artificial Satellite," Astronomical Journal, Vol. 66, No. 1290, June 1961.

90. Brouwer, D. and Clemence, G. M., Methods of Celestial Mechanics, New York, New York: Academic Press 1961.

91. Dahlquist, Germund and Bjorck, Ake, Numerical Methods, Englewood Cliffs, New Jersey: Prentice-Hall Inc., 1974.

92. Danby, John M. A., Fundamentals of Celestial Mechanics, New York, New York: The Macmillan Company, 1964.

93. Bogoliubov, N. N. and Mitropolsky, Y. A., Asymptotic Methods in the Theory of Non-Linear Oscillations, Jawahar Nagar, Delhi-6, India: Hindustan Scientific Press, 1961.

94. Nayfeh, Ali H., Perturbation Methods, New York, New York: John Wiley & Sons, Inc., 1973.

95. Verhulst, F., On the Theory of Averaging in Long-Time Predictions in Dynamics, V. Szebehely and B. D. Tapley editors, D. Reidel Publishing Co., 1976.

96. Kreysig, Erwin, Advanced Engineering Mathematics, New York, New York: John Wiley & Sons, Inc., 1972.

97. Slutsky, Mark, First Order Short-Periodic Motion of an Artificial Satellite Due to Third Body Perturbations, Draper Laboratory, Division 15Z, IOC, AOD/SD-021-15Z-MS, 30 November 1982.

98. Smith, Richard L. and Mollick M.K., Definitive Orbit Determination for the HEAO-2 Spacecraft. Computer Science Corporation, Contract # NAS5-26122, Greenbelt, Maryland, November 1982.

99. Lichten, Bertiger and Katsigris, "Sub-meter GPS Orbit Determination and High Precision User Positioning: A Demonstration," Paper No. 88-4211, to be presented at the AIAA/AAS Astrodynamics Conference, Minneapolis, Minnesota, 15-17 August 1988.

BIOGRAPHY

Darrell Lee Herriges was born on 31 July 1956 in Hustisford, Wisconsin. He grew up in Hartford, Wisconsin and graduated from Hartford Union High School in 1974. He then entered the USAF Academy and graduated in 1978 as a distinguished graduate. His first assignment on active duty was in the F-16 SPO at Wright-Patterson AFB, Ohio. This was a temporary assignment until he entered pilot training at Williams AFB, Arizona, in January of 1979. Upon graduation, in November, 1979, Second Lieutenant Herriges was introduced to the Tactical Air Command at Holloman AFB, New Mexico, during his Fighter Lead-In Training. Following this three month initiation to the art and science of combat flying, he arrived at Homestead AFB, Florida, to learn how to fly the F-4 Phantom. On October 6th, 1980, First Lieutenant Herriges graduated from F-4 training, and thereby became a fighter pilot. His first operational assignment was at Hahn AB, Germany. After spending a year as a "new guy"/ wingman Lieutenant Herriges was assigned the 401st Tactical Fighter Wing at Torrejon AB, Madrid, Spain. While at Torrejon, Captain Herriges became a flight leader and he was introduced to his wife-to-be, who was visiting her sister in Madrid. His follow-on assignment was to George AFB, California, where Captain Herriges got married to Bev-Ann Lynn Frownfelter; had a baby daughter, Audra; and became a "Wild Weasel" F-4G instructor pilot. The family moved to Boston in May of 1986 when Captain Herriges was selected to attend graduate school at MIT. While writing his thesis in Boston, the second addition to the family arrived, Travis, a new son. Following completion of his degree, Captain Herriges will report to duty in Los Angeles.